Developmental regulators and secreted effector molecules of the fungal pathogen *Verticillium* spp.

Dissertation

For the award of the degree

“Doctor rerum naturalium”

of the Georg-August-Universität Göttingen

within the doctoral program

“Plant Responses To Eliminate Critical Threats“

of the Georg-August University School of Science (GAUSS)

submitted by

Miriam Anna Leonard

from Stade

August 2019

Thesis Committee and members of the Examination Board

Referee: **Prof. Dr. Gerhard Braus**
Department of Molecular Microbiology and Genetics
Georg-August-Universität Göttingen

2nd referee: **apl. Prof. Dr. Kai Heimel**
Department of Molecular Microbiology and Genetics
Georg-August-Universität Göttingen

3rd referee: **Prof. Dr. James Kronstad**
Michael Smith Laboratories
University of British Columbia Vancouver

Further members of the Examination Board:

Prof. Dr. Volker Lipka
Department of Plant Cell Biology
Georg-August-Universität Göttingen

Dr. Marcel Wiermer
Department of Molecular Biology of Plant-Microbe Interactions
Georg-August-Universität Göttingen

Dr. Till Ischebeck
Department of Plant Biochemistry
Georg-August-Universität Göttingen

Date of oral examination: 30th September 2019

This work was accomplished in the group of Prof. Dr. Gerhard H. Braus in the Department of Molecular Microbiology and Genetics at the Institute of Microbiology and Genetics, Georg-August-Universität Göttingen.

Parts of this work are published in:

Bui T, Harting R, Braus-Stromeyer SA, Tran V, **Leonard M**, Höfer A, Abelmann A, Bakti F, Valerius O, Schlüter R, Stanley CE, Ambrósio A & Braus GH (2019) *Verticillium dahliae* transcription factors Som1 and Vta3 control microsclerotia formation and sequential steps of plant root penetration and colonisation to induce disease. *New Phytol*. **221**: 2138-2159.

Leonard M, Kühn A, Harting R, Maurus I, Nagel A, Starke J, Kusch H, Valerius O, Feussner K, Feussner I, Kaever A, Landesfeind M, Morgenstern B, Becher D, Hecker M, Braus-Stromeyer SA, Kronstad JW & Braus GH (2020) *Verticillium longisporum* elicits media-dependent secretome responses with capacity to distinguish between plant-related environments. *Front. Microbiol.* **11**: eCollection 2020.

Table of Contents

Summary

The haploid *Verticillium dahliae* and the allodiploid *V. longisporum* are two filamentous fungal pathogens, which colonize the plant vascular system of a broad host range including important crops. They survive outside of the plant for years in the soil with microsclerotia as resting structures and colonize specific host plants through the roots. In the xylem they form conidia to facilitate transportation within the plant. This life cycle requires a tight control of fungal development and a cautious communication with the host through the secretome without causing extensive plant defense reactions. The focus of this work was (i) to explore the regulatory function of two transcriptional regulators in development, Frq (Frequency) and Sfl1 (Suppressor of flocculation 1), and (ii) to compare fungal secretomes in different environmental conditions. One major result was that Frq and Sfl1 are required for microsclerotia and conidia formation of *V. dahliae*. The circadian clock component Frq acts as light-dependent microsclerotia formation repressor and has the opposite function for conidia where it operates as activator. Sfl1 functions as well as activator of conidia, but also as activator of microsclerotia formation in *V. dahliae*. A genetic analysis using deletion mutant strains revealed that *SFL1* is epistatic to *FRQ* because the absence of *SFL1* leads to the same severe reduction of microsclerotia formation in single as in double deletion mutant strains. This suggests that *SFL1* is genetically located downstream in the regulation of fungal development. This genetic analysis demonstrated as second major result that both genes are required for full virulence of *V. dahliae* on tomato. The fungal communication with the host plant was examined by the secretome of allodiploid *V. longisporum* as pathogen of rape seed. Minimal or complete media delivered a similar broad exoprotein pattern. In contrast, cultivation in the plant-related media, a pectin-rich medium or pure xylem sap isolated from *Brassica napus*, triggered the secretion of another exoproteome pattern that includes similar but also distinct features. This corroborates significant differences in the sensing of the fungus of different environments resulting in different secretion responses. The xylem sap-specific exoproteome included carbohydrate-active enzymes (CAZys), peptidases and proteins with effector domains. Deletion strains of the corresponding homologs of haploid *V. dahliae* were phenotypically similar to wildtype growth *ex planta*. Whereas single deletions of CAZy encoding genes, and even a double deletion of the *MEP1* and *MEP2* genes encoding metallopeptidases or the *CP1* and *CP2* encoding cerato-platanin proteins did not alter virulence, the single metalloprotease Mep1 and the necrosis and ethylene inducing-like proteins Nlp2 and Nlp3 are necessary for *V. dahliae* pathogenicity on tomato. Therefore, the exoproteome approach pinpointed Mep1, Nlp2 and Nlp3 as single effectors required for successful *V. dahliae* colonization whereas other secreted proteins might provide redundant functions. This study shows the flexibility of the *Verticillium* response throughout the life cycle to adjust to distinct external stimuli. Developmental regulators such as the Frq and Sfl1 proteins are essential for microsclerotia or conidia production and for pathogenicity. The secretome response adapts with a distinct pattern to different nutrient combinations in the environment. En masse, these findings revealed Frq, Sfl1, Mep1 and Nlp2/3 as factors important for *V. dahliae* virulence, which all display potential targets for new growth control strategies of the fungus.

Zusammenfassung

Der haploide Pilz *Verticillium dahliae* und sein allodiploider Verwandter *V. longisporum* gehören zu den filamentösen Pflanzenpathogenen. Sie kolonisieren das vaskuläre System eines breiten Wirtsspektrums einschließlich wichtiger Nutzpflanzen. Durch die Ausbildung von Mikrosklerotien als Überdauerungsstrukturen überleben diese Pilze außerhalb der Pflanze über Jahre im Boden und kolonisieren spezifische Wirtspflanzen über die Wurzeln. Dieser Lebenszyklus ist abhängig von einer strengen Kontrolle der pilzlichen Entwicklung und einer umsichtigen Kommunikation mit dem Wirt über das Sekretom um das Auslösen umfassender Pflanzenabwehrreaktionen zu vermeiden. Der Fokus dieser Arbeit lag (i) auf der Untersuchung der regulatorischen Funktionen zweier transkriptioneller Regulatoren in der Entwicklung, Frq (Frequency) und Sfl1 (Suppressor of flocculation 1), und (ii) auf dem Vergleich pilzlicher Sekretome unter unterschiedlichen Umweltbedingungen. Ein bedeutendes Ergebnis war, dass Frq und Sfl1 für die Mikrosklerotien- und Sporenbildung von *V. dahliae* benötigt werden. Als Komponente der zirkadianen Uhr agiert Frq als Licht-abhängiger Repressor der Mikrosklerotienbildung und hat als Aktivator eine entgegengesetzte Funktion auf die Konidienbildung. Sfl1 zeigt ebenfalls eine Aktivatorfunktion auf die Konidienbildung, aber auch auf die Ausbildung von Mikrosklerotien in *V. dahliae*. Eine genetische Analyse unter der Nutzung von Deletionsstämmen zeigte, dass *SFL1* epistatisch zu *FRQ* ist, da die Abwesenheit von *SFL1* in Einzel- und Doppeldeletionen zu einer ähnlich starken Reduktion der Mikrosklerotienbildung führte. Die genetische Analyse demonstrierte als zweites bedeutendes Ergebnis, dass beide Gene für die vollständige Virulenz von *V. dahliae* in Tomatenpflanzen benötigt werden. Die pilzliche Kommunikation mit der Wirtspflanze wurde anhand des Sekretoms des allodiploiden Rapspathogens *V. longisporum* untersucht. Minimal- oder Vollmedium lieferten ein ähnlich breites Exoproteinmuster. Im Gegensatz führte die Kultivierung in den Pflanzen-ähnlichen Umgebungen, einem Pektin-reichen Medium oder purem Xylemsaft, welcher aus *Brassica napus* isoliert wurde, zur Sekretion eines weiteren Exoproteinmusters, welches sowohl gemeinsame als auch spezifische Eigenschaften aufwies. Dies bekräftigt, dass signifikante Unterschiede in der Wahrnehmung von unterschiedlichen Umgebungen in spezifischen Sekretionsantworten resultieren. Das Xylemsaft-spezifische Exoproteom enthält „carbohydrate-active enzymes“ (CAZys), Peptidasen und Proteine mit Effektordomänen. Deletionsstämme der entsprechenden Homologe des haploiden *V. dahliae* waren außerhalb der Pflanze phänotypisch ähnlich zum Wildtyp. Einzeldeletionen der CAZy-kodierenden Gene, eine Doppeldeletion der Metalloproteasen-kodierenden *MEP1* und *MEP2* Gene oder der Ceratoplataninprotein-kodierenden *CP1* und *CP2* Gene veränderten die Virulenz nicht. Im Gegensatz dazu werden „necrosis and ethylene inducing-like“ Proteine Nlp2 and Nlp3 und die einzelne Metalloprotease Mep1 für die Pathogenität von *V. dahliae* in Tomaten benötigt. Die Analyse des Exoproteoms hat Mep1, Nlp2 und Nlp3 als einzelne Effektoren identifiziert, welche für die erfolgreiche Kolonisierung durch *V. dahliae* benötigt werden. Andere sekretierte Proteine hingegen haben möglicherweise redundante Funktionen. Diese Untersuchung zeigt die Flexibilität der Antwort, mit welcher *Verticillium* sich während seines Lebenszyklus an bestimmte externe Stimuli anpasst. Regulatoren der Entwicklung

wie die Proteine Frq und Sfl1 sind sowohl essentiell für die Mikrosklerotien- und Konidienbildung als auch für die Pathogenität. Die Sekretomantwort passt sich mit bestimmten Mustern an unterschiedliche Nährstoffbedingungen in der Umwelt an. Zusammenfassend wurden Frq, Sfl1, Mep1 und Nlp2/3 als wichtige Faktoren der Virulenz von *V. dahliae* identifiziert, welche potentielle Angriffspunkte für die Entwicklung von neuen Strategien zur Wachstumskontrolle des Pilzes bieten.

1 Introduction

1.1 *Verticillium* spp., the destructive pathogen of Verticillium wilt

Species of the *Verticillium* genus are soil-borne plant pathogenic Ascomycetes that are capable of infecting hundreds of plant species world-wide resulting in enormous economic losses (Pegg & Brady, 2002; Fradin & Thomma, 2006; Klosterman *et al*, 2009). Infections occur predominantly in temperate regions, but also appear in the subtropics and tropical regions of the world (Inderbitzin & Subbarao, 2014). Outbreaks of the devastating Verticillium wilt disease, which is a vascular wilt, lead to economic losses of up to 50% on high value crops such as cotton, lettuce, strawberry, olive and potato (Inderbitzin & Subbarao, 2014). Symptoms of Verticillium wilt include stunting, foliar chlorosis and necrosis, vascular discoloration, early senescence and the characteristic wilting, but vary among hosts (Fradin & Thomma, 2006).

The history of *Verticillium* taxonomy and the identification of individual species has been controversial (Inderbitzin & Subbarao, 2014). In 1816 Nees von Esenbeck identified the first *Verticillium* species, which established the *Verticillium* genus (Nees von Esenbeck, 1817; Klosterman *et al*, 2009). The name derived from the verticillate shaped conidiophore morphology. The phialides are arranged in whorls around the conidiophores and form conidia at their terminal ends (Isaac, 1967). *V. dahliae* is the most destructive causal agent of Verticillium wilt and was first found by Klebahn in 1913 as the cause of wilted dahliae (*Asteraceae* family) (Klebahn, 1913; Pegg & Brady, 2002; Klosterman *et al*, 2009). *V. dahliae* alone is able to infect more than 200 plant species (Klosterman *et al*, 2009; Inderbitzin & Subbarao, 2014). Latest morphological and multigene phylogenetic data include the designation of ten *Verticillium* species, *V. dahliae*, *V. albo-atrum*, *V. alfalfae*, *V. isaacii*, *V. klebahnii*, *V. longisporum*, *V. nonalfalfae*, *V. nubilum*, *V. tricorpus* and *V. zaregamsianum* (Inderbitzin *et al*, 2011a; Inderbitzin & Subbarao, 2014). *Verticillium* spp. are plant-associated, however, they have different characteristics such as their host range preferences (Inderbitzin *et al*, 2011a; Klimes *et al*, 2015). *V. longisporum*, for example, has a narrow host range as it primarily infects brassicaceous hosts. *V. dahliae* has the broadest host range and is able to adapt to new hosts (Klosterman *et al*, 2009). Other differences between the species include the morphology of the microsclerotia. *V. dahliae* produces clearly defined

microsclerotia which are thick, melanized resting structures of the fungus that can persist in the soil for more than a decade (Wilhelm, 1955). *V. alfalfae* produces dark resting mycelia that only remain viable for 2-5 years (Schnathorst, 1981; Inderbitzin *et al*, 2011a). Moreover, *V. longisporum*, which produces elongate microsclerotia and longer, ovoid conidia was recognized as a hybrid fungus that evolved by several hybridization events from four different parental lineages (Inderbitzin *et al*, 2011b; Depotter *et al*, 2016). The evolutionary history of the amphidiploid *V. longisporum* is unique among the members of the *Verticillium* genus of which all other members are haploid. Sexual structures have not been observed for any of the *Verticillium* species (Short *et al*, 2014).

Management of Verticillium wilt is very challenging as the fungus is inaccessible once it lives in the vascular tissue of the plants. Soil fumigation with methyl bromide or metam sodium is used for high valuable crops, but is not profitable for all crops. Furthermore, this and other banned fungicides, are associated with environmental issues (Klosterman *et al*, 2009; Yellareddygari & Gudmestad, 2018). While crop rotation is used effectively for other pathosystems, it is not sufficient to combat *Verticillium* spp. for the following reasons. The broad host range of *Verticillium* spp. challenge the farmer to grow resistant crops. Melanized microsclerotia can survive in the soil for a long time without any suitable host (Klosterman *et al*, 2009; Lo Presti *et al*, 2015). Therefore, it is indispensable to use resistant plant varieties, but these are not available in most crops. The selection pressure on fungal strains to quickly overcome genetic resistance makes it even more difficult to develop new resistant traits (Klosterman *et al*, 2009; Lo Presti *et al*, 2015). Consequently, increased understanding of the infection process of *Verticillium* spp. is necessary to reveal new angles of how to control the disease.

1.2 Disease cycle of *Verticillium* spp.

The life cycle of *Verticillium* spp. can be divided into a dormant and a parasitic phase (Figure 1). The parasitic lifestyle begins with the penetration of the host roots. The fungus then grows towards the xylem vessels where it produces conidia and uses the xylem stream to colonize the whole system. This leads to the induction of disease symptoms and the subsequent death of the plant. *Verticillium* then forms microsclerotia to survive in the soil (Schnathorst, 1981; Fradin & Thomma, 2006).

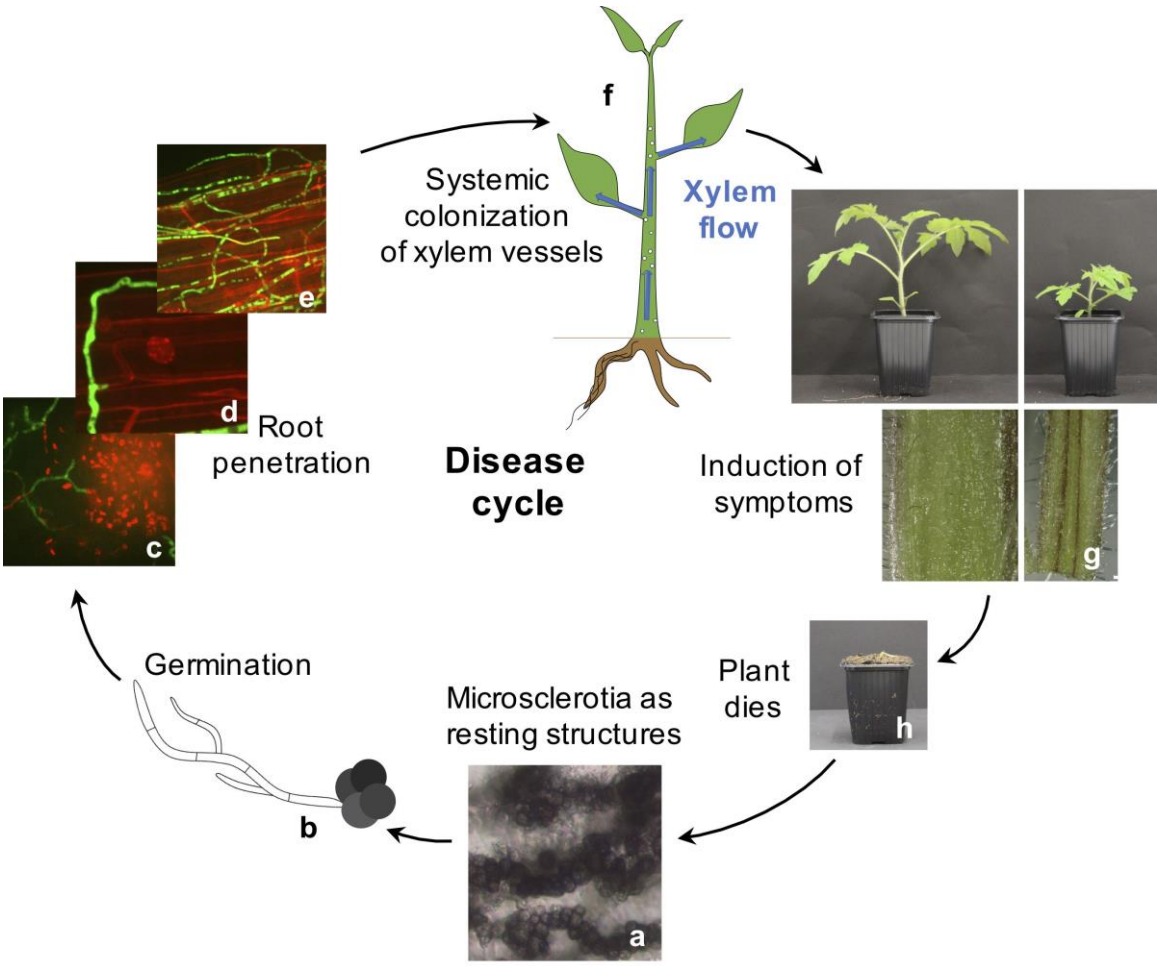

Figure 1. Disease cycle of *Verticillium* spp.
Verticillium spp. form resistant, black microsclerotia that are melanized hyphal cells clumped together **(a)**. Once the fungus senses root exudates microsclerotia germinate and grow towards the root **(b)**. **(c-d)** Fluorescence microscopy of *V. dahliae* expressing free *GFP*. Root cells were stained with 0.05% propidium iodide/0.01% silwet solution. Hyphae can enter the root at the tip **(c)** or grow along the root and form hyphopodia, which appear as hyphal swelling **(d)**. Hyphae cover the whole root **(e)**, grow inter- and intracellularly until reaching the xylem vessels. Here, conidia are produced and exploit the xylem flow to systematically colonize the whole plant **(f)**. Disease symptoms such as stunting, foliar chlorosis and necrosis as well as vascular discolorations become visible **(g)**. Xylem vessels are blocked by the fungal mass and other substances secreted by the fungus or by plant response products. The fungus senses the lack of nutrition as the plant dies **(h)** and produces microsclerotia that are released into the soil with the plant debris and the cycle can begin again with the next growing season.

The dormant microsclerotia in the soil are the primary propagules that initiate the infection. To build up microsclerotia, hyphae start to swell by forming septa, until the hyphal mass is globular and separates from the parent mycelium. These masses later become melanized and form the mature microsclerotia (Figure 1a) (Pegg & Brady, 2002; Klimes *et al*, 2015). Microsclerotia are able to sense root

exudates upon which the germination process is initiated and the hyphae grow towards the root of the plant (Figure 1b) (Gao *et al*, 2010; Schnathorst, 1981). First, hyphae often colonize the root tips (Figure 1 c) or the root hairs, achieving a tight attachment by intermingling with the hair. Then hyphae subsequently colonize the whole root surface (Figure 1e) (Eynck *et al*, 2007; Zhou *et al*, 2006; Klosterman *et al*, 2009).

To penetrate the root, fungi like *Magnaporthe oryzae* require the formation of an appressorium-like invasion structure to attach to plant roots and enter the plants (Eynck *et al*, 2007). For *V. dahliae,* Vallad and Subbarao (2008) reported that the fungus grows along the epidermal cell junctions where it develops appressoria and then penetrates a neighboring epidermal cell. In contrast, other studies observed only slight hyphal swelling leading to the formation of so-called hyphopodia as penetration structure (Figure 1d). In addition, *Verticillium* spp. secrete molecules such as adhesins and effectors that soften the cell wall for easier penetration (Eynck *et al*, 2007; Luo *et al*, 2014; Tran *et al*, 2014; Bui *et al*, 2019; Reusche *et al*, 2014; Zhao *et al*, 2016; Zhou *et al*, 2017).

Success of infections also depends on the penetration site. Hyphae entering at the root cap or root elongation zone result in whole plant colonization compared to unsuccessful penetrations at the mature root regions above the tip (Vallad & Subbarao, 2008; Klosterman *et al*, 2009; Reusche *et al*, 2014). Upon penetration, hyphae then grow inter- and intracellular towards the vascular cylinder and colonize the xylem vessels (Eynck *et al*, 2007; Prieto *et al*, 2009; Reusche *et al*, 2014). Here, the fungus remains for most of its life cycle. Conidia are produced that are passively dispersed throughout the whole plant by exploiting the transpiration stream (Figure 1f) (Eynck *et al*, 2007). The fungus has adapted to growth in the xylem sap which is a nutrient-limited environment with low amounts of sugars, inorganic salts, and amino acids (Eynck *et al*, 2007; Singh *et al*, 2010). In addition to the yeast-like budding growth, *Verticillium* switches to hyphal growth to penetrate into adjacent vessels when conidia become trapped in pit membranes (Klimes *et al*, 2015; Klosterman *et al*, 2009). Not only the mycelia and spores of the fungus lead to clogging of vessels, but also the plant initiates defense responses and thereby releases gums or tyloses to the vessel lumen (Klimes *et al*, 2015; Agrios, 2005a). The plant is disabled in transporting the water to reach upper parts. Verticillium wilt symptoms such as stunting, foliar chlorosis and necrosis become

visible (Fradin & Thomma, 2006). Secretion of fungal enzymes that attack plant cells lead to oxidation of the breakdown products, which results in the brown discoloration of affected vascular tissues (Figure 1g) (Agrios, 2005a). As these processes continue, the plant senesces and the pathogen produces microsclerotia in the dying plant cells (Figure 1h). As microsclerotia are capable of surviving unfavorable environmental conditions, they remain in the field and display the primary inoculum for the following growing season (Schnathorst, 1981; Neumann & Dobinson, 2003; Eynck *et al*, 2007; Klimes *et al*, 2015).

The life cycle of *Verticillium* spp. incorporates many steps and structures that are crucial for plant infections. The resistant microsclerotia play an important role as the primary infection propagules. Adhesion to the root is essential for fungal infection. And the adaptation to the nutrient-limiting xylem sap, where the fungus competes with plant defense reactions, is a lead that requires further investigations to understand the success of this fungus. Shedding light on these infection processes is crucial to find novel control strategies.

1.2.1 Microsclerotia as primary infectious propagule

The resistant microsclerotia formed by *V. dahliae* and *V. longisporum* represent the primary source of inoculum as they are able to survive in the fields for up to 14 years without any host plant (Wilhelm, 1955). Upon perception of a plant root exudates, the microsclerotia germinate and hyphae grow towards the plant roots. Only few microsclerotia per gram of soil are required to establish a 100% infection rate in various susceptible crops (Agrios, 2005b).

Microsclerotia are resistant to UV-light, heat, nutrient deprivation and molecules produced by the plant immune system such as hydrolytic enzymes and oxidizing agents (Brandt, 1964; Wang *et al*, 2018a; Casadevall *et al*, 2017; Bell & Wheeler, 1986; Fan *et al*, 2017; Fang *et al*, 2019). The component protecting the fungus from these stresses is melanin, which is generally deposited in the outer cell wall layer of the microsclerotia (Brandt, 1964; Wang *et al*, 2018a; Butler & Day, 1998). Microsclerotia mostly appear as dark resting structures. However, unpigmented microsclerotia exist as well, indicating that melanin production can be uncoupled from microsclerotia development in *V. dahliae* (Bell *et al*, 1976; Duressa *et al*, 2013). Melanins are mostly black or brown macromolecules composed of phenolic or indolic compounds (Casadevall *et al*, 2017; Butler & Day, 1998; Langfelder *et*

al, 2003). The phenolic structure of melanin is composed of aromatic rings that can absorb light and heat energy and bind toxic chemicals. These features lead to the protection of microsclerotia (Henson *et al*, 1999).

Most fungi, including *Verticillium* spp., produce DHN melanin, which is named after one of its precursors 1,8-dihydroxynaphthalene (DHN) (Fan *et al*, 2017; Bell & Wheeler, 1986). In the DHN pathway, malonyl-CoA or acetyl-CoA is converted to 1,3,6,8-tetrahydroxynaphthalene (THN) by the polyketide synthase (Figure 2). Reductases and dehydratases catalyze the reduction of 1,3,6,8-THN to scytalone and the subsequent dehydration to 1,3,8-THN. These reactions are repeated, 1,3,8-THN is reduced to vermelone and then dehydrated to DHN. Laccases further catalyze the oxidation and polymerization of DHN monomers to DHN melanin (Bell *et al*, 1976; Bell & Wheeler, 1986; Langfelder *et al*, 2003; Duressa *et al*, 2013; Wang *et al*, 2018a). The pathway illustrates that several enzymes are required for correct production of melanized microsclerotia. Several genes involved in melanogenesis turned out to cluster together in a 48.8 kb region of the *V. dahliae* genome (Duressa *et al*, 2013). The organization of melanin biosynthetic genes in a cluster is present in other fungi such as the plant pathogen *Cochliobolus heterostrophus* (Wang *et al*, 2018a; Duressa *et al*, 2013).

Melanin protects the fungus from various stresses. Plant pathogenic fungi such as *M. oryzae* and *Colletotrichum lagenarium* even require the production of melanin to build up sufficient pressure in their penetration structures, the melanized appressoria (Butler & Day, 1998; Henson *et al*, 1999). Although *Verticillium* forms non-melanized hyphopodia as infection structures and therefore not directly requires melanin for plant penetration, several studies report a correlation between impairment in melanin biosynthesis and compromised virulence. Depletion of *VAYG1,* which catalyzes the polyketide shortening step of the polyketide synthase product into 1,3,6,8-THN, leads to melanin and microsclerotia deficient mutant strains that show reduced pathogenicity (Fan *et al*, 2017). The polyketide synthase Pks1 in *V. dahliae* isolate V592 has a positive role on melanin production and virulence on cotton (Zhang *et al*, 2017a). In another *V. dahliae* isolate, VdLs.17, however, Pks1 is required for melanin production but not for virulence on tobacco and lettuce (Wang *et al*, 2018a). Additionally, the melanogenesis cluster-specific transcription factor VdCmr1 is not required for *V. dahliae* pathogenicity despite its involvement in the regulation of melanin biosynthesis-associated gene expression.

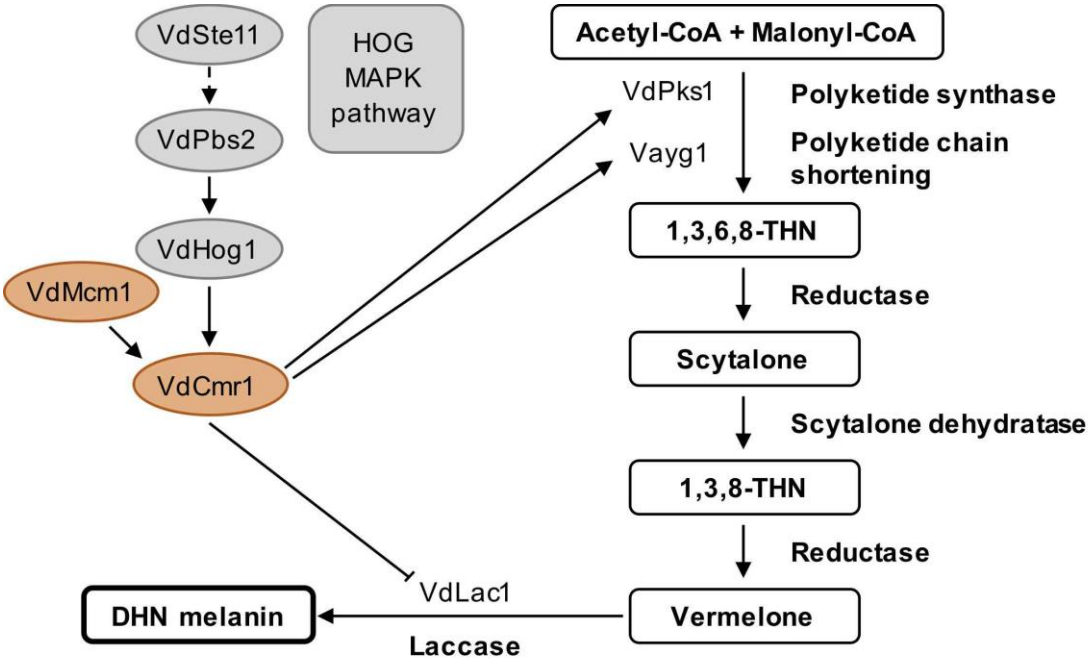

Figure 2. **DHN melanin biosynthesis in *V. dahliae* and involvement of transcription factor VdCmr1.**
DHN melanin biosynthesis pathway with key enzymes in *V. dahliae* is displayed (in bold) with details given in the text. Additionally, *V. dahliae* proteins are involved in melanin biosynthesis, which is connected to the high-osmolarity glycerol (HOG) mitogen-activated protein kinase (MAPK) pathway through VdCmr1. Further details are given in the text. This figure was modified from Y. Wang *et al* (2018).

VdCmr1 positively regulates expression of VdPks1 and Vayg1 and inhibits VdLac1 expression (Figure 2) (Wang *et al*, 2018a). VdCmr1 further controls the expression of a gene cluster encoding proteins involved in secondary metabolism and stress responses, which protects the fungus from high temperatures and UV irradiation (Fang *et al*, 2019). Here, the high osmolarity glycerol (HOG) mitogen-activated protein kinase (MAPK) cascade (Ste11-Pbs2-Hog1) and the MADS-box transcription factor VdMcm1 play key roles in VdCmr1 regulation (Figure 2) (Wang *et al*, 2018a).

The involvement of regulators and signal transduction pathways that translate external signals into responses such as the induction of the melanin and microsclerotia forming processes aid the fungus to initiate appropriate responses. Therefore, signaling mutant strains are impaired in melanin or microsclerotia production. Disruption of the *VdPKAC1* gene, which encodes the catalytic subunit of a cAMP-dependent kinase, resulted in elevated microsclerotia levels on several media, but showed less severe disease symptoms in tomato and eggplant (Tzima

et al, 2010a). Kinases of the MAPK pathways are essential for microsclerotia development and *V. dahliae* virulence such as Vmk1 (Rauyaree *et al*, 2005; Starke, 2019, Dissertation), VdMsb (Tian *et al*, 2014), VdPbs2 (Tian *et al*, 2016) and VdHog1 (Wang *et al*, 2016b). In addition, genes encoding transcriptional regulators with roles in microsclerotia development and *V. dahliae* pathogenicity have been characterized such as the mentioned MADS-box transcription factor VdMcm1 (Xiong *et al*, 2016), the calcineuron-dependent transcription factor VdCrz1 (Xiong *et al*, 2015), as well as, Vta2, Vta3 and Som1, which are transcriptional activators of adhesion and will be discussed further in the following chapter (Tran *et al*, 2014; Bui *et al*, 2019). Latter two regulate microsclerotia formation and expression of the hydrophobin protein Vdh1, which plays a key role in production of microsclerotia (Klimes & Dobinson, 2006; Tran *et al*, 2014; Bui *et al*, 2019).

Studies on microsclerotia deficient mutant strains revealed that concerning virulence, the major functions of the microsclerotia lie in resting in the soil for years and responding to the availability of an appropriate host plant. Regulatory processes controlling pathogenicity and developmental programs such as microsclerotia share common regulatory factors resulting in an intertwined complex network regulating gene expression.

1.2.2 Adhesion as first contact to the plant

Plant pathogenic fungi produce adhesive substances to enable attachment of the hyphae to the plant (Agrios, 2005b). This displays a crucial step of infection. Several studies revealed an association between adhesion and virulence. Pathogens forming appressoria such as *Colletotrichum gloeosporioides* and *M. oryzae* were reported to require CAP20 and the fasciclin-like protein MoFLP1, respectively, for adhesion and virulence (Hwang *et al*, 1995; Liu *et al*, 2009). Other proteins, e.g. the adhesins Mad1 and Mad2 were also shown to be directly required for these processes (Wang & St Leger, 2007).

In the yeast *Saccharomyces cerevisiae*, the flocculation (*FLO*) genes are essential for adhesion to surfaces and other cells (Braus *et al*, 2003; Fichtner *et al*, 2007; Brückner & Mösch, 2012). Among the *FLO* genes, *FLO11*, which encodes a hydrophobic cell wall protein, is involved in several processes such as surface adhesion, biofilm formation, filamentous agar invasion and cell-cell adhesion. It confers cell surface hydrophobicity and acts similar to fungal hydrophobins

(Brückner & Mösch, 2012). Regulation of *FLO11*-mediated adhesion is complex and involves cyclic AMP (cAMP)-dependent protein kinase A (PKA) and MAPK signal transduction pathways (Figure 3) (Rupp *et al*, 1999; Fichtner *et al*, 2007; Brückner & Mösch, 2012).

The 3 kb long promoter region of *FLO11* comprises activation and repression elements for several transcription factors (Brückner & Mösch, 2012). Besides other factors (reviewed in e.g. Brückner and Mösch, 2012), Flo8 and Ste12 play activating roles whereas Sfl1, named suppressor gene for flocculation, leads to repression of *FLO11* expression (Pan & Heitman, 2002; Brückner & Mösch, 2012; Fujita *et al*, 1989). The transcription factor Flo8 is activated through the cAMP-dependent PKA pathway by the PKA subunit Tpk2 and competes with the transcriptional repressor Sfl1 for the same binding site in the *FLO11* promoter. Sfl1, at the same time, is inhibited by Tpk2, which prevents it from binding (Rupp *et al*, 1999; Pan & Heitman, 2002; Brückner & Mösch, 2012).

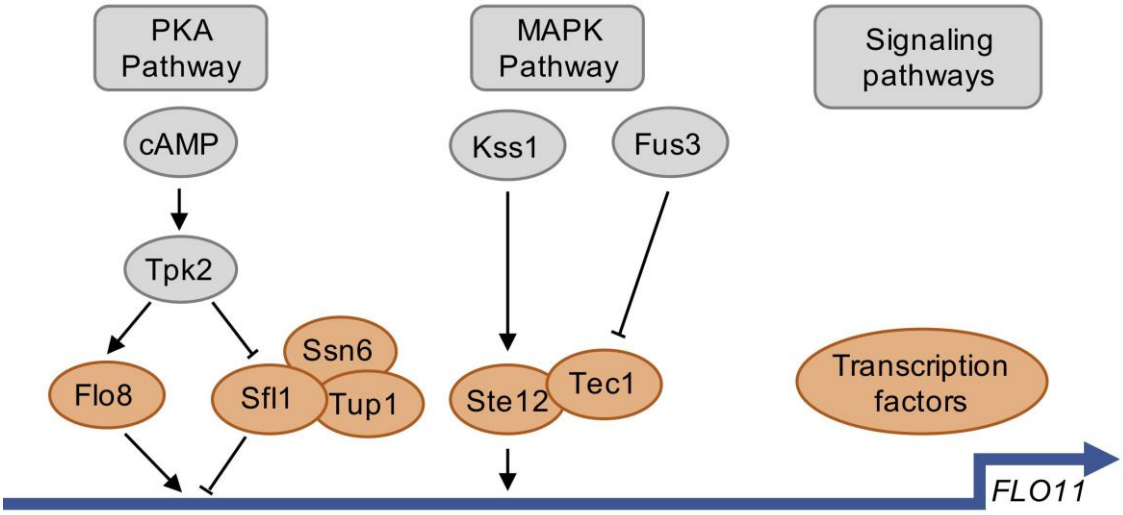

Figure 3. Regulation of *FLO11* expression by PKA and MAPK pathways in *S. cerevisiae*.
Expression of *FLO11* is required for adhesion in yeast. Flo8 is activated through the cyclic AMP (cAMP)-dependent protein kinase A (PKA) pathway via the PKA subunit Tpk2. When cAMP concentrations are low, Tpk2-mediated inhibition of Sfl1 terminates and Sfl1 together with the corepressor complex Ssn6-Tup1 binds to *FLO11* promoter to repress *FLO11* expression. Transcriptional activation and repression binding sites of Flo8 and Sfl1 are overlapping. Mitogen-activated protein kinases (MAPK) Kss1 or Fus3 regulate *FLO11* via the Ste12 and Tec1 complex. This figure was adapted from Brückner and Mösch (2012).

With low cAMP levels, Tpk2-mediated repression of Sfl1 is released and Sfl1 recruits the Ssn6-Tup1 corepressor complex to suppress *FLO11* transcription (Conlan & Tzamarias, 2001). The PKA-mediated *FLO11* activation may be part of a quorum sensing mechanism connecting environmental sensing and adhesion (Brückner & Mösch, 2012).

Further, the Kss1 MAPK pathway is involved in sensing nutritional signals and initiating cell-surface adhesion by activating *FLO11* expression. Upon phosphorylation, the MAPK Kss1 activates transcription factor Tec1, which, on its own or in a complex with Ste12, binds to the *FLO11* promoter and activates *FLO11* transcription (Brückner & Mösch, 2012). An additional MAPK Fus3, which is involved in the mating pathway, interferes with *FLO11* expression. Fus3 phosphorylates Tec1, which leads to its degradation (Brückner & Mösch, 2012). Additionally to the role as flocculation repressor, Sfl1 acts as an activator of stress-responsive genes in yeast providing a link between adhesion and stress responses (Ansanay Galeote *et al*, 2007).

In the vascular wilt pathogen *V. dahliae*, studies on homologous genes show that these pathways are involved in pathogenicity and for some proteins the association to adherence was shown. The transcription factor Som1, which is encoded by a *FLO8* homolog additionally plays key roles in *V. dahliae* adhesion and penetration (Bui *et al*, 2019). The PKA subunit *VdPKAC1* controls virulence (Tzima *et al*, 2010a). Deletion of *VdCYC8* (*SSN6*), coding for a glucose repression mediator protein, resulted in reduction of pathogenicity (Li *et al*, 2015). The *FUS3* homolog *VMK1* was deleted in different *V. dahliae* isolates. Deletion strains were severely impaired in infection of their host (Rauyaree *et al*, 2005; Starke, 2019, Dissertation). Deletion strains of the *STE12* homolog, *VPH1*, failed to form hyphopodia and penetrate the root surface or cellophane paper and were not able to infect plants (Sarmiento-Villamil *et al*, 2018b). All mentioned *V. dahliae* deletion strains were additionally impaired in regulation of developmental structures such as microsclerotia. The deletion mutants exhibited a decrease in microsclerotia formation except for the *VdPKAC1* deletion strain, which resulted in enhanced microsclerotia production (Tzima *et al*, 2010a; Bui *et al*, 2019; Li *et al*, 2015; Rauyaree *et al*, 2005; Sarmiento-Villamil *et al*, 2018b).

An approach using a *S. cerevisiae* strain lacking *FLO8* was used to screen for adhesion genes from *V. longisporum*. The yeast strain was unable to express

FLO11 and consequently lost the ability to adhere to surfaces. Twenty-two genes were identified that reprogrammed the non-adhering mutant to adhesion including putative transcription regulators named *Verticillium* transcription activator of adhesion Vta1-6 (Tran *et al*, 2014). Vta2 has a suppressing role on microsclerotia production but is required for conidia and disease symptom induction (Tran *et al*, 2014). Vta3 is encoded by a homolog of the yeast *RFX1*/*CRT1*, which is associated with the recruitment of the co-repressor Ssn6-Tup1 complex. Deletion of *VTA3* resulted in reduced conidia and microsclerotia formation and impaired colonization of plants (Bui *et al*, 2019). Furthermore, data indicate that the *FLO8* homolog coding for Som1 regulates expression of *VTA* genes such as *VTA2* and *VTA3*. Vta3 positively regulates *SFL1* expression in *V. dahliae* (Bui *et al*, 2019). Som1, Vta2 and Vta3 additionally regulate expression of genes encoding putative adhesin-like cell wall proteins (Tran *et al*, 2014; Bui *et al*, 2019).

V. dahliae adhesion to roots is necessary for successful plant colonization (Zhao *et al*, 2016; Bui *et al*, 2019). Hyphopodia enable *Verticillium* spp. to adhere to the plant surface. The tetrapspanin VdPls1 and the catalytic subunit of membrane-bound NADPH oxidase VdNoxB were reported to be essential for mature hyphopodia formation (Zhao *et al*, 2016). It was suggested that VdPls1 is required to recruit and activate VdNoxB. Following ROS production leads to Ca^{2+} accumulation at the hyphal tip, which activates calcineuron-VdCrz1 signaling (Zhao *et al*, 2016). VdCrz1 is important for virulence, more precisely the penetration peg formation on cotton roots (Xiong *et al*, 2015; Zhao *et al*, 2016).

Collectively, these data provide evidence of a possible connection between the adhesion associated pathways and the regulation of pathogenicity. Whether this link solely is a consequence of the impairment of adherence or other involved developmental regulations remains to be elucidated. Nevertheless, these pathways represent potential targets for the control of *Verticillium*.

1.2.3 Conidia as colonization tool

Verticillium spp. propagate by asexual conidiation and the formation of microsclerotia whereas a sexual cycle has not yet been observed (Klosterman *et al*, 2009; Inderbitzin *et al*, 2011a). The conidia are sensitive and easily killed by short exposure to drought or high temperatures and only survive in liquid cultures for about 3 weeks at room temperature (Schnathorst, 1981). Therefore, conidia do

not play a big role in the spread of the disease on the field compared to the long-lived microsclerotia. However, conidia are of great importance during colonization of the plant. Once the fungus reaches the xylem, it suppresses mycelia production and switches to a rapid spore budding growth (Schnathorst, 1981; Pegg & Brady, 2002). Spores are passively dispersed throughout the whole plant with the xylem stream. When trapped at the end of a vessel, conidia can germinate to enter the adjacent vessel where sporulation continues (Schnathorst, 1981; Sewell & Wilson, 1964).

Proper regulation of conidia formation is beneficial for *Verticillium* pathogenicity. The fungus is more virulent if it is able to reproduce quickly by conidiation in the xylem (Schnathorst, 1963; Fradin & Thomma, 2006). This proposition is confirmed by several studies with deletion strains that are impaired in conidia production. These strains also exhibited reduced colonization of the host. For *Verticillium* transcription factors such as Vta2, Vta3 and Som1 expression levels of conidiation associated genes such as *CON8* and *ABA1* were reduced in corresponding single deletion strains (Tran *et al*, 2014; Bui *et al*, 2019). Consequently, reduced conidiation coincided with the inability of the single deletion mutants to colonize tomato plants (Tran *et al*, 2014; Bui *et al*, 2019).

1.3 Fungal responses to the environment

Fungi require sensing and adapting mechanisms throughout their life cycle. Different environmental cues induce different secretion responses enabling the pathogen to react to changes in e.g. nutrient supply or host defense responses (McCotter *et al*, 2016; Agrios, 2005b).

1.3.1 Fungal responses to amino acid imbalances

Verticillium spp., as mentioned in 1.2.1, form melanized resting structures whenever nutrients are unavailable or no host plant is present. However, the fungus spends most of its life time in the xylem of its host plant where it exploits the vascular system to colonize the whole plant (Eynck *et al*, 2007; Singh *et al*, 2010). The plant requires the xylem stream primarily to transport water and soluble minerals from the soil to upper parts of the plant (de Boer & Volkov, 2003). It as well contains plant defense proteins, hormones and low concentrations of amino acids and sugars (Singh *et al*, 2010; Carella *et al*, 2016). Due to this low and

imbalanced nutrient supply, xylem sap displays a very unique environment for fungal growth.

Although fungi are prototroph for amino acids, they preferably acquire amino acids from their environment by uptake systems (Braus *et al*, 2004; Singh *et al*, 2010). The fungus can sense the nutrient supply and change its own cellular biosynthesis accordingly (Singh *et al*, 2010). Studies on *V. longisporum* addressed the question whether the fungus depends on its own amino acid biosynthesis during growth in xylem sap of its host *B. napus* where amino acids are scarce. Growth of *V. longisporum* in the xylem sap depends on the chorismate synthase encoding gene *VlARO2*. This is required for the production of aromatic acids and for expression of the cross-pathway transcription factor *CPC1* for the initiation of the cross-pathway control (Singh *et al*, 2010; Timpner *et al*, 2013). This pathway is induced by fungi to increase biosynthesis of amino acids if the basal biosynthesis is not sufficient for cellular translation (Timpner *et al*, 2013; Carsiotis & Jones, 1974; Carsiotis *et al*, 1974). *CPC1* was additionally associated with control of secondary metabolism and is therefore required for crosstalk with the plant (Timpner *et al*, 2013). Knockdowns of the mentioned genes consequently resulted in decreased *V. longisporum* pathogenicity (Singh *et al*, 2010; Timpner *et al*, 2013). These data indicate that *Verticillium* spp. are able to sense the nutrient-low environment and have means to adapt accordingly.

1.3.2 Fungal responses to plants

As mentioned, xylem sap as well contains plant defense proteins as part of the immune system (Singh *et al*, 2010; Carella *et al*, 2016). Cultivation of *V. longisporum* in the presence of xylem sap leads to the upregulation of six proteins with functions in oxidative stress response. One of these proteins was a catalase peroxidase encoded by *VlCPEA*. This protein is essential for response to oxidative stress and full *V. longisporum* virulence (Singh *et al*, 2012). These findings indicate that *V. longisporum* induces the expression of enzymes that function in protection of the fungus from the oxidative stress response of the plant. During plant colonization the fungus is exposed to several plant responses. To overcome the plant immune response and establish a successful infection, it responds to the host by effector secretion (McCotter *et al*, 2016). These back and

forth reactions have been characterized as arms race between the host and pathogen (Jones & Dangl, 2006).

The first line of plant defense provides basal defense against all pathogens and depends on pattern recognition receptors representing transmembrane receptor proteins. These are localized at cell surfaces and recognize conserved microbial molecules and structural motifs summarized as pathogen-associated molecular patterns (PAMPs) or microbe-associated molecular patterns (MAMPs) (Figure 4a) (Rovenich *et al*, 2014). An example for a PAMP is the fungal cell-wall polymer chitin (Sorrell & Chen, 2009). Upon recognition of PAMPs or MAMPs, the plant initiates the PAMP-triggered immunity (PTI) (Figure 4b) such as the production of reactive oxygen species (ROS) or the secretion of chitinases (Figure 4c). Host-adapted pathogens circumvent this response by secretion of specific effector proteins as virulence factors for different phases of the infection cycle to avoid recognition by the plant or fend off the defense responses (Figure 4, inhibitory arrows) (Dodds & Rathjen, 2010). Such effectors are, for example, Avr4 and Ecp6 from the leaf mold fungus *Cladosporum fulvum* that inhibit plant chitinases by binding chitin to prevent elicitation of PTI (van Esse *et al*, 2007; de Jonge *et al*, 2010). Nep1-like proteins (Necrosis and ethylene inducing protein-like proteins, NLP) induce immune responses and cell death in their host tissues and were found to be conserved among fungi including *Verticillium* spp. (Gijzen & Nürnberger, 2006; Santhanam *et al*, 2013). The best characterized *V. dahliae* effector is Ave1, which acts as a virulence factor in tomato and *Arabidopsis* plants that lack the Ve1 resistance protein (de Jonge *et al*, 2012).

As plants evolve to encode different immune receptors that recognize novel fungal effectors, this evolutionary arms race puts effector genes under selection pressure (de Jonge *et al*, 2011). Fungi often comprise effector genes in dynamic and repeat-rich genome regions enabling faster diversification of the effector repertoire (Dong *et al*, 2015; Möller & Stukenbrock, 2017). *V. dahliae* as well evolves under such a two-speed regime to accelerate effector evolution (de Jonge *et al*, 2013; Faino *et al*, 2016). However, these repeat-rich lineage specific regions in *V. dahliae* are conserved among other *Verticillium* species. Therefore, it was suggested that *V. dahliae* preferably promotes effector evolution by presence or absence polymorphism rather than nucleotide substitution events as reported for other fungi (Depotter *et al*, 2019).

This evolving effector repertoire represents yet another challenge in the control of Verticillium wilt. As *Verticillium* spp. colonize the vascular system of their hosts, further insights into the processes of specific secretion could lead to new control strategies.

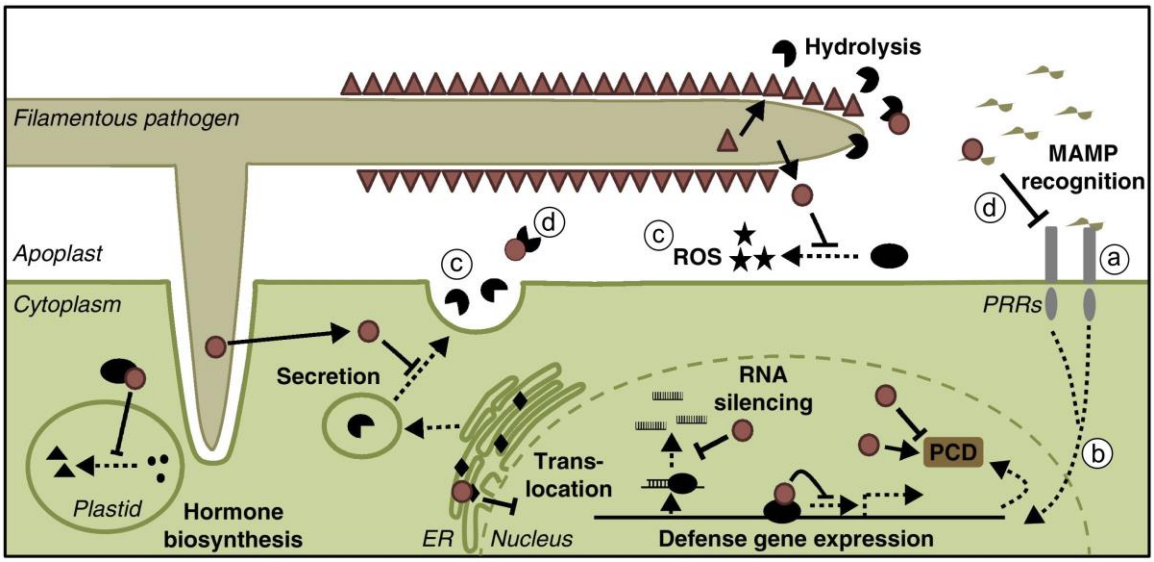

Figure 4. Cross-talk during host-pathogen interaction.
Upon perception of a pathogen plants initiate defense responses (a, b, c, black shapes), which the pathogen combats by secreting effectors. Effectors aid the fungus by shielding hyphae against hydrolytic enzymes of the host (red triangles). Other effectors inactivate these enzymes or inhibit other plant immunity processes (red circles, d). More details are given in the text. MAMP = Microbe-associated molecular pattern, PRR = pattern recognition receptor, PCD = programmed cell death, ROS = reactive oxygen species, ER = endoplasmic reticulum. This model was modified from (Rovenich *et al*, 2014).

1.3.3 Fungal responses to light

For a soil-borne pathogen light sensing provides another external cue for the adaptation to a different environment. Underground the fungus relies primarily on the perception of nutrients in order to migrate towards roots of host plants. Once inside the plant, light serves as additional external factor for the fungus. Light is conducted in plant tissues and even transmitted to the roots, however, only with a linear attenuation (Beattie *et al*, 2018; Sun *et al*, 2005). If plant pathogens were able to sense and differentiate light quality and intensity, it would provide them yet another system to regulate development and growth direction accordingly.

As a matter of fact, light responsive elements for the perception of different wavelengths are found in pathogens across the fungal kingdom (Yu & Fischer,

2019; Salichos & Rokas, 2010) indicating that light sensing may be conserved. The main blue-light receptors, White Collar-1 (WC-1) and White Collar-2 (WC-2) were reported to exist in most filamentous fungi whereas the presence of other light responsive elements differs. Other photoreceptors include cryptochromes that sense UV- and blue-light, opsins for green-light detection, phytochromes for red-light and VIVIDs as additional blue-light receptors (Hevia *et al*, 2016).

The nonpathogenic *Neurospora crassa* has been exploited as the ultimate model for light regulation. Different light-depended processes in this fungus were observed and include the carotenoid biosynthesis, conidiation, protoperithecia production and the circadian clock (Rodriguez-Romero *et al*, 2010). The characteristics of a circadian clock include free-running oscillations that persist in the absence of environmental inputs and the entrainment of the cycle by temperature or light cycles (Hevia *et al*, 2016). Extensive studies on *N. crassa* followed to dissect the components involved in the circadian rhythm revealing a complex network including a transcriptional translational negative feedback loop (Figure 5). FREQUENCY (FRQ), also called the circadian oscillator, is the main central component. By night, transcript levels of the *frq* gene coding for the circadian oscillator are low. The blue-light receptors WC-1 and WC-2 together form the white collar complex (WCC) and act as transcription factors. The WCC activates *frq* transcription by binding to the Clock box in the *frq* promoter (Dunlap & Loros, 2006, 2017; Montenegro-Montero *et al*, 2015). FRQ protein is produced in the early morning and as homodimer binds to the FRQ-interacting RNA helicase (FRH). This protein complex named FFC can enter the nucleus (Dunlap & Loros, 2006; Cheng *et al*, 2001). FFC recruits the casein kinases CK1 and CK2 to promote phosphorylation of the WCC and FRQ (Montenegro-Montero *et al*, 2015; Baker *et al*, 2012; Yu & Fischer, 2019). The WCC becomes inactivated, loses its affinity to the clock box promoter region and is released. This way, FRQ acts as negative regulator of its own transcription. As FRQ becomes hyperphosphorylated, its interaction with WCC is inhibited (Schafmeier *et al*, 2006; He *et al*, 2006; Cha *et al*, 2011). Specific amino acid groups of FRQ are additionally phosphorylated, which mark the protein for recognition by the SCF (Skp1-Cul1-F-box-protein)-type ubiquitin ligase FWD-1.

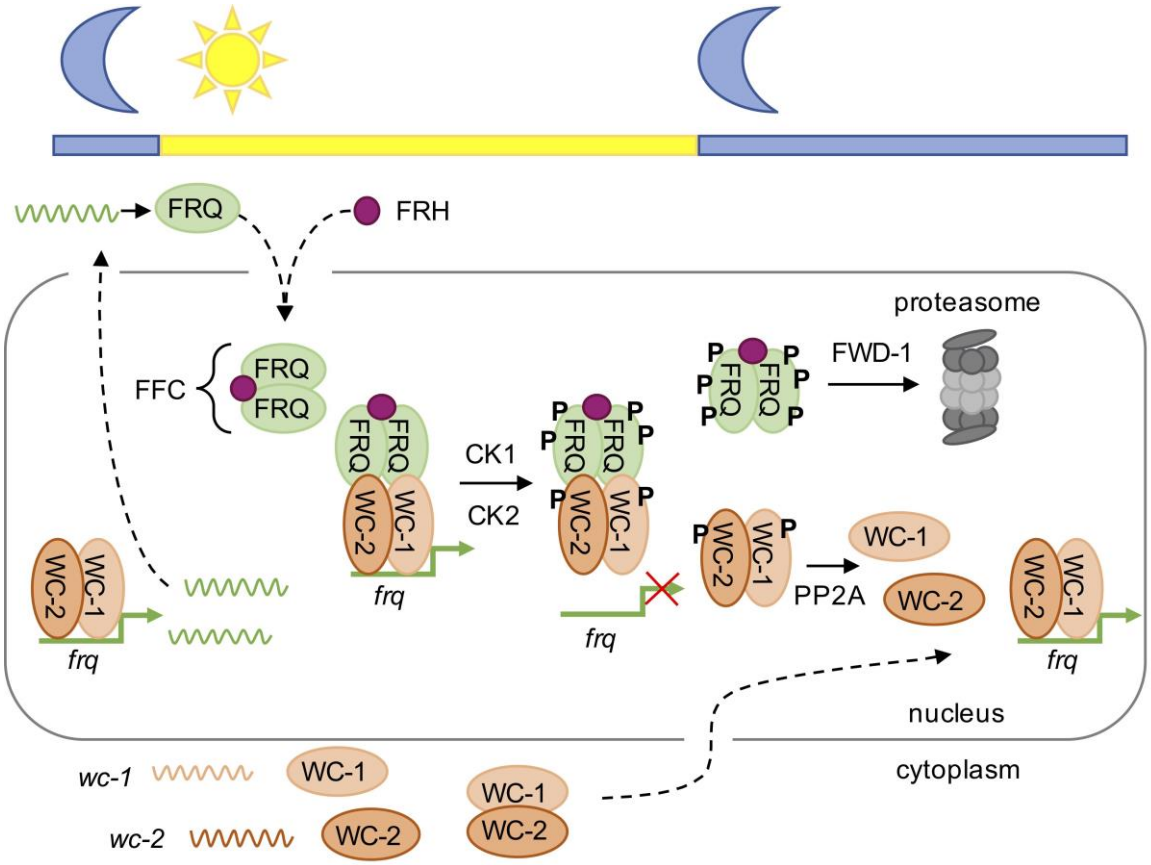

Figure 5. Model of circadian rhythm in *Neurospora crassa*.
Sequential molecular actions of the *N. crassa* circadian oscillations are displayed as function of time. Details are given in the text. Sun and moon indicate day and night, respectively. 'P' indicates phosphorylation of a protein. FRQ = Frequency, FRH = Frq interacting RNA helicase, FFC = FRQ-FRH complex; WC-1/2 = White collar-1/2; CK1/2 = casein kinases; FWD-1 = ubiquitin ligase, PP2A = phosphatase. This image was modified from Dunlap and Loros (2017).

This leads to FRQ ubiquitination and subsequent degradation by the proteasome (He *et al*, 2003; Dunlap & Loros, 2017). Dephosphorylation of WC-1 and WC-2 by the phosphatase PP2A and *de novo* synthesis lead to new accumulation of WCC to reinitiate the cycle (Dunlap & Loros, 2017; Yu & Fischer, 2019).

Additional to this free-running circadian rhythm, light input activates *frq* expression through WC-1. WC-1 absorbs blue-light and directly activates the expression of light responsive genes including *frq* (Crosthwaite *et al*, 1995). In this situation, WC-1 binds to the proximal light regulatory element in the *frq* promoter close to the transcription start site, which leads to a faster accumulation of FRQ protein compared to the circadian driven synthesis (Froehlich *et al*, 2002).

As plants evolved to regulate their defense reactions according to their own circadian clock (Roden & Ingle, 2009; Liversage *et al*, 2018), it is beneficial for plant

pathogens to anticipate the downregulation of the plant immune system and time the infection process accordingly. The infection success of the plant pathogen *Botrytis cinerea* depends on a functional circadian clock and the day time of initial infection (Hevia *et al*, 2015, 2016). The fungus did not show an obvious phenotypical circadian behavior under constant conditions (Canessa *et al*, 2013), however, *bcfrq1* transcript and BcFRQ1 protein levels oscillate and therefore provide evidence for a functional circadian clock in *B. cinerea* (Hevia *et al*, 2015). Besides the role in circadian rhythm during infection, BcFRQ1 has additional non-circadian functions in sexual/asexual reproduction (Hevia *et al*, 2015). This is a major difference to the roles of FRQ in *N. crassa* where no circadian-independent altered phenotype was assigned to FRQ (Hevia *et al*, 2015; Aronson *et al*, 1994). This represents only one disparity in the light regulation between these fungi indicating that the way light is perceived and signals are forwarded may vary among different pathogens, especially between fungi with different life styles.

Light perception is connected to other pathways, which provides a mechanism to transduce an external signal to the cell and control a whole set of genes at once. This allows the fungus to differentially regulate biological processes under and above ground. In *Aspergillus nidulans* the HOG MAPK pathway has been linked to light signal transduction. The red-light absorbing phytochrome FphA is proposed to be involved as it has a histidine kinase domain that is likely to phosphorylate other proteins. In response to light it may activate the cascade leading to phosphorylation of the MAPK SakA. It, as well, interacts with the WCC that activates *frq* transcription (Pöggeler *et al*, 2018; Yu & Fischer, 2019; Schumacher, 2017). Studies on *B. cinerea* detected light- and stress-depending increased transcript and phosphorylation levels of the MAPK BcSAK1 supporting the connection between the HOG MAPK pathway and light regulation (Schumacher, 2017).

Furthermore, PKA was implicated in regulation of *frq* trancription (Yu & Fischer, 2019; Liu *et al*, 2015). PKA phosphorylates RCM-1, which interacts with RCO-1. RCO-1 and RCM-1 are encoded by homologs of the co-repressor complex Ssn6-Tup1 in yeast. Phosphorylation of RCM-1 leads to the release of the complex, and therefore the inhibition of *frq* repression. (Yu & Fischer, 2019; Liu *et al*, 2015). These data indicate a WC-independent *frq* transcriptional control by PKA and further present a connection to the pathways involved in adhesion (1.2.2).

Most of the circadian clock components (FRQ, WC-1, WC-2, FRH, FWD-1) are conserved among different fungal classes except FRQ, which is mainly restricted to the Sordariamycetes including *V. dahliae* (Salichos & Rokas, 2010). For *Verticillium* spp. no circadian rhythm was observed so far, however, it possesses the required elements, which prompts the question what functions they fulfill.

1.4 Aim of this study

The haploid *V. dahliae* and the allodiploid *V. longisporum* produce highly melanized resting structures called microsclerotia when nutrients are scarce. As they can survive for a long time without any host, they display persistent infectious propagules. Microsclerotia germinate upon sensing root exudates (Wilhelm, 1955). The hyphae migrate towards the plant. To establish an infection, it needs to adhere to the roots and penetrate it. The formation of these microsclerotia additionally depends on other external factors such as light. To control different developmental steps, the fungus requires regulators that translate external factors into appropriate responses.

This study addressed the role of two regulators, the homolog of yeast suppressor of flocculation *SFL1* and the circadian oscillator *FREQUENCY* (*FRQ*). In yeast, *SFL1* has roles in activation and repression of different processes such as adhesion and stress responses (Conlan & Tzamarias, 2001; Ansanay Galeote *et al*, 2007). In *V. dahliae*, *SFL1* expression is regulated by Vta3, a *Verticillium* transcription activator of adhesion (Bui *et al*, 2019). Vta3 was reported to be important for fungal root colonization, infection as well as conidia and microsclerotia formation (Bui *et al*, 2019). In this work, the role of Sfl1 in fungal development and virulence was dissected. Adhesion to the root surface, microsclerotia production and overall pathogenicity on tomato were analyzed with the *SFL1* deletion strain to shed a light on the function of Sfl1. Further, the regulation of development by light was investigated with the *FRQ* deletion strain. *Verticillium* spp. possess important elements for light regulation and the circadian rhythm (Salichos & Rokas, 2010), yet, none of the involved proteins have been characterized thus far. Therefore, *FRQ*, the central component of the circadian clock, was deleted in frame of this work to reveal first insights into light-regulated processes in *V. dahliae*. Adhesion and light-regulated pathways may be connected by other signaling cascades that orchestrate external inputs to appropriate

responses. Experiments with a double deletion mutant of *SFL1* and *FRQ* allowed further investigations of a possible link between these pathways. Signaling cascades are as well required to aid the fungus in sensing of different infection steps to secrete different effectors.

How the fungus changes its secretome according to different environments was assessed in this study. *V. longisporum* secreted proteins derived from cultivation in different growth media were identified by a proteomic approach and the protein patterns induced by different environments were compared. Our goal was to obtain a more comprehensive overview of the secreted factors of *Verticillium* and identify potential effector proteins specific for interaction with the host. We analyzed the exoproteomes of *V. longisporum* on a broad range of media from water to minimal and complete media. Additionally, simulated xylem medium was used as this pectin-rich medium was developed to mimic the infection environment in the plant (Neumann & Dobinson, 2003). All exoproteomes were compared to the exoproteomes of fungal cultures grown in extracted xylem sap of the oilseed rape *B. napus*. The xylem sap-specific proteome was further examined and potential effector candidates were analyzed in the haploid *V. dahliae*. These included the carbohydrate-active enzymes Gla1 (glucoamylase), Cbd1 (putative polysaccharide mono-oxygenase) and Amy1 (α-amylase), the metallopeptidases Mep1 and Mep2, cerato-platanin proteins Cp1 and Cp2 and necrosis and ethylene inducing-like proteins Nlp2 and Nlp3. Single or double deletions were generated to investigate on their impact in *V. dahliae* pathogenicity on tomato.

2 Materials and Methods

2.1 Material and Chemicals

Media for strain cultivation, buffers and other solutions were prepared with products from APPLICHEM GMBH (Darmstadt, Germany), BD BIOSCIENCES (Heidelberg, Germany), BIOZYM SCIENTIFIC GMBH (Hessisch Oldendorf, Germany), CARL ROTH GMBH & CO. KG (Karlsruhe, Germany), FLUKA (Neu-Ulm, Germany), INVITROGEN (Carlsbad, CA, USA), MERCK KGAA (Darmstadt, Germany), OXOID DEUTSCHLAND GMBH (Wesel, Germany), ROCHE DIAGNOSTICS GMBH (Mannheim, Germany), SERVA ELECTROPHORESIS GMBH (Heidelberg, Germany), SIGMA-ALDRICH (Munich, Germany), TH. GEYER GMBH & CO. KG (Renningen, Germany), THERMO FISHER SCIENTIFIC (Schwerte, Germany) and VWR INTERNATIONAL GMBH (Darmstadt, Germany).

For pH determination a WTW bench pH/mV Routine meter pH 526 from SIGMA-ALDRICH was used. Ampicillin purchased from CARL ROTH GMBH & CO. KG, cefotaxime from WAKO CHEMICALS GMBH (Neuss, Germany), chloramphenicol from APPLICHEM GMBH, clonNAT (nourseothricin dihydrogen sulfate) from WERNER BIOAGENTS GMBH (Jena, Germany), hygromycin B from INVIVOGEN (San Diego, CA, USA) and kanamycin from APPLICHEM GMBH were used for the selection of microorganisms.

Polymerases, restriction enzymes and corresponding buffers were obtained from NEW ENGLAND BIOLABS (NEB, Frankfurt am Main, Germany), or THERMO FISHER SCIENTIFIC. Primers were obtained from EUROFINS GENOMICS GMBH (Ebersberg, Germany) or SIGMA-ALDRICH. Polymerase chain reactions (PCRs) were performed in T Professional Standard 96, T Professional Trio 48, and T Professional Standard 96 Gradient thermocyclers from BIOMETRA GMBH (Göttingen, Germany) and in Primus 96 Thermal Cyclers from MWG BIOTECH AG (Ebersberg, Germany). The GeneRuler 1 kb DNA ladder and the PageRuler™ Prestained Protein Ladder (THERMO FISHER SCIENTIFIC) were used for DNA and protein *on-gel* band size determination. DNA was purified with the NucleoSpin Plasmid Kit/NucleoSpin Gel and PCR clean up Kit from MACHEREY-NAGEL GMBH & CO. KG (Düren, Germany) or the QIAprep® Spin Miniprep Kit/QIAquick® Gel Extraction Kit from QIAGEN (Hilden, Germany). RNA was extracted with the Direct-zol™ RNA MiniPrep Kit from

ZYMO RESEARCH (Freiburg im Breisgau, Germany). Concentrations of DNA and RNA samples were measured with the Nanodrop™ ND-1000 spectrophotometer from PEQLAB BIOTECHNOLOGIE GMBH (Erlangen, Germany). Protein concentrations were measured with an Infinite M200 microplate reader operated with Magellan software from TECAN TRADING AG (Männedorf, Switzerland). The Savant SPD 111V SpeedVac Concentrator (THERMO FISHER SCIENTIFIC) was used to concentrate samples. Agarose gel electrophoresis was performed with Mini-Sub® Cell GT chambers and SDS-polyacrylamide gel electrophoresis was performed with the Mini-Protean® Tetra Cell and Mini Trans-Blot® Electrophoretic Cell with the PowerPac™ 3000 power supply from BIO-RAD LABORATORIES GMBH. DNA was transferred from agarose gels onto Amersham™ Hybond-N™ nylon membranes and proteins were blotted from SDS-polyacrylamide gels onto Amersham™ Protran™ 0.45 µm NC nitrocellulose blotting membranes from GE HEALTHCARE (Little Chalfont, United Kingdom). For Southern hybridization analysis the Amersham™ AlkPhos Direct™ Labeling and Detection System from GE HEALTHCARE was used. Chemiluminescence of Southern and Western hybridization was detected by developing the Amersham™ Hyperfilm™-ECL (GE HEALTHCARE) with the use of the Optimax® X-ray Film Processor from PROTEC GMBH & CO. KG (Oberstenfeld, Germany). As primary antibody α-GFP antibody sc-9996 was purchased from SANTA CRUZ BIOTECHNOLOGY (Dallas, TX, USA). As secondary antibody horseradish peroxidase-coupled α-mouse antibody 115-035-003 from JACKSON IMMUNORESEARCH (West Grove, PA, USA) was used. For fluorescence microscopy the µ-Slide 8 well microscopy chambers from IBIDI GMBH (Martinsried, Germany) were used for localization studies and nuclei were visualized with 4′,6-Diamidin-2-phenylindol (DAPI) from CARL ROTH GMBH & CO. KG.

Plastic and other consumables such as pipet tips, petri dishes, reaction tubes etc. were purchased from EPPENDORF AG (Hamburg, Germany), NERBE PLUS GMBH (Winsen/Luhe, Germany), SARSTEDT AG & CO. KG (Nümbrecht, Germany), SARTORIUS (Göttingen, Germany) and STARLAB GMBH (Hamburg, Germany). Centrifugation of 1.5 and 2 ml reaction tubes was performed with Heraeus™ Biofuge Fresco (refrigerated) and Pico™ Microcentrifuges from HERAEUS INSTRUMENTS GMBH (Hanau, Germany). For centrifugation of 15 and 50 ml

centrifuge tubes Centrifuge 5804R from EPPENDORF AG was used. For bigger volumes the SorvallRC-3B Plus Refrigerated Centrifuge and Sorvall RC-5B Plus Refrigerated Centrifuge from THERMO FISHER SCIENTIFIC were used. The Shaking Water Bath 1086, the Orbital shaker 3005 and 3020 from GFL (Burgwedel, Germany), Rotamax 120 from HEIDOLPH INSTRUMENTS GMBH & CO. KG (Schwabach, Germany) and the rotator Infors HT AG15 from INFORS AG (Bottmingen, Switzerland) were used for incubations.

Planting pots (70x70x80 mm) from SOPARCO GMBH (Saarbrücken, Germany), Fruhstorfer Erde Typ T Struktur 1 (fein) from ARCHUT GMBH & CO. KG (Lauterbach, Germany) and 0.4-0.8 mm crystal silica sand from DORSILIT (Hirschau, Germany) were purchased. As phyto chamber the BrightBoy GroBank from CLF PLANTCLIMATICS (Emersacker, Germany) was used. Photographs and photomicrographs were obtained with the following devices: Perfection V600 Photo Scanner from EPSON (Suwa, Japan), the binocular microscope SZX12-ILLB2-200 from OLYMPUS GMBH (Hamburg, Germany) with illumination of the KL1500-LCD light source (OLYMPUS GMBH) and the Axiolab light microscope from ZEISS (Oberkochen, Germany). Fluorescence microscopy was performed with the AxioObserver Z1 inverted confocal microscope equipped with Plan-Neofluar 63x/0.75 (air) objective (ZEISS).

Materials and instrumentations, which were not listed here, are indicated in the following chapters.

2.2 Media and growth conditions

All liquid and solid media used in this study were dissolved in deionized H_2O and sterilized by autoclaving at 120°C for 20 min at 2 bar. Heat-sensitive compounds were filter-sterilized with a 0.2 µm pore size syringe filter and added to the medium after autoclaving.

2.2.1 Cultivation of bacteria

Escherichia coli and *Agrobacterium tumefaciens* were cultivated in liquid lysogeny broth (LB) (Bertani, 1951) [1% (w/v) tryptone/peptone from casein, 0.5% (w/v) yeast extract, 1% (w/v) NaCl] on a rotary shaker at 37°C for *E. coli* and 25°C for *A. tumefaciens*. For solid media 2% (w/v) agar (CARL ROTH GMBH & CO. KG) was added to the medium before autoclaving. Selection was performed by

supplementing the media with 100 µg/ml ampicillin or kanamycin. Bacteria were conserved in a final concentration of 50% glycerol and stored at -80°C.

2.2.2 Cultivation of *Verticillium* strains

2.2.2.1 Cultivation of *Verticillium dahliae*

In general, *V. dahliae* strains were cultivated in liquid simulated xylem medium (SXM), which was prepared as described by Hollensteiner *et al* (2017), for conidiospore formation and in liquid potato dextrose medium (PDM) [2.65% (w/v) Potato Dextrose broth (CARL ROTH GMBH & CO. KG)] for mycelial growth. Cultures were incubated at 25°C under constant agitation at 115 – 125 rpm.

Conidia were filtered with Miracloth from CALBIOCHEM MERCK (Darmstadt, Germany), washed twice with sterile water and resuspended in sterile water. Spore concentrations of *V. dahliae* strains (spore size of 1.9-4.5 µm) were determined with the Beckman Coulter Z2 Cell and Particle Counter and Coulter Isoton II Diluent from BECKMAN COULTER GMBH (Krefeld, Germany). *V. dahliae* strains were conserved by resuspending freshly harvested spores in a sodium-tween solution (0.5% NaCl, 0.01% Tween 80) at a concentration of $2x10^7$ spores/ml mixed with an equal volume of 50% glycerol. The glycerol stocks were kept at -80°C. Mycelium was harvested from PDM cultures for genomic DNA or protein extraction and from SXM cultures for extraction of RNA.

Selection of *Verticillium* transformants was performed on solid PDM [3.9% (w/v) Potato Dextrose agar (CARL ROTH GMBH & CO. KG), 0.5% (w/v) agar] supplemented with antimycotics clonNAT nourseothricin dihydrogen sulfate (72 µg/ml) or hygromycin B (50 µg/ml) and the antibiotic cefotaxime (300 µg/ml) after autoclaving.

2.2.2.2 Cultivation of *Verticillium longisporum*

For the exoproteome comparison, *V. longisporum* 43 (*Vl*43) was inoculated with $1x10^6$ spores/ml in 150 ml liquid PDM at constant agitation. After 4 days, each culture was centrifuged and the mycelium/spore sediment was resuspended in 150 ml extracted xylem sap of *B. napus*, SXM, CDM supplemented with 7% extracted xylem sap or plant proteins, H_2O and H_2O supplemented with 0.1% glucose, YNB [yeast nitrogen base: 1.5 g/l YNB, 5 g/L $(NH_4)_2SO_4$, 20 g/l glucose,

ad 1 l H_2O] and vegetable juice (V8 from CAMPBELL SOUP COMPANY, Camden, NJ, USA). After an additional incubation period of 4 days, proteins of the supernatant were precipitated with TCA/acetone.

2.2.2.3 Xylem sap extraction from *Brassica napus*

B. napus seeds were surface sterilized with 70% ethanol and sown on sand. Plants were grown on long-day condition (16h light: 8h dark) at 22°C. Seven-day-old seedlings were transferred into soil-sand (1:1) and grown for 42 days. For xylem sap extraction plants were cut at the height of the first internode and xylem sap was collected. The xylem sap was filtered through Vivaspin 15R columns (SARTORIUS) and directly used as medium for inoculation.

2.3 Nucleic acid methods

2.3.1 Purification of nucleic acids

2.3.1.1 Isolation of plasmid DNA from *Escherichia coli*

E. coli strains carrying the plasmid of interest were grown overnight at 37°C under constant agitation in liquid LB supplemented with the appropriate antibiotic for selection. For extraction of plasmid DNA the QIAprep® Spin Miniprep Kit (QIAGEN) or the NucleoSpin® Plasmid Kit (MACHEREY-NAGEL) were used according to the manufacturer's instructions. Plasmid DNA was eluted from spin columns with dH_2O.

2.3.1.2 Isolation of *V. dahliae* genomic DNA

V. dahliae was grown in liquid PDM cultures for at least three days at 25°C under constant agitation. For isolation of genomic DNA (gDNA) the method modified from Kolar *et al* (1988) was used. Mycelium was harvested through Miracloth filters, washed with 0.96% (w/v) NaCl, dried and ground in liquid nitrogen with a mortar and pestle. Approximately 500 µl of the fine powder were mixed with 800 µl of lysis buffer [50 mM Tris (pH 7.5), 50 mM EDTA (pH 8), 3% (w/v) SDS and 1% (v/v) ß-mercaptoethanol] and incubated at 65°C for at least one hour. To the mixture 800 µl phenol were added and then centrifuged for 20 min at 13000 rpm. The upper aqueous phase was transferred to a new tube. To denature the proteins, 500 µl chloroform were added, mixed and centrifuged for 10 min at 13000 rpm. The upper

phase was transferred to a new tube and 400 µl of isopropanol were added, followed by a centrifugation step of 2 min at 13000 rpm for precipitation of gDNA. After the removal of the supernatant, the pelleted gDNA was washed with 70% (v/v) ethanol by centrifuging for 1 min at 13000 rpm. The supernatant was removed and the sediment was dried at 65°C for approximately 25 min. The pelleted gDNA was dissolved in up to 100 µl deionized H_2O containing 2 µl RNase A (10 mg/ml) and treated at 65°C for 30 min to remove RNA. Quality and concentration of gDNA were checked by agarose gel electrophoresis.

2.3.2 Polymerase chain reaction (PCR)

DNA fragments were amplified by PCR (Saiki *et al*, 1988) for construction of plasmids or Southern probes. Colony PCRs were performed to identify the *E.coli* or *A. tumefaciens* transformants containing the plasmid of interest (Bergkessel & Guthrie, 2013). As polymerases the Phusion® High Fidelity Polymerase, *Taq* DNA Polymerase (both THERMO FISHER SCIENTIFIC) and Q5® High Fidelity Polymerase (NEW ENGLAND BIOLABS) were used. PCR programs and oligonucleotides were designed according to manufacturer's specifications.

2.3.3 Agarose gel electrophoresis

By agarose gel electrophoresis DNA and RNA fragments were separated according to size. For the gel 1% (w/v) agarose (BIOZYM SCIENTIFIC GMBH) was dissolved in TAE buffer [40 mM Tris, 20 mM acetic acid, 1 mM EDTA] and 0.001 mg/ml ethidium bromide was added. The DNA was mixed with 6x loading dye [0.25% (w/v) bromophenolblue, 0.25% (w/v) xylene cyanole, 40% (w/v) sucrose] prior to loading it on the agarose gel. As size standard the GeneRuler™ 1 kb DNA (THERMO FISHER SCIENTIFIC) was used. By applying a current of 90 V to the running chamber negatively charged DNA molecules migrate to the positive electrode and separate according to size. TAE buffer was used as electrophoresis buffer. *In-gel* visualization was enabled by exposure to UV-light (λ = 254 nm) with the Gel iX20 Imager Windows Version and the Intas GDS gel documentation software from INTAS SCIENCE IMAGING INSTRUMENTS GMBH (Göttingen, Germany) or on a TFX-20 MX Vilber Lourmat Super Bright transilluminator (SIGMA-ALDRICH).

2.3.3.1 Purification of DNA from agarose gels

PCR amplification or enzymatic restriction fragments were excised from agarose gels and purified for further cloning reactions or the use as probes in Southern hybridizations. For purification steps the QIAquick® Gel Extraction Kit (QIAGEN) or the NucleoSpin® Gel and PCR Clean-up Kit from MACHEREY-NAGEL GMBH & CO. KG were utilized according to manufacturer's instructions. Purified DNA was eluted from spin columns with dH_2O.

2.4 Southern hybridization

Integration of DNA at the desired locus of the *V. dahliae* genome was verified by Southern hybridization (Southern, 1975). Total gDNA of the respective strains was treated with appropriate restriction enzymes that cleave at two sites in the linear DNA sequence or in the neighboring DNA sequence resulting in recognizable different sizes between the transformation host and the constructed strain. Enzyme restriction was conducted overnight and the cut gDNA was separated on an agarose gel. The agarose gel was washed in three subsequent steps: 10 min in buffer 1 [0.25 M HCl], 25 min in a denaturing buffer 2 [0.5 M NaOH, 1.5 M NaCl] and 30 min in a neutralizing buffer 3 [0.5 M Tris, 1.5 M NaCl, pH 7.4]. The DNA was transferred to Amersham™ Hybond™-N nylon membranes (GE HEALTHCARE) from the agarose gel during dry-blotting for at least 90 min. The membrane was dried at 70°C for 10 min and the DNA was crosslinked to the membrane by exposure to UV-light (λ = 254 nm) for 3 min per membrane side. For pre-hybridization and probe labeling the Amersham™ Gene Images AlkPhos Direct Labelling and Detection System (GE HEALTHCARE) was used according to the manufacturer's instructions. The rotating incubation steps at 60°C were performed in HERA hybrid R hybridization oven (HERAEUS INSTRUMENTS). During overnight hybridization, the probe binds to a specific DNA sequence excised by the restriction enzymes. The membrane was washed twice in post-hybridization buffer 1 [1 mM $MgCl_2$, 3.5 mM SDS, 50 mM Na_3PO_4 buffer, 150 mM NaCl, 2 M urea, 0.2% (w/v) blocking reagent] for 10 min at 60°C in the hybridization oven and twice in post-hybridization buffer 2 [50 mM Tris, 100 mM NaCl (pH 10) and freshly added 2 mM $MgCl_2$] for 5 min under constant agitation. Probe detection was performed with CDP-Star Detection Reagent (GE HEALTHCARE) and subsequent exposure to

Amersham™ Hyperfilm™ ECL (GE HEALTHCARE). The film was developed with the Optimax film processor (PROTEC GMBH & CO. KG).

2.5 Organisms, plasmids and strains

2.5.1 Organisms

2.5.1.1 Bacterial strains

Plasmid construction and cloning were performed with *E. coli* strain DH5α (Woodcock *et al*, 1989). *A. tumefaciens* strain AGL-1 (Lazo *et al*, 1991) was used in an *A. tumefaciens* mediated transformation (ATMT) for the construction of *V. dahliae* strains.

2.5.1.2 *Verticillium* strains

In this study the *V. dahliae* strain JR2 (Fradin *et al*, 2009) isolated from *Solanum lycopersicum* was used as background for generation of all *V. dahliae* mutant strains (Table 1). Up to three strains for one genotype were saved with individual VGB (*Verticillium* strain collection Gerhard H. Braus) numbers. *V. longisporum* 43 isolated from *B. napus* (Zeise & von Tiedemann, 2002) was used for the exoproteome comparison.

Table 1. *Verticillium dahliae* strains used and constructed in this study.

Strain	Genotype	Reference
JR2	*Solanum lycopersicum* isolate	(Fradin *et al*, 2009)
JR2-*GFP*	^{p}*gpdA:GFP:trpC*^{t}:^{p}*gpdA:HYG*^{R}*:trpC*^{t}	(Tran *et al*, 2014)
VGB126/ VGB133	Δ*MEP2::*^{p}*gpdA:NAT*^{R}*:trpC*^{t}	This study
VGB127/ VGB132	Δ*CBD1::*^{p}*gpdA:NAT*^{R}*:trpC*^{t}	This study
VGB128/ VGB130	Δ*AMY1::*^{p}*gpdA:NAT*^{R}*:trpC*^{t}	This study
VGB129/ VGB131	Δ*GLA1::*^{p}*gpdA:NAT*^{R}*:trpC*^{t}	This study
VGB203/ VGB204	Δ*MEP1::*^{p}*gpdA:HYG*^{R}*:trpC*^{t}*;* Δ*MEP2::*^{p}*gpdA:NAT*^{R}*:trpC*^{t}	This study
VGB226/ VGB227	Δ*MEP1::*^{p}*gpdA:HYG*^{R}*:trpC*^{t}	This study

Strain	Genotype	Reference
VGB266/ VGB348/ VGB349	Δ*SFL1::^{p}gpdA:NAT^{R}:trpC^{t}; ^{p}gpdA:GFP:SFL1:trpC^{t}:^{p}gpdA:HYG^{R}:trpC^{t}*	This study
VGB296	Δ*FRQ::^{p}gpdA:NAT^{R}:trpC^{t}*	This study
VGB316/ VGB317	Δ*CP1::^{p}gpdA:NAT^{R}:trpC^{t}*	This study
VGB324/ VGB325	Δ*SFL1::^{p}gpdA:NAT^{R}:trpC^{t}*	(Bui *et al*, 2019)/ This study
VGB340/ VGB341	Δ*SFL1::^{p}gpdA:NAT^{R}:trpC^{t}; ^{p}gpdA:GFP:trpC^{t}:^{p}gpdA:HYG^{R}:trpC^{t}*	(Bui *et al*, 2019)
VGB342/ VGB343	Δ*SFL1::^{p}gpdA:NAT^{R}:trpC^{t}; ^{p}SFL1:SFL1:SFL1^{t}:^{p}gpdA:HYG^{R}:trpC^{t}*	(Bui *et al*, 2019)
VGB350/ VGB351/ VGB352	Δ*SFL1::^{p}gpdA:NAT^{R}:trpC^{t}; ^{p}gpdA:SFL1:GFP:trpC^{t}:^{p}gpdA:HYG^{R}:trpC^{t}*	This study
VGB384/ VGB385	Δ*NLP3::^{p}gpdA:NAT^{R}:trpC^{t}*	This study
VGB390/ VGB391	Δ*NLP2::^{p}gpdA:HYG^{R}:trpC^{t}*	This study
VGB400/ VGB401	Δ*NLP3::^{p}gpdA:NAT^{R}:trpC^{t}; ΔNLP2::^{p}gpdA:HYG^{R}:trpC^{t}*	This study
VGB402/ VGB403	Δ*FRQ::^{p}gpdA:HYG^{R}:trpC^{t}*	This study
VGB404/ VGB405	Δ*SFL1::^{p}gpdA:NAT^{R}:trpC^{t}; ΔFRQ::^{p}gpdA:HYG^{R}:trpC^{t}*	This study
VGB406/ VGB422	Δ*CP2::^{p}gpdA:HYG^{R}:trpC^{t}*	This study
VGB411	Δ*FRQ::^{p}gpdA:NAT^{R}:trpC^{t}; ^{p}FRQ:FRQ:FRQ^{t}:^{p}gpdA:HYG^{R}:trpC^{t}*	This study
VGB423/ VGB424	Δ*CP2::^{p}gpdA:HYG^{R}:trpC^{t}; ΔCP1::^{p}gpdA:NAT^{R}:trpC^{t}*	This study
VGB425/ VGB426	Δ*NLP3::^{p}gpdA:NAT^{R}:trpC^{t}; ^{p}NLP3:NLP3:NLP3^{t}:^{p}gpdA:HYG^{R}:trpC^{t}*	This study
VGB427/ VGB428	Δ*NLP2::^{p}gpdA:HYG^{R}:trpC^{t}; ^{p}NLP2:NLP2:NLP2^{t}:^{p}gpdA:NAT^{R}:trpC^{t}*	This study
VGB429/ VGB430	Δ*CP2::^{p}gpdA:HYG^{R}:trpC^{t}; ^{p}CP2:CP2:CP2^{t}:^{p}gpdA:NAT^{R}:trpC^{t}*	This study
VGB431/ VGB432	Δ*NLP3::^{p}gpdA:NAT^{R}:trpC^{t}; ^{p}gpdA:GFP:trpC^{t}:^{p}gpdA:HYG^{R}:trpC^{t}*	This study

Strain	Genotype	Reference
VGB433/ VGB434	$^{p}SFL:GFP:SFL1:^{p}gpdA:HYG^{R}:trpC^{t}:SFL1^{t}$	This study
VGB435/ VGB436	$\Delta FRQ::^{p}gpdA:NAT^{R}:trpC^{t};$ $^{p}gpdA:GFP:SFL1:trpC^{t}:^{p}gpdA:HYG^{R}:trpC^{t}$	This study
VGB441/ VGB442	$\Delta FRQ::^{p}gpdA:HYG^{R}:trpC^{t};$ $^{p}FRQ:FRQ:FRQ^{t}:^{p}gpdA:NAT^{R}:trpC^{t}$	This study
VGB489/ VGB490	$\Delta CP1::^{p}gpdA:NAT^{R}:trpC^{t};$ $^{p}CP1:CP1:CP1^{t}:^{p}gpdA:HYG^{R}:trpC^{t}$	This study

^{p}: promoter, ^{t}: terminator, HYG^{R}: hygromycin B resistance marker, NAT^{R}: nourseothricin resistance marker, several VGB numbers for one genotype indicate independent transformants.

2.5.1.3 Plants

Plants used in this study are listed in Table 2. All plants were grown in a climate chamber at long day conditions with 16 hours of light (fluorescence: 60, GroLEDs: 100, illumination: 95µmol) at 25°C and eight hours in the dark at 22°C.

Table 2. Plants used in this study

Strain	Description	Reference
Arabidopsis thaliana (Columbia-0)	thale cress, family: *Brassicaceae*, used for root colonization analysis by *V. dahliae*	N1902; NOTTINGHAM ARABIDOPSIS STOCK CENTRE (Nottingham, United Kingdom)
Brassica napus (Falcon)	rapeseed, family: *Brassicaceae*, used for xylem sap extraction for exoproteome studies	NORDDEUTSCHE PFLANZENZUCHT (Holtsee, Germany)
Solanum lycopersicum (Moneymaker)	tomato, family: *Solanaceae*, used as host for *V. dahliae*	BRUNO NEBELUNG GMBH & CO. KIEPENKERL-PFLANZENZÜCHTUNG (Everswinkel, Germany)

2.5.2 Plasmid and strain constructions

For PCRs the following polymerases were used: Phusion® High Fidelity Polymerase, *Taq* DNA Polymerase (both THERMO FISHER SCIENTIFIC) and Q5® High Fidelity Polymerase (NEW ENGLAND BIOLABS). For enzymatic restriction controls restriction enzymes and corresponding buffers were obtained from NEB or THERMO FISHER SCIENTIFIC. For plasmid propagation the *E. coli* strain DH5α was utilized.

A. tumefaciens AGL-1 was exploited to transform *V. dahliae* strains with the desired construct. All constructed plasmids were sequenced by MICROSYNTH SEQLAB (Göttingen, Germany) and the genetically modified strains were checked by Southern hybridization if not indicated otherwise.

2.5.2.1 Cloning strategy

Plasmid constructions were performed with GeneArt® Seamless Cloning and Assembly Kit purchased from THERMO FISHER SCIENTIFIC. For this strategy fragments required border sequences that share a 15 bp homology region. Therefore, primers were designed with an overhang of 15 bp to the desired neighboring fragments. All primers used in this study are listed in Table 3. Genes or surrounding flanking regions were amplified by PCR from *V. dahliae* gDNA. As resistance markers the nourseothricin resistance marker (*NAT*^{R}) and the hygromycin B resistance marker (*HYG*^{R}) were used under control of the *A. nidulans* glyceraldehyde-3-phosphate dehydrogenase *gpdA* (AN8041; *A. nidulans* FGSC A4) promoter and the tryptophan biosynthesis gene *trpC* (AN0648; *A. nidulans* FGSC A4) terminator for constitutive gene expression (Punt *et al*, 1987). If more than three fragments were to be incorporated into one plasmid, fusion PCRs (Szewczyk *et al*, 2006) were performed prior to Seamless Cloning.

Table 3. Primers designed and used in this study.

Name	Sequence (5' to 3')	Size	Overhang (at indicated site)
AO84	CAC GGA CGA GTC TCT CGG A	19 mer	-
AO85	ACC GGT CAC TGT ACA GTT GGA AGT TGA GGG GTG AT	35 mer	*gpdA* promoter
AO86	AGG TAA TCC TTC TTT GGC GTC TGC GTT ATT AGA G	34 mer	*trpC* terminator
AO87	CTC GGC AAA GGG TTT CTT	18 mer	-
AO131	ATT CTT AAT TAA GAT CAC GGA CGA GTC TCT CG	32 mer	pPK2 (*Eco*RV)
AO132	GGT ACC GAG CTC GAT CTC GGC AAA GGG TTT C	31 mer	pPK2 (*Eco*RV)
JST27	GTA TGT TGT GTG GAA AAC AGG CTC TAT GGC GGG	33 mer	pME4564 (ML1)

Name	Sequence (5' to 3')	Size	Overhang (at indicated site)
JST28	AAG ATC CCC GGG TAC CGG GAC GCG CAG GTT GTA AT	35 mer	*gpdA* promoter
JST29	AGG TAA TCC TTC TTT ATA GTT CAT TCT GTT TGC ATC	36 mer	*trpC* terminator
JST30	CAC AGT ACA CGA GGA TAG ACC CGA CGA CTT GTT	33 mer	pME4564 (ML2)
ML1	TTC CAC ACA ACA TAC GAG CC	20 mer	-
ML2	TCC TCG TGT ACT GTG TAA GC	20 mer	-
ML8	AAA GAA GGA TTA CCT CTA AAC AA	23 mer	-
ML9	TGT ACA GTG ACC GGT GAC	18 mer	-
ML12	GTA TGT TGT GTG GAA CCA CAC CGC TGG CTT ATC TT	35 mer	pME4564 (ML1)
ML13	ACC GGT CAC TGT ACA GGT GAC GAT TGA GAA CCC GC	35 mer	*gpdA* promoter
ML14	AGG TAA TCC TTC TTT ACG GAG AGT TGA AAC ACT CT	35 mer	*trpC* terminator
ML15	CAC AGT ACA CGA GGA TTG TCA AGC AGA GCG CTA AC	35 mer	pME4564 (ML2)
ML16	GTA TGT TGT GTG GAA GCC ACC TTG TTC AAC GTT GA	35 mer	pME4564 (ML1)
ML17	ACC GGT CAC TGT ACA TTT GTG AGG ATT GTC GAC TGT C	37 mer	*gpdA* promoter
ML18	AGG TAA TCC TTC TTT GCT ACC GCG GAC ACT ACC A	34 mer	*trpC* terminator
ML19	CAC AGT ACA CGA GGA CAA CTC GAC AGT CTG CTG GG	35 mer	pME4564 (ML2)
ML20	GTA TGT TGT GTG GAA GCT AGT CAA CAA TGC AAG AG	35 mer	pME4564 (ML1)
ML21	ACC GGT CAC TGT ACA ATT GAA TTG ATA CCG AGC CG	35 mer	*gpdA* promoter
ML22	AGG TAA TCC TTC TTT GTC GAC TCT CCT TCG TTG GT	35 mer	*trpC* terminator
ML23	CAC AGT ACA CGA GGA CTT GGC ACC TTG CTC AGG AG	35 mer	pME4564 (ML2)
ML24	GTA TGT TGT GTG GAA GCT TGC CTT GTT GAA CTT GA	35 mer	pME4564 (ML1)

Name	Sequence (5’ to 3’)	Size	Overhang (at indicated site)
ML25	ACC GGT CAC TGT ACA GAT GAT GGT GAT GCC TCG TC	35 mer	*gpdA* promoter
ML26	AGG TAA TCC TTC TTT TGA GCA GGA TTG TGC TTG C	34 mer	*trpC* terminator
ML27	CAC AGT ACA CGA GGA GTA GTC GGC ATA TAG GAC AGC	36 mer	pME4564 (ML2)
ML30	GGT GGT AGC GGT GGT ATG GTG AGC AAG GGC GAG	33 mer	Linker
ML67	GGT ACC GAG CTC GAT TTT CTG AGG AGA TGC GAG AAG	36 mer	pPK2 (*Eco*RV)
ML69	ATT CTT AAT TAA GAT AGC GTC CCC TTG CCC ATT	33 mer	pPK2 (*Eco*RV)
ML70	GGT ACC GAG CTC GAT ACG AAA CCG ATA AGC TCT CCA	36 mer	pPK2 (*Eco*RV)
ML71	AAT CGC GGC AGC CAT GGT GAT GTC TGC TCA AGC G	34 mer	*SFL1*
ML72	ACC ACC GCT ACC ACC CTG CAT CCG TTT GCG TTT C	34 mer	Linker
ML73	GGT GGT AGC GGT GGT ATG GCT GCC GCG ATT GAG A	34 mer	Linker
ML74	AAA CGG ATG CAG TGA TCC ACT TAA CGT TAC TGA AAT CAT	39 mer	*SFL1*
ML77	GCC CTT GCT CAC CAT TTG CGC TGC ACG ATG C	31 mer	GFP
ML78	AGA TCC CCG GGT ACC TCA CTG CAT CCG TTT GCG	33 mer	*gpdA* promoter
ML79	AGA TCC CCG GGT ACC GGA TAT GGT GCG TCC CCA	33 mer	*gpdA* promoter
ML81	CTA CAG CGC CGC CTT CT	17 mer	-
ML86	ATT CTT AAT TAA GAT AAT GGT GTA ACG TGA CGC G	34 mer	pME4564/ pPK2 (*Eco*RV)
ML87	ACC GGT CAC TGT ACA GGT GGA GAT TGC TGA TTG TT	35 mer	*gpdA* promoter
ML88	AGG TAA TCC TTC TTT ATG GAC CCG AGG GGC GA	32 mer	*trpC* terminator
ML89	AGG ACT TCT AGA AGG CTT CGA CCT CGC GTC GA	32 mer	pME4564 (*Stu*I)
ML90	ATT CTT AAT TAA GAT TAG AAT GAA GTT CTG GGG TCG	36 mer	pME4564 (*Eco*RV)

Name	Sequence (5’ to 3’)	Size	Overhang (at indicated site)
ML91	AGA TCC CCG GGT ACC GGG ATC TTC CCT CCC ACC T	34 mer	*gpdA* promoter
ML92	AGG TAA TCC TTC TTT TCT GGG TTG TGA GGA AGA GC	35 mer	*trpC* terminator
ML94	ATT CTT AAT TAA GAT ACT CCC AGT TTC TGC TAC TTC ATT	39 mer	pME4564 (*Eco*RV)
ML95	AGA TCC CCG GGT ACC GAC CAC GGC GCA TGT CTT	33 mer	*gpdA* promoter
ML96	AGG TAA TCC TTC TTT AAA TTG GGG GCG TTG CG	32 mer	*trpC* terminator
ML97	AGG ACT TCT AGA AGG TTG ACA ATT CAA CGC GAA CAC TAC	39 mer	pME4564 (*Stu*I)
ML98	GGT ACC GAG CTC GAT CTT CGA CCT CGC GTC GA	32 mer	*gpdA* promoter
ML102	TGT TGT GTG GAA GAT TAG AAT GAA GTT CTG GGG TCG	36 mer	pME4815 (*Eco*RV)
ML104	TGT TGT GTG GAA GAT ACT CCC AGT TTC TGC TAC TTC A	37 mer	pME4815 (*Eco*RV)
ML105	GGT CAC TGT ACA GAT TTG ACA ATT CAA CGC GAA C	34 mer	pME4815 (*Eco*RV)
ML106	AGG ACT TCT AGA AGG ATT GGG TGA CGT TTT CAT GG	35 mer	pME4564 (*Stu*I)
ML107	GGT CAC TGT ACA GAT ATT GGG TGA CGT TTT CAT GG	35 mer	pME4815 (*Eco*RV)
ML108	GAT CTT GGA AAC CAT GGT GGA GAT TGC TGA TTG TTG	36 mer	*NLP3*
ML109	ATG GTT TCC AAG ATC TTC TCC A	22 mer	-
ML111	AAG GCG GCG CTG TAG TCT GGG TTG TGA GGA AGA GC	35 mer	*NLP2*
ML114	TGT TGT GTG GAA GAT AGG CCA CAC CAT CCC ACT	33 mer	pME4815 (*Eco*RV)
ML115	GGT CAC TGT ACA GAT TTT CTG AGG AGA TGC GAG AAG	36 mer	pME4815 (*Eco*RV)
RH631	ATT CTT AAT TAA GAT AGG CCA CAC CAT CCC ACT	33 mer	pME4564/ pPK2 (*Eco*RV)
RH632	ACC GGT CAC TGT ACA GGA TAT GGT GCG TCC CCA	33 mer	*gpdA* promoter
RH633	AGG TAA TCC TTC TTT TGC TGC CAC GGA CGT ATT	33 mer	*trpC* terminator

Name	Sequence (5' to 3')	Size	Overhang (at indicated site)
RH634	AGG ACT TCT AGA AGG TTT CTG AGG AGA TGC GAG AAG	36 mer	pME4564 (*Stu*I)
RH635	GGT ACC GAG CTC GAT GTG ACC GGT GAC TCT TTC TG	35 mer	pPK2 (*Eco*RV)
RH636	ATT CTT AAT TAA GAT CGA GTG GAG ATG TGG AGT G	34 mer	pPK2 (*Eco*RV)
RH659	ACC GGT CAC TGT ACA TTG CGC TGC ACG ATG C	31 mer	*gpdA* promoter
RH660	AGG TAA TCC TTC TTT TAT CGT CTC TCC GCA ACC G	34 mer	*trpC* terminator
RH661	TCT AGA GGG CCC AGG ACG AAA CCG ATA AGC TCT CCA G	37 mer	pME4548 (*Eco*RV)
RH664	ATG GCT GCC GCG ATT GA	17 mer	-
RH665	TCA CTG CAT CCG TTT GCG	18 mer	-
RH667	ATT CTT AAT TAA GAT AGC GTC CCC TTG CCC ATT	33 mer	pME4548 (*Eco*RV)
RH668	GTC GCA CAA AAG AGG AGA TGT TG	23 mer	-
RO3	GGT ACC CGG GGA TCT TTC G	19 mer	-
SZ19	ACC TCT GGA GGC AAG GCT T	19 mer	-
SZ20	GCT TGG CCT TCT TCT TCT GC	20 mer	-
ZQY10	ATG GTG AGC AAG GGC GAG	18 mer	-
ZQY11	ACC ACC GCT ACC ACC CTT GTA CAG CTC GTC CAT GC	35 mer	Linker

2.5.2.2 Genetic manipulation of microorganisms

2.5.2.2.1 Transformation of *Escherichia coli*

E. coli strain DH5α was utilized for cloning reactions and propagation of plasmids. Transformation of the *E. coli* was performed based on a heat shock method (Inoue *et al*, 1990). Up to 200 µl chemically competent *E. coli* cells were thawed on ice, DNA was added followed by another 30 min incubation on ice. The heat shock occurred for 60 seconds at 42°C. The cells were cooled down on ice for 2 min

before 800 µl liquid SOC medium [2% tryptone/peptone from casein, 0.5% yeast extract, 10 mM NaCl, 2.5 mM KCl, 10 mM $MgCl_2$, 10 mM $MgSO_4$, 20 mM glucose] were added. To induce cell growth, the cells were incubated at 37°C under agitation for 40 to 60 min and then spread on LB agar plates containing 100 µg/ml kanamycin for selection of positive transformants. Agar plates were incubated at 37°C overnight and the clones were tested by colony PCRs.

2.5.2.2.2 Transformation of *Agrobacterium tumefaciens*

A. tumefaciens AGL-1 cells were used for an ATMT of *V. dahliae* spores. *A. tumefaciens* was transformed via a freeze-thaw method (Jyothishwaran *et al*, 2007). 200 µl competent *A. tumefaciens* cells were thawed on ice and mixed with 1 µg plasmid DNA and incubated on ice for another 10 min. The mixture was frozen in liquid nitrogen for 10 min. The heat shock was performed at 37°C for 5 min before 800 µl liquid SOC were added. The cell growth was initiated by a one-hour incubation in a shaking water bath at 28°C. Cells were then spread on LB agar plates containing 100 µg/ml kanamycin for selection and incubated at 25°C for 3 days. Plasmid uptake was verified by colony PCR.

2.5.2.2.3 Transformation of *Verticillium dahliae*

The ATMT of *V. dahliae* was performed based on the method described in Mullins *et al* (2001). *A. tumefaciens* cells were grown in liquid LB supplemented with 100 µg/ml kanamycin at 25°C on a rotary shaker overnight. The pre-culture was used to inoculate liquid induction medium [1x MM salts (2.5x stock: 3.625 g/l KH_2PO_4, 5.125 g/l K_2HPO_4, 0.375 g/l NaCl, 1.25 g/l $MgSO_4 \cdot 7\ H_2O$, 0.165 g/l $CaCl_2 \cdot 2\ H_2O$, 6.2 mg/l $FeSO_4 \cdot 7\ H_2O$, 1.25 g/l $(NH_4)_2SO_4$), 10 mM glucose, 0.5% (v/v) glycerol, 40 mM MES, 200 µM acetosyringone]. The supplementation of acetosyringone allowed the upregulation of virulence genes in *A. tumefaciens,* which improves transformation efficiency. The culture was incubated for approximately 5 hours in a 28°C shaking water bath before an equal volume of the culture was mixed with spores of the *V. dahliae* host (1 x 10^6 spores/ml). Of the mixture 200 µl were spread on filter paper (85 mm, SARTORIUS) placed on solid induction medium [1x MM salts, 5 mM glucose, 0.5% (v/v) glycerol, 40 mM MES (pH 5.3), 10 mM acetosyringone (pH 8), 1.5 % (w/v) agar]. Plates were incubated at 25°C for three days in the dark. The filter paper was then transferred to solid

PDM plates containing 300 µg/ml cefotaxime to kill *A. tumefaciens* cells and other antimycotica that were required for selection of positive transformants (50 µg/ml hygromycin B, 72 µg/ml nourseothricin). Filters were removed after approximately six days and transformants were singularized in another two steps on PDM selection plates. To generate fungal spore suspensions, single colonies were used to inoculate SXM cultures containing 300 µg/ml cefotaxime. Spores were collected, used for inoculation of PDM cultures and mycelia were harvested as described in 2.2.2. Genomic DNA was extracted as mentioned in 2.3.1.2 and correct DNA integration was verified by Southern hybridization (2.4).

2.5.2.3 Plasmid and strain constructions

All plasmids used and constructed in this study (listed in Table 4) contain a left and right border for ATMT.

Table 4. Plasmids generated and used in this study

Plasmid	Description	Reference
pGreen2	^{p}*gpdA:GFP:trpC*^{t}:^{p}*gpdA:HYG*^{R}*:trpC*^{t}*; KAN*^{R}, use *Eco*RV site for integration	(Tran *et al*, 2014)
pPK2	^{p}*gpdA:HYG*^{R}*:trpC*^{t}*; KAN*^{R} Cloning vector with *KAN*^{R} *and HYG*^{R}, use *Eco*RV site for integration	(Covert *et al*, 2001)
pME4548	^{p}*trpC:NAT*^{R}*; KAN*^{R} Cloning vector with *KAN*^{R} *and NAT*^{R}	(Bui *et al*, 2019)
pME4564 (pKO1)	^{p}*trpC:HYG*^{R}*; KAN*^{R} Cloning vector with *KAN*^{R} *and HYG*^{R} without terminator, use *Eco*RV and *Stu*I for exchange of ^{p}*trpC:HYG*^{R} with the desired fragment or ML1 and ML2 for amplification of backbone	(Tran, 2011, Dissertation)
pME4727	^{p}*SFL1:*^{p}*gpdA:NAT*^{R}*:trpC*^{t}*:SFL1*^{t} in pME4548	(Bui *et al*, 2019)
pME4728	^{p}*SFL1:SFL1:SFL1*^{t}, ^{p}*gpdA:HYG*^{R}*:trpC*^{t} in pPK2	(Bui *et al*, 2019)
pME4815	^{p}*gpdA:NAT*^{R}*:trpC*^{t}*; KAN*^{R} Cloning vector with *KAN*^{R} *and NAT*^{R}, use *Eco*RV site for integration	(Balnojan, 2016, Master thesis)
pME4876	^{p}*gpdA:GFP:SFL1:trpC*^{t}:^{p}*gpdA:HYG*^{R}*:trpC*^{t} in pPK2	This study

Plasmid	Description	Reference
pME4877	^{p}*SFL:GFP:SFL1:*^{p}*gpdA:HYG*^{R}*:trpC*^{t}*:SFL1*^{t} in pME4727	This study
pME4878	^{p}*gpdA:SFL1:GFP:trpC*^{t}*:*^{p}*gpdA:HYG*^{R}*:trpC*^{t} in pPK2	This study
pME4879	^{p}*FRQ:*^{p}*gpdA:NAT*^{R}*:trpC*^{t}*:FRQ*^{t} in pME4564	This study
pME4880	^{p}*FRQ:FRQ:FRQ*^{t}*:*^{p}*gpdA:HYG*^{R}*:trpC*^{t} in pPK2	This study
pME4881	^{p}*FRQ:*^{p}*gpdA:HYG*^{R}*:trpC*^{t}*:FRQ*^{t} in pME4564	This study
pME4882	^{p}*FRQ:FRQ:FRQ*^{t}*:*^{p}*gpdA:NAT*^{R}*:trpC*^{t} in pME4815	This study
pME4883	^{p}*NLP3:*^{p}*gpdA:NAT*^{R}*:trpC*^{t}*:NLP3*^{t} in pME4564	This study
pME4884	^{p}*NLP3:NLP3:NLP3*^{t}*:*^{p}*gpdA:HYG*^{R}*:trpC*^{t} in pPK2	This study
pME4885	^{p}*NLP2:*^{p}*gpdA:HYG*^{R}*:trpC*^{t}*:NLP2*^{t} in pME4564	This study
pME4886	^{p}*NLP2:NLP2:NLP2*^{t}*:*^{p}*gpdA:NAT*^{R}*:trpC*^{t} in pME4815	This study
pME4887	^{p}*CP1:*^{p}*gpdA:NAT*^{R}*:trpC*^{t}*:CP1*^{t} in pME4564	This study
pME4888	^{p}*CP1:CP1:CP1*^{t}*:*^{p}*gpdA:HYG*^{R}*:trpC*^{t} in pPK2	This study
pME4889	^{p}*CP2:*^{p}*gpdA:HYG*^{R}*:trpC*^{t}*:CP2*^{t} in pME4564	This study
pME4890	^{p}*CP2:CP2:CP2*^{t}*:*^{p}*gpdA:NAT*^{R}*:trpC*^{t} in pME4815	This study
pME4891	^{p}*MEP1:*^{p}*gpdA:HYG*^{R}*:trpC*^{t}*:MEP1*^{t} in pME4564	This study
pME4892	^{p}*MEP2:*^{p}*gpdA:NAT*^{R}*:trpC*^{t}*:MEP2*^{t} in pME4564	This study
pME4894	^{p}*GLA1:*^{p}*gpdA:NAT*^{R}*:trpC*^{t}*:GLA1*^{t} in pME4564	This study
pME4895	^{p}*CBD1:*^{p}*gpdA:NAT*^{R}*:trpC*^{t}*:CBD1*^{t} in pME4564	This study
pME4896	^{p}*AMY1:*^{p}*gpdA:NAT*^{R}*:trpC*^{t}*:AMY1*^{t} in pME4564	This study

HYG^{R}: hygromycin B resistance marker, *KAN*^{R}: kanamycin resistance marker, *NAT*^{R}: nourseothricin resistance marker, ^{p}: promoter, ^{t}: terminator.

Plasmid and strain construction of *GFP-SFL1* complementation strain

Construction of the *SFL1* (*VDAG_JR2_ Chr4g02790a*) deletion and ectopic complementation strain was described in a previous study (Bui *et al*, 2019). The resulting deletion (VGB324 and VGB325) and complementation transformants (VGB342 and VGB343) were used in this study and VGB324 was used as background strain for integration of *GFP-SFL1*. The 5' region of *SFL1* together with the backbone of pME4548 and 3' region were amplified from pME4727 (9 101 bp) with ML77/RH660, *GFP* (lacking the stop codon) fused to *SFL1* was amplified as one PCR product from pME4876 with ZQY10/ML78 (3 942 bp), the hygromycin resistance cassette was amplified from pPK2 with RO3/ML8 (3 942 bp). All fragments were ligated together resulting in pME4877. In an ATMT this plasmid was utilized to transform VGB324 resulting in the transformants VGB433 and VGB434. Verification of the correctly integrated fragment was performed by Southern hybridization (Figure S1) for which gDNA was cut with *Pst*I and part of the *SFL1* gene was used as probe (664 bp at the beginning ot the *SFL1* ORF amplified with RH664/RH668).

Plasmid and strain construction of the ectopic N- and C-terminally *GFP*-tagged *SFL1* strains

To overexpress N- or C-terminally *GFP*-tagged *SFL1* in the *SFL1* deletion strain, constructs were generated including the hygromycin resistance cassette and integrated into the *SFL1* deletion strain VGB324. For the *GFP-SFL1* harboring construct, *GFP* (lacking the stop codon) under control of the *gpdA* promoter was amplified from pGreen2 with ZQY11/RH635 (1 609 bp). ZQY11 includes a sequence coding for GGSGG that serves as a flexible linker to allow independent protein folding (van Rosmalen *et al*, 2017). The *SFL1* ORF was amplified from wildtype (WT) gDNA with primer pair ML73/RH665 (2 069 bp) and the *trpC* terminator from pGreen2 with ML74/RH636 (772 bp). Latter two fragments were fused by PCR with ML74/RH636 before all fragments were ligated to linearized pPK2 (cut with *Eco*RV, 10 751 bp) resulting in pME4876. For construction of the *SFL1-GFP* possessing construct the *gpdA* promoter was amplified from pGreen2 with ML71/RH635 (874 bp), the *SFL1* sequence without the stop codon was amplified from genomic WT DNA with RH664/ML72 (2 066 bp). ML72 possesses an overhang to the linker sequence. These fragments were fused in another PCR

using primer pair ML72/RH635. *GFP* fused to *trpC* terminator was obtained by PCR of pGreen2 with ML30 (including the linker sequence)/RH636 (1 510 bp). These fragments were ligated to *Eco*RV linearized pPK2. The constructed plasmid was named pME4878. These plasmids were used to transform the desired fragments into VGB324. Transformants were tested by Southern hybridization to possess the ectopically integrated fragments (Figure S1). Genomic DNA of WT and the transformants was cut by *Pst*I. Part of the *SFL1* gene (664 bp) was used as probe to verify the correct strains. VGB266, VGB348 and VGB349 were verified as *GFP-SFL1* overexpressing transformants whereas VGB350, VGB351 and VGB352 harbored the *SFL1-GFP* overexpressing construct.

Plasmid and strain construction of the *FRQ* deletion (*NAT^R*) and corresponding complementation strain

For deletion of *FRQ* (*VDAG_JR2_Chr1g01960a*) the 5' and 3' flanking regions were amplified from *V. dahliae* WT gDNA with RH631/RH632 (1 425 bp) and RH633/RH634 (866 bp), respectively. The *NAT^R* cassette was obtained by amplification of pME4815 with ML8/ML9 (2194 bp). For the backbone pME4564 was cut with *Stu*I and *Eco*RV and the linearized backbone (6 804 bp) was ligated with the fragments resulting in pME4879. This plasmid was used for transformation of the WT. The obtained *FRQ* deletion transformants were tested for correct integration of the construct by Southern hybridization (Figure S2). Restriction enzyme *Sac*II was used to cut gDNA of WT and deletion transformants and the 3' *FRQ* region was used as probe to verify the *FRQ* deletion strain VGB296.

For construction of the complementation strain, the *FRQ* ORF was amplified from WT gDNA including its 5' and 3' flanking regions with RH631/ML67 (5 296 bp) and ligated to pPK2 (10 751 bp), which was linearized with *Eco*RV. The resulting plasmid was named pME4880, which was used to transform the *FRQ* deletion strain VGB296. The received transformants were analyzed for ectopic integration of the construct by Southern hybridization with the same enzyme and probes as the deletion transformants (Figure S2). VGB411 was confirmed as ectopic complementation strain and was conserved in the strain collection.

Strain construction of the *FRQ* deletion strain ectopically overexpressing *GFP-SFL1*

Plasmid pME4876 harboring *GFP-SFL1* under control of the constitutively active *gpdA* promoter was used for ectopic integration of the desired fragments into VGB296. Transformants were tested by Southern hybridization to possess the ectopically integrated fragments (Figure S2). Genomic DNA of WT, VGB296 and the transformants was cut by *Pst*I and part of the *SFL1* gene (664 bp amplified with RH664/RH668) was used as probe to confirm the integration. Correct transformants were conserved as VGB435 and VGB436.

Plasmid and strain construction of the *FRQ* deletion (*HYG^R*) and respective complementation strain

Another *FRQ* deletion construct was designed with a hygromycin cassette in order to enable the construction of a Δ*FRQ*Δ*SFL1* double mutant strain. The 5' and 3' flanking regions of *FRQ* (*VDAG_JR2_Chr1g01960a*) were amplified from *V. dahliae* WT gDNA with RH631/ML79 (1 425 bp) and RH633/RH634 (866 bp), respectively. The *HYG^R* cassette was received by amplification of pPK2 with ML8/RO3 (3 942 bp). Plasmid pME4564 was cut with *Stu*I and *Eco*RV and the linearized backbone (6 804 bp) was ligated with the fragments resulting in pME4881. With this plasmid the WT was transformed to achieve replacement of the *FRQ* ORF with the hygromycin resistance cassette. Transformants were analyzed with Southern hybridization for correct integration of the construct (Figure S3). Restriction enzyme *Bam*HI was used to restrict gDNA of the strains and with a probe based on the 5' *FRQ* region (RH631/ML79) *FRQ* deletion transformants VGB402 and VGB403 were verified.

To construct complementation strain, the *FRQ* ORF flanked with 5' and 3' regions was amplified with ML114/ML115 (5 296 bp) from WT gDNA and ligated to the *Eco*RV linearized pME4815 (8 928 bp) resulting in pME4882. Complementation transformants were verified by Southern hybridization with 3' *FRQ* region (RH633/RH634) as probe after gDNA treatment with *Nco*I (Figure S3). As result VGB441 and VGB442 were conserved.

Plasmid and strain construction of Δ*FRQ*Δ*SFL1* double mutant

SFL1 (*VDAG_JR2_Chr4g02790a*) and *FRQ* (*VDAG_JR2_Chr1g01960a*) ORFs were both deleted to construct a double deletion mutant. The plasmid pME4881 harboring the hygromycin resistance cassette flanked with 5' and 3' regions of *FRQ* was used for transformation of the *SFL1* deletion strain. The sequence was replaced with *HYG*^{R} by homologous recombination. Correct transformants were verified by Southern hybridization (Figure S3). Genomic DNA of WT and the deletion transformants was processed with restriction enzyme *Bam*HI. As probes the 5' flanking regions of *SFL1* (RH659/RH667) and *FRQ* (RH631/ML79) were used and confirmed VGB404 and VGB405 as Δ*FRQ*Δ*SFL1* mutant transformants.

Plasmid and strain construction of *NLP3* deletion and complementation strains and *NLP3* deletion strain overexpressing free GFP

For deletion of the *NLP3* (*VDAG_JR2_Chr4g05950a*) ORF, the 5' and 3' flanking regions were amplified from *V. dahliae* WT gDNA with ML86/ML87 (1 561 bp) and ML88/ML89 (1 284 bp), respectively. The nourseothricin resistance cassette was obtained by amplification from pME4815 with ML8/ML9 (2 194 bp). To receive the backbone, pME4564 was cut with *Stu*I and *Eco*RV and the linearized backbone (6 804 bp) was ligated with the fragments resulting in pME4883. *V. dahliae* WT was transformed with this construct resulting in *NLP3* deletion transformants.

For the complementation strain, the 5' flanking region of *NLP3* and the ORF including the 3' flanking region were amplified of WT gDNA with ML86/ML108 (1 561 bp) and ML109/ML98 (2 131 bp), respectively. To receive the plasmid backbone pPK2 was linearized with *Eco*RV (10 751 bp) and the inserts were ligated to the backbone to generate pME4884. The *NLP3* deletion strain was transformed with this construct to generate complementation strains. Transformants were tested for correct integration of the constructs by Southern hybridization (Figure S4). The gDNA of WT and transformants was cut with *Xho*I and the 5' flanking region of *NLP3* was prepared as probe to verify the *NLP3* deletion (VGB384, VGB385) and complementation transformants (VGB425, VGB426).

Additionally, an *NLP3* deletion strain (VGB384) was transformed with pGreen2 to generate the *NLP3* deletion strain expressing ectopically integrated GFP.

Transformants were screened for their fluorescence signal. VGB431 and VGB432 were conserved.

Plasmid and strain construction of *NLP2* single and *NLP2/NLP3* double deletion and *NLP2* complementation strain

To generate an *NLP2* (*VDAG_JR2_Chr2g05460a*) deletion strain, the 5' flanking region was amplified with ML90/ML91 (975 bp), the 3' flanking region with ML92/ML106 (1 165 bp) from WT gDNA and the HYG^R cassette with ML8/RO3 (3 942 bp) of pPK2. Plasmid pME4564 was cut with *Stu*I and *Eco*RV and the linearized backbone (6 804 bp) was ligated with the fragments resulting in pME4885. *V. dahliae* WT and the *NLP3* deletion strain were transformed with the construct and by homologous recombination the *NLP2* deletion strain and the *NLP2/NLP3* double deletion strains were generated, respectively.

An *NLP2* complementation strain was generated by amplifying the *NLP2* ORF including the 5' flanking region with ML81/ML102 (1 892 bp) and the 3' flanking region with ML107/ML111 (1 165 bp) of *V. dahliae* WT gDNA. The inserts were ligated to the *Eco*RV linearized pME4815 (8 928 bp) resulting in pME4886, which was ectopically introduced into the *NLP2* deletion strain to generate a complementation strain. All transformants were analyzed for integration of the construct via Southern hybridization (Figure S4). Genomic DNA was processed with *Pst*I to verify *NLP2* deletion and complementation transformants with 3' *NLP2* as probe confirming VGB390 and VGB391 as deletion and VGB427 and VGB428 as *NLP2* complementation transformants. Verification of the double deletion strain was obtained by cutting gDNA with *Xho*I and 5' *NLP3* and 5' *NLP2* were used as probes to confirm VGB400 and VGB401.

Plasmid and strain construction of *CP1* deletion and complementation strain

For construction of the *CP1* (*VDAG_JR2_Chr7g00860a*) deletion strain, the 5' and 3' flanking regions were amplified of WT gDNA with AO84/AO85 (891 bp) and AO86/AO87 (1 205 bp), respectively. The nourseothricin resistance cassette was obtained by amplification of pME4815 with ML8/ML9 (2 194 bp) and all three fragments were fused by PCR with AO84/AO87 (4 291 bp) and then phosphorylated with T4 Polynucleotide Kinase (THERMO FISHER SCIENTIFIC). The backbone of pME4564 (6 804 bp) was received by enzyme restriction with *Eco*RV

and *Stu*I. It was dephosphorylated with FastAP Thermosensitive Alkanline Phosphatase (THERMO FISHER SCIENTIFIC) and ligated to the insert with T4 DNA Ligase. The resulting plasmid pME4887 was used to generate the *CP1* deletion strain by transforming *V. dahliae* JR2 with the construct. To generate the corresponding complementation strain, the *CP1* ORF was amplified including the 5' and 3' flanking regions with AO131/AO132 (2 626 bp) and ligated to *Eco*RV linearized pPK2 (10 751 bp) resulting in pME4888. The complementation construct was ectopically integrated into the *CP1* deletion strain. To verify the constructed transformants, they were subjected to Southern hybridization (Figure S5). For confirmation of the *CP1* deletion (VGB316 and VGB317) and *CP1* complementation (VGB489 and VGB490) strains, gDNA of WT and the transformants was cut with *Sal*I while 3' *CP1* region was used as probe.

Plasmid and strain construction of *CP2* single, *CP1/CP2* double deletion and *CP2* complementation strains

Construction of *CP2* (*VDAG_JR2_Chr2g07000a*) deletion strain required amplification of 5' and 3' flanking region of *CP2* with ML94/ML95 (778 bp) and ML96/ML97 (1 343 bp), respectively, of WT gDNA. As resistance cassette to replace the ORF, the HYG^R cassette with ML8/RO3 (3 942 bp) of pPK2 was amplified. All inserts were ligated to pME4564, which was linearized with *Stu*I and *Eco*RV (6 804 bp). The resulting plasmid pME4889 was used to transform *V. dahliae* WT resulting in the *CP2* deletion transformants VGB406 and VGB422. For the complementation, the plasmid pME4890 was constructed by amplifying the *CP2* ORF including its 5' and 3' flanking regions with ML104/ML105 (2 913 bp) of WT gDNA, which was ligated to *Eco*RV linearized pME4815. This construct was utilized to transform *CP2* deletion strain VGB406 resulting in the ectopic complementation transfromants VGB429 and VGB430. Additionally, VGB406 was transformed with pME4887 to generate the Δ*CP1*Δ*CP2* double deletion strains VGB423 and VGB424. All strains were confirmed in Southern hybridizations (Figure S5). To test *CP2* strains gDNA was cut with *Sma*I and correct fragments were detected with 3' *CP2* region as probe resulting in the verification of *CP2* deletion and ectopic complementation strains. For verification of Δ*CP1*Δ*CP2* transformants, gDNA was cut with *Mfe*I or *Hind*III and as probes the 5' flanking region of *CP1* or *CP2* were utilized, respectively.

Plasmid and strain construction of *MEP1* and *MEP2* single and double deletion strains

For the deletion of *MEP1* (*VDAG_JR2_Chr8g09760a*) the annotation of VdLs.17 *MEP1* (*VDAG_03418*) starting 341 bp upstream of the JR2 prediction was considered in addition to the prediction for *V. dahliae* JR2 to make sure the whole gene is deleted. Upstream of this region, 1 500 bp were amplified with JST27/JST28 as 5' flanking region and 3' flanking region of *MEP1* was amplified with JST29/JST30 (1 000 bp) of WT gDNA, respectively. The hygromycin resistance cassette was amplified of pPK2 with ML8/RO3 (3 942 bp). The fragments were ligated together with the pME4564 backbone, which was obtained by PCR amplification with ML1/ML2 (6 727 bp), resulting in pME4891. The deletion construct was introduced into *V. dahliae* WT to obtain the *MEP1* deletion transformants VGB226 and VGB227, which were confirmed by Southern hybridization (Figure S6). Genomic DNA was cut with *Bgl*II and *MEP1* 3' flanking region was used as probe to verify the correct integration of the deletion construct. To generate the *MEP2* (*VDAG_JR2_Chr1g21900a*) deletion strain the 5' and 3' flanking regions of *MEP2* were amplified with ML12/ML13 (960 bp) and ML14/ML15 (1 000 bp) of WT gDNA, respectively and the nourseothricin resistance cassette was obtained by PCR amplification of pME4815 with ML8/ML9 (2 194 bp). The fragments were ligated to the backbone of pME4564, which was generated by PCR amplification with ML1/ML2 (6 727 bp). The resulting plasmid pME4892 was used for construction of the *MEP2* deletion strain by transformation of *V. dahliae* WT. Genomic DNA of transformants and WT was processed with *Sac*I and *MEP2* deletion transformants VGB126 and VGB133 were confirmed by Southern hybridization with 3' *MEP2* as probes (Figure S6). VGB126 was further transformed with pME4891 to obtain the double deletion strain Δ*MEP1*Δ*MEP2*. VGB203 and VGB204 were verified by Southern hybridization with *Kpn*I treated gDNA and 3' *MEP1* as probe or *Nco*I treated gDNA and 3' *MEP2* as probe.

Plasmid and strain construction of *GLA1*, *CBD1 and AMY1* single deletion strains

Plasmids for the generation of *GLA1, CBD1* and *AMY1* deletion strains all contain the nourseothricin resistance cassette, which was obtained by PCR amplification of pME4815 with ML8/ML9 (2 194 bp). 5' and 3' flanking regions of the respective

genes were amplified of *V. dahliae* WT gDNA and, together with *NAT*^{R}, ligated to the backbone of pME4564 that was gained by PCR amplification with ML1/ML2 (6 727 bp).

The *GLA1* (*VDAG_JR2_Chr8g11020a*) deletion construct contains the upstream 5' flanking region amplified with ML20/ML21 (990 bp) and 3' flanking region with ML22/ML23 (1 095 bp). The fragments were ligated to *NAT*^{R} and the backbone of pME4564 resulting in pME4894. After transformation of *V. dahliae* WT with this construct, the resulting transformants were tested for their correct insert by Southern hybridization with *Xho*I treatment of the gDNA and 5' flanking region as probe (Figure S7A). The confirmed *GLA1* deletion transformants VGB129 and VGB130 were conserved.

For the *CBD1* (*VDAG_JR2_Chr4g04440a*) deletion construct the 5' and 3' flanking regions were amplified with ML16/ML17 (982 bp) and ML18/ML19 (996 bp), respectively. Ligating these fragments to the nourseothricin resistance cassette and the pME4564 backbone results in pME4895. This plasmid was used to generate *CBD1* deletion transformants. VGB127 and VGB132 were confirmed by Southern hybridization (Figure S7B). The gDNA was cut with *Pvu*I and 3' flanking region of *CBD1* was used as probe.

Construction of *AMY1* (*VDAG_JR2_Chr7g03330a*) deletion construct involves amplification of the 5' flanking region with ML24/ML25 (1 013 bp) and of the 3' flaking region with ML26/ML27 (814 bp). After amplification of the backbone of pME4564, the inserts and the *NAT*^{R} cassette are ligated together to form pME4896. This construct was utilized for transformation of *V. dahliae* WT resulting in *AMY1* deletion transformants VGB128 and VGB130. The strains were verified by Southern hybridization with *Kpn*I treated gDNA and 3' flanking region as probe (Figure S7C).

2.6 Microbiological methods

2.6.1 Phenotypic analysis

For phenotypic analysis, 50 000 spores were point inoculated on plates containing 100 ml of the desired solid media. As minimal medium Czapek-Dox Medium (CDM, modified from Czapek (1902) and Dox (1910)) [3% (w/v) sucrose, 2% (v/v) 50x AspA (3.5 mM $NaNO_3$, 350 mM KCl, 550 mM KH_2PO_4 (pH 5.5)), 2 mM $MgSO_4$, 1%

(w/v) $FeSO_4$, 2% (w/v) agar] was used for *ex planta* characterization of all constructed *V. dahliae* transformants. For observation of regular vegetative growth, solid SXM and PDM agar plates were included in phenotypic analysis. Additionally, the phenotype on different carbon sources was tested by replacing sucrose in CDM with either cellulose (Carboxymethylcellulose sodium salt), galactose or glucose. Plates were incubated for ten or 14 days at 25°C. Photomicrographic pictures of colonies on agar plates and cross sections of colonies were obtained using the binocular microscope SZX12-ILLB2-200 from OLYMPUS GMBH. Pictures of microsclerotia were taken with Axiolab microscope (ZEISS). The OLYMPUS SC30 digital camera was used together with both microscopes. Pictures were edited with the cellSens software (OLYMPUS GMBH).

2.6.2 Stress tests

For phenotypic analysis of tolerance to oxidative and cell wall stress 50 000 spores were point inoculated on CDM supplemented with 0.00075% (v/v) H_2O_2, 0.004% (w/v) SDS or 1% (v/v) ethanol and characterization of phenotypes was carried out as previously described (2.6.1).

Another approach for analysis of stress tolerance was conducted for *V. dahliae SFL1* deletion strains. Here, 1 000 000 spores were spread on PDM agar plates containing cefotaxime (300 µg/ml). A filter disc was placed in the center of the plate and 10 µl of 10% (v/v) H_2O_2 or 100 mg/ml menadione dissolved in DMSO were pipetted onto the disc. Plates were incubated at 25°C for four days and the inhibition zone was observed of triplicates.

2.6.3 Quantification of melanization

The quantification of melanization was performed for *V. dahliae* colonies grown on 30 ml containing CDM agar plates. In the center of the plate 50 000 spores were point inoculated. Plates were incubated at 25°C for 14 days. Aerial hyphae were removed and top-view pictures were scanned. The brightness of the melanized area was determined with ImageJ (Schindelin *et al*, 2012). The mean value was taken from three plates and normalized to WT. The experiment was repeated three times and significances were calculated by one-way ANOVA and t-test statistical analyses with *SISA* online tool (Uitenbroek, 1997) using standard deviations.

2.6.4 Quantification of conidiospores

Freshly harvested spores were used for this experiment. Conidiospore solutions of 1 x 10^6 spores/ml were determined with the Beckman Coulter Z2 particle counter (BECKMAN COULTER GMBH). Exactly 50 ml liquid SXM were inoculated with 200 µl of the 1 x 10^6 spores/ml spore solutions. Every strain was inoculated in triplicates. Cultures were incubated at 25°C and 125 rpm for five days. Conidia were harvested by filtering cultures through Miracloth. Spores were spun down for 10 min at 3 500 rpm. The centrifugation step was performed at 4°C to keep the spores from germinating. Spore pellets were suspended in 30 ml dH_2O and the spore concentration was determined with the particle counter. The experiment was repeated at least three times and significances were calculated as described in 2.6.3.

2.6.5 Fluorescence microscopy

Fluorescence microscopy was performed to investigate subcellular localization of proteins and to select positive transformants expressing free *GFP*. Strains were grown in an 8-well chambered coverslip system (IBIDI GMBH) with approximately 1 000 000 spores inoculated in 300 µl liquid PDM per well. The well chamber was incubated at 25°C overnight before GFP signals were detected the following day.
Nuclei were visualized with 4′,6-diamidino-2-phenylindole (DAPI from CARL ROTH GMBH & CO. KG). On glass cover slips 500 µl liquid PDM were inoculated with spores and incubated at 25°C overnight. The droplets were transferred to 1.5 ml tubes and spun down. The pelleted mycelia were resuspended in 0.5% (v/v) DAPI staining solution (dissolved in staining buffer [100 mM Tris-HCl (pH 7), 150 mM NaCl, 1 mM $CaCl_2$, 1% (v/v) Nonidet^{TM} P-40 from SIGMA-ALDRICH]) and washed with dH_2O after 15 min before fluorescence signals were monitored.
Fluorescence signals were detected with a Zeiss AxioObserver Z.1 inverted confocal microscope, equipped with Plan-Neofluar 63x/0.75 (air) objectives (ZEISS) and QuantEM:512SC digital camera (PHOTOMETRICS, Tucson, AZ, USA). The SlideBook 6.0 software (INTELLIGENT IMAGING INNOVATIONS, Göttingen, Germany) was used for picture processing.

2.6.6 Plant infection assays

2.6.6.1 *Solanum lycopersicum* infection assay with *Verticillium dahliae*

To evaluate the virulence of *V. dahliae,* plant infections with *S. lycopersicum* (Moneymaker) as host plants were conducted. Seeds were sterilized by incubation in 70% (v/v) EtOH, 0.05% Tween 20 for 5 min while shaking and another 5 minutes shaking incubation in 96% (v/v) EtOH. Seeds were dried and distributed on a damp sand:soil (1:1) mixture (DORSILIT, ARCHUT GMBH & CO. KG). Tomato plants were grown in a climate chamber at long day conditions with 16 hours of light (fluorescence: 60, GroLEDs: 100, illumination: 95µmol) at 25°C and eight hours in the dark at 22°C. After ten days the tomato seedlings were root-inoculated by incubating the roots in 50 ml spore solutions of 10^7 spores/ml for 40 min under constant agitation at ~35 rpm. Mock control plants were treated similarly with dH_2O. Treated seedlings were planted in 70x70x80 mm planting pots with a sand:soil (1:1) mixture (DORSILIT, ARCHUT GMBH & CO. KG) and 3 000 000 spores or 3 ml dH_2O for mock plants were added to the soil. For each strain or control 15 plants were infected. Plants were incubated in the climate chamber at long day conditions for another 21 days before disease symptoms were scored.

Disease scoring

At 21 days post inoculation the following measures were taken: fresh weight of the aerial parts, the length of the longest leaf and the height of the vegetation point. These parameters were calculated into a disease score ranking relative to uninfected mock plants. The mean values of mock plants of each parameter were set to 100%. All values from 80% and above were assigned the disease score 1 (‘healthy’), 60-79% scored 2 (‘mild symptoms’), 40-59% scored 3 (‘strong symptoms’), lower than 40% scored 4 (‘very strong symptoms’) and dead plants scored 5. The scores for each strain were visualized in a stack diagram displaying the number of plants per disease score relative to the total amount of tested plants from all experiments. As another measure the discoloration of the tomato hypocotyl was observed with a binocular microscope SZX12-ILLB2-200 from OLYMPUS GMBH.

Stem assay

All treated plants were tested for fungal outgrowth 21 days after infection. The tomato stems were surface sterilized by incubation in 70% (v/v) EtOH for eight minutes, followed by 6% (v/v) sodium hypochlorite solution for eight minutes and two washing steps with dH_2O. Dismissing the outer parts of the sterilized stems the stem was sliced and pieces were placed on PDM agar plates containing 100 µg/ml chloramphenicol. Plates were incubated at 25°C for seven days and the fungal outgrowth was observed.

2.6.6.2 *Arabidopsis thaliana* root colonization assay

Infections of *Arabidopsis thaliana* Col-0 seedlings with *V. dahliae* strains overexpressing free *GFP* enabled the monitoring of the hyphal growth on the roots by fluorescence microscopy. The assay was performed based on the protocol described in Bui *et al*, 2019. Seeds were sterilized with a five-minute washing step in 70% (v/v) EtOH, 0.05% Tween 20, followed by another five minutes in 96% (v/v) EtOH. The seeds were then dried in a 1.5 ml tube at 35°C. Seeds were sown on Murashige and Skoog (MS) agar (Murashige & Skoog, 1962) [0.22% MS including vitamins (DUCHEFA BIOCHEMIE, Haarlem, Netherlands), 0.05% MES monohydrate (CARL ROTH GMBH & CO. KG), 1% sucrose and 1.5% plant agar (DUCHEFA BIOCHEMIE), pH 5.7], incubated at 4°C overnight and then incubated in the climate chamber at long day conditions. Three weeks later the seedlings were transferred to water agarose (1% w/v) plates for overnight incubation. Then the seedlings were root-inoculated. The roots were incubated in spore solutions with 100 000 spores/ml for 35 minutes and then placed on water agarose again. The root part of the plate was covered in aluminum foil to shade the roots. The plates were further incubated in the plant chamber and colonization on the roots was monitored at indicated time points. The root was incubated in a staining solution [0.0025% (v/v) propidium iodide, 0.005% (v/v) silwet] for five minutes in the dark. Then the roots were placed on an object slide with 200 µl H_2O and 20 µl staining solution. RFP signals of the stained root and GFP signals of the fungal hyphae were monitored by fluorescence microscopy.

2.7 Protein methods

2.7.1 Protein extraction

For general western hybridization analysis strains were grown in liquid PDM or SXM cultures. Mycelia were harvested through sterile Miracloth filter, rinsed with 0.96% NaCl solution, dried and directly frozen in liquid nitrogen. For time point experiments with GFP-Sfl1 fusion protein, the fungus was additionally grown on SXM agar plates overlaid with Amersham™ Hybond™-N nylon membranes (GE HEALTHCARE) which allowed to easily scrape off the mycelia (Neumann & Dobinson, 2003). The mycelia were dried and frozen in liquid nitrogen. Frozen mycelia were ground in liquid nitrogen with a mortar and pestle or small amounts were ground with a table mill (RETSCH TECHNOLOGY GMBH). Similar amounts of powder were mixed with B* buffer [300 mM NaCl, 100 mM Tris (pH 7.5), 10% glycerol, 1 mM EDTA, 0.02% NP-40) supplemented with 2 mM DTT, 10 µl/ml (v/v) complete EDTA-free protease inhibitor cocktail (ROCHE; stock solution: one tablet in 500 µl dH_2O) and centrifuged for 20 min at 13 000 rpm at 4°C. Supernatants were transferred into fresh test tubes and protein concentrations were measured with Bradford.

2.7.2 Protein precipitation of extracellular proteins

For the exoproteome comparison *V. longisporum* 43 was cultivated as described in 2.2.2.2. Proteins of the supernatant were precipitated with TCA/acetone. To 45 ml of the supernatant 5 ml of 10% trichloroacetic acid (w/v) in acetone were added and incubated at 4°C overnight. This mixture was centrifuged at 4 000 rpm for 60 min at 4°C. The protein sediment was washed three times with 80% (v/v) acetone and once with 100% (v/v) acetone and then resolved in 8 M urea/ 2 M thiourea.

2.7.3 Determination of protein concentration by Bradford assay

Protein concentrations were determined based on the Bradford assay (Bradford, 1976). As Coomassie Brilliant Blue-G250 containing dye Roti®-Quant from CARL ROTH GMBH & CO. KG was purchased and used according to manufacturer's instructions. Binding of the dye to the protein leads to a shift in absorption to 595 nm, which was measured with the Infinite M200 microplate reader and data

were evaluated with Magellan software from TECAN TRADING AG. For calibration standard the bovine serum albumin (BSA) from CARL ROTH GMBH & CO. KG was used.

2.7.4 SDS-PAGE

Proteins were subjected to sodium dodecyl sulfate polyacrylamide gel electrophoresis (SDS-PAGE) gels to separate them by their molecular weight. By applying an electrical field small molecular weight proteins migrate faster through the polyacrylamide gel than proteins with high molecular weight (Laemmli, 1970). Protein extracts were mixed with SDS sample buffer [250 mM Tris-HCl (pH 6.8), 15% (v/v) β-mercaptoethanol, 30% (v/v) glycerol, 7% (w/v) SDS, 0.3% (w/v) bromophenol blue]. The protein mixtures were denatured at 95°C for ten minutes. SDS gels (12%) consist of a short stacking gel [1.835 ml H_2O, 313 µl 1 M Tris (pH6.8), 15 µl 10% (w/v) SDS, 333 µl 30% (v/v) acrylamide, 5 µl N,N,N′,N′-tetramethylethane-1,2-diamine (TEMED), 30 µl 10% (w/v) ammonium persulfate (APS)] and a longer separation gel [1.05 ml H_2O, 1.875 ml 1 M Tris (pH 8.8), 50 µl 10% (w/v) SDS, 2 ml 30% (v/v) acrylamide, 5 µl TEMED, 25 µl 10% (w/v) APS]. For proteins larger than ~80 kDa, 8% SDS gels were used where acrylamide is reduced to 8%. SDS gels were placed in running buffer [25 mM Tris, 250 mM glycerol, 0.1% (w/v) SDS] in Mini-Protean® Tetra Cell (BIO-RAD LABORATORIES GMBH). Proteins were loaded onto the SDS gels and Prestained Protein Ladder (THERMO FISHER SCIENTIFIC) was used as size marker.

2.7.5 Western hybridization

Equal amounts of protein extracts were separated by SDS-PAGE. By western hybridization the proteins on the gel were transferred to a nitrocellulose membrane (Amersham™ Protran™ 0.45 µm NC nitrocellulose blotting membranes from GE HEALTHCARE) in transfer buffer [25 mM Tris, 192 mM glycerol, 0.02% (w/v) SDS, 20% (v/v) methanol] using Trans-Blot® Electrophoretic Cell with the PowerPac™ 3000 power supply from BIO-RAD LABORATORIES GMBH. Blotting took place either at 35V at room temperature overnight or ice-cooled at 100V for 90 minutes. The following steps were all performed under constant agitation. Membranes were stained with Ponceau S (3% (v/v) trichloroacetic acid, 0.2% (w/v) Ponceau S) for visualization of transferred proteins as loading control (Romero-Calvo *et al*, 2010).

The membrane was blocked by a one-hour incubation in 5% (w/v) skim milk powder (SUCOFIN TSI GMBH & CO. KG) in TBS-T [10 mM Tris-HCl (pH 8), 150 mM NaCl, 0.05% (w/v) Tween 20]. Next, the membrane was probed with the primary antibody α-GFP (sc-9996, SANTA CRUZ BIOTECHNOLOGY) during incubation overnight at 8°C. Of the primary antibody 1:250 or 1:500 dilutions in TBS-T buffer with 5% (w/v) milk powder were used for endogenous expression or overexpression, respectively. Following, membranes were washed three times for 10 minutes in TBS-T. Then horseradish peroxidase-coupled α-mouse antibody (115-035-003, JACKSON IMMUNORESEARCH) was applied as secondary antibody in a dilution of 1:1500 or 1:2000 in TBS-T buffer with 5% (w/v) milk powder for extracts from strains with endogenous expression or overexpression of *GFP*, respectively. The membranes were incubated in the secondary antibody for at least one hour. Three ten-minute washing steps with TBS-T buffer followed the antibody probing. Subsequently, detection of chemiluminescent signals was conducted with horseradish peroxidase substrate luminol based chemiluminescence. A 1:1 mixture of detection solution A [2.5 µM luminol, 400 µM paracoumarat, 100 mM Tris-HCl (pH 8.5)] and detection solution B [5.4 mM H_2O_2, 100 mM Tris-HCl (pH 8.5)] was applied to the membrane for a two-minute incubation in the dark. Signals were detected with an Amersham™ Hyperfilm™-ECL film (GE HEALTHCARE), which was developed with the Optimax® X-ray Film Processor from PROTEC GMBH & CO. KG.

2.7.6 Tryptic digestion, mass spectrometry analysis and exoprotein identification

For protein analysis with liquid chromatography – tandem mass spectrometry (LC-MS/MS), 30 µg of the extracellular protein extract was separated by SDS-PAGE 2.7.4. The gels were incubated for 1h in fixing solution [40% (v/v) EtOH, 10% (v/v) acetic acid] and then washed twice for 20 min with dH_2O. Gels were colloidal Coomassie stained [0.12% (w/v) Coomassie Brilliant Blue-G250, 5% (w/v) aluminum sulfate-(14-18)-hydrate, 10% (v/v) methanol, 2% (v/v) orthophosphoric acid (85%)]. For each growth condition one lane was cut into ten pieces of equal size, which was subsequently *in-gel* digested with trypsin to cut the proteins into small peptides and make them accessible for LC-MS/MS analysis (Shevchenko *et al*, 1996). The gel pieces were incubated in acetonitrile for 10 minutes under constant agitation. The supernatant was discarded and gel pieces were dried using

the SpeedVac Concentrator (Savant SPD 111V from THERMO FISHER SCIENTIFIC). The gel pieces were then incubated in 10 mM DTT solved in 100 mM ammonium bicarbonate (NH_4HCO_3) for one hour at 56°C on a heating block to denature and reduce disulfide bonds of the proteins. After removal of the DTT solution, pieces were covered with 55 mM iodacetamide solution for cysteine alkylation at room temperature for one hour in the dark. The solution was removed and three washing cycles with alternating 100 mM NH_4HCO_3 and acetonitrile for 10 min each followed. Supernatants were discarded after every step. The gel pieces were dried in the SpeedVac for ten minutes at 55°C and the trypsin solution (Trypsin NB Sequencing Grade (PROMEGA GMBH) prepared according to manufacturer's specifications) was added for an incubation period of 45 min on ice. The supernatant was discarded and the gel pieces were incubated in 25 mM NH_4HCO_3 at 37°C overnight. The supernatants of the following steps were collected in a Protein LoBind tube (EPPENDORF AG). First, the pieces were covered in 20 mM NH_4HCO_3 and incubated for ten minutes under constant agitation. Then the gel pieces were incubated in 50% acetonitrile, 5% formic acid solution for 20 min at room temperature under agitation and then spun down at 13 000 rpm for one minute to separate and collect the supernatant. Latter step was repeated three times. The collected supernatants were dried completely in the SpeedVac. The dried samples were resolved in a resuspension buffer [2% (v/v acetonitrile, 0.1% (v/v) formic acid]. Resulting tryptic peptide mixtures were separated by a reversed-phase liquid chromatographic column (Acclaim PepMap RSLC column, 75 µm x 15 cm, C18, 3 µm, 100 Å, P/N164534, THERMO FISHER SCIENTIFIC) to further reduce sample complexity prior to mass analyses with an LTQ Velos Pro mass spectrometer (THERMO FISHER SCIENTIFIC). To identify matches of the peptides, the draft genome-wide protein sequence database of *V. longisporum*, VertiBase (http://biofung.gobics.de:1555/; coordinated by Prof. Dr. Gerhard H. Braus, Georg-August-Universität Göttingen), was used. The analysis was performed by a Thermo Proteome Discoverer™ (version 1.3) workflow that integrates Sequest and Mascot search engines. The search was performed with an initial precursor mass tolerance of 10 ppm and fragment mass tolerance of 0.8 Da Carbamidomethylcysteine was used as a fixed modification, oxidized methionine was included as variable modification and two miscleavages were allowed for each

peptide. For peptide and protein validation, a 0.5% false discovery rate was set and determined by using peptide validator with a reverse decoy database. Resulting lists of identified proteins were semi-quantitatively processed by a statistical workflow using MarVis Suite (Kaever *et al*, 2012). The data set was annotated using the online database VertiBase. Proteins were ranked according to the positive directed signal-to-level (s/l) ratio using as maximum the SXM and XyS conditions. Proteins with an s/l ratio above 0.3 were considered as candidates with higher intensities in that medium compared to the rest and therefore belong to the specifically enriched proteins in the corresponding medium whereas proteins below a s/l ratio of 0.3 were considered not to be specifically enriched and belong to the shared core proteome.

2.8 Computational methods

Sequences, gene predictions and accession numbers for *Verticillium* were retrieved from Ensembl Fungi (Kersey *et al*, 2018) and VertiBase (http://biofung.gobics.de:1555/; coordinated by Prof. Dr. Gerhard H. Braus, Georg-August-Universität Göttingen). Sequences of other fungal species were obtained from National Center for Biotechnology Information (NCBI) (Geer *et al*, 2010). Multiple sequence alignments were performed using Clustal Omega (Madeira *et al*, 2019). Motif prediction was performed with InterProScan (Jones *et al*, 2014). Nuclear localization signal (NLS) prediction was conducted with the NLS mapper software (Kosugi *et al*, 2009) and subcellular localization was predicted with DeepLoc-1.0 (Almagro Armenteros *et al*, 2017).

SeqBuilder (DNASTAR, Madison, USA) or SnapGene (GSL Biotech LLC) software were used for plasmid and primer design and prediction of enzyme restriction reactions. Annealing temperatures of primers were calculated with the online NEB Tm Calculator (NEW ENGLAND BIOLABS). Sanger sequencing of plasmid DNA or PCR products was performed by the Microsynth Seqlab in Göttingen.

3 Results

3.1 Microsclerotia formation of *V. dahliae* is controlled by the light regulator Frq (Frequency) and by Sfl1 (suppressor of flocculation)

Microsclerotia development is crucial for the long-term survival of *V. dahliae* as these clustered, melanized hyphae enable the fungus to persist in the soil without a host for more than a decade (Wilhelm, 1955). Upon stimulation by e.g. root exudates, microsclerotia start germinating and *V. dahliae* grows towards the root to initiate the infection cycle (Schnathorst, 1981). Therefore, infection success of *V. dahliae* depends on microsclerotia survival. In this study, two regulators of microsclerotia production were investigated.

3.1.1 *V. dahliae* Frq is a light-dependent repressor for microsclerotia formation

3.1.1.1 *V. dahliae* possesses a *FRQ* homolog

Microsclerotia production depends on different external stimuli such as nutrient availability and light (Brandt, 1964; Klimes *et al*, 2008; Heale & Isaac, 1965). Light delays formation of microsclerotia in most *Verticillium* isolates (Brandt, 1964). However, light sensing of *V. dahliae* is poorly understood although the genome contains homologs to all the light-responsive elements required for the circadian clock as described for *N. crassa* and other filamentous fungi (Montenegro-Montero *et al*, 2015; Salichos & Rokas, 2010). *V. dahliae* even harbors the *FREQUENCY* (*FRQ*) gene, which is only well conserved among the Sordariaceae (Dunlap & Loros, 2006). Frq is known as the pace maker of the circadian clock as described for *N. crassa* (Dunlap & Loros, 2006; Montenegro-Montero *et al*, 2015). Furthermore, Frq responds to light stimuli (Crosthwaite *et al*, 1995), thus, was subject to our investigations on microsclerotia formation depending on light.

The protein sequence of the well characterized *N. crassa* FRQ (XP_011395125.1) was used to search against the *V. dahliae* JR2 proteome (Ensembl Fungi) to identify the *V. dahliae* Frq encoding gene *VDAG_JR2_Chr1g01960a*. BLAST search and similarity of pairwise and multiple sequence alignments of corresponding Frq homologs in other Ascomycetes were calculated to show the amino acid sequence conservation between the different fungi (Figure 6A). While all Frq proteins of the Sordariomycetes (*N. crassa*, *M. oryzae*, *Fusarium*

oxysporum, *Trichoderma reesei* and *V. dahliae*) share a relatively high degree of amino acid sequence identity (between 42 and 53%), they only share about 30% to the corresponding protein in *B. cinerea* from the Leotiomycetes. *V. dahliae* Frq was compared to *N. crassa* FRQ in more detail. The full-length protein of *V. dahliae* (983 aa) is similar in length to *N. crassa* FRQ (989 aa) and both Frequency clock proteins (PF09421) are recognized as such by InterProScan revealing an incorporated coiled coil region (Figure 6B).

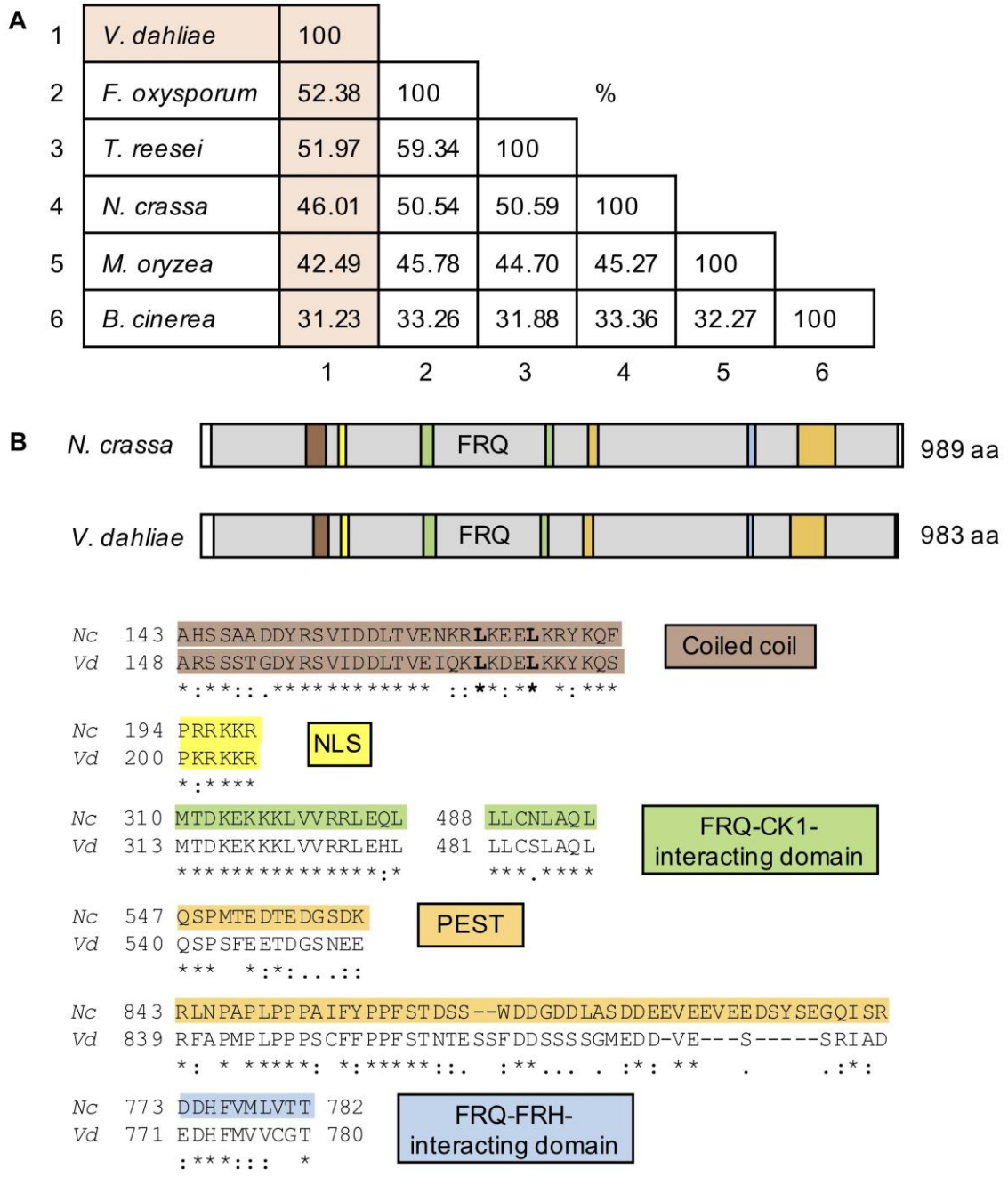

Figure 6. Comparison of circadian oscillator Frq in *V. dahliae*, *N. crassa* and other fungi.
(A) Protein sequence identity matrix of *V. dahliae* Frq and corresponding proteins in related Ascomycetes is shown in %. The matrix includes *N. crassa* (XP_011395125.1), *M. oryzae* (QBZ62296.1), *V. dahliae* (VDAG_JR2_Chr1g01960a), *F. oxysporum* (RKK71427.1), *T. reesei* (XP_006965164.1) from the Sordariomycetes and *B. cinerea* (XP_001547609.1) from the Leotiomycetes. Amino acid sequences were retrieved from NCBI database. The multiple sequence alignment was performed using Clustal Omega (Madeira *et al*, 2019). **(B)** The protein structures of *N. crassa* FRQ and *V. dahliae* Frq were analyzed by InterProScan assigning both proteins to the Frequency clock protein family (PF09421, grey), which incorporates a coiled coil region (brown). The nuclear localization signals (NLS) predicted by the NLS mapper software (Kosugi *et al*, 2009) are indicated in yellow. Additional motifs that were described in *N. crassa* (*Nc*) (Traeger & Nowrousian, 2015) are highlighted and alignments with corresponding amino acid sequences in *V. dahliae* (*Vd*) Frq by Clustal Omega are shown to display the level of conservation: FCD1 and 2 (FRQ-CKI)-interacting domain (green), PEST-1 and 2 (orange), FFD (FRQ-FRH-interacting domain, blue). Asterisks (*): fully conserved residue; colon (:): conserved between groups of strongly similar properties, period (.): conserved between groups of weakly similar properties.

With NLS mapper software (Kosugi *et al*, 2009) a nuclear localization signal (NLS) was assigned to both proteins . Amino acid sequence alignments of these regions in *N. crassa* FRQ and *V. dahliae* Frq show that the coiled coil region and the NLS are well conserved between these two fungi. The coiled coil motif includes two leucines important for protein binding that are also found in *V. dahliae*. Additional motifs of FRQ that are involved in its regulation are well characterized in *N. crassa*: FRQ-CK1-interacting domains (FCD), PEST motifs and FRQ-FRH (Frequency-interacting RNA helicase)-interacting domain (FFD) (Montenegro-Montero *et al*, 2015; Traeger & Nowrousian, 2015; Querfurth *et al*, 2011; Guo *et al*, 2010). Protein sequence alignments of *V. dahliae* Frq and *N. crassa* FRQ show a high conservation of the functionally important motifs suggesting that the complex roles of these domains in *N. crassa* FRQ may also be assigned to the corresponding protein in *V. dahliae* and may be involved in clock functions and light signaling. Until now, no circadian rhythmicity of developmental growth under constant light conditions has been observed for *V. dahliae*. Thus, as first objective, the role of Frq dependent on light was investigated.

3.1.1.2 *V. dahliae* Frq represses microsclerotia formation in the light

The deletion strain of *FRQ* was constructed to elucidate its function in *V. dahliae* development and virulence. The full *FRQ* open reading frame (ORF) was replaced

by a nourseothricin resistance cassette (*NAT*^{R}) by homologous recombination resulting in the Δ*FRQ* (*NAT*^{R}) strain. To complement this strain, the *FRQ* ORF including 5' flanking and 3' flanking regions was ectopically integrated into the deletion strain. Correct integration of the constructs was confirmed by Southern hybridization (Figure S2).

Vegetative growth of the *FRQ* deletion strain was tested under constant light or darkness at 25°C or under light:dark and 25°C:22°C cycles. Spores were point inoculated on different media and grown for 14 days. The most prominent phenotypes are depicted in Figure 7A. When grown on minimal medium under light, Δ*FRQ* strain exhibits an increased melanized colony center compared to *V. dahliae* WT and the complementation strain (*FRQ*-C). This effect was abolished when the fungus was incubated in the dark as WT and *FRQ*-C strains also showed stronger melanized colony centers compared to growth in the light. Another difference was observed in production of aerial hyphae on simulated xylem medium (SXM) in the light. WT and *FRQ*-C strains exhibit dense aerial hyphae formation of which Δ*FRQ* produces fewer. Similar to the microsclerotia effect, the difference of aerial hyphae production was only visible when grown at constant light, as overall aerial hyphae formation was reduced in WT and *FRQ*-C strains. The *V. dahliae* Δ*FRQ ex planta* phenotype was further tested under growth conditions closer to plant infection situation, incubating the fungus in light:dark cycles on SXM plates (Figure 7B). *V. dahliae* WT produced concentric zones of greater and lesser density of microsclerotia and aerial hyphae. Rings with more microsclerotia production seemed to exhibit less aerial hyphae density whereas zones with less microsclerotia exhibit higher aerial hyphae density.

This corresponds to alternating phenotypes observed under constant light and dark conditions for the WT. These alternating concentric zones are almost abolished in Δ*FRQ*. The light:dark incubation was also analyzed on minimal and complete medium where no alternating rings of developmental structures were observed for both strains (Figure S8). Overall aerial hyphae formation of the WT colony on CDM is stronger than of the deletion strain. On PDM the *FRQ* deletion strain formed a larger dark area of melanized microsclerotia and fewer aerial hyphae.

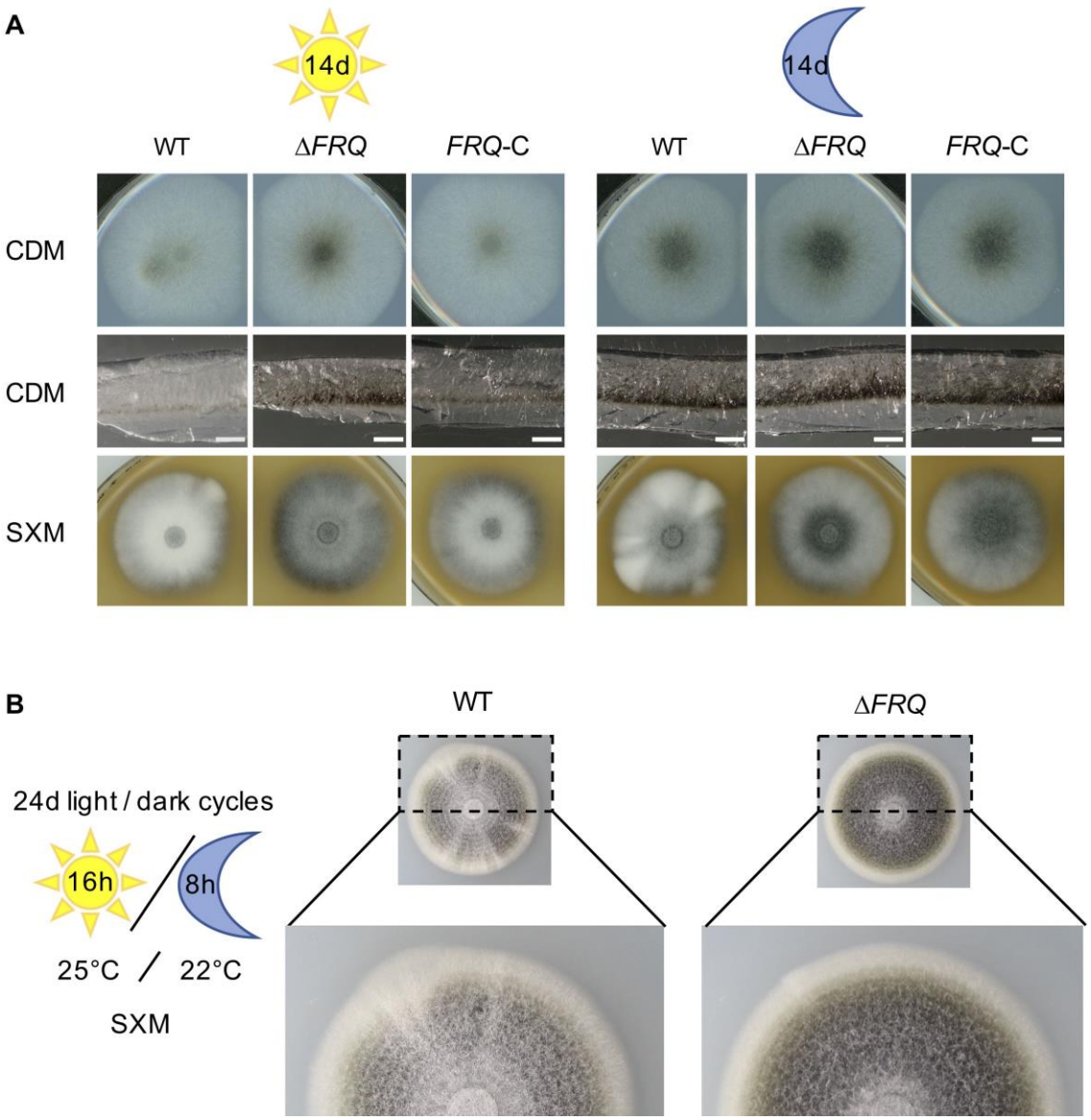

Figure 7. *V. dahliae* Frq represses microsclerotia formation in the light.
(A) 50 000 spores of *V. dahliae* JR2 (WT), *FRQ* deletion (VGB296, Δ*FRQ* containing a nourseothricin resistance cassette (*NAT*^{R})) and *FRQ* complementation strain (*FRQ*-C – VGB411) were point inoculated on minimal medium (CDM) and simulated xylem medium (SXM) and incubated at 25°C for 14 days in light or in the dark as indicated by a sun or moon, respectively. Top-view scans of the colony (1st and 3rd rows) and cross sections of the colony center (2nd row) show the enhanced microsclerotia production of Δ*FRQ* compared to WT and the complementation strain when grown in the light. In the dark no difference in microsclerotia production was observed for the *FRQ* deletion strain in comparison to WT and the *FRQ* complementation strain, which produce more microsclerotia than in light. Scale bars = 1 mm. **(B)** 50 000 spores of *V. dahliae* JR2 (WT) and *FRQ* deletion strain were point inoculated on SXM and incubated for 14 days with cycles of 16 h of light at 25°C and 8 h of darkness at 22°C. Top views of the colonies display the different phenotypes. Close up views of the colonies show that WT growth results in a more prominent ring-like structure than *FRQ* deletion strain.

Together, these results suggest that *V. dahliae* senses light and represses the production of microsclerotia during incubation in light. The *FRQ* deletion mutant is unable to reduce the microsclerotia production to WT-level and, hence, is involved in light-dependent microsclerotia repression.

3.1.2 The transcription factor Sfl1 is a light-independent activator of *V. dahliae* microsclerotia formation

3.1.2.1 The *SFL1* gene encodes a protein containing a heat shock factor-type DNA-binding domain

Another potential developmental regulator was characterized in parallel, namely Sfl1 (suppressor of flocculation). In previous studies, *V. dahliae SOM1* and *VTA3*, homologs of yeast *FLO8* and *RFX1*, respectively, were identified as genes encoding for positive regulators of microsclerotia production (Bui *et al*, 2019). Som1 and Vta3 are involved in numerous developmental programs and are required for sequential steps in plant root infections. While deletion of *SOM1* leads to the inability of *V. dahliae* to produce microsclerotia, deletion of *VTA3* only reduces microsclerotia formation (Bui *et al*, 2019). Vta3 regulates *SFL1* gene expression, thus, Sfl1 might function in between Vta3 and activation of microsclerotia biosynthesis. In yeast, Sfl1 is a well characterized repressor of several genes by interacting with the repressor complex Ssn6(Cyc8)-Tup1, which as well interacts with Rfx1 to inhibit the transcription of target genes (Conlan & Tzamarias, 2001). Sfl1 additionally activates gene expression in yeast (Ansanay Galeote *et al*, 2007). Thus, the role of Sfl1 in *V. dahliae* was analyzed concentrating on the role of microsclerotia production and virulence on tomato.

The sequence of *S. cerevisiae SFL1* (SGD: S000005666) was retrieved from the *Saccharomyces* Genome Database (SGD) (Cherry *et al*, 2012). BLAST search of the amino acid sequence against the *V. dahliae* JR2 proteome (Ensembl Fungi) (Kersey *et al*, 2018) revealed that *VDAG_JR2_Chr4g02790a* codes for Sfl1 in *V. dahliae*. On protein level *S. cerevisiae* Sfl1 and *V. dahliae* Sfl1 only share 28% identity whereas a search for protein domains with InterProScan (Jones *et al*, 2014) detected a heat shock factor-type DNA-binding domain (HSF, PF00447) in both proteins (Figure 8). Additionally, analysis with NLS mapper software (Kosugi *et al*, 2009) proposed an NLS at the C-terminal end of the HSF domains indicating that both proteins may have a nuclear function. When comparing specifically the HSF

domain, the sequence similarity with 59% amino acid identity is higher and shows that the Sfl1 characteristic domain is conserved in *V. dahliae*. In yeast, Sfl1 functions as an activator and repressor (Conlan & Tzamarias, 2001; Ansanay Galeote *et al*, 2007), thus, it is intriguing to test the regulatory role of Sfl1 in *V. dahliae*.

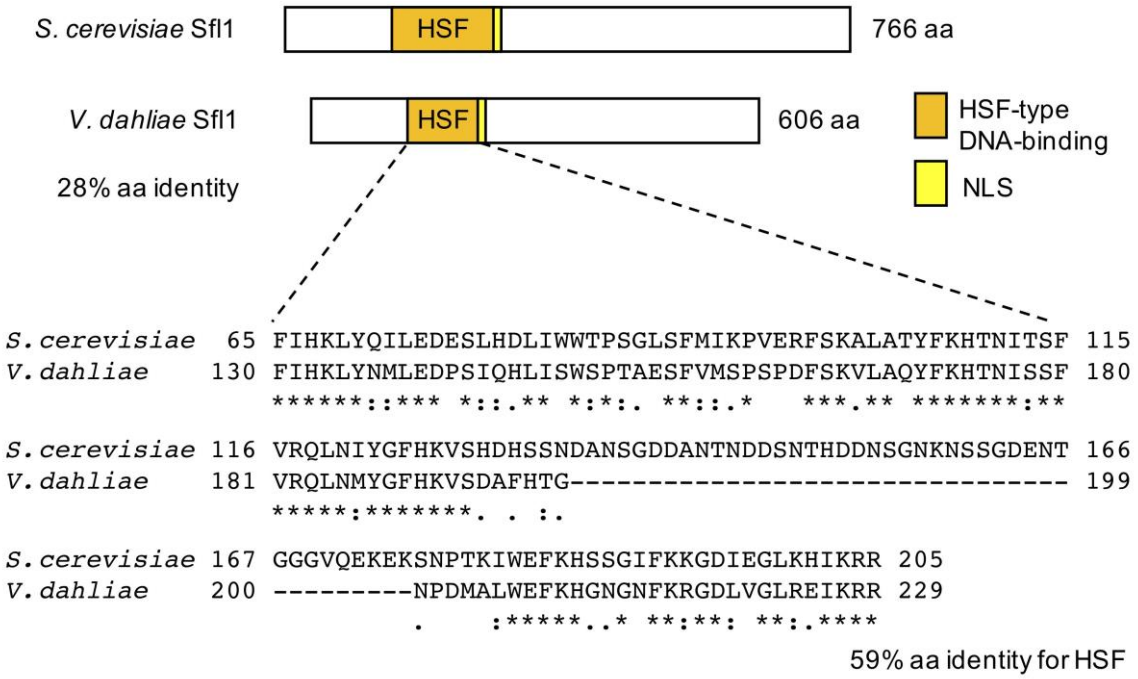

Figure 8. Comparison of the protein structure of *S. cerevisiae* and *V. dahliae* Sfl1. The protein structures of *V. dahliae* Sfl1 (VDAG_JR2_Chr4g02790a) and *S. cerevisiae* Sfl1 (SGD: S000005666) are shown in comparison. The nuclear localization signals (NLS) predicted by the NLS mapper software (Kosugi *et al*, 2009) are indicated in yellow and the heat shock factor-type DNA-binding domain (HSF, PF00447) in orange. Protein domains were predicted by InterProScan. Clustal Omega (Madeira *et al*, 2019) was used for the sequence alignment of the *V. dahliae* and *S. cerevisiae* HSF domains. Asterisks (*): fully conserved residue; colon (:): conserved between groups of strongly similar properties, period (.): conserved between groups of weakly similar properties.

3.1.2.2 Nuclear Sfl1 is required for microsclerotia production in *V. dahliae*

For analysis of the role of Sfl1 in *V. dahliae* an *SFL1* deletion strain (Δ*SFL1*) was constructed and phenotypically examined. The full *SFL1* ORF was replaced with a nourseothricin resistance cassette by homologous recombination with the WT strain. The *SFL1* ORF flanked with 5' and 3' regions was ectopically integrated into

the deletion strain to test if the deletion phenotypes could be complemented. Strains were verified by Southern hybridization (Figure S3).

The *SFL1* deletion strain produces no visible amounts of microsclerotia when grown on minimal or complete medium for 14 days (Figure 9). *V. dahliae* WT exhibits production of melanized microsclerotia on minimal medium when grown in the light. This phenotype is restored in the *SFL1* complementation strain (*SFL1*-C). Cross sections of the colony center of Δ*SFL1* on minimal medium do not show any dark structures whereas for WT and *SFL1*-C black structures can be observed in the agar. Zooming into the picture, on microscopic level these black structures are recognized as microsclerotia, which are clusters of pigmented hyphal cells (Heale & Isaac, 1965). Without *SFL1*, *V. dahliae* was impaired in producing mature microsclerotia under these conditions. Before forming melanized microsclerotia, hyphal cells start to swell and cluster together before becoming pigmented (Hall & Ly, 1972), which can be observed for the *SFL1* deletion strain. Here, pigmented microsclerotia are scarce and more non-pigmented initial microsclerotia structures can be seen as displayed in the microscopic view. As experiments with the *FRQ* deletion strain exhibited that incubation in the dark resulted in enhanced microsclerotia production of the WT strain, depletion of light was also tested on the *SFL1* deletion strain. Intriguingly, incubation in the dark led to stronger microsclerotia production in all strains. The colonies of WT and *SFL1*-C strains show a larger melanized area. Cross sections as well as microscopic views also indicate a denser production of melanized microsclerotia. In the dark, the *SFL1* deletion strain also produces microsclerotia, which can be observed in the cross section of the colony center.

This suggests that depletion of *SFL1* clearly compromises microsclerotia formation but does not disable the strain to produce microsclerotia. Furthermore, growth phenotypes on PDM and SXM exhibit differences. On PDM, incubation in light and darkness leads to excessive formation of aerial mycelia in the absence of *SFL1* whereas WT and *SFL1*-C strains produce moderate amounts when incubated in the light and even less amounts in the dark. On SXM, in contrast, aerial hyphae of the *SFL1* deletion strain have a less dense appearance compared to WT and *SFL1*-C in the light and incubation in the dark leads to a decreased formation of aerial hyphae in all strains. The alterations in aerial hyphae production show that deletion of *SFL1* results in higher aerial hyphae formation on PDM and slightly less

formation on SXM in the light. The strongest phenotype of the *SFL1* deletion strain, however, was observed in microsclerotia formation, in which Sfl1 functions as a positive regulator.

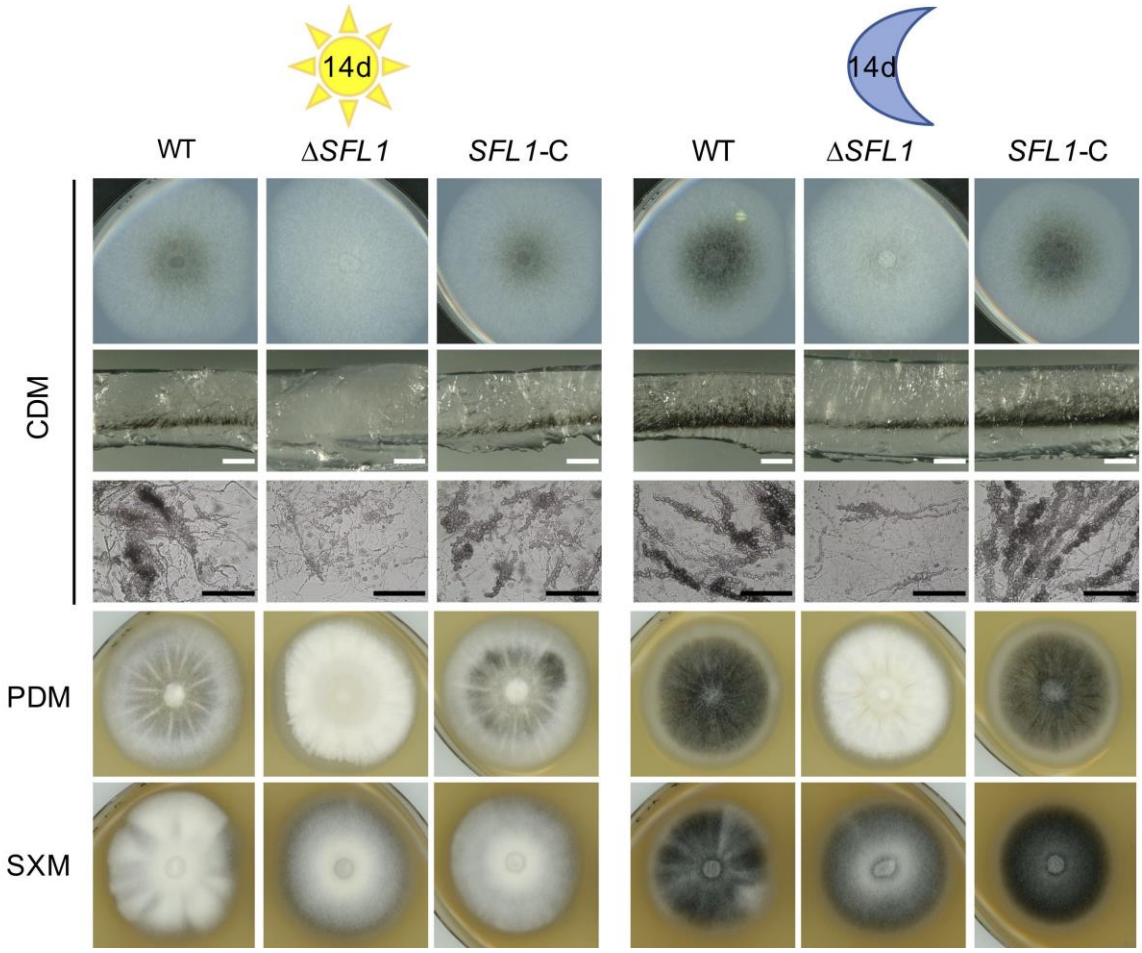

Figure 9. The transcription factor Sfl1 is required for *V. dahliae* microsclerotia formation.
50 000 spores of *V. dahliae* JR2 wildtype (WT), *SFL1* deletion (Δ*SFL1* – VGB324) and complementation strain (*SFL1*-C – VGB342) were point inoculated on different media and incubated at 25°C for 14 days in the light (left panel) or in the dark (right panel). Top-view scans of the colonies (1st row) on minimal medium (CDM), cross sections of the colony center (2nd row) and microscopic views (3rd row) display the decrease of microsclerotia production of Δ*SFL1.* Top-view scans of the colonies on potato dextrose medium (PDM, 4th row) and simulated xylem medium (SXM, 5th row) show the differences in aerial hyphae growth. White scale bars = 1 mm, black scale bars = 100 µm.

Consistent with the idea of a transcriptional regulator should be a nuclear localization of the Sfl1 protein. This idea is supported by the presence of the NLS sequence within the HSF domain of Sfl1 (Figure 8). To investigate on the localization of Sfl1, *SFL1* N- or C-terminally fused to *GFP* was ectopically

overexpressed in the *SFL1* deletion background (*GFP-SFL1* OE and *SFL1-GFP* OE, respectively). The overexpression ensures expression of sufficient amounts of the fusion protein that can be detected by fluorescence microscopy. The constructed strains were verified by Southern hybridization (Figure S1).

GFP-SFL1 or *SFL1-GFP* OE strains were phenotypically analyzed to see whether the strains restore the microsclerotia deficient phenotype of *SFL1* deletion. Strains were grown on minimal medium for 14 days under constant light or in darkness (Figure 10A). The melanized area of the colony center of *GFP-SFL1* OE and, especially of the *SFL1-GFP* OE strain, was not as dark as the WT colony center. Increased production of both fusion proteins in the *SFL1* deletion strain did, however, lead to enhanced microsclerotia production compared to the deletion strain. Thus, all transformants were tested for the production of the full-length fusion protein. Western hybridization experiments with α-GFP antibody were performed with protein crude extracts derived from three-day-old mycelia grown in liquid complete medium at 25°C (Figure 10B). As control *V. dahliae* WT expressing free *GFP* driven by the constitutively active *gpdA* promoter was included (WT *GFP* OE). Western hybridization analysis of all *SFL1* deletion transformants overexpressing either *GFP-SFL1* or *SFL1-GFP* resulted in a signal that migrates between 100 and 130 kDa, which is higher than the predicted molecular weight of the fusion protein (~93 kDa). Higher migrating signals raise the idea of a post-translationally modified fusion protein. Free GFP is observed for the WT *GFP* OE control as expected at a size of around 27 kDa.

Next, the subcellular localization of the fusion protein was studied. Freshly harvested spores were used to inoculate liquid complete medium. After 16 hours of growth the GFP signals were monitored by fluorescence microscopy (Figure 10C). Strains overproducing GFP-Sfl1 predominantly showed strong nuclear GFP signals and only low diffuse signals throughout the cytoplasm whereas Sfl1-GFP was detected throughout the cytoplasm additional to GFP signals at sites of DAPI staining in the nuclei. The localization of fusion protein accumulation correlates with the extent of the microsclerotia phenotype restoration. *GFP-SFL1* OE strains exhibit specific localization to the nuclei with less diffuse GFP signals throughout the cytoplasm. This strain also results in stronger microsclerotia production than the *SFL1-GFP* OE strain and, therefore, restores the WT phenotype to a higher extent.

These results suggest that GFP fused to the N- or C-terminal end of Sfl1 interferes with the localization regulation of Sfl1. However, none of the GFP fusions hinders the protein completely from localizing to the nucleus possibly enabling Sfl1 to positively regulate microsclerotia production.

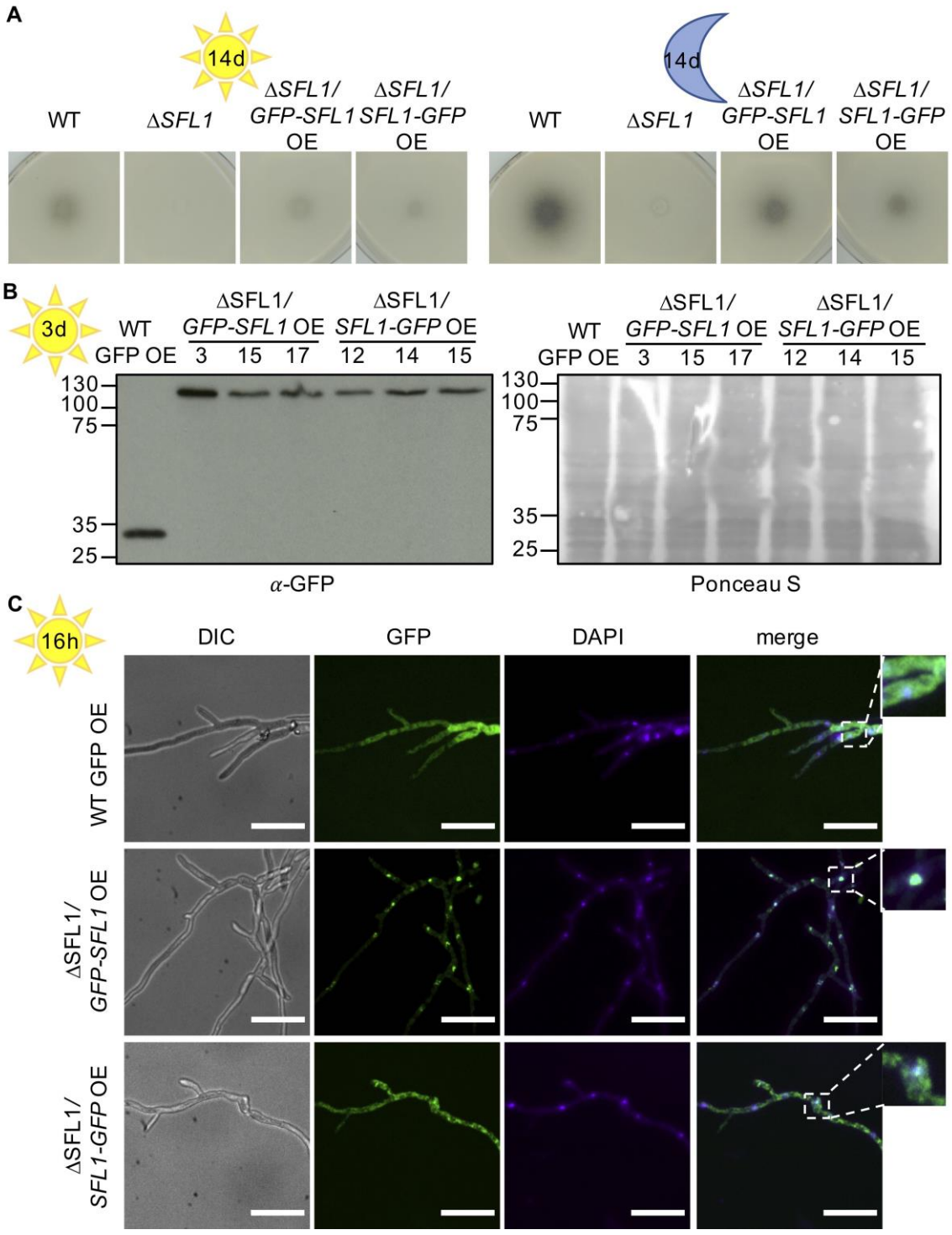

Figure 10. The regulatory protein Sfl1 of *V. dahliae* is localized in the nucleus.
SFL1 deletion strains ectopically overexpressing *GFP-SFL1* or *SFL1-GFP* were tested for production of microsclerotia **(A)**, production of the intact full-length fusion protein **(B)** and subcellular localization **(C)**. Three transformants of each strain were tested and representative pictures are shown. **(A)** 50 000 spores of *V. dahliae* JR2 wildtype (WT), Δ*SFL1* (VGB324) and Δ*SFL1* overexpressing *GFP-SFL1* or *SFL1-GFP* were point inoculated on minimal medium (CDM) and incubated at 25°C for 14 days in light or darkness as depicted. Representative top-views of the colonies show that melanization is restored when *GFP-SFL1* or *SFL1-GFP* is expressed. **(B)** Western hybridization with α-GFP antibody was performed with 80 µg protein extracts that were isolated from fungal strains grown in liquid potato dextrose medium (PDM) for three days at 25°C. Ponceau S staining served as loading control. WT overexpressing ectopically integrated *GFP* (~27 kDa) was used as control. Three transformants of *SFL1* deletion strains overexpressing *GFP-SFL1* (ΔSFL1*/GFP-SFL1* OE #3 – VGB266, #15 – VGB348, #17 – VGB349) or *SFL1-GFP* (ΔSFL1*/SFL1-GFP* OE #12 – VGB350, #14 – VGB351, #15 – VGB352) were tested. The fusion protein runs higher than the predicted size of ~93 kDa. **(C)** Subcellular localization of GFP-Sfl1 and Sfl1-GFP was analyzed by fluorescence microscopy after spores were incubated at 25°C in PDM for 16h. Nuclei were stained with DAPI (blue). GFP-Sfl1 predominantly localized to the nucleus (as seen on the zoom in pictures) while the localization of Sfl1-GFP is more diffuse. Scale bar = 20 µm.

3.1.2.3 Sfl1 is present in young hyphae of *V. dahliae*

Sfl1 is important for microsclerotia development. To investigate whether the presence of Sfl1 is required at different developmental steps, the protein abundance of Sfl1 was analyzed at different time points in liquid and on solid simulated xylem medium. A strain expressing endogenous levels of *GFP-SFL1* was constructed to enable the analysis of Sfl1 protein levels by Western hybridization. *GFP-SFL1* and the hygromycin resistance cassette were integrated into the *SFL1* deletion strain *in locus* by homologous recombination to enable expression under control of the native *SFL1* promoter. Correct integration was verified by Southern hybridization (Figure S1).

The *GFP-SFL1* complementation strain was tested for its growth phenotype to see whether the endogenous expression of the fusion protein *GFP-SFL1* was able to restore the microsclerotia production. WT, *SFL1* deletion strain and the *GFP-SFL1* complementation strain were spotted on solid minimal medium and were incubated at 25°C for ten days under constant light or dark conditions. The production of GFP-Sfl1 results in microsclerotia formation after growth in light and dark conditions (Figure 11A). However, the melanized area is slightly less enlarged compared to WT, which is visible in cross sections of the colony center. The strain was also

investigated for subcellular localization by fluorescence microscopy (Figure 11B). In *GFP-SFL1* expressing hyphae GFP signals were observed with higher accumulation at certain points in the hyphae, presumably the nuclei. This is consistent with the nuclear localization of GFP-Sfl1 in the *SFL1* deletion strains overexpressing *GFP-SFL1* (Figure 10).

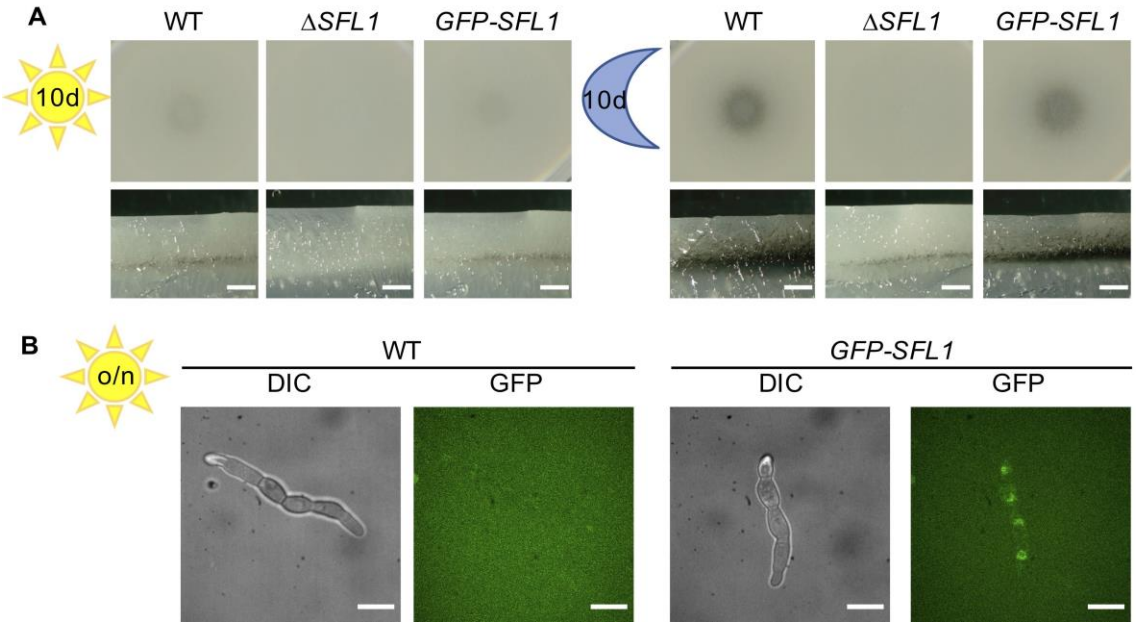

Figure 11. Expression of GFP-Sfl1 under control of its native promoter allows wildtype-like microsclerotia production in *V. dahliae*.
Strains expressing endogenous levels of *GFP-SFL1* (VGB433, VGB434) were tested for microsclerotia phenotype **(A)** and subcellular localization **(B)**. Data of a representative transformant are shown. **(A)** 50 000 spores of *V. dahliae* JR2 WT, *SFL1* deletion strain (VGB324) and *SFL1* deletion strain expressing *GFP-SFL1* were point-inoculated on minimal medium (CDM) and incubated at 25°C for ten days in light (left panel) or in the dark (right panel). Top-view of the colony (1st row) and the cross sections of the colony center (2nd row) show that the microsclerotia producing phenotype is restored in the *GFP-SFL1* expressing strain. Scale bars = 1 mm. **(B)** Subcellular localization of GFP-Sfl1 was analyzed by fluorescence microscopy after spores were incubated at 25°C in PDM overnight (o/n). GFP signals can be detected at distinct points. WT was used as negative control. Scale bars = 10 µm.

The production of the intact fusion protein was tested in Western hybridization experiments. Immunoblots with α-GFP antibody showed two different protein bands, one migrating at the expected size of the GFP-Sfl1 fusion protein at ~93 kDa and a higher migrating band at a size between 100 and 130 kDa, which could account for a modified fusion protein (Figure 12A). These two bands were observed

for all tested transformants. To investigate whether Sfl1 is required at a specific developmental stage, protein abundance of the fusion protein was analyzed at different time points in simulated xylem medium. One million spores of WT and *SFL1-GFP* complementation strain were spread on solid SXM agar plates overlaid with nylon membranes for analysis on solid medium or were used to inoculate SXM liquid cultures. Mycelia were harvested after two, four and six days of growth at 25°C and continuous light. Similar to Western analyses with protein extracts from PDM (Figure 12A), two bands were observed for the GFP-Sfl1 fusion protein (Figure 12B). The strength of these bands overall decreased with age of the culture indicating that the fusion protein is degraded. At two days of growth on SXM plates and in SXM liquid cultures the lower migrating GFP-Sfl1 signal (~93 kDa) exhibits the highest protein abundance that is decreasing at four and six days post inoculation. This correlates with the appearance of microsclerotia production on plate.

The fusion protein product seems to be stable during early time points when microsclerotia production is initiated, but no microsclerotia are visible yet, and is then degraded once microsclerotia are detectable (Figure 12C). The higher migrating band may correlate with degradation of the fusion protein. When grown on SXM plates, the higher migrating band is less prominent after two days where the lower band is very prominent. After four and six days of growth the 93 kDa fusion protein becomes less abundant while the signal of the higher migrating band is stronger at four days and then decreases in intensity after six days. The increase of signal at the second time point may correlate with the decrease in signal of the lower band corroborating the hypothesis of protein modification prior to the degradation of the fusion protein. The signal strength at ~27 kDa displaying free GFP increases with age of the culture, which is another indication for the degradation of the fusion protein. The WT control expressing no *GFP* shows no unspecific bands. A similar picture is seen for liquid cultures where the signal of the lower and higher migrating band of the fusion protein GFP-Sfl1 decreases with advanced culture age. In liquid SXM cultures, however, microsclerotia are not predominantly produced, but spore production is induced. Pictures of the culture flasks at the different time points show that only at six days after growth, the culture becomes darker, but that cultures are turbid from the beginning where spores are

produced. These results indicate that Sfl1 is abundant at time points where spore and microsclerotia production are initiated.

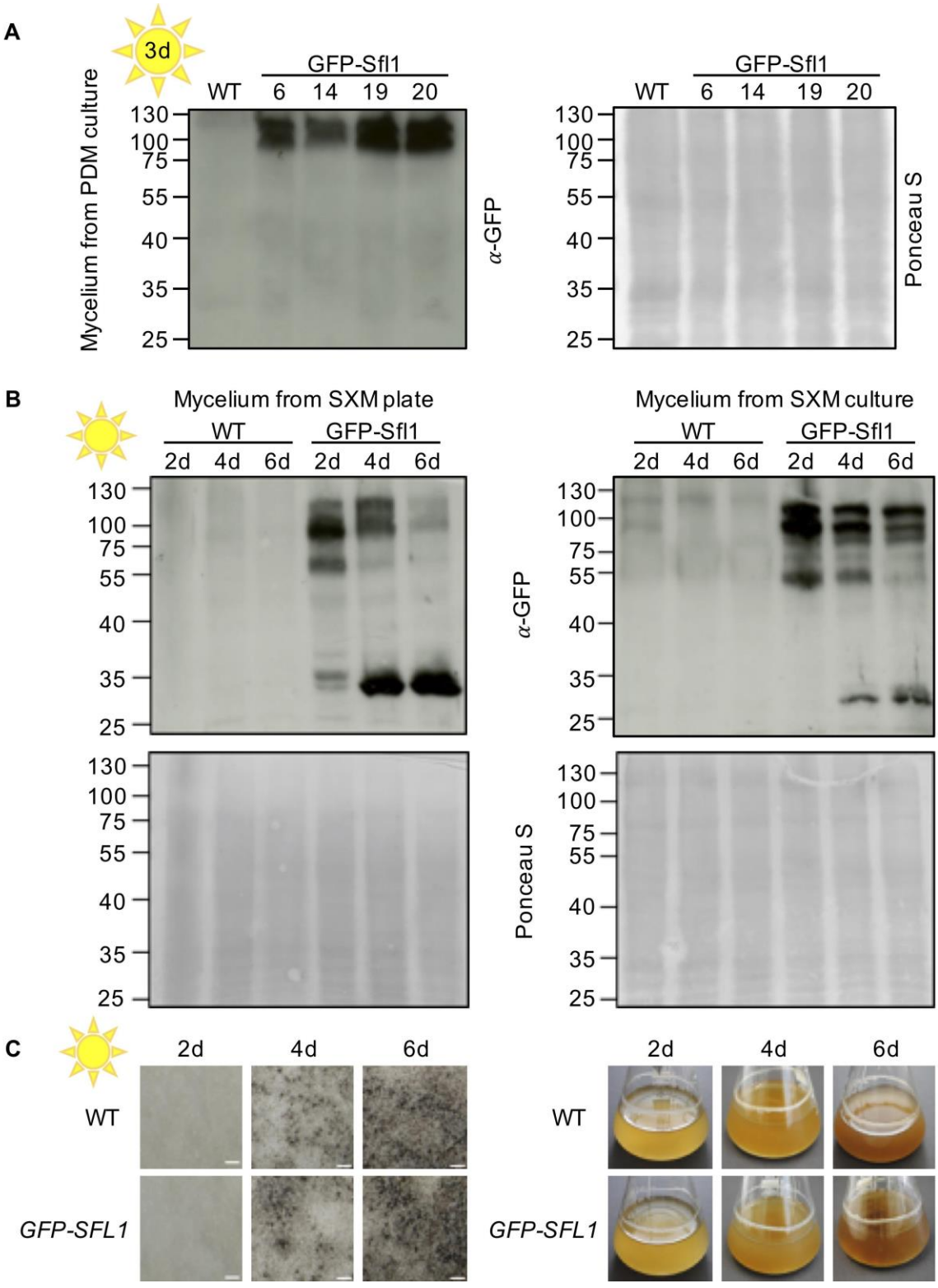

Figure 12. The Sfl1 protein is required in the initial phases of *V. dahliae* microsclerotia and conidia production.
A strain expressing endogenous levels of *GFP-SFL1* (VGB434) was tested for Sfl1 protein abundance at time points before, during and after microsclerotia production. Western hybridizations with α-GFP antibody were performed. *V. dahliae* JR2 was used as negative control and Ponceau S staining served as loading control. **(A)** Proteins were extracted from fungal mycelium grown in liquid complete medium (PDM) for three days. For Western hybridization 150 µg protein extracts of four different transformants (#6, #14, #19 – VGB433 and #20 – VGB434) was tested. (**B**, **C**) 1 000 000 spores of *V. dahliae* WT and *GFP-SFL1* expressing strain were used for inoculation. Fungal material was harvested after two, four and six days. **(B)** Western hybridization was performed with 50 µg protein extracts from fungal mycelium grown on a Hybond^{TM}-Nylon membrane on simulated xylem medium (SXM) agar (left) or from mycelium grown in liquid SXM cultures. **(C)** Pictures of the plates (left) and liquid cultures (right) indicate the level of microsclerotia abundance by the darkness of the culture at the different time points. Scale bars = 200 µm.

Overall, the protein abundance at different time points shows that Sfl1 may have a function in young cultures as the protein abundance was higher here. It is intriguing to speculate that the abundance of GFP-Sfl1 on plate negatively correlates with the presence of microsclerotia in a way that Sfl1 is degraded upon microsclerotia formation. Furthermore, data support a potential role in spore formation.

3.1.2.4 The stress response of *V. dahliae* is independent of Sfl1

Microsclerotia are required for the fungus to survive in nutrient-limited conditions and therefore are involved in stress resistance. *V. dahliae* Sfl1 possesses the characteristic HSF domain, which is required for the transcriptional activation of heat shock genes in yeast. Heat shock proteins are produced in response to exposure to stressful conditions. Thus, it is intriguing to analyze the phenotype of *SFL1* deletion regarding its stress response.

Spores were point inoculated on minimal medium containing different stress-inducing agents. As cell wall perturbing agents sodium dodecyl sulfate (SDS) and ethanol (EtOH) were added and for induction of oxidative stress hydrogen peroxide (H_2O_2) was utilized. Apart from the reported microsclerotia defect of the *SFL1* deletion no differences in radial growth were detected after two weeks of incubation at 25°C in continuous light or dark conditions (Figure 13A). Additionally, an inhibition test was performed to test stress responses of the *SFL1* deletion strain. Again, the *SFL1* deletion is reduced in microsclerotia development but no differences in the inhibition zones between WT and Δ*SFL1* were detectable in

response to the oxidative stressors menadione or H_2O_2 after four days of growth at 25°C in the light (Figure 13B). These results indicate that under tested conditions Sfl1 is dispensable for stress tolerance to SDS, H_2O_2, menadione and EtOH in *V. dahliae*.

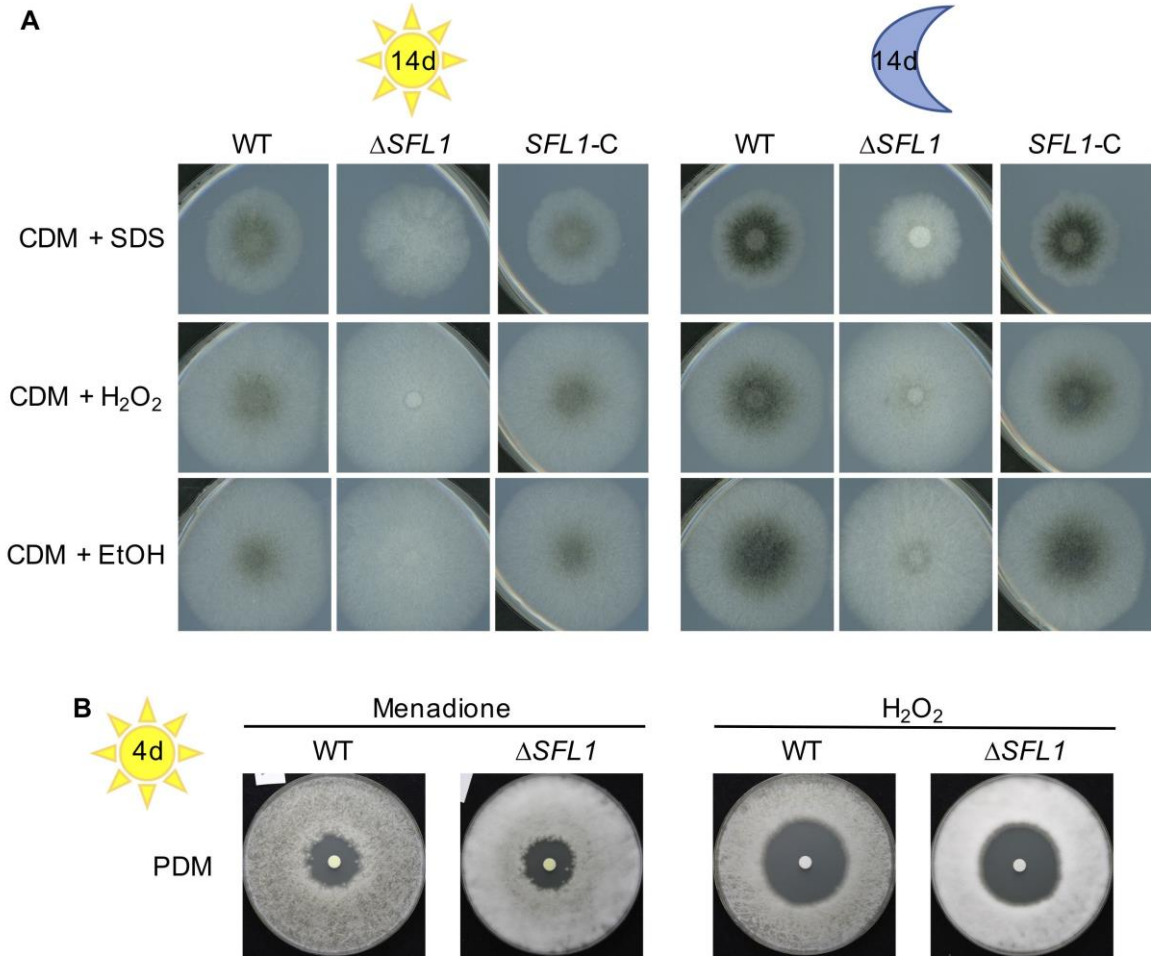

Figure 13. Transcription factor Sfl1 is dispensable for *V. dahliae* stress tolerance to several cell stressors.
SFL1 deletion strain was tested for stress tolerance to sodium dodecyl sulfate (SDS), hydrogen peroxide (H_2O_2), menadione and ethanol (EtOH). Two transformants of the *SFL1* deletion (Δ*SFL1* – VGB324, VGB325) and complementation strain (*SFL1*-C – VGB342, VGB343) were tested. Representative results of one transformant each are shown. **(A)** 50 000 spores of *V. dahliae* JR2 wildtype (WT), *SFL1* deletion and complementation strain were spotted on minimal medium (CDM) containing different stressors and incubated at 25°C for 14 days in light or dark (as depicted). Top-view scans of the colonies show that the *SFL1* deletion strain produces less microsclerotia compared to WT, but displays no additional growth defect. **(B)** 1 000 000 spores of *V. dahliae* WT and Δ*SFL1* deletion strain were spread on potato dextrose agar (PDM) plates containing 300 µg/ml cefotaxime and 10 µl of a stressor was pipetted on a paper disc in the center of the plate (100 mg/ml menadione in DMSO, 10% H_2O_2 in DMSO). Triplicates of each transformant were tested and the experiment was repeated with similar results. No significant differences in the inhibition zone between the *SFL1* deletion strain and WT were observed.

3.1.3 The regulatory protein Sfl1 and the light regulator Frq are opposing regulators in *V. dahliae* microsclerotia development

3.1.3.1 *SFL1* is epistatic to *FRQ* in the regulation of *V. dahliae* microsclerotia production

This study revealed two *V. dahliae* mutants with regulatory functions in microsclerotia development. Frq was shown to be important in light-dependent microsclerotia repression whereas Sfl1 is required for microsclerotia formation. To further shed light on the regulation of microsclerotia development and to investigate on a possible connection of these two regulators, the Δ*FRQ*Δ*SFL1* double deletion was generated and analyzed. As both single deletion strains harbored the nourseothricin resistance cassette, a new *FRQ* deletion was generated by replacing the full *FRQ* ORF in *V. dahliae* WT with the hygromycin resistance cassette (*HYG*^{R}) via homologous recombination. The same construct was integrated into the *SFL1* deletion strain to generate the double deletion strain. An ectopic complementation (*FRQ*-C) of Δ*FRQ* (*HYG*^{R}) was constructed by ectopically integrating the *FRQ* ORF including 5' and 3' flanking regions into the *FRQ* deletion strain. Strains were tested in Southern hybridizations to verify correct integrations of the desired constructs (Figure S3).

Strains were analyzed for their phenotypic growth on solid media. Spores of Δ*FRQ*, Δ*SFL1* and Δ*FRQ*Δ*SFL1* strains were point inoculated on various media and incubated at 25°C in light or darkness for ten days. The most prominent phenotypes were observed on minimal medium and SXM (Figure 14A). Overall, the double deletion strain resembles the phenotype of the *SFL1* deletion strain. When grown on CDM in constant light, depletion of *FRQ* led to enhanced microsclerotia production only in the single deletion strain as displayed by top-view and cross sections of the colony. Microscopic views indicate that microsclerotia formed in the *FRQ* deletion strain are as well darker indicating more melanization than WT microsclerotia. These results confirm that the microsclerotia phenotype in a *FRQ* deletion strain is independent of the resistance cassette used. Depletion of *SFL1*, in contrast, leads to the absence of darkened areas in the colonies and only initial developmental stages of microsclerotia can be detected microscopically. This applies for the *SFL1* single as for the Δ*FRQ*Δ*SFL1* double deletion strain. When incubated in the dark mature microsclerotia were observed for all strains.

However, as WT exhibited enhanced microsclerotia production compared to growth in the light, *FRQ* deletion strain resembles the WT phenotype in darkness. Growth of Δ*SFL1* and Δ*FRQ*Δ*SFL1* strain in the dark and overall growth on SXM shows that deletion of *SFL1* does not lead to total inhibition of microsclerotia production. Nevertheless, compared to WT and *FRQ* deletion strains microsclerotia production is significantly decreased. Cultivation on solid SXM displays differences in aerial hyphae production. After incubation in the light, the *FRQ* deletion strain exhibits a decrease in production of aerial hyphae compared to WT and the *SFL1* deletion strains. Depletion of light leads to a general decrease in aerial hyphae production on SXM in all tested strains.

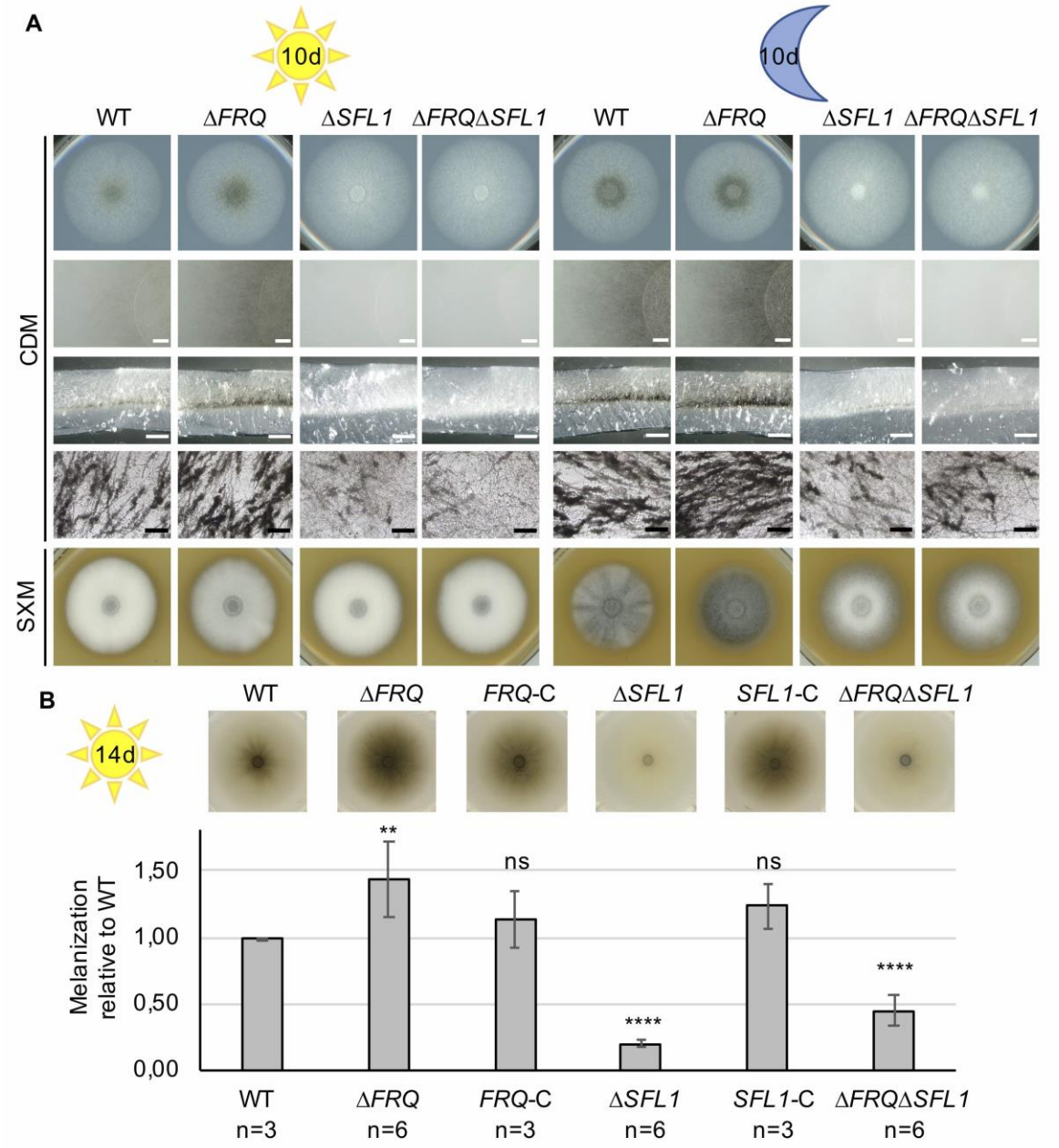

Figure 14. Light regulator Frq is required for microsclerotia repression and regulatory protein Sfl1 for microsclerotia production in *V. dahliae*.
V. dahliae JR2 wildtype (WT), *FRQ* and *SFL1* single deletion strains (Δ*FRQ* (*HYG*^{R}) – VGB402, VGB403; Δ*SFL1* – VGB324, VGB325) with the corresponding complementations (*FRQ*-C – VGB441; *SFL1*-C – VGB342) and the double deletion strain Δ*FRQ*Δ*SFL1* (VGB403, VGB404) were analyzed for microsclerotia production. **(A)** 50 000 spores of indicated *V. dahliae* strains were point inoculated on minimal medium (CDM) (1st to 4th row) and simulated xylem medium (SXM) (5th row) and incubated at 25°C for ten days in the light (left panel) and in the dark (right panel). Top-view pictures of the colony on CDM (1st row) and the colony center without aerial hyphae (2nd row), cross sections of the colony center (3rd row) and microscopic views (4th row) display the differences in microsclerotia production. Top-view pictures of the colony on SXM (5th row) show that Δ*FRQ* produces less aerial hyphae compared to WT and *SFL1* deletion strains. White scale bars = 1mm, black scale bars = 100 µm. **(B)** 50 000 spores were point inoculated on CDM and incubated at 25°C for 14 days. For melanization quantification top-view scans of the colonies were taken after the removal of aerial hyphae. The brightness factor of the melanized areas was measured with ImageJ software while blank agar was set to 0 and WT to 1. Triplicates of two independent transformants (n=2) of the deletion strains were tested and for the complementation strains one transformant (n=1) each was used. The diagram displays the mean values with standard deviation of three independent experiments. Significant differences compared to WT are indicated and were calculated with one-way Anova and Student's t-test with *p*-values: **: $p < 0.01$, ****: $p < 0.0001$. Non-significant differences to WT are indicated with "ns".

The microsclerotia producing defect was further quantified. Strains were point inoculated on CDM agar plates and incubated for 14 days at 25°C in the light. One experimental set-up was tested in the dark and dismissed for further repetitions due to undetectable differences between WT and the *FRQ* deletion strain. Top-view scans were taken of the colonies after removal of aerial mycelia and the melanized area was quantified relative to WT. Melanization levels were significantly increased by ~40% in Δ*FRQ* compared to the WT whereas the melanization was significantly decreased to less than half in strains lacking *SFL1* (Figure 14B). Ectopic complementation of *FRQ* and *SFL1* restored the phenotype and showed no significant alteration in microsclerotia production compared to WT.
These data verify the opposing roles of Frq and Sfl1 in microsclerotia production. While Frq is required for repression, Sfl1 acts as activator. The phenotypical resemblance of Δ*SFL1* and Δ*FRQ*Δ*SFL1* leads to the conclusion that *SFL1* must act epistatic to *FRQ* in the regulation pathway.
To test whether the microsclerotia production in the *FRQ* deletion strain is altered by high abundance of Sfl1, a *FRQ* deletion strain ectopically overexpressing *GFP-*

SFL1 was constructed. Correct integration of *GFP-SFL1* driven by the constitutively active *gpdA* promoter into the *FRQ* (*NAT*^{R}) deletion strain was verified by Southern hybridization (Figure S2).

The presence of the fusion protein GFP-Sfl1 was verified by Western hybridization using protein extracts derived from fungal mycelia from three-day-old liquid PDM cultures (Figure 15A).

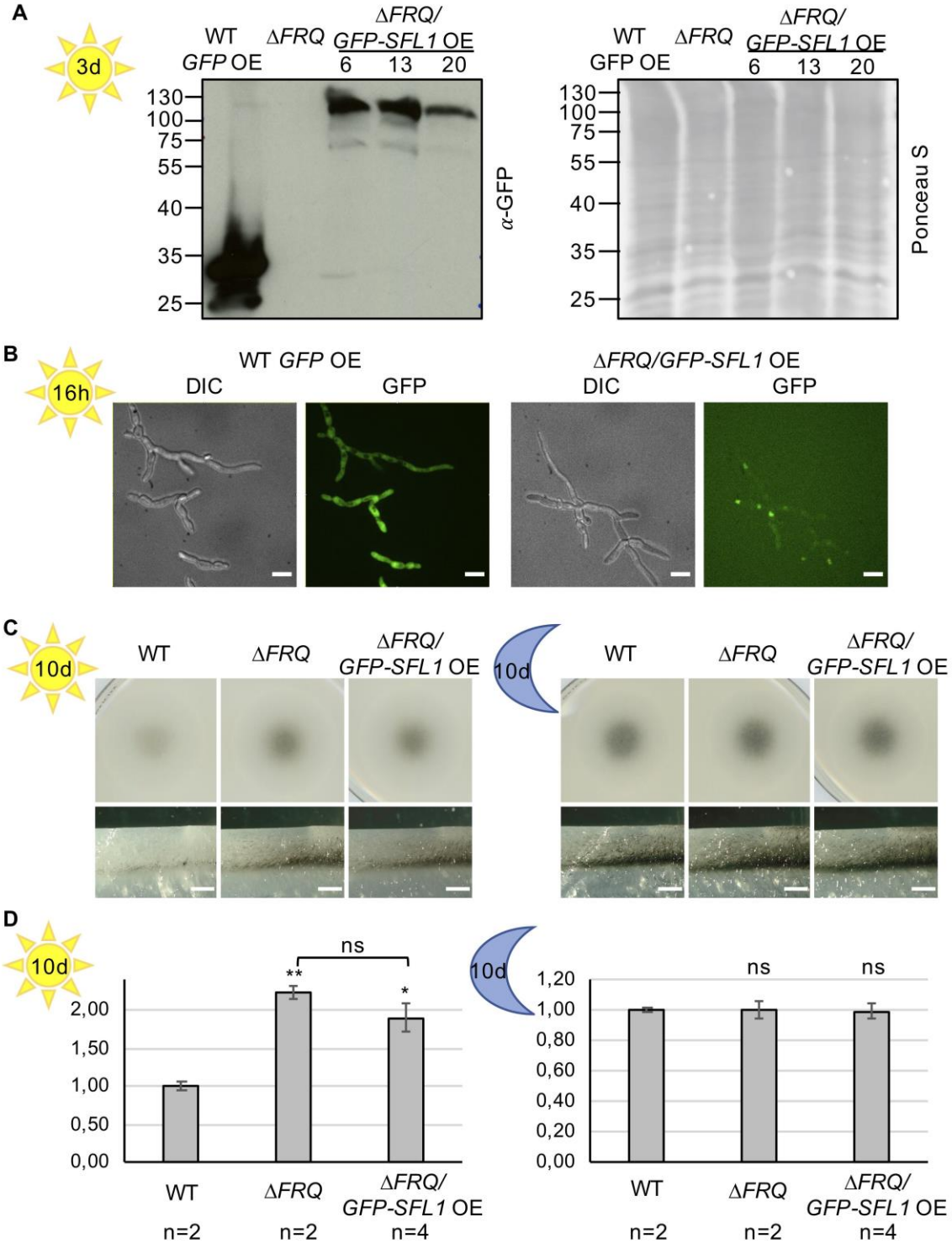

Figure 15. High abundance of the regulator Sfl1 reduces strong microsclerotia production of *V. dahliae* Δ*FRQ*.
FRQ deletion strains ectopically overexpressing *GFP-SFL1* (Δ*FRQ/GFP-SFL1* OE #13 – VGB435, #20 – VGB436) were tested for production and localization of the fusion protein and for microsclerotia production. As background strain the *FRQ* deletion strain VGB296 (Δ*FRQ* containing a nourseothricin resistance cassette (*NAT*^{R})) was used. **(A)** Western hybridization with α-GFP antibody was performed with 150 µg protein extracts from fungal mycelium grown in liquid potato dextrose medium (PDM) for three days at 25°C. Three transformants were tested of the Δ*FRQ/GFP-SFL1* OE strain, WT overexpressing free GFP (WT *GFP* OE) and Δ*FRQ* were used as controls. Ponceau S staining served as loading control. The fusion protein GFP-Sfl1 runs slightly higher than the predicted size of ~93 kDa while accumulation of free GFP is seen at the size of 27 kDa. **(B)** Subcellular localization of GFP-Sfl1 was analyzed by fluorescence microscopy after spores were incubated at 25°C in PDM for 16h. Scale bars = 10 µm. **(C)** 50 000 spores of WT, Δ*FRQ* and Δ*FRQ/GFP-SFL1* OE were spotted on minimal medium (CDM). Plates were incubated at 25°C for ten days in the light (left) or in the dark (right). Top-view of the colony (1st row) and cross sections of the colony center (2nd row) display the phenotypes. Scale bars = 1 mm. **(D)** After the removal of aerial hyphae the brightness level of the colonies in **C** was quantified with ImageJ for duplicates of each strain and an additional transformant of the *GFP-SFL1* OE. Blank agar was set to 0 while WT was set to 1. Significant differences were calculated with one-way Anova and Student's t-test with *p*-values: *: $p < 0.05$, **: $p < 0.01$. Non-significant differences are indicated by "ns".

The most prominent signal migrated at a size with a molecular weight of above 100 kDa which is higher than the predicted ~93 kDa and could correspond to a post-translationally modified fusion product. A fainter band is displayed at the predicted size and another faint band with a size smaller than 75 kDa. WT control overexpressing *GFP* resulted in a strong expected band at 27 kDa with a putative degradation pattern of bands at smaller sizes. GFP signals were further investigated by fluorescence microscopy 16 hours post inoculation in liquid PDM. WT control overexpressing *GFP* shows a diffuse signal in the cytoplasm whereas the GFP signal in the *GFP-SFL1* overexpressing strain accumulated at distinct spots suggesting that it is functional and localized to the nucleus (Figure 15B). Microsclerotia production was analyzed in ten-day-old colonies after growth on various solid media including simulated xylem medium, complete medium, minimal medium, and minimal medium with cellulose as carbon source or minimal medium supplemented with stress inducing agents such as SDS or H_2O_2. Vegetative growth of two tested transformants of *FRQ* deletion overexpressing *GFP-SFL1* resembled the *FRQ* deletion phenotype on all tested media. The enhanced microsclerotia producing phenotype of Δ*FRQ* was most apparent on minimal medium (Figure

15C). Quantification of the melanized area was performed once with duplicates and confirmed that depletion of *FRQ* leads to a melanization increase of about 100% compared to WT when grown in the light (Figure 15D). Overexpression of *GFP-SFL1* in the *FRQ* deletion background exhibited slightly less melanization compared to the *FRQ* deletion strain showing that high protein levels of Sfl1 may interfere with microsclerotia production. The difference in the melanized area was constant in repetitions, but not significant. Strains incubated in the dark did not differ from WT-levels of melanization.

These observations suggest that Sfl1 is required for microsclerotia production, but high abundance of Sfl1 does not support excessive microsclerotia formation.

3.1.3.2 Sfl1 and Frq are positive regulators of conidia production in *V. dahliae*

Once inside the plant, *V. dahliae* produces conidia exploiting the vascular system to systematically colonize the whole plant making conidia production a crucial step in plant infection. Thus, we investigated the roles of *V. dahliae* Frq and Sfl1 in conidia production.

The same number of spores of *V. dahliae* WT, *FRQ* and *SFL1* single deletion with corresponding complementation strains and the Δ*FRQ*Δ*SFL1* strain was inoculated in liquid simulated xylem medium and spore concentrations were determined after five days of growth at 25°C. All deletion strains displayed significantly reduced spore concentrations compared to the WT (Figure 16). *FRQ* deletion showed a reduction of about 40% compared to WT while *SFL1* deletion resulted in a minor reduction in spore formation of about 15% to WT level whereas the double deletion strain exhibited the most severe reduction to half of the WT level. All complementation strains restored the conidiospore production to WT levels.

In summary, Frq and Sfl1, both positively regulate conidiation and may have an additive effect on conidia production.

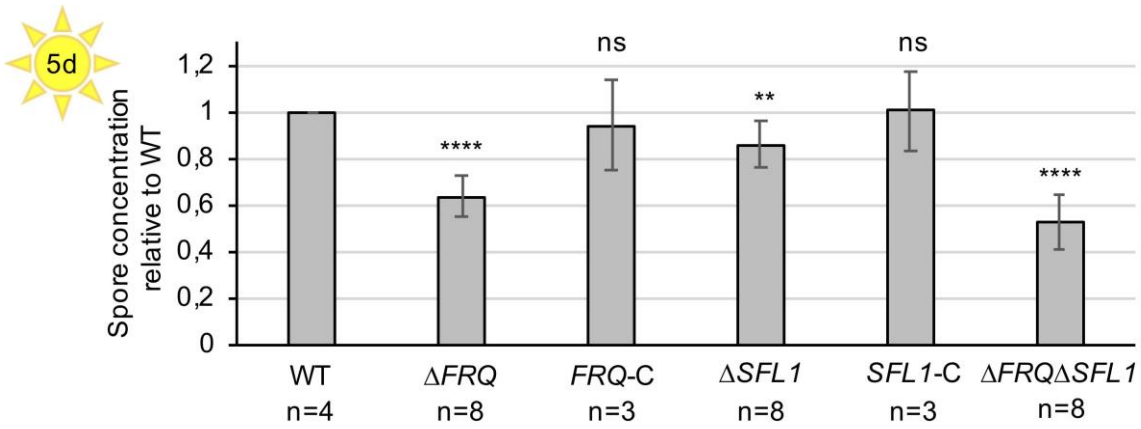

Figure 16. Regulator proteins Frq and Sfl1 are required for *V. dahliae* conidiospore production.
V. dahliae JR2 wildtype (WT), *FRQ* and *SFL1* single deletion strains (Δ*FRQ* (*HYG*^{R}) – VGB402, VGB403 and Δ*SFL1* – VGB324, VGB325), indicated complementations (*FRQ*-C – VGB441 and *SFL1*-C – VGB342) and Δ*FRQ*Δ*SFL1* strain (VGB403, VGB404) were analyzed for conidiospore production. Liquid simulated xylem medium (SXM) cultures inoculated with 200 000 spores were incubated at 25°C for five days under constant agitation. For the *V. dahliae* single and double deletion strains two independent transformants were tested for each strain and one transformant of each complementation strain. For conidia quantification spores of each culture were collected, the spore concentration was determined and normalized to WT. The experiment was repeated three times with all strains and one additional time without the complementation strains. Significant differences compared to WT are indicated and were calculated with one-way Anova and Student's t-test with *p*-values: **: $p < 0.01$, ****: $p < 0.0001$. Non-significant differences are marked with "ns".

3.1.3.3 Light regulator Frq and regulatory protein Sfl1 contribute to *V. dahliae* virulence on tomato

As mentioned, the production of conidia is required for *V. dahliae* to colonize the plant. As *FRQ* and *SFL1* deletion mutants are impaired in the production of WT level conidiospores, this defect may lead to the induction of less severe disease symptoms, which was analyzed in tomato infections. Furthermore, the involvement of Sfl1 in adherence to the root was tested in an *Arabidopsis* root infection assay as this process was impaired in *V. dahliae VTA3* deletion strains (Bui *et al*, 2019) and Vta3 regulates expression of *SFL1* in *V. dahliae*.

To monitor the growth of fungal hyphae, an *SFL1* deletion strain expressing ectopically integrated *GFP* controlled by the *gpdA* promoter (Δ*SFL1 GFP* OE) was used. Root colonization was investigated on thin and low-fluorescent *Arabidopsis* roots rather than on the thicker tomato roots (Geldner & Salt, 2014). Three-week-old *Arabidopsis* roots were infected with the same number of spores of WT and

Δ*SFL1* overexpressing free GFP via root dipping. Both strains showed similar initial colonization of the roots at two days post inoculation and further whole root proliferation after five days (Figure 17A). Thus, the *SFL1* deletion strain is well able to grow on *Arabidopsis* roots suggesting that *Arabidopsis* root colonization behavior of *V. dahliae* is independent of Sfl1. For tomato infections the same number of spores of *SFL1* and *FRQ* single and double deletion strains were used to root-inoculate ten-day-old tomato seedlings. Disease symptoms were scored 21 days after infection. Plants colonized with *FRQ* deletion strains, either expressing the nourseothricin (Figure 17B) or hygromycin resistance genes (Figure 17C), resulted in compromised virulence on tomato compared to WT infection. Almost 70% of plants infected with Δ*FRQ* displayed no or only mild symptoms compared to 40% of WT treated plants. This indicates that the less severe disease symptoms of Δ*FRQ* colonized plants are independent of the resistance cassette. *SFL1* deletion strain caused no or only mild symptoms in about 60% plants whereas infection with the Δ*FRQ*Δ*SFL1* strain was even less pathogenic leading to almost 80% of healthy or mildly affected plants (Figure 17C). Overall, depletion of *SFL1* and *FRQ* led to the induction of less symptoms compared to WT treated plants. Infections with all tested strains, however, induced discolorations of the hypocotyls and the fungus was re-isolated from all infected stems after surface sterilization (Figure 17B,C).

These data suggest that *V. dahliae* lacking *SFL1* and *FRQ* is still able to penetrate the root and is able to induce disease symptoms, however, not to the extent as *V. dahliae* WT. Concluding, Frq and Sfl1 are required for full virulence of *V. dahliae* on tomato, but only after penetration. As both proteins are positively regulating conidiospore production this may hinder the fungus to proliferate in the plant and induce infection to the same level as WT.

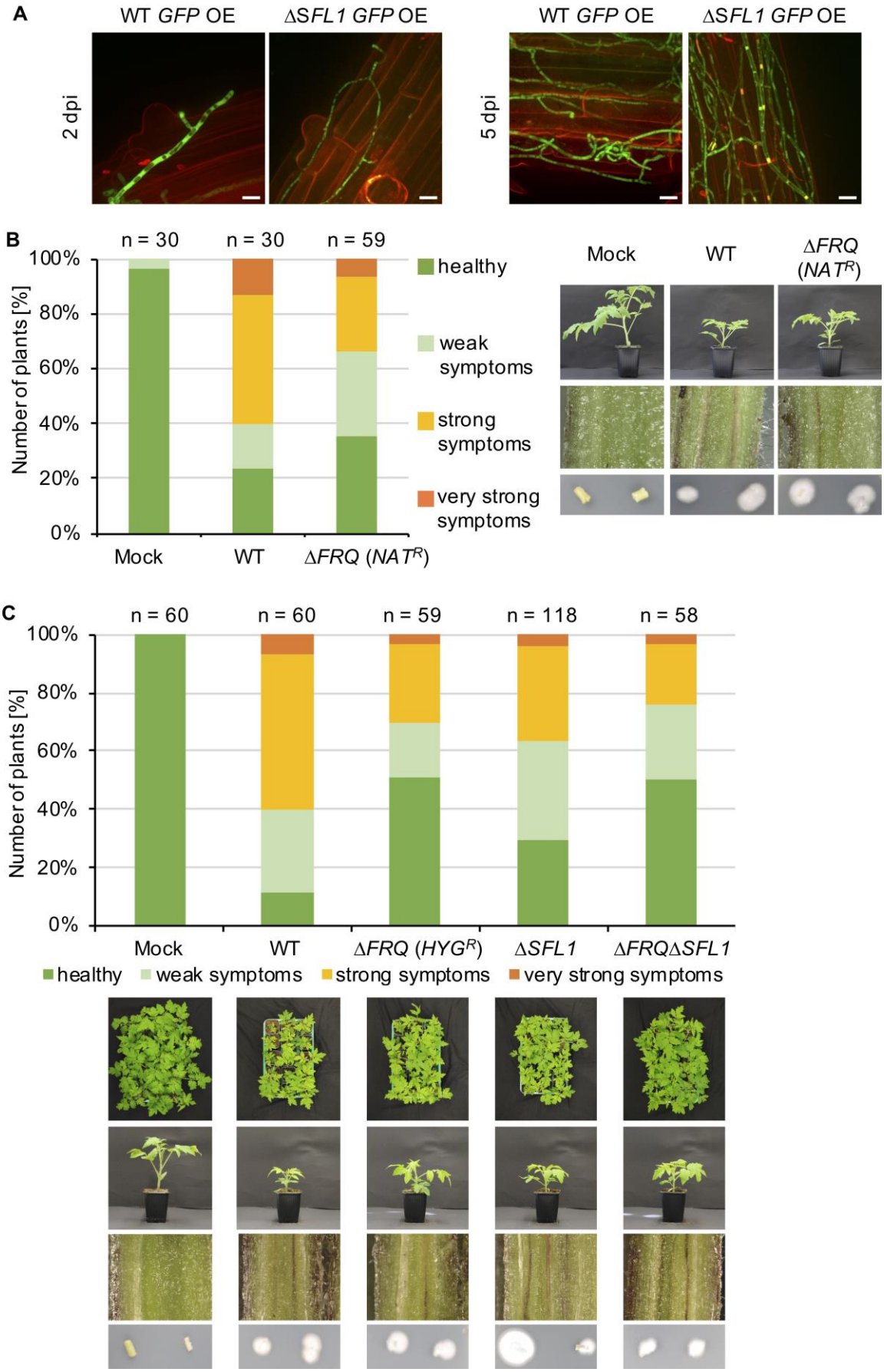
A
WT GFP OE
ΔSFL1 GFP OE
WT GFP OE
ΔSFL1 GFP OE
2 dpi
5 dpi
B
n = 30
n = 30
n = 59
100%
80%
60%
40%
20%
0%
Number of plants [%]
healthy
weak symptoms
strong symptoms
very strong symptoms
Mock
WT
ΔFRQ (NATR)
Mock
WT
ΔFRQ (NATR)
C
n = 60
n = 60
n = 59
n = 118
n = 58
100%
80%
60%
40%
20%
0%
Number of plants [%]
Mock
WT
ΔFRQ (HYGR)
ΔSFL1
ΔFRQΔSFL1
healthy
weak symptoms
strong symptoms
very strong symptoms

Figure 17. Light regulator Frq and regulatory protein Sfl1 contribute to *V. dahliae* virulence on tomato.

Single and double deletion strains of *FRQ* and *SFL1* were tested in tomato infections and *Arabidiospis thaliana* root colonization. Infected plants were incubated in the climate chamber under 16h:8h light:dark at 22-25°C. **(A)** Three-week-old *A. thaliana* seedlings were infected with *V. dahliae* JR2 and *SFL1* deletion strain overexpressing ectopically integrated *GFP* (WT *GFP* OE and Δ*SFL1 GFP* OE, respectively) via root dipping in a 100 000 spores/ml spore solution. At two and five days post inoculation (dpi) the colonization of the fungal hyphae on the roots was monitored. Root cells were stained with 0.05% propidium iodide/0.01% silwet solution. The experiment was repeated twice with two individual Δ*SFL1 GFP* OE transformants (VGB340, VGB341). Representative fluorescence microscopy pictures show similar initial colonization of *V. dahliae* WT and *SFL1* deletion strain on the root surface at two dpi and whole root colonization at five dpi. Scale bars = 10 µm. **(B, C)** Ten-day-old tomato seedlings were root-infected with spores of WT and the indicated deletion strains. Uninfected plants (mock) served as control. The disease index was assessed at 21 dpi and includes the height of the plant, the longest leaf length and the weight of the plant. Representative plants, discolorations of the hypocotyls and the fungal outgrowth of the stems are shown. The number (n) of treated plants is shown for each fungal strain. The experiments were repeated twice with two transformants of each deletion strain. **(B)** Infection with *FRQ* deletion strain harboring the nourseothricin resistance cassette (NAT^R) (Δ*FRQ* (NAT^R) – VGB295, VGB296) results in reduced disease symptoms compared to WT infection. **(C)** Tomato infections with *FRQ* deletion strain (carrying the hygromycin resistance cassette (HYG^R); Δ*FRQ* (HYG^R) – VGB402, VGB403), *SFL1* deletion (Δ*SFL1* – VGB324, VGB325) and Δ*FRQ*Δ*SFL1* strain (Δ*FRQ*Δ*SFL1* – VGB403, VGB404) lead to a lower disease index compared to WT infection.

3.2 Xylem sap and pectin-rich medium trigger specific secretome responses compared to other media

Verticillium spp. grow in the xylem sap to infect rapeseed. They are also able to grow in different environments, which requires adaptation to changing nutrients and other biotic and abiotic factors. This study addressed the question how different growth media affect the secretion response of *Verticillium* spp. with specific focus on identification of distinct exoproteomic patterns triggered by different plant related contents and how they differ from responses to various other cultivation environments. As model fungi for this approach, the allodiploid *V. longisporum* 43 that mainly infects *Brassicaceae* including the economically important oilseed rape (Novakazi *et al*, 2015) was used.

3.2.1 *V. longisporum* is able to form different media-dependent secretome responses

V. longisporum was precultured in liquid complete medium for four days and transferred to different media: dH_2O, minimal medium, yeast nitrogen base (YNB), vegetable juice (V8), SXM and xylem sap extracted from *B. napus*. After another four days of cultivation the proteins of the supernatants of the *V. longisporum* cultures were precipitated, separated by SDS-PAGE and subjected to tryptical protein digestion. Peptides were analyzed by LC-MS/MS, bioinformatically processed and mapped to the protein sequence database of *V. longisporum* (http://biofung.gobics.de:1555/; coordinated by Prof. Dr. Gerhard H. Braus, Georg-August-Universität Göttingen). Information of the peptides were combined in an exoproteomic data matrix and calculated into a principle component analysis (PCA) plot with MarVis software (Figure 18A, initial data sets were provided by A. Kühn and bioinformatic analysis were performed by A. Kaever, both Georg-August-Universität Göttingen). The PCA plot displays the exoproteome signature of each culture. In total, protein patterns of six biological replicates for each medium were tested and the secretion response of the replicates generated similar signatures. Cultivation in all tested media, however, result in different secretion response clusters. Exoproteomes of *V. longisporum* derived from the diverse non-plant related media such as water, minimal medium, YNB and V8 form a similar pattern as reflected by sample clustering in the PCA plot analysis. In contrast, the secretion response in the pectin-rich SXM or xylem sap each result in a different

exoproteome pattern, but include similar features as displayed by the close proximity on the x-axis. These results propose that the fungus has the potential to differentiate between various environments and is able to form media-dependent responses in exoproteome production.

Analysis of the specific exoproteomic responses of *V. longisporum* in the plant related media, SXM and xylem sap, was further refined. The lists of identified candidates included more than 1000 proteins in the SXM and xylem sap exoproteomes. To exclude only weakly enriched or unsuitable proteins, the lists were semi-quantitatively processed by a statistical workflow using MarVis Suite (Kaever *et al*, 2012).

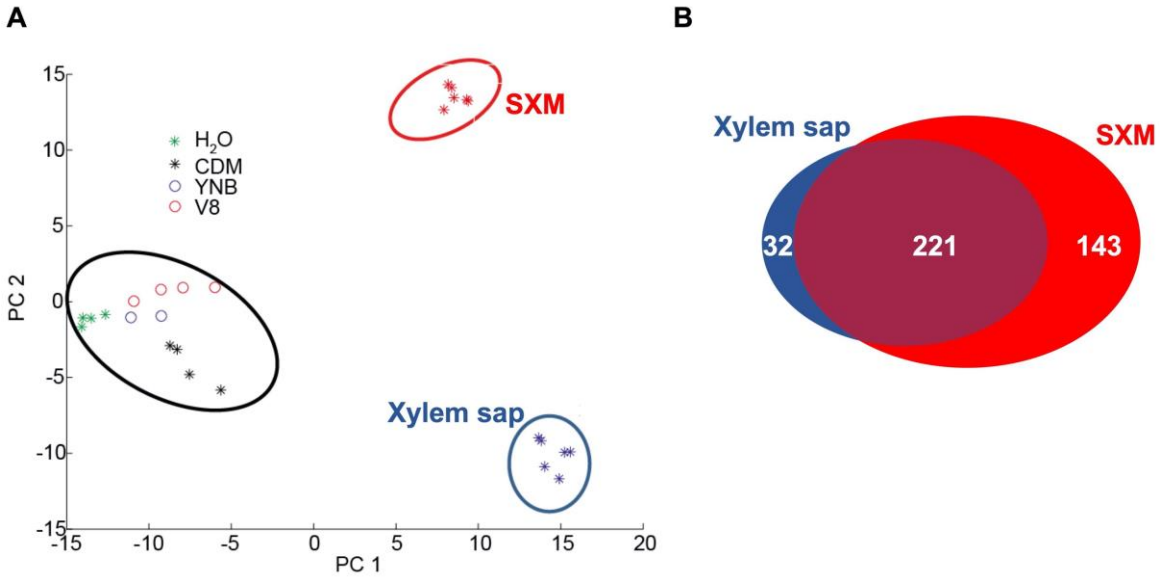

Figure 18. Exoproteome signatures of *V. longisporum* in different growth media.
V. longisporum 43 was cultivated in complete medium (PDM) for four days before the sedimented mycelia and spores were dissolved in different media (dH_2O, minimal medium (CDM), yeast nitrogen base (YNB), vegetable juice (V8), simulated xylem medium (SXM) and extracted xylem sap from *B. napus*) and cultivated for four more days. Proteomic secretome analyses via LC-MS/MS and initial data analysis were performed by A. Kühn and A. Kaever, both Georg-August-Universität Göttingen. **(A)** Principle component analysis (PCA plot, created with MarVis software) of a combined exoproteomic data matrix is based on spectral countings with each dot representing one biological sample, which is an independent culture. The compared exoproteomic signatures cluster in three groups: a first cluster is formed by all xylem sap culture samples (blue); the second cluster contains all SXM culture samples (red) and the third cluster consists of all other samples (black). **(B)** Lists of identified proteins were semi-quantitatively processed by a statistical workflow using MarVis Suite (Kaever *et al*, 2012). The Venn diagram displays the number of proteins specifically enriched in xylem sap (blue) and proteins enriched in SXM (red). All proteins below the statistical threshold form the core exoproteome that is similarly enriched in both media (blue and red).

A group of 396 identified proteins fulfilled the criteria of a threshold of at least 2 peptides in at least two independent cultivations and a high intensity ratio of 0.83 of all replicates together in one condition. The list was sorted according to the positive directed signal-to-level (s/l) ratio using as maximum the SXM and xylem sap conditions. Polypeptides with an s/l ratio above 0.3 were considered as candidates with higher intensities in the specific medium and therefore belong to the specifically enriched proteins in that medium whereas an s/l ratio below 0.3 was considered not to be specifically enriched and formed the shared core proteome. The groups are displayed in a Venn diagram (Figure 18B), which shows that cultivation of *V. longisporum* in both, SXM and xylem sap, triggers the release of a large group of identical proteins as 221 proteins belong to the core set. These proteins are similar in abundance in both media. SXM, additionally, induces the secretion of another 143 proteins that are specifically enriched during cultivation in this medium. Xylem sap, however, triggers a smaller unique exoproteome response as only 32 proteins are specifically enriched here (Table 5).
Summarizing these results, the different secretion responses in SXM, which is thought to substitute xylem sap *in vitro,* and xylem sap indicates that the fungus is able to fine-tune its secretion response.

3.2.2 Xylem sap triggers the release of potential effectors such as NLPs

V. longisporum formed a specific secretion response in xylem sap compared to other media. This indicates that the fungus can distinguish between xylem sap and the presence of other plant material and accordingly fine-tunes its protein secretion. As these proteins are specifically secreted in the host xylem sap, their function is probably fulfilled during colonization of the plant. They may be more important during this step than proteins that are also secreted in other media. Therefore, the list of identified candidates after cultivation in xylem sap was further examined (Table 5).
Domain predictions of *V. longisporum* protein sequences were assigned with InterProScan (Jones *et al*, 2014) and classification of carbohydrate-active enzyme (CAZys) families was specified with dbCAN2 (Zhang *et al*, 2018) to address putative functions of all xylem sap-specific proteins (Table 5). Accordingly, proteins were sorted into different groups. The 32 xylem sap-specific proteins comprise 20 CAZys, five proteins with domains of known effectors, four metallopeptidases

and three proteins with either no domain or domains assigned to neddylation or redox processes. CAZys include enzymes and sugar-binding proteins that are important for degradation of the plant cell wall and successful invasion of the plant. Additional to the CAZys, several potential virulence factors were identified. The five *V. longisporum* proteins comprising domains of already characterized *V. dahliae* effectors incorporate either necrosis inducing protein (NPP1, also necrosis-inducing *Phytophtora* protein) or cerato-platanin (CP) domains. NPP1 domains are characteristic for Nep1-like proteins (NLP) of which *Verticillium* spp. contain up to eight members (Santhanam *et al*, 2013). Nlp1 and Nlp2 were shown to differentially contribute to *V. dahliae* pathogenicity on different hosts (Santhanam *et al*, 2013; Wang *et al*, 2004; Zhou *et al*, 2012). Our secretome approach identified four isogene products corresponding to two NLPs, Nlp2 and Nlp3, that were included in further analysis. Of the CP domain-containing proteins, one isogene assigned to Cp2, was identified as specifically enriched in xylem sap. *V. dahliae* possesses two CP proteins of which one CP protein, Cp1, affects virulence on cotton (Zhang *et al*, 2017b). Additionally, four isogenes of two metallopeptidases were found in the xylem sap-specific secretome. Metalloproteases are able to truncate host defense proteins such as chitinases and therefore have the potential to act as virulence factors (Naumann *et al*, 2011). In *V. dahliae,* the serine protease VdSsep1 also acts as virulence factor and absence of this protein results in reduced pathogenicity on cotton (Han *et al*, 2019).

These findings show that *V. longisporum* induces the secretion of xylem sap-specific exoproteins which include known and potential effectors important for plant colonization or infection.

Table 5. Xylem sap-specific exoproteins of *V. longisporum*.

	Name	*Vl*43 identifier	Best Hit *V. dahliae* JR2	Protein domain - *Vl*43	Peptide counts SXM	Peptide counts XyS	XyS/ SXM	s/l ratio
Characterized *Vd* effector domains	Nlp3	vl43-au16.g9727.t1	VDAG_JR2_Chr4g05950a	Necrosis inducing protein	0.3	8.3	>8.3	0.84
		vl43-au16.g96.t1			0.2	6.3	>6.3	0.81
	Nlp2	vl43-au16.g3884.t1	VDAG_JR2_Chr2g05460a	Necrosis inducing protein	1.0	4.8	4.8	0.61
		vl43-au16.g12566.t1			1.8	6.5	3.6	0.47
	Cp2	vl43-au16.g16459.t1	VDAG_JR2_Chr2g07000a	Cerato-platanin	0.3	1.8	>1.8	0.41
Metallo-peptidases	Mep2	vl43-au16.g19470.t1	VDAG_JR2_Chr1g21900a	Peptidase M43	1.0	8.8	8.8	0.57
		vl43-au16.g11262.t1			1.3	8.7	6.7	0.55
	Mep1	vl43-au16.g19320.t1	VDAG_JR2_Chr8g09760a	FTP domain, Peptidase M36, fungalysin	1.7	14.0	8.2	0.69
		vl43-au16.g14388.t1			1.8	13.5	7.5	0.65
CAZys	Gla1	vl43-au16.g17458.t1	VDAG_JR2_Chr8g11020a	Glycoside hydrolase 15, Carbohydrate binding module family 20	0.0	8.2	>8.2	0.76
		vl43-au16.g13024.t1			0.0	3.8	>3.8	0.62
	Cbd1	vl43-au16.g11636.t1	VDAG_JR2_Chr4g04440a	Auxiliary activity 13, Carbohydrate binding module family 20	1.7	13.8	8.1	0.71
		vl43-au16.g3945.t1			1.3	6.8	5.2	0.55
	Amy1	vl43-au16.g6892.t1	VDAG_JR2_Chr7g03330a	Glycoside hydrolase 13	1.5	12.0	8.0	0.68
		vl43-au16.g6746.t1	VDAG_JR2_Chr3g11080a	Glycoside hydrolase 43	1.2	7.8	6.5	0.68
		vl43-au16.g12522.t1			1.0	5.8	5.8	0.61
		vl43-au16.g12596.t1	VDAG_JR2_Chr6g04040a	Glycosyl hydrolases 11	0.8	5.2	>5.2	0.55
		vl43-au16.g15027.t1	VDAG_JR2_Chr6g09340a	Pectate lyase 6	2.2	11.2	5.1	0.57
		vl43-au16.g5309.t1			2.3	10.8	4.7	0.59
		vl43-au16.g207.t1	VDAG_JR2_Chr1g06940a	Glycoside hydrolase 16	2.2	9.0	4.1	0.56
		vl43-au16.g14986.t1			2.3	9.5	4.1	0.55
		vl43-au16.g5519.t1	VDAG_JR2_Chr6g09790a	Auxiliary activity 9, Carbohydrate binding module family 1	2.0	8.2	4.1	0.51
		vl43-au16.g20506.t1			2.3	8.8	3.8	0.46
		vl43-au16.g15947.t1	VDAG_JR2_Chr3g00250a	Glycoside hydrolase 131	1.0	4.0	4.0	0.43
		vl43-au16.g9097.t1	*V. alfalfae*: VDBG_03110	Glycoside hydrolase 12	1.0	2.8	2.8	0.38
		vl43-au16.g2684.t1	VDAG_JR2_Chr8g10630a	Auxiliary activity 7	6.0	13.2	2.2	0.33
		vl43-au16.g13340.t1			8.0	15.3	1.9	0.34
		vl43-au16.g16765.t1	VDAG_JR2_Chr1g04240a	Glycosyl transferase 1	0.3	1.7	>1.7	0.49
		vl43-au16.g9025.t1	VDAG_JR2_Chr7g01210a	Carbohydrate esterase 1 , Carbohydrate binding module family 1	0.2	1.3	>1.3	0.49
Other proteins		vl43-au16.g9360.t1	*V. alfalfae*: VDBG_05827		0.0	7.5	>7.5	0.77
		vl43-au16.g11273.t1	VDAG_JR2_Chr6g05220a	Quinoprotein alcohol dehydrogenase-like superfamily, WSC	3.2	11.7	3.7	0.46
		vl43-au16.g18734.t1	VDAG_JR2_Chr1g04640a	Ubiquitin 3 binding protein But2, C-terminal	9.7	18.8	1.9	0.37

*Vl*43 = *V. longisporum* 43; SXM = simulated xylem medium; XyS = xylem sap; s/l = signal-to-level; CAZys = carbohydrate-active enzymes; *Vd* = *V. dahliae*; FTP = fungalysin/thermolysin propeptide; WSC = putative carbohydrate-binding domain

V. longisporum 43 used in this study is an allodiploid fungus derived from two haploid parents in an A1xD1 hybridization event. A1 and D1 are hypothetical species of which D1 is closely related to *V. dahliae* and A1 is distantly related to *V. alfalfae* (Inderbitzin & Subbarao, 2014). Consequently, most genes are encoded in two copies, reflecting the two isogenes of both parental lineages.

Following analyses of these proteins were conducted with the haploid strain *V. dahliae* JR2, which is the close relative to the parental species D1, due to the fact that genetic manipulations with the haploid strain are much easier to facilitate than with an allodiploid strain. Therefore, BLAST searches against the *V. dahliae* JR2 proteome (Ensembl Fungi) were conducted. The best hit in *V. dahliae* is displayed in Table 5, except for the *V. alfalfae* specific proteins that were searched against the *V. alfalfae* VaMs.102 proteome. Domain predictions of *V. dahliae* or *V. alfalfae* proteins resembled the *V. longisporum* predictions.

Of the 32 xylem sap-specific proteins eleven were detected with two isogene products, which can be assigned to one of the parental strains related to *V. dahliae* or *V. alfalfae*. Another eight proteins were found of which only one copy was detected in the xylem sap-specific exoproteome. The other isogene product was either detected in the core exoproteome or not at all. Two proteins were detected in the xylem sap-specific secretome with only one copy in *V. longisporum* that were assigned to *V. alfalfae*. Table 5 displays the proteins grouped according to “Characterized *V. dahliae* (*Vd*) effector domains”, “Metallopeptidases”, “CAZys” and “Other proteins”. The isogenes are paired up and the assigned *V. dahliae* or *V. alfalfae* protein accession number is displayed. Within these groups, proteins were ranked according to the quotient of peptide counts identified in xylem sap (XyS) by the number detected in simulated xylem medium (SXM). Displayed peptide counts were averaged from six biological replicates. If the number was below 1, it was calculated as 0 and the quotient was given as bigger as the average XyS peptide counts (>).

To investigate whether the proteins that were uniquely enriched in xylem sap play a major role in fungal infections, the top candidates of the protein groups that have been shown to play critical roles in plant colonization (Fradin & Thomma, 2006; Santhanam *et al*, 2013; Zhang *et al*, 2017b) were analyzed in this study. These groups are the proteins with domains of known effectors, metallopeptidases and CAZys and chosen proteins are marked in Table 5 with a colored given name. From

the first mentioned group all identified candidates were included. These comprise two NLPs, Nlp2 and Nlp3, and the Cp2. For further investigations the *V. dahliae* JR2 homolog of *VdCP1* was tested, as well. VdCp1 is a virulence factor of *V. dahliae* strain XH-8 in infections on cotton (Zhang *et al*, 2017b). The metallopeptidases that were identified as specifically enriched in xylem sap were named Mep1 and Mep2 and were both included in the study. Of the latter group, the CAZys, three top candidates, a glucoamylase Gla1, a carbohydrate-binding module containing protein Cbd1 and the α-amylase Amy1 were further investigated.

Protein domain structures as predicted by InterProScan (Jones *et al*, 2014) and dbCAN2 (Zhang *et al*, 2018) are displayed in Figure 19. Consistent with the idea of a secreted protein all candidates were predicted to contain an N-terminal signal peptide (SP). Cp2 and Nlp2, however, required closer examination. Following the *V. dahliae* JR2 annotations (Ensembl Fungi) Cp2 has a predicted size of 195 aa with no predicted SP whereas Nlp2 is annotated as 184 aa protein, which results in a long uncharacteristic N-terminal SP. Incorrect annotation of the ORFs in *V. dahliae* JR2 with premature Start codons is possible. Using the annotation of the homologous genes for *CP2* and *NLP2* in *V. dahliae* VdLs.17, *VDAG_01852* and *VDAG_01995*, respectively, protein domain predictions are more likely as shown in Figure 19. Apart from the signal peptides the proteins contain the characteristic domains. The CPs and NLPs contain the name-giving CP and NPP1 domain, respectively. The metalloproteases belong to two different types of peptidases. Mep1 contains a fungalysin/thermolysin propeptide and the catalytic peptidase domain of family M36 whereas Mep2 comprises the M43 family domain. The CAZys all contain protein motifs related to carbohydrate catalytic activity. The glucoamylase Gla1 was predicted to contain a glycosyl hydrolase family 15 domain and a non-catalytic Carbohydrate-binding module family 20 domain (CBM20). The protein Cbd1, as well, incorporates a CBM20 domain and a lytic polysaccharide mono-oxygenase domain. It was assigned to enzymes with auxiliary activity 13 (AA13) meaning it has the potential to aid other CAZys to gain access to the carbohydrates encrusted in the plant cell wall (Levasseur *et al*, 2013). Amy1 comprises the glycosyl hydrolase family 13 domain.

As these proteins were specifically enriched during cultivation in xylem sap compared to simulated xylem medium, they are thought play a critical role during colonization of the host plant. Therefore, these candidates were further analyzed.

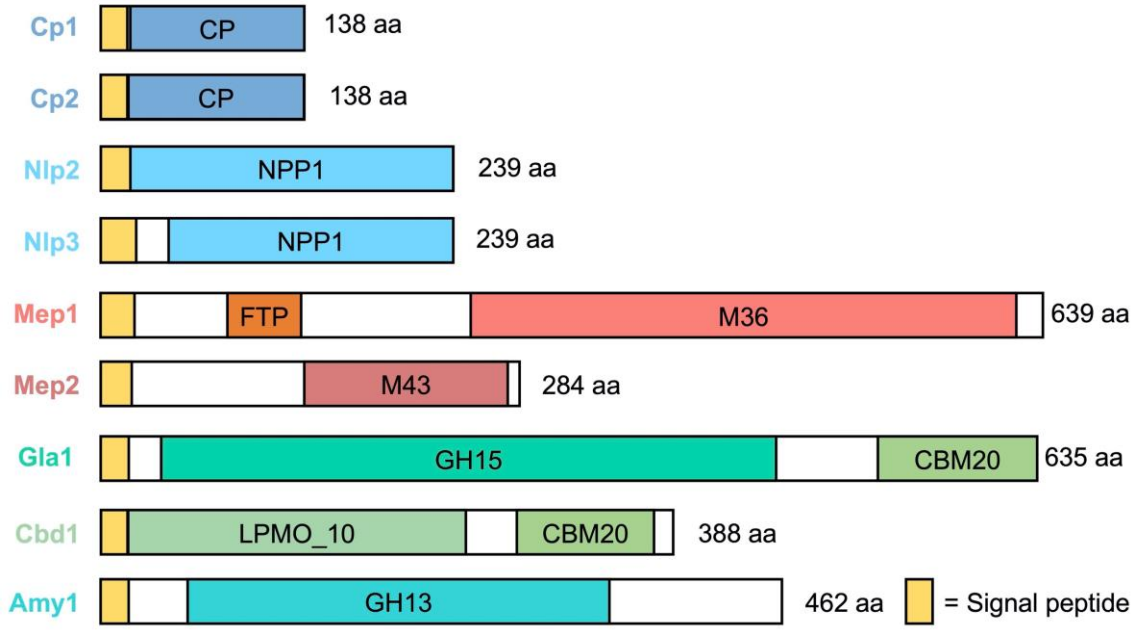

Figure 19. *V. dahliae* protein domain structures of effectors enriched in xylem sap. The protein domain structures of analyzed *V. dahliae* proteins were predicted by InterProScan (Jones *et al*, 2014) and dbCAN2 (Zhang *et al*, 2018). All proteins were predicted to contain a secretory signal peptide (SP, yellow) and the following characteristic domains: Cp1 and Cp2 – Cerato-platanin domain (CP, PF07249), Nlp2 and Nlp3 – necrosis-inducing protein domain (NPP1, PF05630), Mep1 – Fungalysin/thermolysin propeptide (FTP, PF07504), Peptidase M36 domain (PF02128), Mep2 – Peptidase M43 domain (PF05572), Gla1 – glycosyl hydrolase family 15 (GH15, PF00723) and Carbohydrate-binding module family 20 domain (CBM20, PF00686), Cbd1 – Lytic polysaccharide mono-oxygenase domain (LPMO_10, PF03067) belonging to enzymes with auxiliary activity 13 and CBM20, Amy1 – glycosyl hydrolase family 13 domain (GH13, PF00128).

3.2.3 Exoproteins enriched in xylem sap are dispensable for the *V. dahliae ex planta* phenotype

To analyze the function of the secreted proteins, deletion strains were constructed. Genes coding for Cp1, Cp2, Nlp2, Nlp3, Mep1, Mep2, Gla1, Cbd1 and Amy1 were deleted in *V. dahliae* JR2. The full ORFs of the genes were replaced by a resistance cassette flanked with the corresponding 5' and 3' regions by homologous recombination. The CAZys, *GLA1*, *CBD1* and *AMY1* were replaced by the nourseothricin resistance cassettes. The metallopeptidases were additionally analyzed in double deletions as synergistic action may occur as shown

for *F. oxysporum* virulence on tomato (Jashni *et al*, 2015). Therefore, the *MEP1* and *MEP2* ORFs were replaced with hygromycin and nourseothricin resistance cassettes, respectively, and single and double deletions were constructed. Similarly, double deletions for *NLP2*/*NLP3* and *CP1/CP2* were constructed. *NLP2* was replaced by the hygromycin and *NLP3* by the nourseothricin resistance cassette. *NLP2* and *NLP3* were also ectopically complemented where the respective ORF including the 5' and 3' flanking regions was introduced into the deletion strain again. *CP1* was replaced by the nourseothricin and *CP2* by the hygromycin resistance marker. Here, also ectopic complementations were generated with the similar procedure as for the *NLP* complementation strains. Correct integration of the deletion or complementation constructs was verified by Southern hybridizations (Figure S4-7).

The *ex planta* phenotypes of all generated strains were tested on several solid media such as minimal and complete medium and simulated xylem medium. Additionally, the strains were tested for the involvement in stress responses with at least one stressor tested for each strain. The stress inducing agent was added to minimal medium. As cell wall perturbing agents SDS and EtOH or as oxidative stressor H_2O_2 were used. All single deletion, double deletion and complementation strains exhibited similar morphological development as *V. dahliae* WT, which is exemplified by growth on SXM (Figure 20). All colonies show WT-like aerial hyphae and microsclerotia development indicating that the tested proteins are dispensable for growth on SXM agar. The simulated xylem medium is supposed to reflect the nutritional conditions in the plant's xylem and therefore represents the closest environment to the actual xylem sap. Nonetheless, there are differences to the xylem sap where the proteins were found to be enriched, which was as well sensed by the fungus in the exoproteome experiment. Furthermore, these phenotypes were conducted on solid agar plates that also triggers different morphological fungal structures compared to growth in liquid media.

Therefore, these results are in accordance with the exoproteome pattern. As *Verticillium* induces the secretion of a small specific exoprotein set that is uniquely secreted in xylem sap, it is not surprising if these proteins have no role in other media such as the pectin rich SXM agar.

Concluding, the xylem sap-specific enriched proteins Cp1, Cp2, Nlp2, Nlp3, Mep1, Mep2, Gla1, Cbd1 and Amy1 are dispensable for the *ex planta* phenotype. Growth

rates and formation of microsclerotia was indistinguishable between all tested strains and *V. dahliae* WT suggesting that, under the tested conditions, the function of the proteins is dispensable for vegetative growth, development and stress response of *V. dahliae*. Whether the specific role lies in the xylem sap of the host during plant infection was further investigated.

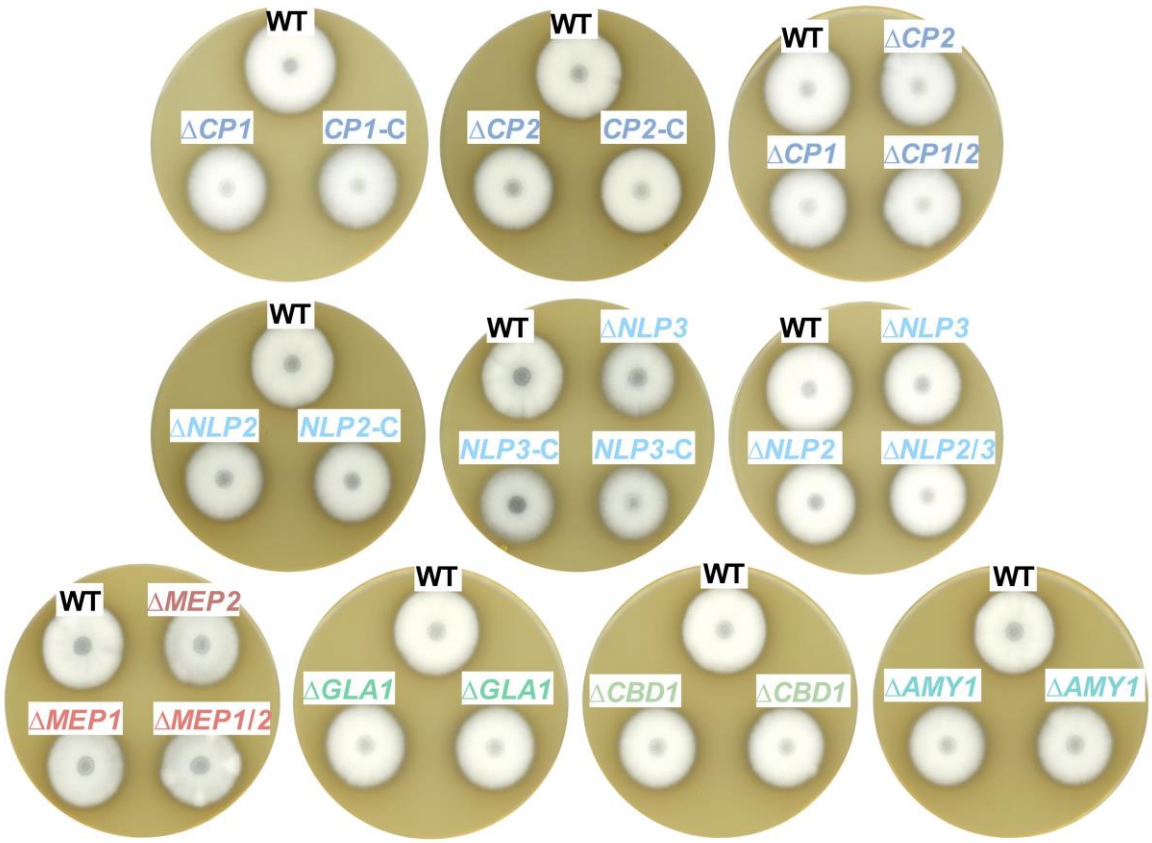

Figure 20. Exoproteins specifically secreted in xylem sap are dispensable for *V. dahliae ex planta* phenotype.
50 000 spores of *V. dahliae* JR2 wildtype (WT) and indicated deletion (Δ*CP1* – VGB316, ΔCP2 – VGB406, Δ*CP1/2* – VGB423, Δ*NLP2* – VGB390, Δ*NLP3* – VGB384, Δ*NLP2/7* – VGB400, Δ*MEP1* – VGB226, Δ*MEP2* – VGB126, Δ*MEP1/2* – VGB203, Δ*GLA1* – VGB129, VGB131, Δ*CBD1* – VGB127, VGB132, Δ*AMY1* – VGB128, VGB130) and complementation (*CP1*-C – VGB489, *CP2*-C – VGB429, *NLP2*-C – VGB427, *NLP3*-C – VGB425, VGB426) strains were point inoculated on simulated xylem medium (SXM) plates and incubated at 25°C for ten days. Of three deletion mutants (Δ*AMY1*, Δ*GLA1*, Δ*CBD1*) two transformants were spotted as of the *NLP3* complementation strain. Top-view scans of the colonies show a similar phenotype of all strains.

3.2.4 Exoproteins specifically enriched in xylem sap can contribute to *V. dahliae* virulence on tomato

The comparative exoproteomic approach revealed a small set of xylem sap-specifically enriched proteins. The function of these proteins is expected to be in

the interaction with plant substrates in the xylem sap of the host. Therefore, all *V. dahliae* single and double deletion strains were tested for their virulence on tomato.

3.2.4.1 Necrosis and ethylene inducing-like effectors Nlp2 and Nlp3 are required for full virulence of *V. dahliae* on tomato

In this study, the contribution of *NLP2* (*VDAG_JR2_Chr2g05460a*) and *NLP3* (*VDAG_JR2_Chr4g05950a*) to *V. dahliae* JR2 pathogenicity was examined. Nlp2 and Nlp3 were both detected in the xylem sap-specific exoproteome. NLPs are known to be effectors for *V. dahliae* pathogenicity (Santhanam *et al*, 2013; Zhou *et al*, 2012; Wang *et al*, 2004). Nlp1 and Nlp2 contribute to *V. dahliae* JR2 virulence on tomato and *Arabidopsis* (Santhanam *et al*, 2013) whereas corresponding proteins in *V. dahliae* V592 did not alter virulence on cotton (Zhou *et al*, 2012). Nlp3 did not show any cytotoxic activity on *N. benthamiana* and has not been further characterized (Santhanam *et al*, 2013). However, as the cytotoxic effect was studied on *N. benthamiana,* it is nevertheless possible that Nlp3 has a role in a different host. *V. dahliae* isolates contain up to eight NLP homologs (Santhanam *et al*, 2013; Zhou *et al*, 2012) whereas many fungi only contain up to three NLPs (Gijzen & Nürnberger, 2006). It is intriguing to speculate that not all NLPs have a function in virulence on the same host and, therefore, the higher number of NLP members may correlate with the broad host range of *V. dahliae*. Thus, the two xylem sap-specific enriched NLPs, Nlp2 and Nlp3, were investigated in this study. Npl2 has already been tested in the *V. dahliae*-tomato system, but only exhibited minor effects (Santhanam *et al*, 2013). It would be interesting to see if a possible synergistic effect of two NLPs was visible. This question was addressed utilizing the double deletion Δ*NLP2*Δ*NLP3*.

First, the adherence to the root and further root colonization of the *NLP3* deletion strain on *A. thaliana* was monitored with fluorescence microscopy. The *NLP3* deletion strain expressing free *GFP* under the control of the *gpdA* promoter (Δ*NLP3 GFP* OE) and the WT control overexpressing GFP (WT *GFP* OE) were used to root inoculate three-week-old *Arabidopsis* seedlings. The root colonization at three and five days post inoculation is indistinguishable between WT *GFP* OE and Δ*NLP3 GFP* OE (Figure 21A). Initial root colonization was observed at three days following

inoculation and after five days whole roots were covered with fungal hyphae suggesting that Nlp3 is dispensable for root colonization, at least on *A. thaliana*.

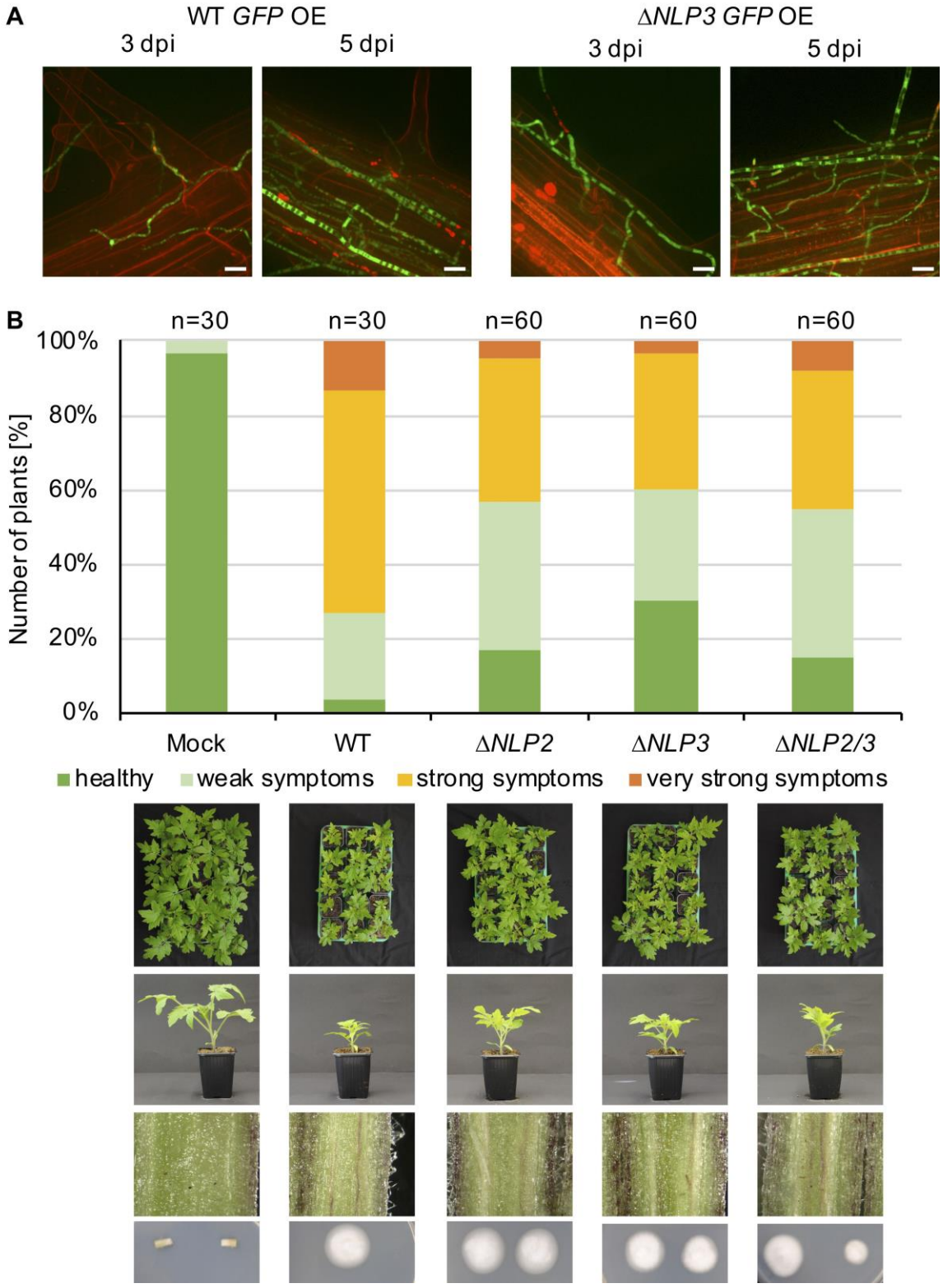

Figure 21. Necrosis and ethylene inducing-like effectors Nlp2 and Nlp3 contribute to *V. dahliae* virulence on tomato.

NLP3 deletion strain was tested in *A. thaliana* root colonization and single and double deletion strains of *NLP2* and *NLP3* were tested for pathogenicity on tomato. Infected plants

were incubated in the climate chamber under 16h:8h light:dark at 22-25°C. **(A)** Three-week-old *A. thaliana* seedlings were infected with *V. dahliae* JR2 and *NLP3* deletion strain overexpressing free *GFP* (WT *GFP* OE and Δ*NLP3 GFP* OE, respectively) via root dipping in a 100 000 spores/ml spore solution. At three and five days post inoculation (dpi) the colonization of the fungal hyphae was monitored with root cells stained by 0.05% propidium iodide/0.01% silwet solution. The experiment was repeated twice with two individual transformants of Δ*NLP3 GFP* OE (VGB431, VGB432). Representative fluorescence microscopy pictures show similar initial colonization of *V. dahliae* WT *GFP* OE and Δ*NLP3 GFP* OE on the root surface at three dpi and whole root colonization at five dpi. Scale bar = 10 µm. **(B)** Ten-day-old tomato seedlings were infected with spores of *V. dahliae* JR2 and the indicated *NLP2* (Δ*NLP2* – VGB390, VGB391) and *NLP3* single (Δ*NLP3* – VGB384, VGB385) and double deletion strains (Δ*NLP2/3* – VGB400, VGB401) via root-dipping. Uninfected plants (mock) served as control. The disease index was assessed at 21 dpi and includes the height of the plant, the longest leaf length and the weight of the plant. Representative plants, discolorations of the hypocotyls and the fungal outgrowth of the surface sterilized stems are shown. The number of treated plants (n) is shown for each fungal strain. The experiment was repeated twice. For the deletion strains two individual transformants were tested.

Further, the effect on pathogenicity towards tomato was investigated. Ten-day-old tomato seedlings were root-inoculated with *NLP2* and *NLP3* single and double deletion strains and WT as control. Plants treated with dH_2O were used as mock control. The infection study was repeated twice including two transformants of each deletion strain. The height of the plant, longest leaf length and the fresh weight of the aerial part of the plant were measured. Average means of the mock treated plants were set to 100%, data of the infected plants were calculated accordingly and sorted into different categories. The stack diagram displays the percentage of plants exhibiting the respective symptoms (Figure 21B). All tested deletion strains were compromised in virulence compared to WT. However, plants still developed symptoms. All infected plants exhibited stem discoloration and fungal outgrowth was detected after stems were surface sterilized. But symptom development in plants colonized with deletion strains was less severe compared to WT infection. Overviews of the treys with 15 treated plants, which is a representative number of plants considering fluctuations in the infection success, nicely demonstrate the differences (Figure 21B). Whereas the trey with WT infected plants exhibited the least visible green leaf mass, deletion strain infections led to an elevated mass of greens. Translating the disease symptoms into the different categories, it shows that about 60% of tested plants exhibited no or only mild symptoms compared to approximately 25% of the WT treated plants. Infections with the Δ*NLP2*Δ*NLP3*

double deletion strain resulted in a similar disease index compared to the single deletion strains and, therefore, does not show an additive effect of the two deleted *NLP* genes.

Concluding, this infection study demonstrated that *NLP2* and *NLP3* contribute to *V. dahliae* JR2 virulence on tomato. Deletion of the genes still resulted in induction of disease symptoms suggesting that the strains are well able to penetrate the plant and Nlp2 and Nlp3 may play a role inside of the plant. These experiments provide evidence that the xylem sap-specific exoproteome does contain effectors with roles in the xylem sap.

3.2.4.2 *V. dahliae* pathogenicity on tomato is independent of Cp1 and Cp2

Cerato-platanin (CP) domain containing proteins are spread among the fungal kingdom and several functions could be assigned to the CP family. CPs act as elicitors of plant defense responses in their hosts, they were speculated to function in fungal cell wall formation due to their chitin binding activity and could function in host colonization by weakening plant cellulose (de O. Barsottini *et al*, 2013; Baccelli *et al*, 2014). In *V. dahliae* one CP protein, VdCp1, was identified in the secretome of *V. dahliae* strain XH-8 and functions in chitin scavenging to prevent the fungal recognition by plants. *VdCP1* knockout mutants were affected in cotton virulence (Zhang *et al*, 2017b). A *VdCP1* homolog was also detected in the exoproteome studies, more precisely in the xylem sap-specific secretome, which was named *CP2* (*VDAG_JR2_Chr2g07000a*). However, the closest *V. dahliae* JR2 homolog (*VDAG_JR2_Chr7g00860a*) of *VdCP1* was not detected in the secretome approach, but was included in this study to investigate on a putative combined effect of *CP1* and *CP2*.

To assess the role of *V. dahliae CP1* and *CP2* in pathogenicity on tomato plants, *CP1* and *CP2* single and double deletion strains were root inoculated on susceptible tomato plants along with WT JR2. Additionally, *CP1* and *CP2* complementation strains were included in the infection assay and mock plants were treated similarly with dH_2O as control. Infection experiments and evaluations were carried out as explained for *NLP* deletion strains (3.2.4.1).

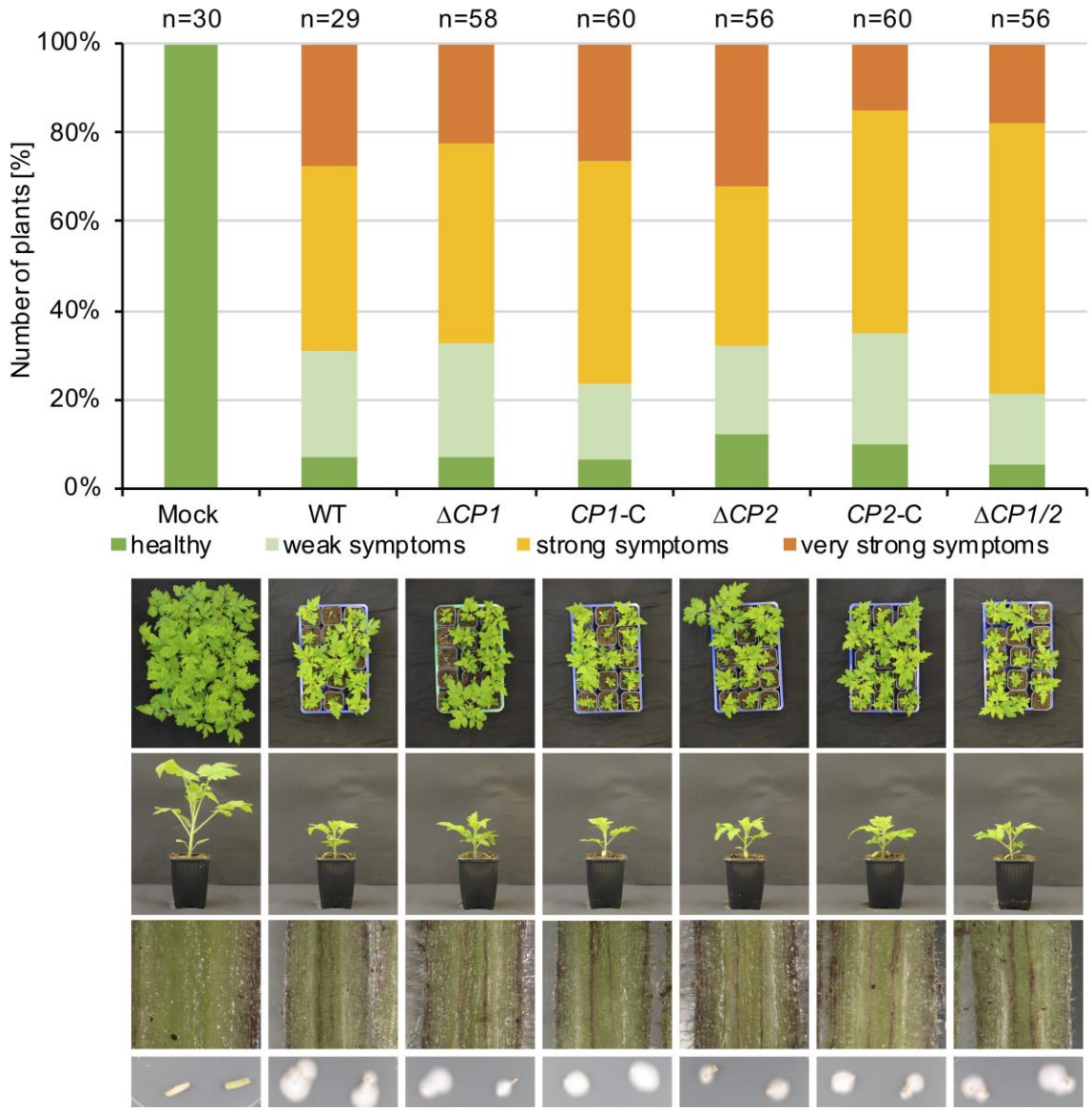

Figure 22. Exoproteins Cp1 and Cp2 are dispensable for *V. dahliae* virulence on tomato.

Ten-day-old tomato seedlings were infected with spores of *V. dahliae* JR2 wildtype (WT) and the indicated deletion (Δ*CP1* – VGB316, VGB317, ΔCP2 – VGB406, VGB422, Δ*CP1/2* – VGB423, VGB424) and complementation strains (*CP1*-C – VGB489, VGB490, *CP2*-C – VGB429, VGB430) via root-dipping. Uninfected plants (mock) served as control. Plants were incubated in the climate chamber under 16h:8h light:dark at 22-25°C. The disease index was assessed at 21 days post inoculation and includes the height of the plant, the longest leaf length and the weight of the plant. Representative plants, discolorations of the hypocotyls and the fungal outgrowth of the stems are shown. The number (n) of treated plants is shown for each fungal strain. The experiment was repeated twice. *CP1* and *CP2* deletion strains infect tomato plants to the same extent as WT and the complementation strains.

All tested deletion and complementation strains were found to be as virulent as WT. The plants developed similar severe disease symptoms (Figure 22). Fungal outgrowth assays upon plating of sterilized stem sections harvested from inoculated plants demonstrated that the fungus could be re-isolated. Additionally, all hypocotyls of infected plants showed plant defense reactions, which was visible by the discoloration of the hypocotyl.

Concluding, *V. dahliae* virulence on tomato plants is independent of Cp1 and Cp2 under tested conditions. Not even the deletion of both CP encoding genes resulted in a visible effect when using the corresponding deletion strains for plant infection experiments. The double deletion strain was able to colonize tomato plants whereas on cotton the deletion of *VdCP1* resulted in reduced virulence (Zhang *et al*, 2017b). Together these data provide evidence for a host-specific role of CPs.

3.2.4.3 Metalloprotease Mep1 can contribute to *V. dahliae* pathogenicity on tomato whereas Mep2 is dispensable

Metalloproteases are able to truncate host defense proteins such as chitinases and, therefore, act as virulence factors (Naumann *et al*, 2011). *V. dahliae* is impaired in virulence on cotton if the serine protease *VdSSEP1* was knocked out. The protease cleaves chitinase 28 that is important for plant defense (Han *et al*, 2019). In *F. oxysporum* the double deletion of a serine protease *FoSep1* and a metalloprotease *FoMep1* resulted in reduced virulence on tomato (Jashni *et al*, 2015). It was reported that the effect of the single deletion strains on *Fusarium* virulence was not measurable, but the double deletion strain resulted in a significant less diseased phenotype compared to WT infected plants. These data indicate the importance of the investigation on synergistic actions of proteases (Jashni *et al*, 2015). In our secretome approach proteins of the two metallopeptidase families M36 and M43 were found to be uniquely enriched in xylem sap. According to similarities to the homologous protease Mep1 (FVEG_13630.0) of *F. oxysporum*, the corresponding *V. dahliae* protein containing M36 domain was named Mep1 (VDAG_JR2_Chr8g09760a, 63.7% aa sequence identity) and the M43 containing protein Mep2 (VDAG_JR2_Chr1g21900a, 19.1% aa sequence identity). This study aimed to investigate on a putative additive effect of Mep1 and Mep2 in *V. dahliae*.

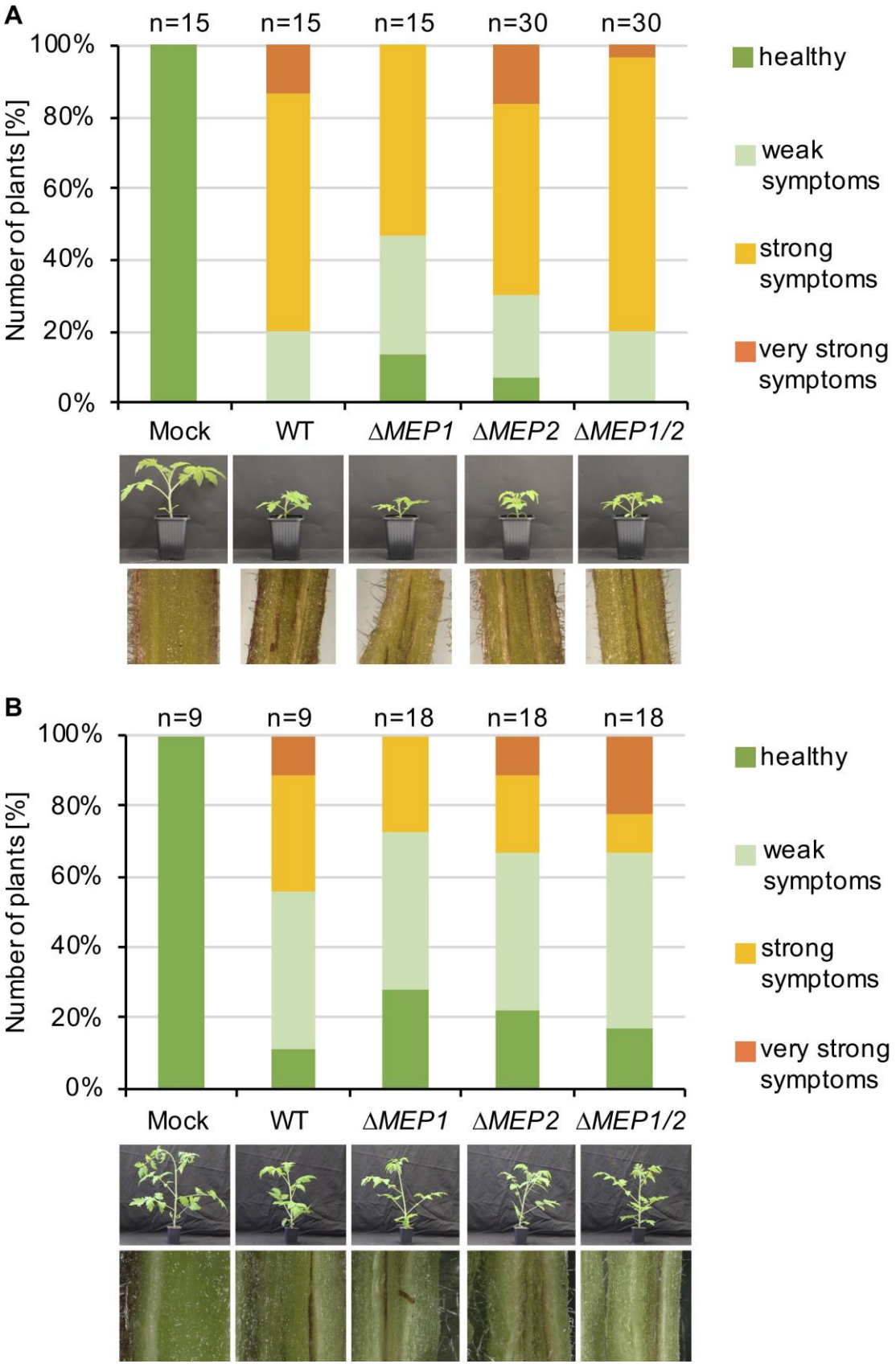
A
n=15
n=15
n=15
n=30
n=30
100%
80%
60%
40%
20%
0%
Number of plants [%]
Mock
WT
ΔMEP1
ΔMEP2
ΔMEP1/2
healthy
weak symptoms
strong symptoms
very strong symptoms
B
n=9
n=9
n=18
n=18
n=18
100%
80%
60%
40%
20%
0%
Number of plants [%]
Mock
WT
ΔMEP1
ΔMEP2
ΔMEP1/2
healthy
weak symptoms
strong symptoms
very strong symptoms

Figure 23. Absence of both metalloproteases Mep1 and Mep2 results in wildtype-like *V. dahliae* pathogenicity on tomato.
Ten-day-old tomato seedlings were root-infected with the same number of spores of *V. dahliae* JR2 (WT) and single (Δ*MEP1* – VGB226, VGB227, Δ*MEP2* – VGB126, VGB133) and double deletions (Δ*MEP1/2* – VGB203, VGB204) of the metalloproteases *MEP1* and *MEP2*. Uninfected plants (mock) served as control. Plants were incubated in the climate chamber under 16h:8h light:dark at 22-25°C. The disease index was assessed at 21 **(A)** or 35 days post inoculation **(B)** and includes the height of the plant, length of the 2nd true leaf and weight of the plant. Representative plants and discolorations of the hypocotyls are shown for each infection. The number (n) of plants is shown for each infection or mock treatment. Infection with the deletion strains resulted in the same stunting phenotype as WT infections.

Tomato infections were conducted with *MEP1* and *MEP2* single and double deletion strains and WT control infections, as well as the mock negative control. Virulence assays were conducted as described for *NLP* deletion strains. Infections with all fungal strains resulted in induction of disease symptoms similar to WT colonization (Figure 23A). A small effect of the *MEP1* deletion strain was observed as approximately 45% of the plants showed no or only mild symptoms compared to 20% of mild symptom induction of the WT strain. The plants inoculated with the double deletion strain Δ*MEP1*Δ*MEP2*, however, were more affected and resembled the WT treated plants. Nevertheless, the possible effect of *MEP1* was further investigated in tomato infections with longer incubations in which disease symptoms were evaluated after five weeks. A putative small defect in virulence may be better visible if the fungus has more time to colonize the plant. However, the difference in disease symptoms induced after five weeks were comparable to results after 3 weeks of infection (Figure 23B).
These results suggest that Mep2 is dispensable for *V. dahliae* pathogenicity on tomato whereas it is possible that Mep1 contributes to virulence.

3.2.4.4 Single *V. dahliae* carbohydrate-active enzymes are dispensable for induction of disease symptoms in tomato

CAZys include cell wall degrading enzymes (CWDE) that are important for successful plant invasion due to their potential to degrade plant material. As they have redundant functions, their analysis remains a major challenge. Nevertheless, other studies were able to exhibit virulence effects of single CWDEs. In *V. dahliae* isolate Vd991 a pectate lyase was detected that triggered plant defense responses

and conferred resistance to *B. cinerea* and *V. dahliae* in tobacco and cotton plants (Yang *et al*, 2018). Glycoside hydrolase 12 proteins, VdEG1 and VdEG3 from *V. dahliae* were shown to contribute to *V. dahliae* virulence to *N. benthamiana* and cotton plants (Gui *et al*, 2017).

Therefore, we decided to investigate on the best CAZy candidates detected in our exoproteomic approach that were specifically highly enriched in xylem sap. These include a glucoamylase Gla1, a putative polysaccharide mono-oxygenase Cbd1 and an α-amylase Amy1. Deletion strains were constructed and tested in tomato infections as described previously. Deletion of *GLA1* (*VDAG_JR2_Chr8g11020a*), *CBD1* (*VDAG_JR2_Chr4g04440a*) or *AMY1* (*VDAG_JR2_Chr7g03330a*) did not lead to any differences in disease symptom induction compared to WT infections (Figure 24). All fungal infections resulted in a similar stunting phenotype as WT colonization and plant defense reactions were observed by the discoloration of the hypocotyls in all infected plants.

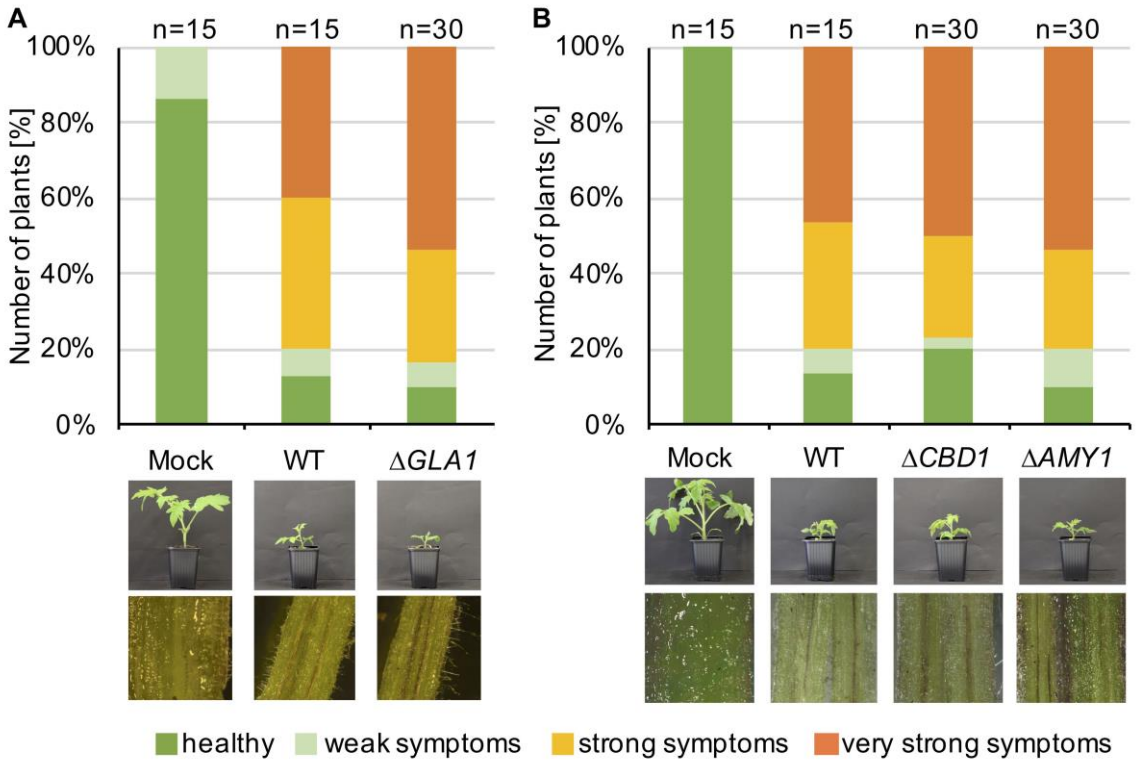

Figure 24. Carbohydrate-active enzymes Gla1, Cbd1 and Amy1 are dispensable for *V. dahliae* virulence on tomato.
Ten-day-old tomato seedlings were root-infected with the same number of spores of *V. dahliae* JR2 (WT) and the indicated deletion strains (Δ*GLA1* – VGB129, VGB131, Δ*CBD1* – VGB127, VGB132, Δ*AMY1* – VGB128, VGB130). Uninfected plants (mock) served as control. Plants were incubated in the climate chamber under 16h:8h light:dark at 22-25°C. The disease index was assessed at 21 days post inoculation and includes the height of the plant, length of the 2nd true leaf and weight of the plant. Representative plants and discolorations of the hypocotyls are shown for each infection. The number (n) of plants is shown for each fungal strain or mock treatment. **(A)** Infections with *GLA1* (glycoamylase) deletion strains resulted in the same stunting phenotype as WT infections. **(B)** Strains with deletion of the carbohydrate-binding domain containing *CBD1* or the amylase *AMY1* resulted in a WT-like induction of disease symptoms.

This study demonstrated that it is not sufficient to delete one single gene coding for one of the tested CAZys to affect *V. dahliae* virulence on tomato under the tested conditions. Due to redundant functions of other CAZys, it is possible that the single effect is neglectable. However, the exoproteomic approach revealed that *Verticillium* is able to sense different environments as it induces the secretion of three different response patterns. The xylem sap-specific set of proteins was revealed to include proteins with different effects on *V. dahliae* virulence. The CAZys, Mep2 and CPs did not affect *V. dahliae* pathogenicity in our virulence assays. However, the xylem sap-specific proteins also included effectors such as Mep1, Nlp2 and Nlp3 that, even with single deletions of the corresponding genes in *V. dahliae*, resulted in compromised *V. dahliae* pathogenicity on tomato.

4 Discussion

Verticillium spp. colonize the vascular system of a broad host range. During infection of the plant, it mainly restricts growth to spore production and exploits the xylem stream to spread throughout the whole plant (Pegg & Brady, 2002). The lifestyle of *Verticillium* spp. requires communication with the host plant to circumvent detection by the plant or to combat plant defense responses by the secretion of effectors. In the soil, the fungus as well depends on the perception of environmental cues to initiate formation of appropriate developmental structures, the resistant, melanized microsclerotia.

To translate these signals into cellular responses, the fungus requires developmental regulators. The functions of two transcriptional regulators were dissected in this study (Figure 25). The circadian clock component Frq was revealed to be a light-dependent suppressor of microsclerotia formation whereas it activates conidia formation. The protein Sfl1, known for suppression of flocculation genes in yeast, is required for conidia and microsclerotia production in *V. dahliae*. Genetic analyses using double deletion strains suggest that *SFL1* is epistatic to *FRQ* in microsclerotia development. Frq and Sfl1, both, are required for full virulence on tomato.

Insights into the fungal communication with the plant were received by comparing the secretome of allodiploid *V. longisporum* in different media including the simulated xylem medium (SXM) and xylem sap of the host plant *B. napus*. Different exoproteome patterns were formed after cultivation in non-plant related media and SXM and xylem sap. The secretion response that was uniquely induced in xylem sap includes CAZys, peptidases and proteins with domains of known effectors. Several candidates were analyzed in the haploid parental strain *V. dahliae*. Single deletion strains of CAZy encoding genes, single and double deletion strains of *MEP2* and *MEP1*/*MEP2*, respectively, coding for metallopeptidases as well as single and double deletion strains of *CP1* and *CP2* encoding cerato-platanin proteins did not affect *V. dahliae* pathogenicity. In contrast, the deletion of *MEP1* and the necrosis inducing *NLP2* and *NLP3* resulted in reduced virulence on tomato (Figure 25).

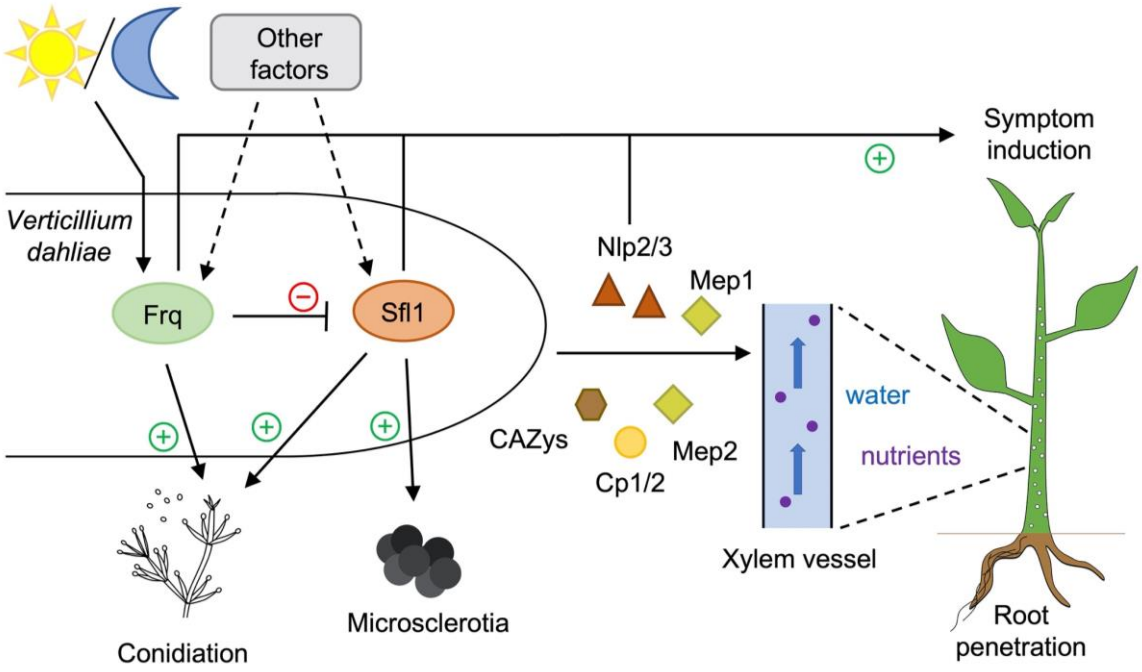

Figure 25. The light regulator Frq, regulatory protein Sfl1, metalloprotease Mep1 and necrosis and ethylene inducing-like effectors Nlp2/3 are required for *V. dahliae* pathogenicity.
Verticillium dahliae Frq (Frequency) suppresses microsclerotia production in the light (indicated by the sun) and positively regulates conidiation and virulence on tomato. Sfl1 (Suppressor of flocculation) is required for conidiation, microsclerotia formation and full virulence of *V. dahliae*. In microsclerotia formation *SFL1* functions epistatic to *FRQ* (this connection is displayed by the inhibitory effect of Frq to Sfl1). Other factors influencing the fungus might include temperature, availability of nutrients, plant signals and other external stimuli. To colonize the xylem vessels, the fungus secretes xylem sap-specific effectors such as Nlp2/3 (necrosis and ethylene inducing-like proteins), CAZys (carbohydrate-active enzymes), Cp1/2 (cerato-platanin domain containing protein) and Mep1/2 (metalloproteases). Mep1 and Nlp2/3 are required to promote disease symptom induction.

4.1 Frq is involved in light-dependent, but circadian-independent suppression of *V. dahliae* microsclerotia production

Circadian clocks allow organisms to synchronize to daily environmental changes. Mammals are known to use the internal timing system to adapt to and anticipate the cyclic environmental changes such as temperature or light and regulate biological processes accordingly (Dunlap & Loros, 2017). Plants also coordinate their defense responses in a circadian manner to anticipate pathogen attacks (Wang *et al*, 2011). Therefore, plant pathogenic fungi would be more successful if they on the other side can anticipate the plant's defense responses and adapt to it. For the necrotrophic plant pathogen *B. cinerea*, the fungal circadian clock was

proven to be important for the plant-pathogen interaction outcome (Hevia *et al*, 2015). The best characterized circadian system in fungi is presented by the nonpathogenic fungus *N. crassa* (Dunlap & Loros, 2006, 2017; Lombardi & Brody, 2005). In *N. crassa* sexual and asexual development, growth rate and gene expression are under the control of the circadian rhythm (Dunlap & Loros, 2017).
In *V. dahliae* no circadian rhythm has been reported thus far. However, *V. dahliae* does possess the components that were described to be required for the circadian clock in *N. crassa* such as FRQ, WC-1, WC-2, FRH and FWD-1 (Salichos & Rokas, 2010). We observed that *V. dahliae* preferable forms microsclerotia in the dark and more aerial hyphae in the light. This growth resulted in alternating rings of darker (increased microsclerotia) and lighter (increased aerial hyphae) developmental structures, but only when incubated in light:dark cycles. This effect was abolished in growth under constant conditions (Figure 7). Darkness generally induced higher production of microsclerotia compared to incubation in the light. A true circadian clock would include free-running oscillations that remain in the absence of environmental inputs (Hevia *et al*, 2016). These observations indicate that a circadian rhythm is not involved in the development of obvious phenotypical structures. Similarly, in *Aspergillus fumigatus* the light-induced melanin production was not confirmed as circadianly controlled as it is only light-dependent and not maintained under free-running conditions (Dunlap & Loros, 2017). *N. crassa* shows rhythmic conidiation patterns even in constant darkness (Baker *et al*, 2012). However, it is still possible that the initial growth must be entrained by light cycles first and therefore, in this study with *V. dahliae*, no alternating rings of enhanced microsclerotia and aerial hyphae were observed under constant conditions. Additionally, biological processes may be controlled circadianly on transcriptional level. However, results did show that *V. dahliae* is able to sense light and responds by adapting its developmental structures. When subjected to light, the fungus suppresses microsclerotia and enhances aerial hyphae production.
Although no visible involvement of the oscillator Frq in a circadian rhythm was observed, results did show that Frq in *V. dahliae* is required for suppression of microsclerotia and activation of conidia formation as the deletion strain showed enhanced microsclerotia production and reduced conidiation compared to WT and the complementation strain (Figure 7A). The microsclerotia phenotype was solely observed when incubated in the light. In the dark, WT and the *FRQ*

complementation strain exhibited enhanced microsclerotia production compared to incubation in the light, and, therefore, resembled the phenotype of the *FRQ* deletion strain. These results indicate that Frq in *V. dahliae* is involved in the light-dependent suppression of microsclerotia. Additionally, it is required for production of WT amounts of conidia. As none of these phenotypes showed rhythmicity under constant conditions, results suggest that Frq serves non-circadian roles in developmental regulation in this fungus.

Similar observations were reported for *B. cinerea* where macroconidiation is induced by light and is absent in darkness. These phenotypes result in a banding pattern after light:dark cycles, but under constant darkness the rhythmic pattern was lost (Canessa *et al*, 2013). However, *bcfrq1* mRNA levels were detected to oscillate not only in light:dark cycles, but also in constant darkness, which provides evidence for the presence of a circadian clock (Hevia *et al*, 2015).

These findings show that although no morphological phenotype is circadianly controlled, *V. dahliae* may nevertheless show circadian rhythmicity at the molecular level. In *V. dahliae* the components of the circadian clock are present supporting a possible role of the circadian rhythm (Salichos & Rokas, 2010). Possible oscillating transcripts need to be investigated in future studies.

4.1.1 *V. dahliae* Frq possesses motifs for post-translational modifications

For a functional circadian rhythm the oscillator FRQ in *N. crassa* interacts with other proteins in a complex network. For regulation of these interactions and control of subcellular localization of FRQ, the protein is post-translationally modified (Dunlap & Loros, 2017). When comparing *V. dahliae* Frq (VdFrq) to *N. crassa* FRQ (NcFRQ) on protein sequence level, similar motifs were observed. The full-length proteins exhibit 46% amino acid sequence identity and alignments of motifs required for functions of FRQ show that these regions are specifically well conserved (Figure 6).

These include the NLS, coiled coil region, FRQ-CK1-interacting domains (FCD), PEST motifs and FRQ-FRH-interacting domain (FFD) (Traeger & Nowrousian, 2015). The coiled coil region possesses two conserved leucines (additionally marked in bold, Figure 6). This motif enables FRQ to interact with itself and, furthermore, is a prerequisite to bind the WC proteins that are involved in light signal transduction in *N. crassa* (Crosthwaite *et al*, 1997; Cheng *et al*, 2001;

Traeger & Nowrousian, 2015). Nuclear localization of FRQ is essential in *N. crassa* for its repression of the light-sensing WC proteins (Luo *et al*, 1998), which is enabled by the NLS. The FCD1 and FCD2 motifs are highly conserved in *V. dahliae* and various fungal FRQ homologs. These interacting domains function in binding of kinase CK1 leading to phosphorylation of the protein, which mediates its localization and degradation status (He *et al*, 2006; Querfurth *et al*, 2011; Diernfellner *et al*, 2009). Moreover, the PEST motifs, PEST-1 and PEST-2, have distinct functions in *N. crassa.* Phosphorylation of PEST-1 is crucial for FRQ protein turnover (Görl *et al*, 2001) whereas phosphorylation of the second motif further downstream is required for circadian rhythmicity (Schafmeier *et al*, 2006; Baker *et al*, 2012). The FFD was defined as the minimal region required for binding of the helicase FRH to FRQ that together builds up the FFC complex. This complex represses activity of the light-sensing WC complex and subsequently represses *frq* transcription (Guo *et al*, 2010). The PEST motifs and the FRQ-FRH-interacting domain are only moderately conserved in *V. dahliae*. However, *in silico* analysis of PEST motifs in *V. dahliae* Frq with epestfind (http://emboss.bioinformatics.nl/cgi-bin/emboss/epestfind) supports a putative function of the corresponding region in phosphorylation. Furthermore, an *FRH* homolog is as well present in the *V. dahliae* JR2 genome (*VDAG_JR2_Chr4g00070aa*) and its deduced protein exhibits a high amino acid sequence identity of 70% compared to *N. crassa* FRH (XP_956298.1). Concluding, *V. dahliae* Frq exhibits similar motifs as the *N. crassa* protein. As homologs of genes coding for FRQ-interacting proteins are present in the *V. dahliae* genome, post-translational modifications as observed for NcFRQ are possible for VdFrq. However, these processes remain to be investigated.

4.1.2 *V. dahliae* responds to light

Light presents an external cue for fungi to orientate themselves and adapt accordingly (Yu & Fischer, 2019). Plants also perceive light and transmit it throughout their tissues with attenuation over distance (Beattie *et al*, 2018; Sun *et al*, 2005). *Verticillium* spp. colonize the plant vascular system starting by penetrating the roots underground. Light often signals the fungus to adapt to stressful conditions, which as well applies to the situation of *V. dahliae* in the plant aboveground (Yu & Fischer, 2019).

Results showed that *V. dahliae* clearly responds to light. It exhibits enhanced microsclerotia formation in the dark and stronger aerial hyphae formation in the light (Figure 7B). These morphological changes display the obvious light-dependent observations, however, additional responses are possible as reported for other plant pathogenic fungi. *B. cinerea*, for example, was shown to induce stress responses upon light induction (Schumacher, 2017). *V. dahliae* not only possess all the prerequisites for a circadian clock (Salichos & Rokas, 2010), but it also contains homologs of the genes encoding light-responsive proteins described in *N. crassa,* the model system for light sensing (Figure 26).

Photoreceptors bind different chromophores for light sensing. The three main classes of receptors bind flavin-based chromophores to the PAS (found in Per – period circadian protein; Arnt – Ah receptor nuclear translocator protein and Sim – single-minded protein) domains for blue-light. Green-light sensing is achieved by binding retinal. Linear tetrapyrrole is bound by the GAF (named after vertebrate cGMP-specific photodieasterases, cyanobactrial adenylate cyclases, and the transcription activator FhlA) and PHY (phytochrome-specific PAS-related) domains for red-light perception (Fischer *et al*, 2016).

Homologs of all genes coding for *N. crassa* blue-, green- and red-light photoreceptors were found in *V. dahliae*. Deduced proteins share a similar domain structure as determined with InterProScan. The white collars act as transcription factors with their GATA-type zinc finger DNA binding domain (Fischer *et al*, 2016). Upon light perception the WC-1 and WC-2 form the WCC and activate gene expression of *frq* and other light-responsive genes. Accumulation of FRQ protein leads to repression of the WCC activity displaying the regulatory role of FRQ (Wang *et al*, 2016a). WC-1 has activating and repressing conidiation roles conidiation in fungi such as *N. crassa* and *M. oryzae,* respectively (Liversage *et al*, 2018). WC-1 was as well implicated to be required for melanin biosynthesis, which is essential for mature microsclerotia formation in *Alternaria alternata*, *A. fumigatus* and *B. cinerea* (Pruß *et al*, 2014; Fuller *et al*, 2013; Canessa *et al*, 2013).

In *V. dahliae* microsclerotia production is light-dependent. It is possible that WC1 is activated by light to drive gene expression required for microsclerotia. If Frq is present, it inhibits WCC activity and suppresses enhanced microsclerotia production. According to the *Neurospora* circadian clock model (Figure 5), Frq would be phosphorylated leading to the release of WCC inhibition in the dark.

Therefore, WC1 could activate microsclerotia production in the dark. In absence of *FRQ*, WC1 would not be inhibited by Frq activating formation of microsclerotia even during light conditions.

Vivids interact with the WCC to fine-tune light responses. Additionally, the cryptochromes CRY-DASH (*Drosophila*, *Arabidopsis*, *Synechocystis*, *Homo*) and PHR-1 (Photolyase-related) function in DNA repair and light signaling (Schumacher, 2017; Bayram *et al*, 2008a). Whereas in *N. crassa* PHR-1 is only required for light-driven DNA repair and CRY-DASH for light signaling, the cryptochrome in the Ascomycete *A. nidulans* (CryA) is crucial for both, DNA repair and signaling function in response to light (Schumacher, 2017; Bayram *et al*, 2008a). In *A. nidulans* light induces asexual reproduction during which CryA plays an inhibitory role of sexual development.

Light inhibits the formation of cleistothecia as sexual structures that are covered with protective Hülle cells (Bayram *et al*, 2008a; Sarikaya Bayram *et al*, 2010). These fruiting bodies display robust sexual structures that are governed by light, which shows parallels to the resting structures of *V. dahliae*. The plant pathogenic fungus *B. cinerea* harbors two cryptochromes with specific functions similar to *N. crassa* (Cohrs & Schumacher, 2017). It is also possible that *V. dahliae* exerts similar strategies as homologs coding for PHR-1 and CRY-DASH were detected in the genome.

Phytochromes absorb red-light and contain signal output domains characteristic for histidine kinases. PHY-1 consists of a histidine kinase domain, an ATP-binding domain followed by a response receiver domain, which are presumably involved in phosphotransfer and connect light signaling to MAPK pathways (Yu & Fischer, 2019; Schumacher, 2017). In *A. nidulans* the phytochrome FphA interacts with the white collars as well as VeA of the velvet family. This interaction integrates external signals including blue- and red-light into responses such as developmental growth and secondary metabolite production (Bayram *et al*, 2010; Bayram & Braus, 2012). VeA is essential for this communication and the corresponding homolog is also required for full photoadaptation in *N. crassa* (Olmedo *et al*, 2010). VeA in *A. nidulans* additionally requires the velvet-like protein VelB to coordinate light signals with fungal development and secondary metabolism (Bayram *et al*, 2008b). Single deletion strains of the homologs in *V. dahliae*, *VEL1* and *VEL2*, were analyzed.

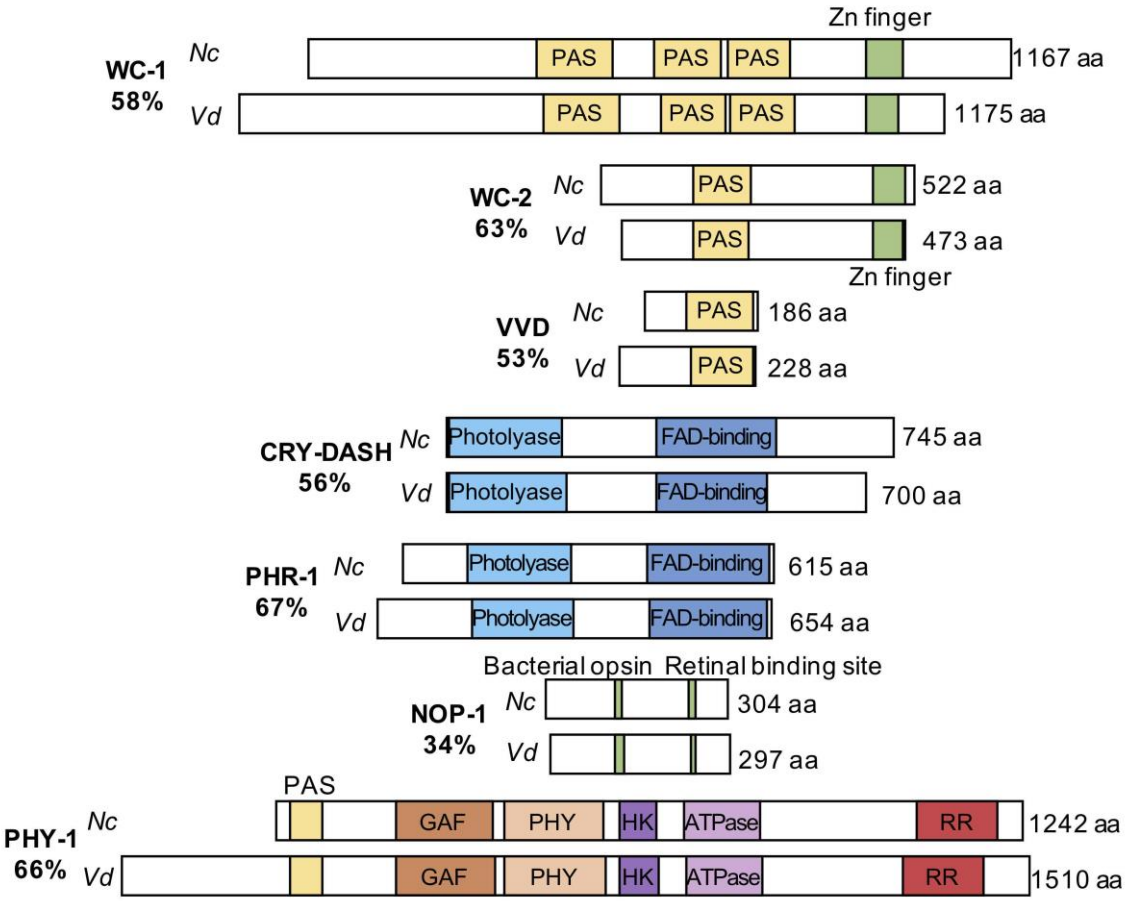

Figure 26. Photoreceptor protein structures in *N. crassa* and *V. dahliae*.
Amino acid sequences of *N. crassa OR74A* (*Nc*) proteins were retrieved from NCBI database. Corresponding proteins were identified by reciprocal BLAST search against the *V. dahliae* JR2 (*Vd*) proteome (Ensembl Fungi). Protein sequence identities were calculated using Clustal Omega (Madeira *et al*, 2019). Protein structures were analyzed with InterProScan and revealed similar domains for *Nc* and *Vd* proteins. The white collar proteins (WC-1 and WC-2) contain the GATA-type Zinc finger transcription factor (IPR000679) and PAS (Per – period circadian protein; Arnt – Ah receptor nuclear translocator protein; Sim – single-minded protein) domains (IPR000014). PAS is also present in VIVID (VVD). The cryptochromes CRY-DASH and PHR-1 possess a DNA-photolyase (IPR006060) and an FAD-binding domain (IPR005101). These four proteins are involved in blue-light sensing. The green-light photoreceptor NOP-1 (new eukaryotic opsin-1) exhibits the motifs, bacterial opsin and a retinal binding site (IPR018229). The protein structure of the red-light-sensing phytochrome exhibits a PAS, a GAF domain (IPR003018) required for chromophore binding, a phytochrome domain (IPR013515), histidine kinase domain (IPR003661), ATPase domain (IPR003594) and a signal transduction response receiver (RR) domain (IPR001789). Following gene accession numbers were used: *wc-1*: *Nc – XP_011395152*; *Vd - VDAG_JR2_Chr2g01990a*; *wc-2*: *Nc - XP_009855773*; *Vd - VDAG_JR2_Chr7g03830a*; *vvd*: *Nc – XP_957606*; *Vd - VDAG_JR2_Chr3g10380a*; *cry-dash*: *Nc – XP_965722*; *Vd - VDAG_JR2_Chr1g17210a*; *phr-1*: *Nc – XP_964834*; *Vd - VDAG_JR2_Chr7g00170a*; *nop-1*: *Nc – XP_959421*; *Vd - VDAG_JR2_Chr1g29230a*; *phy-1*: *Nc – XP_960393*; *Vd - VDAG_JR2_Chr4g09150a*.

Absence of Vel1 exhibits a severe reduction in growth and compromised pathogenicity on tomato as well as the inability to form microsclerotia. Vel2 shows a light-dependent reduction of microsclerotia formation (personal communication, A. Höfer, Georg-August-Universität Göttingen).

Additionally, green light is absorbed by opsins, NOP-1 in *N. crassa* (Yu & Fischer, 2019; Adam *et al*, 2018). The best BLAST hit to *N. crassa* NOP-1 in *V. dahliae* shows only 34% amino acid identity. A higher conservation of 58% resulted from comparison to the opsin CarO (CAD97459.1) from plant pathogen *Fusarium fujikuroi*. CarO is predominantly present in plant pathogenic fungi (Wang *et al*, 2018b) and was shown to be essential in fungus-plant interactions (Adam *et al*, 2018). As *V. dahliae* is a plant pathogen, the green-light receptor CarO may also be involved in plant infection.

Concluding, this study shows that *V. dahliae* responds to light by forming microsclerotia and aerial hyphae in darkness and light, respectively. The *N. crassa* photoreceptors are highly conserved in *V. dahliae* and may also play crucial roles in photoadaptation in this fungus. If *V. dahliae* was able to sense light of different wavelengths, it would provide information for the fungus to locate itself and to adapt accordingly. In this study, *V. dahliae* Frq was investigated as central component of the circadian clock. Frq interacts with light-sensing proteins upon perception of light in other fungi. Results indicate that Frq is required for proper light regulation as the *FRQ* deletion was impaired in light-dependent repression of microsclerotia formation. First insights into a possible connection of light sensing and light-depending regulation of developmental structures in *V. dahliae* are provided. This indicates that future work on the photoreceptors can provide a better understanding of the fungal infection success.

4.1.3 *V. dahliae* Frq may regulate microsclerotia suppression, conidiation and virulence through signaling pathways

Signaling pathways are used to quickly respond to external cues such as stress to control the expression of whole gene sets at once. PKA and MAPK signaling are also involved in light-perception.

In the light-regulation model organism *N. crassa*, PKA and Protein kinase C negatively regulate light-dependent gene transcription as they inhibit the WCC through phosphorylation (Hevia *et al*, 2016; Yu & Fischer, 2019). The WCC is then

released from the *frq* promoter terminating WCC-dependent *frq* transcription. Thereby, PKA and PKC negatively regulate *frq* transcription. On the other side, PKA activates WC-independent *frq* transcription by inhibiting the RCM-1/RCO-1 complex. These proteins are encoded by the yeast *CYC8* and *TUP1* homologs of the co-repressor complex. PKA phosphorylates RCM-1. The repressor complex disassembles and is released from the *frq* promoter. This results in WC-independent *frq* transcription (Liu *et al*, 2015).

In *V. dahliae,* light signaling components are present in the genome. Deletion or disruption of *FRQ* or *VdPKAC1* encoding a catalytic subunit of PKA, respectively, result in similar phenotypes such as enhanced microsclerotia production as well as decreased conidiation and virulence (Tzima *et al*, 2010a). These phenotypes suggest an activating role of PKA on *FRQ* transcription in *V. dahliae*.

Further MAPK signaling cascades have been implicated to be involved in the translation of light signals to cellular responses. The osmotic stress-related HOG MAPK pathway is involved in red-light signaling. In the filamentous Ascomycete *A. nidulans*, the histidine kinase activity of phytochrome FphA mediates phosphorylation of the MAPK via the phosphotransfer protein YpdA. YpdA transfers the light signal via the HOG MAPK signaling cascade (Yu & Fischer, 2019; Yu *et al*, 2016). Additionally the activation of stress signaling was found to depend on blue-light receptor WC-1 in *Trichoderma atroviride* or the plant pathogen *A. alternata* (Esquivel-Naranjo *et al*, 2016; Yu & Fischer, 2019; Igbalajobi *et al*, 2019), which is supported by work in *N. crassa*. Here, the MAPK OS-2 and MAPKKK OS-4 of the osmotic stress-activated pathway were identified as direct targets of the WCC (Wang *et al*, 2019).

Whether stress responses in *V. dahliae* are mediated by light, remains to be elucidated. Nevertheless, a similar regulation as described for other fungi is possible in *V. dahliae* and summarized in Figure 27. The HOG MAPK pathway in *V. dahliae* presents yet another link to microsclerotia production, stress response and virulence as shown by the requirement of MAPK VdHog1, MAPKK VdPbs2 and MAPKKK VdSsk2 (Yu *et al*, 2019; Tian *et al*, 2016; Wang *et al*, 2016b).

These findings support a light-regulatory mechanism in *V. dahliae*. However, deletion strains often result in pleiotropic phenotypes, making it more difficult to dissect putative light effects. Experiments with deletion strains incubated in light at different wavelength need to be conducted to unravel the light regulations in this

fungus. Nevertheless, the described work on light-perception and the involvement of MAPK and PKA signaling pathways in other organisms hint to a similar regulation in *V. dahliae* as this fungus also possesses homologs of the involved genes and was shown to be light-responsive. Further it would be beneficial for the plant pathogen to convert light signals into developmental responses through signaling cascades that target sets of genes at once. This would enable the fungus to adapt to different acute environmental signals throughout the different plant colonization steps and persistence in the soil.

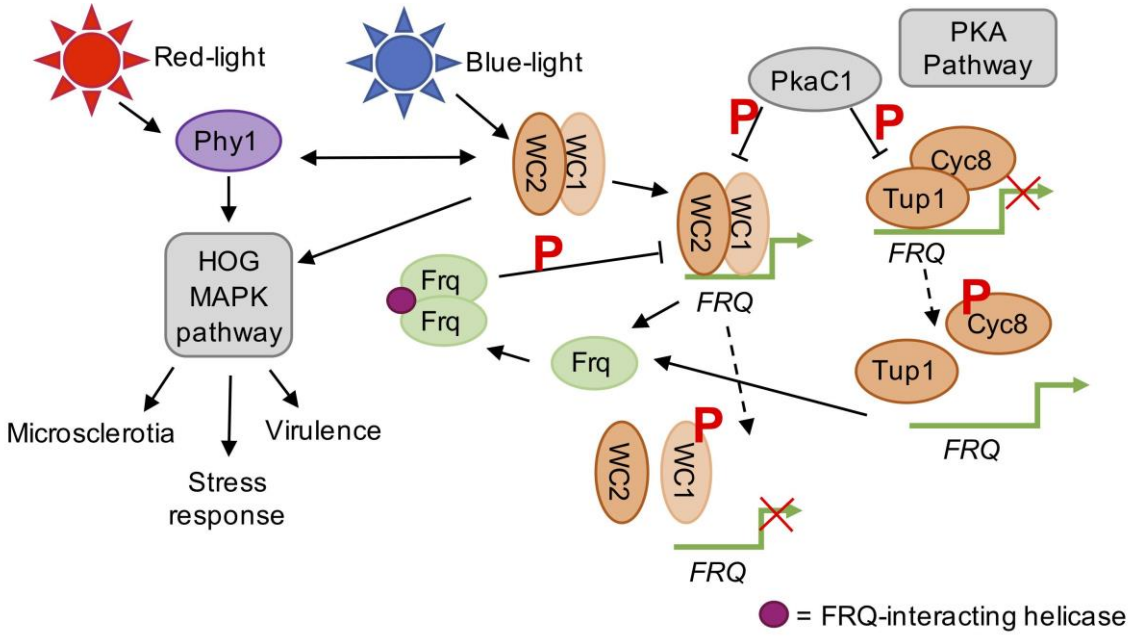

Figure 27. Model of light regulator Frq-dependent signaling in *V. dahliae*.
This model summarizes possible light regulation in *V. dahliae* involving Frequency (Frq), the high osmolarity glycerol (HOG) mitogen-activated protein kinase (MAPK) cascade and cyclic AMP (cAMP)-dependent protein kinase A (PKA) pathway. Indicated interactions and processes have been shown in other fungi as mentioned in the text. Frq proteins form a complex with the Frq-interacting helicase to recruit casein kinases that phosphorylate the white collar complex (WCC). The PKA subunit, PkaC1, as well phosphorylates the WCC. The WCC is then released from the *FRQ* promoter terminating the WCC-dependent expression. The Cyc8-Tup1 co-repressor complex inhibits *FRQ* expression. Upon PKA-mediated phosphorylation it dissociates and WCC-independent *FRQ* expression is activated. The phytochrome Phy1 senses red-light and transfers the signal to the HOG MAPK pathway. This pathway regulates microsclerotia development. Stress responses and virulence. Phy1 also interacts with the WC proteins.

4.2 Sfl1 is required for activation of developmental programs in *V. dahliae*

In addition to the light-dependent regulator Frq, another regulatory protein Sfl1 was analyzed in this study revealing roles in conidiation, microsclerotia formation and pathogenicity of *V. dahliae*. Sfl1 was investigated due to its potential role as transcriptional activator and repressor. The deletion of *SFL1* in yeast resulted in flocculation and increased pseudohyphal and invasive growth (Fujita *et al*, 1989; Robertson & Fink, 1998). Besides its well characterized role as suppressor of flocculation genes, it is additionally required for activation of stress-responsive genes (Conlan & Tzamarias, 2001; Ansanay Galeote *et al*, 2007).

V. dahliae Sfl1 was shown to be positively regulated by Vta3, a protein encoded by the yeast homolog *RFX1/CRT1* (Bui *et al*, 2019). In yeast, Rfx1 has an inhibitory transcriptional role by recruiting the Ssn6-Tup1 repressor complex to promoters (Conlan & Tzamarias, 2001). *V. dahliae* Vta3 was assigned as *Verticillium* activator of adhesion because it restored adhesion in a non-adherent yeast strain (Tran *et al*, 2014). In *V. dahliae,* Vta3 is required for conidiation, microsclerotia formation, plant root colonization and virulence on tomato, but has a repressing function in oxidative stress response to H_2O_2 and menadione (Bui *et al*, 2019). Another factor, which was shown to activate adhesion in the non-adherent yeast strain is Som1 (Bui *et al*, 2019). The *V. dahliae SOM1* homolog in yeast is *FLO8*. Flo8 competes with Sfl1 in binding to the promoter of flocculation gene *FLO11*. While Sfl1 represses *FLO11* expression, Flo8 has an activating role. Both, Sfl1 and Flo8 are controlled through the cAMP-mediated PKA signaling pathway (Conlan & Tzamarias, 2001; Li *et al*, 2011). In *V. dahliae,* deletion of *SOM1* results in a similar but more severe phenotype than the *VTA3* deletion strain and is required earlier during plant infection as it supports fungal adhesion to the root. Som1 further promotes resistance to oxidative stress (Bui *et al*, 2019).

In this study, the *SFL1* homolog was deleted in *V. dahliae*, which resulted in decreased conidia formation and severe reduction of microsclerotia (Figure 9, 16). Further compromised virulence on tomato was observed (Figure 17). A defect in adhesion to the plant roots was not observed for the *SFL1* deletion strain suggesting alternative functions during plant colonization. Microsclerotia are resistant structures usually produced to protect the fungus from environmental stresses such as UV irradiation, temperature extremes or nutrient deprivation (Wang *et al*, 2018a; Butler & Day, 1998). The impairment in the microsclerotia

formation therefore represents a kind of role in stress response. However, no role in response to oxidative stressors was detected. As conidia and microsclerotia production as well as pathogenicity on tomato is impaired in the *SFL1* as well as *VTA3* deletion strain, Vta3-dependent regulation of *SFL1* expression may control genes important for development and virulence. Several genes involved in these processes were found to be differentially regulated in the *VTA3* deletion strain. Expression of the hydrophobin Vdh1 and the putative transcription factor Vta1 encoding genes, that are required for microsclerotia development, is positively regulated by Vta3. (Klimes & Dobinson, 2006; Bui *et al*, 2019). Expression of conidia formation regulating factors *ABA1* and *VTA2* as well as the necrosis-inducing effector *NLP2*, which is required for *V. dahliae* pathogenicity on tomato, depend on Vta3 (Bui *et al*, 2019; Santhanam *et al*, 2013). Whether these genes are directly or indirectly controlled is not known. But as these processes were affected in *SFL1* and *VTA3* deletion strains and Vta3 regulates *SFL1* transcription, it is possible that Vta3 regulates involved genes through Sfl1. This is supported by the transcriptional role of Sfl1 in yeast (Ansanay Galeote *et al*, 2007; Bui *et al*, 2019).

The *VTA3* deletion strain is severely impaired in induction of disease symptoms on tomato whereas the *SFL1* deletion strain is compromised in virulence, but still induces clear stunting of the tomato plants. Therefore, Vta3 seems to regulate additional factors important for pathogenicity independently of Sfl1 (Bui *et al*, 2019). As the stress responses differ between these two deletion strains, Vta3 regulates *SFL1*-independent subsets of genes involved in stress response. Stress responses in this study were only tested with oxidative (ethanol, H_2O_2 and menadione) and cell wall stressors (SDS). Therefore, Sfl1 may respond to a different type of stress. In the rice blast fungus *M. oryzae*, MoSfl1 was not required for hyperosmotic, oxidative and nutritional stress, but deletion of *MoSFL1* resulted in higher sensitivity to elevated temperatures as well as reduced conidia production and virulence (Li *et al*, 2011). These observations were similar to those in the fungal insect pathogen *Beauveria bassiana*. Absence of *SFL1* resulted in decreased conidiation, thermotolerance and virulence (Zhou *et al*, 2018). In *N. crassa* the role of the *SFL1* corresponding gene *hsf2* in conidiation was similar (Thompson *et al*, 2008).

This study demonstrates that the roles of Sfl1 are consistent with those observed in other fungal species. Apart from the stress response, evidence is provided that *V. dahliae* Sfl1 is required for developmental regulation and virulence on tomato. Infection results with complementation strains were not included in this evaluation as the induction of disease symptoms was not as severe as in WT infections. These infection assays need to be repeated with functional complementation strains. The used complementation constructs were ectopically integrated, which may lead to an integration at an undesired locus. Genes may have been disrupted that are required for full virulence or the expression of the integrated gene in this locus is not stable during plant infection conditions. Therefore, complementation constructs will be integrated *in locus* for future investigations to verify the role of Sfl1 in disease symptom induction.

4.2.1 *V. dahliae* Sfl1 requires a functional C-terminal region for proper activation of transcriptional control

The most prominent phenotype of the *V. dahliae SFL1* deletion strain was the lack of microsclerotia, which was analyzed in more detail. A putative role as a transcriptional regulator was supported by nuclear localization of *V. dahliae* Sfl1. These results as well coincide with observations in *Candida albicans* where Sfl1-GFP localized to the nucleus (Li *et al*, 2007; Bauer & Wendland, 2007). Fusion constructs of Sfl1 fused to GFP at the N- or C-terminus under the control of a constitutively active promoter were integrated into the *SFL1* deletion strain. These strains resulted in slight differences in subcellular localization of the fusion proteins as well as in phenotype complementation concerning microsclerotia production (Figure 10). Signals of Sfl1-GFP were not only observed in the nucleus, but were as well present throughout the cytoplasm. Overexpression of GFP-Sfl1 resulted predominantly in nuclear localization as shown by strong GFP signals that co-localized with DAPI signals. Both GFP-fusion strains displayed microsclerotia production, but in lower amounts compared to WT. However, the colony center of the strain expressing Sfl1 N-terminally fused to GFP was darker compared to the C-terminal GFP fusion construct. This indicates that the difference in microsclerotia production of strains overexpressing Sfl1 N- or C-terminally fused to GFP may result from interference with important motifs of Sfl1.

In *C. albicans* Sfl1-GFP fusion proteins were functional as the strain was phenotypically like the WT (Bauer & Wendland, 2007) whereas other studies provide evidence for the requirement of a functional C-terminal region of Sfl1 for proper interaction with Cyc8-Tup1 transcriptional co-repressor in *M. oryzae* and *Fusarium graminearum* (Li *et al*, 2017). Therefore, it is possible that a C-terminal GFP fusion to Sfl1 in *V. dahliae* hinders full functionality of the protein and results in a less melanizing phenotype compared to *V. dahliae* WT. As these overexpressing constructs were integrated ectopically, it is further possible that the genomic context might affect *SFL1* expression. Additionally, increased expression levels of the protein may alter proper function of Sfl1. As we showed that Sfl1 is predominantly present in young hyphae and degraded in ageing hyphae (Figure 12B), artificial overexpression of Sfl1 at later time-points may interfere with regular function of the protein.

4.2.2 Post-translational modifications are likely to regulate transcriptional roles of *V. dahliae* Sfl1

Many regulators are present in the cell at specific developmental stages and are degraded once their specific function is completed. As Sfl1 controls the formation of developmental structures, stability of the protein was investigated at different time-points. Protein abundance of GFP-Sfl1 was predominantly present in young hyphae and degraded in older cultures (Figure 12B). This correlates with the presence of microsclerotia on solid SXM plates and conidia abundance in liquid SXM cultures. When these developmental programs need to be activated, Sfl1 protein abundance is high. With time and after initiating microsclerotia and conidia production, GFP-Sfl1 is degraded. Similarly in *C. albicans*, Sfl1-GFP nuclear signals were also stronger in yeast or pseudohyphal cells compared to long filaments (Bauer & Wendland, 2007).

In our study, Western experiments showed not only a signal at the expected size of the fusion protein (approx. 93 kDa) but in addition a higher migrating band between 100 and 130 kDa, which could present a modified fusion protein. As the abundance of the fusion protein decreases with advanced time-points, it may be targeted with ubiquitin for degradation (Prabakaran *et al*, 2012). The intensity of the higher band does not linearly decrease with advanced time but is more prominent after four days of growth on SXM agar compared to two or six days. This

supports the idea of subsequent degradation of the post-translationally marked protein (Figure 12B). Binding of ubiquitin proteins to the fusion protein adds 9 kDa per ubiquitin and would result in a higher molecular weight. Ubiquitination of proteins often occurs on proteins that are marked by phosphorylation (Ciechanover *et al*, 2000; Ravid & Hochstrasser, 2008).

Phosphorylation of Sfl1, on its own or prior to ubiquitination, may be another possible explanation of the higher migrating band. Although the phosphoproteins do not lead to a detectable mass difference, phosphorylated proteins migrate slower through the SDS-gel due to the negative charge of the added phosphate groups, which leads to a mobility shift on the SDS gel (Kinoshita *et al*, 2009). Phosphorylation of proteins can regulate their subcellular localization or activity. In *M. oryzae,* MoSfl1 is phosphorylated by a MAP kinase and PKA that differentially regulate its transcriptional activity (Li *et al*, 2011, 2017).

The observations of the higher migrating bands for Sfl1-GFP and GFP-Sfl1 would fit a model of *V. dahliae* Sfl1 being subject to phosphorylation events that control the function of the protein while the protein is degraded when the function is not required any longer.

4.2.3 Sfl1 interaction with repressor complex Cyc8-Tup1 is controlled by MAPK and PKA signaling pathways

Possible post-translational events leading to a higher migrating protein on an SDS gel were discussed for *V. dahliae* Sfl1. Modification of the Sfl1 protein by phosphorylation has been observed in several fungi. A MAP kinase docking site, three putative MAPK and two PKA phosphorylation sites were detected in the *SFL1* homolog in *M. oryzae*, which are conserved among various other *SFL1* homologs in filamentous Ascomycetes (Li *et al*, 2011, 2017). The MAP kinase docking site and PKA phosphorylation sites are also found in *V. dahliae* Sfl1 supporting a putative functional conservation. Overall, *V. dahliae* Sfl1 has 64% amino acid sequence identity to *M. oryzae* MoSfl1.

MoSfl1 seems to be differentially regulated by phosphorylation of PKA and Pmk1 (pathogenicity MAP kinase 1). Pmk1 displays the corresponding yeast Fus3/Kss1-like MAPK of the pheromone response and filamentation signaling pathways of which only one ortholog is found in most filamentous Ascomycetes. Pmk1 in plant pathogens is required for infection processes (Jiang *et al*, 2018). On the other side,

the PKA pathway is activated in nutrient-rich conditions in yeast and is involved in the regulation of developmental growth and infection processes in plant pathogens such as hyphopodium formation in *V. dahliae* (Li *et al*, 2017; Sun *et al*, 2019). Different phosphorylation events may lead to expression or repression of different subsets of genes (Li *et al*, 2017; Hamel *et al*, 2012), which may account for *V. dahliae* Sfl1 as well. PKA activity in *M. oryzae* is required for proper function of MoSfl1. The genes encoding the catalytic subunits of PKA, *CPKA* and *CPK2*, were deleted and resulted in impaired growth, conidiation, appressorium formation and virulence but increased activation of MAPK Pmk1 (Li *et al*, 2017). In *M. oryzae* MoSfl1 the C-terminal part was further essential for interaction with the Cyc8-Tup1 co-repressor complex. Phosphorylation of MoSfl1 by PKA leads to termination of this interaction with Cyc8-Tup1 and consequently to activation of expression of Sfl1-controlled genes (Li *et al*, 2017).

In *V. dahliae,* components of the PKA signaling pathway generally suppress microsclerotia production but positively affect virulence (Sarmiento-Villamil *et al*, 2018b). Disruption of genes coding for the G-protein beta subunit VGB or the catalytic subunit of protein kinase A VdPkaC1 result in strains with increased microsclerotia production and impaired pathogenicity (Tzima *et al*, 2010a, 2012). This study revealed that Sfl1 in *V. dahliae* is required for virulence but has a positive effect on microsclerotia production, which is different from PKA pathway. If genes are controlled by PKA phosphorylation of Sfl1, differential regulation of Sfl1 must be the case, which will be explained together with putative MAPK phosphorylation at the end of this chapter.

Disruption of the repressor *VdCYC8* (*SSN6*) in *V. dahliae* results in a similar phenotype as *SFL1* deletion strain. Transcription levels of many genes required for melanin and microsclerotia production were downregulated in the mutant (Li *et al*, 2015). These similar phenotypes corroborate a putative interaction of Sfl1 with the co-repressor complex Cyc8-Tup1 that together control gene expression.

Additionally to phosphorylation by PKA, MoSfl1 as well interacts with the pathogenicity MAP kinase Pmk1 in *M. oryzae* (Li *et al*, 2011). In plant pathogens the corresponding MAPK has a conserved role in plant infection (Jiang *et al*, 2018). In *M. oryzae* Pmk1 positively regulates transcription factors such as MoSfl1 and MADS-box regulator MoMcm1 (Jiang *et al*, 2018). VdMcm1 was identified as key

regulator for conidiation, microsclerotia formation, virulence, and secondary metabolism in *V. dahliae* (Xiong *et al*, 2016).

In appressorium forming fungi such as *M. oryzae*, Pmk1 and corresponding MAPKs are important for formation of the specialized plant penetration structures while orthologs in non-appressoria forming pathogens are also required for plant penetration (Jiang *et al*, 2018). In *V. dahliae* the corresponding MAPK gene *VMK1,* was deleted and resulted in reduced conidiation, microsclerotia formation and pathogenicity (Rauyaree *et al*, 2005; Starke, 2019, Dissertation). This phenotype is similar to the *SFL1* deletion phenotype shown in this study suggesting that Vmk1 if functionally related to Sfl1 in the regulation of these processes. However, the pathogenicity was more severely impaired in the *VMK1* deletion strains, which indicates that Vmk1 controls the expression of additional genes. Vmk1 phosphorylates downstream transcription factors to control expression of genes involved in different processes. It targets Vph1 corresponding to yeast Ste12, which is required for root penetration but not involved in microsclerotia or spore production (Sarmiento-Villamil *et al*, 2018a). These results hint to other Vmk1-regulated factors such as Mcm1 or Sfl1 for regulation of microsclerotia formation and conidiation.

In *M. oryzae*, the MAPK Pmk1 showed increased phosphorylation levels in absence of the PKA catalytic subunits (Li *et al*, 2017). Similarly absence of VdPkaC1 in *V. dahliae* could lead to elevated levels of Vmk1. This would lead to increased Vmk1-mediated activation of Sfl1 as positive regulator of microsclerotia production explaining the enhanced microsclerotia phenotype in the *VdPKAC1* deletion strain. In *V. dahliae* an extra copy of *VdPKAC1* in the *VGB* (G-protein beta subunit) mutant strain results in reduced expression levels of *VMK1* and hydrophobin gene *VDH1*. This shows the opposite situation and correlates with the impairment of microsclerotia production in this strain (Tzima *et al*, 2012). Setting the results into relation of what has been shown in regard to Sfl1-dependent regulation of microsclerotia production a putative model is summarized in Figure 28. PKA phosphorylates Sfl1, which then is released from promoters and cannot interact with Cyc8-Tup1 co-repressor (indicated by red phosphorylation). Sfl1 is as well phosphorylated by Vmk1. Phosphorylation at different sites could differentially regulate interaction of Sfl1 with Cyc8-Tup1. Therefore, a possible scenario would

be that PKA phosphorylation inhibits whereas Vmk1 phosphorylation supports interaction of Sfl1 with Cyc8-Tup1.

In yeast, Sfl1 was shown to be able to activate gene expression. The Cyc8-Tup1 repressor complex not only has inhibiting roles but is also able to positively regulate gene expressions as a result of post-translational modifications (Ansanay Galeote *et al*, 2007). These activating roles would fit the model where Sfl1 together with Cyc8-Tup1 activates microsclerotia production.

In absence of Vmk1, only PkaC1 phosphorylates Sfl1 and inhibits formation of the Sfl1-Cyc8-Tup1 complex, therefore, no microsclerotia are produced. This is similar to situations where Sfl1 or Cyc8 is absent. When PkaC1 is absent, Sfl1 is not phosphorylated by PKA, therefore is able to interact with Cyc8-Tup1 leading to gene expression. Overexpression of Sfl1 may lead to high abundance of unphosphorylated Sfl1 that interferes with proper activation of microsclerotia production, which may explain the less microsclerotia formation phenotype in *SFL1* deletion and *FRQ* deletion strains both overexpressing Sfl1 fused to GFP. However, if the repressor complex together with Sfl1 has a direct inhibitory effect, it is possible that genes are interconnected that negatively regulate microsclerotia production.

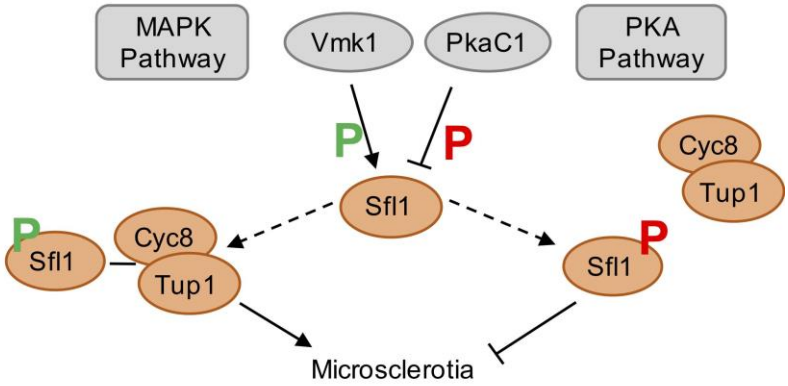

Figure 28. Model of Sfl1-dependent regulation in *V. dahliae*.
A model explaining microsclerotia phenotypes in *V. dahliae* includes phosphorylation of regulatory protein Sfl1 by the mitogen-activated protein kinase (MAPK) and cyclic AMP (cAMP)-dependent protein kinase A (PKA) pathway. Regulatory protein Sfl1 is inhibited by the PKA subunit PkaC1 (red P indicates inhibitory effect of phosphorylation). Sfl1 is phosphorylated and thereby interaction with Cyc8-Tup1 is released. MAPK Vmk1, on the other hand, activates Sfl1 (green P) at different phosphorylation sites and Sfl1 interaction with Cyc8-Tup1 leads to the expression of genes required for microsclerotia production.

This study showed that deletion of *SFL1* severely impacts microsclerotia formation and as well leads to reduced conidiation and pathogenicity on tomato. As *V. dahliae* mutants impaired in the PKA pathway show differences in microsclerotia formation but also positively regulate conidiation and virulence (Tzima *et al*, 2010a, 2012), it is possible that PKA phosphorylation at a different site promotes Sfl1 binding to Cyc8-Tup1 to control gene expression involved in these processes. However, PKA may as well regulate conidiation and virulence through other transcription factors. For full understanding of the role of Sfl1 it will be important to characterize the direct interaction partners of Sfl1 and to investigate on the phosphorylation sites *in vivo* and the regulation of phosphorylation.

4.3 *V. dahliae* regulators Sfl1 and Frq are involved in converging pathways

Regulation of developmental programs relies on conserved pathways such as MAPK and cAMP/PKA signaling in order for the fungus to interpret an external message and translate it into cellular responses. Therefore, it is not surprising that the regulation of Sfl1 and Frq converges at a higher level.

4.3.1 *V. dahliae SFL1* is epistatic to *FRQ* in microsclerotia production

This study revealed that the light-regulator Frq and regulatory protein Sfl1 have opposing roles in microsclerotia production of *V. dahliae*. While Sfl1 is required for the production, Frq seems to suppress excessive microsclerotia formation in light conditions. The severe microsclerotia deficient phenotype of the *SFL1* deletion strain was dominant in the double deletion of *FRQ* and *SFL1* indicating that *SFL1* functions epistatic to *FRQ*.

As Sfl1 and Frq both have been implicated in signaling pathways in other fungi, it is possible that they regulate similar as well as specific targets. Frq is involved in light-sensing and by regulation of the transcriptionally active WCC, it indirectly controls many gene transcripts including MAP kinases that activate whole sets of genes (Wang *et al*, 2019). For Sfl1, work in other organisms found that the protein is regulated by MAP kinases and protein kinases (Li *et al*, 2017, 2011). These findings support that *SFL1* genetically functions downstream of *FRQ*.

4.3.2 *V. dahliae SFL1* and *FRQ* promote virulence on tomato

The developmental regulators Sfl1 and Frq both are required for production of conidia, WT-like formation of microsclerotia and full pathogenicity on tomato.

This may be due to the reduction in conidia formation in both single deletion strains and the *FRQ*/*SFL1* double deletion strain (Figure 16). As *V. dahliae* colonizes its hosts by sporulating in the xylem sap using the vascular stream to spread throughout the whole plant (Schnathorst, 1981), it is likely that strains impaired in conidia production are also compromised in the induction of disease symptoms.

Deletion of the *M. oryzae CON7* homolog coding for the *Verticillium* transcription activator of adhesion Vta2 in *V. dahliae* results in decreased conidiation, increased microsclerotia production and compromised virulence in *V. dahliae* (Tran *et al*, 2014). These results support the correlation between conidiation and infection success. Con7 was detected in *M. oryzae* to be important for spore morphogenesis and later was characterized as a transcription factor with essential roles in infection (Odenbach *et al*, 2007; Shi *et al*, 1998). Vta2 in *V. dahliae* as well acts as transcription factor and controls expression of genes encoding for example adhesin-like cell wall proteins or secreted effector proteins (Tran *et al*, 2014). However, the *VTA2* deletion was impaired in root colonization, which was not altered in the *SFL1* deletion strain, indicating that Vta2 requires Sfl1-independent regulation of genes required for this colonization step (Tran *et al*, 2014; Bui *et al*, 2019).

Other factors involved in the regulation of conidiation such as the MADS-box transcription factor VdMcm1, repressor protein VdCyc8, MAPK Vmk1 and the Verticillium transcription activators of adhesion Vta3 and Som1 were associated with virulence, but also have additional roles in other processes such as microsclerotia formation (Bui *et al*, 2019; Li *et al*, 2015; Rauyaree *et al*, 2005; Starke, 2019, Dissertation; Xiong *et al*, 2016). Therefore, it is complicated to dissect whether a single factor is responsible for the virulence phenotype.

As microsclerotia production was additionally affected in *SFL1* and *FRQ* single and double deletion strains, the compromised virulence may be related to these phenotypes as well. Microsclerotia or melanin-deficient *V. dahliae* deletion strains are not always coupled to compromised virulence (Zhang *et al*, 2017a; Wang *et al*, 2018a; Klimes & Dobinson, 2006). Several examples show that *V. dahliae* strains defective in microsclerotia formation induce less severe disease symptoms in their hosts such as the strains lacking the MADS-box transcription factor VdMcm1, pigment biosynthesis protein Vayg1, transcription factor Som1 and MAP kinase Vmk1 (Xiong *et al*, 2016; Fan *et al*, 2017; Rauyaree *et al*, 2005; Starke, 2019; Bui

et al, 2019). These strains are similar to the *SFL1* deletion and the *SFL1*/*FRQ* double deletion strains that are severely impaired in microsclerotia production and are reduced in pathogenicity (Figure 14, 17). However, *V. dahliae* mutant strains impaired in the PKA signaling pathway show an enhanced microsclerotia phenotype and yet are compromised in virulence (Tzima *et al*, 2010a, 2012), which is similar to the *FRQ* deletion strain (Figure 14, 17). While in appressoria-forming fungi like *M. orzyae* the ability to produce melanin directly correlates with the infection success as the special penetration structures are melanized, this correlation has not been observed for *V. dahliae* as it forms non-melanized hyphopodia to penetrate the roots (Zhao *et al*, 2016). The melanized microsclerotia of *V. dahliae* are thus solely known for the protective function (Wilhelm, 1955).

Frq and Sfl1 serve opposing roles in the regulation of microsclerotia production, however both deletion strains are impaired in infecting tomato plants. These results hint to a stronger role of the impaired conidiation in the outcome of the infection success. Corroborating this hypothesis is the fact that infection studies were conducted with conidial suspensions as it is easier to quantify spore numbers compared to microsclerotia. However, in nature, microsclerotia play a stronger role as primary propagule on the fields as they are able to survive unfavorable environmental conditions (Wilhelm, 1955). Here, both phenotypes represent interesting angles. *SFL1* deletion strains hardly produce any microsclerotia and therefore may not survive on the field if no host is present. Whereas strains lacking *FRQ* show enhanced microsclerotia production and therefore may form microsclerotia in spore-forming conditions and stall colonization of the plant. Infection assays were shown excluding the ectopic complementation strains as the infection phenotype was not fully complemented. Complementation constructs were ectopically integrated into the corresponding single deletion strains. Therefore, the genetic locus is different to the WT and may result in altered expression levels or the integration might affect a gene important for virulence. New complementation strains need to be generated to completely verify the results. Nevertheless, single and double deletion strains showed a reduction in pathogenicity on tomato.

Apart from the visible phenotypes, Frq and Sfl1 may also regulate virulence factors. To pin down the effect of these regulators, the secretome of the fungus can be analyzed and compared to *V. dahliae* WT to detect important effectors involved in

the infection success. However, the germination ability of the microsclerotia and the difference in the secretome were not tested to date.

Concluding, it was shown that the circadian regulator Frq and transcriptional regulator Sfl1 are involved in pathogenicity and the control of different developmental processes such as sporulation and microsclerotia production. These are required for the fungal strategies to disperse in the plant and survive in the soil and therefore display interesting targets for disease control.

4.4 *Verticillium* spp. adapt to their environment with different secretion responses

Plant pathogens do not only regulate their development to efficiently infect plants, but they also continuously secrete proteins throughout the infection process. For example, adhesins play a major role in attachment to the plant and effectors neutralizing the host immune responses are required during colonization of the xylem (Agrios, 2005b). *Verticillium* spp. would save energy and benefit from shutting down such secretion systems when persisting in the soil and activating them when sensing a plant to establish a successful infection. To address the question whether *Verticillium* spp. can sense and adapt to different environments, the media-dependent secretome of the allodiploid *V. longisporum* was investigated. Additionally, xylem sap-specific exoproteins were analyzed for their role in pathogenicity of the haploid parental strain *V. dahliae*.

4.4.1 *V. longisporum* distinguishes between different environments and regulates secretion responses accordingly

A proteomic approach was used to identify *V. longisporum* secreted proteins derived from cultivation in different growth media. Comparison of the exoprotein patterns revealed that *V. longisporum* secretes different proteins after incubation in non-plant related media in contrast to the simulated xylem medium (SXM) and xylem sap from the host *B. napus*. Several cultivation conditions, including water, minimal medium, yeast nitrogen base medium and vegetable juice V8, triggered a similar exoproteome whereas cultivation in SXM or xylem sap each induced a different distinct exoproteome pattern (Figure 18). These findings provide evidence for the ability of *Verticillium* spp. to distinguish between different environments and to induce media-dependent secretion responses.

To study how the fungus communicates with the plant, the direct way would be to monitor its responses during plant infection. Studies on *Verticillium* spp. growth in the plant are quite challenging due to the low amount of fungal material compared to plant tissue. Faino *et al* (2012) showed that RNA sequencing of *V. dahliae*-infected *Nicotiana benthamiana* resulted in only 0.9% fungal reads whereas the rest was mapped to the host plant. Further data are available that aimed to identify effectors required for successful infections. As example, one study compared the *V. dahliae* transcriptome and secretome dependent on Vta2, a global regulator, which is required for successful colonization of tomato plants. The *VTA2* deletion strain was cultivated in SXM and the fungal transcriptome was compared to the extracellular proteome. The exoproteome contained 125 secreted proteins involved in adhesion, detoxification, metabolism and unknown functions whereas RNA-seq data revealed 57 proteins that were classified as secreted. The overlap only contained 21 proteins (Tran *et al*, 2014). These findings point out a major difference between transcriptome and secretome studies and strengthen our approach to identify actual secreted proteins in plant-derived medium to shed a light on the fungal response to the plant.

Studies of the fungus in its natural habitat are scarce due to the technical difficulties to access pure xylem sap. However, for *V. longisporum* it was shown that pure extracted xylem sap inhibits fungal growth whereas filtered xylem sap stimulated growth (Singh *et al*, 2012). These results suggest that plant proteins in the pure xylem sap inhibit fungal growth. Even small traces of filtered xylem sap stimulated mycelial growth suggesting signal molecules trigger the enhanced growth (Singh *et al*, 2012). It as well indicates that *V. longisporum* can sense the presence of xylem sap as it altered growth accordingly.

Studies also showed that *V. longisporum* is able to adapt to the low-nutrient and unbalanced amino acid supply in the xylem sap by activating the cross-pathway (Timpner *et al*, 2013). This pathway is controlled by the cross-pathway control transcription factor Cpc1 in filamentous fungi, which is encoded by the yeast homolog *GCN4* (general control non-derepressed) (Mösch *et al*, 1991; Hoffmann *et al*, 2001; Timpner *et al*, 2013). Knockdowns in *V. longisporum* and knockouts in *V. dahliae* revealed that Cpc1 is required for growth under amino acid starvation conditions and successful colonization of their host (Timpner *et al*, 2013). These

findings suggest that *V. longisporum* senses and reacts to its host environment to survive.

Our study revealed that *V. longisporum* even communicates with its environment. It is able to distinguish between SXM and xylem sap. SXM was developed to mimic the fungal natural habitat (Neumann & Dobinson, 2003). The *Verticillium* exoproteomes derived from SXM and xylem sap share a large core set of 221 fungal proteins that were secreted in both media to a similar extend. However, there are differences in specifically enriched proteins in SXM and xylem sap. The exoproteome in SXM includes a considerable number of pectin degrading enzymes reflecting the adaptation to the medium containing high amounts of pectin as carbon source. With the 143 SXM-enriched proteins it seems to be not as specific as the xylem sap-induced secretome of only 32 proteins. These results further show that SXM lacks the full capacity to mimic the natural growth medium xylem sap and support that the fungus communicates with its host or environment.

Other studies analyzed the *V. dahliae* secretome in minimal medium with cotton roots (Zhang *et al*, 2017b). Several secreted proteins were detected including 12 cellulases, five pectate lyases, two chitinases, 13 proteases and one cerato-platanin domain containing protein (Cp1) (Zhang *et al*, 2017b). Comparing these proteins with our results revealed that most proteins were detected in our SXM-specific and core exoproteome. No overlap to our xylem sap-specific secretome was detected. This suggests that the SXM-induced response of *Verticillium* spp. is more similar to the presence of roots than the actual xylem sap.

In SXM and non-plant related media, the fungus inhibits the expression or at least the secretion of proteins that are uniquely secreted in xylem sap. This suggests that *Verticillium* spp. possess means of a tight and fast adapting control mechanism. Such a regulatory control could be similar to the epigenetic-mediated control of effector expression in *Leptosphaeria maculans.* Effector genes often reside in AT-rich regions of the genome. These are associated with heterochromatin and explain the silenced state of effector expression. Upon leaf infection chromatin-mediated repression is abolished and gene expression is upregulated in *L. maculans* (Tan & Oliver, 2017; Soyer *et al*, 2014). The comparative proteomic approach and other studies indicate that *Verticillium* spp. are able to fine-tune their secretion responses and induce the secretion of specific patterns upon sensing xylem sap or the presence of plant material.

4.4.2 *V. longisporum* induces the secretion of putative effectors in xylem sap

Proteins that were uniquely enriched in the host xylem sap compared to SXM and other media are likely to fulfill their specific function during colonization of the plant. These candidates were analyzed in the haploid parental strain *V. dahliae* and included carbohydrate-active enzymes (CAZys), peptidases and proteins with effector domains. All deletion strains did not show an altered *ex planta* phenotype compared to *V. dahliae* WT, which corroborates a specific function *in planta*.
CAZys, the metallopeptidase Mep2 alone and in combination with Mep1 or the cerato-platanin proteins Cp1 and Cp2 (alone and in combination) were dispensable for WT-like induction of disease symptoms in tomato infections. In contrast, Mep1, the necrosis and ethylene inducing-like proteins Nlp2 and Nlp3 are required for *V. dahliae* pathogenicity on tomato.

4.4.2.1 *V. dahliae* effectors have redundant functions and may be strain specific

Corresponding proteins that were specifically enriched in xylem sap during *V. longisporum* cultivation were analyzed in *V. dahliae*. Many of these secreted proteins did not have a significant effect on pathogenicity in tomato, which can have several causes. One explanation is that *Verticillium* spp. secrete hundreds of effectors (Klosterman *et al*, 2011), which makes it likely that the absence of only one or two effectors is dispensable. *In silico* analysis predicted even 780 secreted proteins in the *V. dahliae* genome with a strikingly high repertoire of pectin-degrading enzymes and other CAZys compared to other fungi. These include mainly enzymes degrading plant cell walls, which are evidently beneficial for the root-penetrating vascular plant pathogen (Klosterman *et al*, 2011). The importance of these enzymes for virulence of *V. dahliae* was demonstrated by the disruption of *VdSNF1* (sucrose nonfermenting 1), which encodes part of a kinase complex. VdSnf1 is involved in catabolite derepression by inducing the expression of carbohydrate-active enzymes. VdSnf1 is essential for growth on medium with pectin or galactose and for virulence on tomato and eggplant (Tzima *et al*, 2010b). The high number of CAZys in the genome and in our secretome approach suggest that *V. dahliae* secretes effectors with redundant functions. *V. dahliae* strains lacking one of the tested CAZys (glucoamylase Gla1, putative polysaccharide

mono-oxygenase Cbd1 and α-amylase Amy1) infected tomato plants similar to WT. This could be explained by similar functions of other CAZys that may not be required solely in xylem sap and were detected in the core exoproteome.

Metalloproteases have been implicated with promoting fungal virulence by degrading host proteins (Jashni *et al*, 2015; Brouta *et al*, 2002). So far, mainly two families were identified as secreted by pathogenic fungi: the deuterolysin (M35) and the fungalysin (M36). A third class, M43 metallopeptidases are poorly described in pathogenic fungi. The only analyzed M43 family metalloprotease is *MEP1* of the human respiratory pathogen *Coccidoides posadasii* where it contributes to evasion of host detection (Hung *et al*, 2005). M36 metallopeptidases are secreted proteins, which occur mainly in pathogenic fungi as shown by phylogenetic analysis (Li & Zhang, 2014). In *Cryptococcus neoformans* M36 is required for invasion of the central nervous system (Vu *et al*, 2014). *Fusarium verticillioides* M36 metallopeptidases truncate and deactivate plant class IV chitinases *in vitro* (Naumann *et al*, 2011; Naumann & Price, 2012). Plant chitinases degrade chitin of the fungus, which elicits the plant defense response (Naumann & Price, 2012).

Our approach identified one M36 (Mep1) and one M43 (Mep2) peptidase in the xylem sap-specific exoproteome. Tomato infection assays with *V. dahliae MEP1* and *MEP2* single and double deletion strains resulted in a similar diseased phenotype as WT infection. One additional M43 peptidase was detected in the core exoproteome. In total, *in silico* analysis identified two M43 and six M36 peptidases in *V. dahliae*. These results suggest that other peptidases complement the absence of Mep1 and Mep2.

In *F. oxysporum* investigations of FoMep1, encoded by the *MEP1* homolog, and an additional serine protease FoSep1, revealed synergistic actions of the proteases on chitinases as well as virulence in tomato infections. The single deletion strains did not result in significant differences in disease induction compared to the WT (Jashni *et al*, 2015). These results provide further evidence of functional redundancy of enzymes and explain why the absence of one or two effectors may not show changes in the infection phenotype. *V. dahliae* possesses the ability to truncate extracellular chitin-binding domain-containing chitinases (Jashni *et al*, 2015). The homolog of the gene encoding FoSep1 is present in the *V. dahliae* genome and was detected in the core exoproteome of our secretome

analysis. A different *V. dahliae* serine protease, *VdSSEP1,* is required for virulence on cotton. This protease cleaves chitinase 28 that is important for plant defense (Han *et al*, 2019). Therefore, it would be interesting to investigate on a possible synergistic effect of Mep1 and Sep1 in *V. dahliae* pathogenicity on tomato.

The cerato-platanin domain containing proteins Cp1 and Cp2 were also found to be dispensable for *V. dahliae* pathogenicity on tomato. Cp1 was not detected in our secretome approach but was included in this study to investigate on putative synergistic actions of the CPs present in the *V. dahliae* genome. Additionally, other studies with the *V. dahliae* strain XH-8 identified Cp1 in the supernatant after incubation in minimal medium supplemented with cotton root fragments. In this system, Cp1 was required for cotton virulence and is suggested to function as a chitin scavenger to prevent fungal recognition by the plant (Zhang *et al*, 2017b). Another example for a host-specific function of effectors was shown with the necrosis and ethylene inducing-like proteins (NLPs). Nlp1 and Nlp2 were dispensable for *V. dahliae* V592 pathogenicity on cotton (Zhou *et al*, 2012). Studies with *V. dahliae* JR2 revealed that Nlp1 and Nlp2 were required for tomato and *A. thaliana* infections whereas Nlp1 was as well essential for full virulence on *N. benthamiana* (Santhanam *et al*, 2013). These results indicate that effectors may work strain- or host-specific or both. As the secretome of *V. longisporum* was analyzed in response to *B. napus* xylem sap, it is possible that *V. dahliae* induces the secretion of a different set of effectors in different hosts.

Similarly, it was found that *V. dahliae* responds differentially in a susceptible and tolerant olive cultivar (Jiménez-Ruiz *et al*, 2019). The fungus significantly induced expression of genes involved in niche-adaptation, pathogenicity and microsclerotia development in the susceptible cultivar (Jiménez-Ruiz *et al*, 2019). These results support that the fungus senses its environment and responds with different secretion patterns. This answer additionally seems to be host-specific.

4.4.2.2 *V. dahliae* Nlp2 and Nlp3 contribute to pathogenicity on tomato

The xylem sap-specific secretome did include effectors with a single effect on infection success, the NLPs. These proteins share an NPP1 domain and are well conserved effectors in plant pathogenicity. An NPP1 domain-containing protein was first described in oomycetes as effector, which is known to elicit plant defense responses in *A. thaliana* (Fellbrich *et al*, 2002). *V. dahliae* possesses eight

members of the NLP family (Santhanam *et al*, 2013). As mentioned in 4.4.2.1, Nlp1 and Nlp2 are differentially required for *V. dahliae* infection on different hosts (Zhou *et al*, 2012; Santhanam *et al*, 2013). However, both were required for WT-like induction of disease symptoms on tomato (Santhanam *et al*, 2013). Nlp3 did not induce necrosis as Nlp1 and Nlp2 when tested on *N. benthamiana* leaves and was not further examined (Santhanam *et al*, 2013).

Two NLPs, Nlp2 and Nlp3 were identified as xylem sap-specific secreted effectors in this study. Single and double deletions of the corresponding genes resulted in compromised pathogenicity on tomato (Figure 21B). The *NLP2* single deletion strain was included as control as it was shown to contribute to *V. dahliae* virulence (Santhanam *et al*, 2013). These findings strengthen our results although no complementation strains are included. Ectopic complementations of the single deletion strains were constructed but did not induce disease symptoms as severe as WT infections. As ectopic integration of constructs leads to a different genetic surrounding, it may be differently expressed. For verification of the roles of Nlp2 and Nlp3 in *V. dahliae* pathogenicity, future work will include new complementation strains. The *NLP3* deletion strain was additionally tested for *A. thaliana* root colonization revealing no differences to WT (Figure 21A). This indicates that Nlp3 is dispensable for root adhesion or colonization but is required during later steps of the infection. The function in the plant is supported by the necrotic lesion formation that is characteristically induced by NLPs (Zhou *et al*, 2012). Additionally, Nlp2 and Nlp3 secretion was triggered by xylem sap and not SXM supporting the role in the plant.

Concluding, this comparative proteomic approach revealed many factors likely to be required for pathogenicity. Many candidates, however, may be complemented by other proteins with similar functions. Moreover, it was shown that effectors also play a host-specific role and are dispensable for infections on other plants. As *Verticillium* spp. have a broad host range, the expression and secretion of required effectors may be induced or inhibited accordingly. This specific communication with the environment was as well corroborated by the different secretion responses that were induced by non-plant related media, the pectin-rich SXM and xylem sap. Our approach identified th metalloprotease Mep1 and the necrosis and ethylene inducing-like proteins Nlp2 and Nlp3 in the xylem sap-specific secretome. These proteins are required for *V. dahliae* pathogenicity with roles in later steps of

infection. These effectors display potential targets for control strategies of Verticillium wilt.

References

Adam A, Deimel S, Pardo-Medina J, García-Martínez J, Konte T, Limón MC, Avalos J & Terpitz U (2018) Protein activity of the *Fusarium fujikuroi* rhodopsins CarO and OpsA and their relation to fungus-plant interaction. *Int. J. Mol. Sci.* **19:** 215.

Agrios GN (2005a) Plant diseases caused by fungi. In *Plant Pathology* pp 265–509. Elsevier Academic Press.

Agrios GN (2005b) Effects of pathogens on plant physiological functions. In *Plant Pathology* pp 175–205. Elsevier Academic Press.

Almagro Armenteros JJ, Sønderby CK, Sønderby SK, Nielsen H & Winther O (2017) DeepLoc: prediction of protein subcellular localization using deep learning. *Bioinformatics* **33:** 3387–3395.

Ansanay Galeote V, Alexandre H, Bach B, Delobel P, Dequin S & Blondin B (2007) Sfl1p acts as an activator of the HSP30 gene in *Saccharomyces cerevisiae*. *Curr. Genet.* **52:** 55–63.

Aronson BD, Johnson KA & Dunlap JC (1994) Circadian clock locus frequency: protein encoded by a single open reading frame defines period length and temperature compensation. *Proc. Natl. Acad. Sci. U. S. A.* **91:** 7683–7687.

Baccelli I, Luti S, Bernardi R, Scala A & Pazzagli L (2014) Cerato-platanin shows expansin-like activity on cellulosic materials. *Appl. Microbiol. Biotechnol.* **98:** 175–184.

Baker CL, Loros JJ & Dunlap JC (2012) The circadian clock of *Neurospora crassa*. *FEMS Microbiol. Rev.* **36:** 95–110.

Balnojan S (2016) Influence of the Fbx15 protein and adjacent elements on the development and virulence of *Verticillium dahliae*. *Master thesis Georg-August-Universität Göttingen.*

Bauer J & Wendland J (2007) *Candida albicans* Sfl1 suppresses flocculation and filamentation. *Eukaryot. Cell* **6:** 1736–1744.

Bayram Ö, Biesemann C, Krappmann S, Galland P & Braus GH (2008a) More than a repair enzyme: *Aspergillus nidulans* photolyase-like CryA is a regulator of sexual development. *Mol. Biol. Cell* **19:** 3254–3262.

Bayram Ö & Braus GH (2012) Coordination of secondary metabolism and development in fungi: the velvet family of regulatory proteins. *FEMS Microbiol. Rev.* **36:** 1–24.

Bayram Ö, Braus GH, Fischer R & Rodriguez-Romero J (2010) Spotlight on *Aspergillus nidulans* photosensory systems. *Fungal Genet. Biol.* **47:** 900–908.

Bayram Ö, Krappmann S, Ni M, Bok JW, Helmstaedt K, Valerius O, Braus-Stromeyer S, Kwon N-J, Keller NP, Yu J-HY & Braus GH (2008b) VelB/VeA/LaeA complex coordinates light signal with fungal development and secondary metabolism. *Science* **320:** 1504–1506.

Beattie GA, Hatfield BM, Dong H & McGrane RS (2018) Seeing the light: the roles of red- and blue-light sensing in plant microbes. *Annu. Rev. Phytopathol.* **56:** 41–66.

Bell AA, Puhalla JE, Tolmsoff WJ & Stipanovic RD (1976) Use of mutants to establish (+)-scytalone as an intermediate in melanin biosynthesis by *Verticillium dahliae*. *Can. J. Microbiol.* **22:** 787–799.

Bell AA & Wheeler MH (1986) Biosynthesis and functions of fungal melanins. *Annu. Rev. Phytopathol.* **24:** 411–451.

Bergkessel M & Guthrie C (2013) Colony PCR. In *Laboratory Methods in Enzymology: DNA*, Lorsch JBT-M in E (ed) pp 299–309. *Academic Press*.

Bertani G (1951) Studies on lysogenesis. I. The mode of phage liberation by lysogenic *Escherichia coli*. *J. Bacteriol.* **62:** 293–300.

de Boer AH & Volkov V (2003) Logistics of water and salt transport through the plant: structure and functioning of the xylem. *Plant, Cell Environ.* **26:** 87–101.

Bradford MM (1976) A rapid and sensitive method for the quantitation of microgram quantities of protein utilizing the principle of protein-dye binding. *Anal. Biochem.* **72:** 248–254.

Brandt WH (1964) Morphogenesis in *Verticillium*: effects of light and ultraviolet radiation on microsclerotia and melanin. *Can. J. Bot.* **42:** 1017–1023.

Braus GH, Grundmann O, Brückner S & Mösch H-U (2003) Amino acid starvation and Gcn4p regulate adhesive growth and *FLO11* gene expression in *Saccharomyces cerevisiae*. *Mol. Biol. Cell* **14:** 4272–84.

Braus GH, Pries R, Düvel K & Valerius O (2004) Molecular biology of fungal amino acid biosynthesis regulation. In *Genetics and Biotechnology* pp 239–269. Berlin, Heidelberg: Springer.

Brouta F, Descamps F, Monod M, Vermout S, Losson B & Mignon B (2002) Secreted metalloprotease gene family of *Microsporum canis*. *Infect. Immun.* **70:** 5676–5683.

Brückner S & Mösch HU (2012) Choosing the right lifestyle: adhesion and development in *Saccharomyces cerevisiae*. *FEMS Microbiol. Rev.* **36:** 25–58.

Bui T, Harting R, Braus-Stromeyer SA, Tran V, Leonard M, Höfer A, Abelmann A, Bakti F, Valerius O, Schlüter R, Stanley CE, Ambrósio A & Braus GH (2019) *Verticillium dahliae* transcription factors Som1 and Vta3 control microsclerotia formation and sequential steps of plant root penetration and colonisation to induce disease. *New Phytol.* **221:** 2138–2159.

Butler MJ & Day AW (1998) Fungal melanins: a review. *Can. J. Microbiol.* **44:** 1115–1136.

Canessa P, Schumacher J, Hevia MA, Tudzynski P & Larrondo LF (2013) Assessing the effects of light on differentiation and virulence of the plant pathogen *Botrytis cinerea*: characterization of the white collar complex. *PLoS One* **8:** e84223.

Carella P, Wilson DC, Kempthorne CJ & Cameron RK (2016) Vascular sap proteomics: providing insight into long-distance signaling during stress. *Front. Plant Sci.* **7:** 651.

Carsiotis M & Jones RF (1974) Cross-pathway regulation: tryptophan-mediated control of histidine and arginine biosynthetic enzymes in *Neurospora crassa*. *J. Bacteriol.* **119:** 889–892.

Carsiotis M, Jones RF & Wesseling AC (1974) Cross-pathway regulation: histidine-mediated control of histidine, tryptophan, and arginine biosynthetic enzymes in Neurospora crassa. *J. Bacteriol.* **119:** 893–898.

Casadevall A, Cordero RJB, Bryan R, Nosanchuk J & Dadachova E (2017) Melanin, radiation, and energy transduction in fungi. *Microbiol Spectr.* **5:** FUNK-0037-2016.

Cha J, Yuan H & Liu Y (2011) Regulation of the activity and cellular localization of the circadian clock protein FRQ. *J. Biol. Chem.* **286:** 11469–11478.

Cheng P, Yang Y, Heintzen C & Liu Y (2001) Coiled-coil domain-mediated FRQ-FRQ interaction is essential for its circadian clock function in *Neurospora*. *EMBO J.* **20:** 101–108.

Cherry JM, Hong EL, Amundsen C, Balakrishnan R, Binkley G, Chan ET, Christie KR, Costanzo MC, Dwight SS, Engel SR, Fisk DG, Hirschman JE, Hitz BC, Karra K, Krieger CJ, Miyasato SR, Nash RS, Park J, Skrzypek MS, Simison M, *et al* (2012) *Saccharomyces* Genome Database: the genomics resource of budding yeast. *Nucleic Acids Res.* **40:** D700-D705.

Ciechanover A, Orian A & Schwartz AL (2000) Ubiquitin-mediated proteolysis: Biological regulation via destruction. *BioEssays* **22:** 442–451.

Cohrs KC & Schumacher J (2017) The two cryptochrome/photolyase family proteins fulfill distinct roles in DNA photorepair and regulation of conidiation in the gray mold fungus *Botrytis cinerea*. *Appl. Environ. Microbiol.* **83:** e00812-17.

Conlan RS & Tzamarias D (2001) Sfl1 functions via the co-repressor Ssn6-Tup1 and the cAMP-dependent protein kinase Tpk2. *J. Mol. Biol.* **309:** 1007–1015.

Covert SF, Kapoor P, Lee M, Briley A & Nairn CJ (2001) *Agrobacterium tumefaciens*-mediated transformation of *Fusarium circinatum*. *Mycol. Res.* **105:** 259–264.

Crosthwaite SK, Dunlap JC & Loros JJ (1997) Neurospora wc-1 and wc-2: Transcription, photoresponses, and the origins of circadian rhythmicity. *Science* **276:** 763–769.

Crosthwaite SK, Loros JJ & Dunlap JC (1995) Light-induced resetting of a circadian clock is mediated by a rapid increase in frequency transcript. *Cell* **81:** 1003–1012.

Czapek F (1902) Untersuchungen über die Stickstoffgewinnung und Eiweißbildung der Pflanzen. *Beiträge zur Chem. Physiol. und Pathol.* **1:** 538–560.

Depotter JRL, Deketelaere S, Inderbitzin P, Tiedemann A von, Höfte M, Subbarao KV., Wood TA & Thomma BPHJ (2016) *Verticillium longisporum*, the invisible threat to oilseed rape and other brassicaceous plant hosts. *Mol. Plant Pathol.* **17:** 1004–1016.

Depotter JRL, Shi-Kunne X, Missonnier H, Liu T, Faino L, Berg GCM van den, Wood TA, Zhang B, Jacques A, Seidl MF & Thomma BPHJ (2019) Dynamic virulence-related regions of the fungal plant pathogen *Verticillium dahliae* display remarkably enhanced sequence conservation. *Mol. Ecol.* **28:** 3482–3495.

Diernfellner ACR, Querfurth C, Salazar C, Höfer T & Brunner M (2009) Phosphorylation modulates rapid nucleocytoplasmic shuttling and cytoplasmic accumulation of *Neurospora* clock protein FRQ on a circadian time scale. *Genes Dev.* **23:** 2192–200.

Dodds PN & Rathjen JP (2010) Plant immunity: towards an integrated view of plant–pathogen interactions. *Nat. Rev. Genet.* **11:** 539–548.

Dong S, Raffaele S & Kamoun S (2015) The two-speed genomes of filamentous pathogens: Waltz with plants. *Curr. Opin. Genet. Dev.* **35:** 57–65.

Dox AW (1910) The intracellular enzymes of Penicillium and Aspergillus with special references to those of P. camenberti. *U.S. Dept. Agr. Bur. Anim. Ind. Bull.,* **120:** 170.

Dunlap JC & Loros JJ (2006) How fungi keep time: circadian system in *Neurospora* and other fungi. *Curr. Opin. Microbiol.* **9:** 579–587.

Dunlap JC & Loros JJ (2017) Making Time: conservation of biological clocks from fungi to animals. In *The Fungal Kingdom* pp 515–534. *NIH Public Access*.

Duressa D, Anchieta A, Chen D, Klimes A, Garcia-Pedrajas MD, Dobinson KF & Klosterman SJ (2013) RNA-seq analyses of gene expression in the microsclerotia of *Verticillium dahliae*. *BMC Genomics* **14:** 1–18.

Esquivel-Naranjo EU, García-Esquivel M, Medina-Castellanos E, Correa-Pérez VA, Parra-Arriaga JL, Landeros-Jaime F, Cervantes-Chávez JA & Herrera-Estrella A (2016) A *Trichoderma atroviride* stress-activated MAPK pathway integrates stress and light signals. *Mol. Microbiol.* **100:** 860–876.

van Esse HP, Bolton MD, Stergiopoulos I, de Wit PJGM & Thomma BPHJ (2007) The chitin-binding *Cladosporium fulvum* effector protein Avr4 is a virulence factor. *Mol. Plant-Microbe Interact.* **20:** 1092–1101.

Eynck C, Koopmann B, Grunewaldt-Stoecker G, Karlovsky P & von Tiedemann A (2007) Differential interactions of *Verticillium longisporum* and *V. dahliae* with *Brassica napus* detected with molecular and histological techniques. *Eur. J. Plant Pathol.* **118:** 259–274.

Faino L, de Jonge R & Thomma BPHJ (2012) The transcriptome of *Verticillium dahliae*-infected *Nicotiana benthamiana* determined by deep RNA sequencing. *Plant Signal. Behav.* **7:** 1065–1069.

Faino L, Seidl MF, Shi-Kunne X, Pauper M, Van Den Berg GCM, Wittenberg AHJ & Thomma BPHJ (2016) Transposons passively and actively contribute to evolution of the two-speed genome of a fungal pathogen. *Genome Res.* **26:** 1091–1100.

Fan R, Klosterman SJ, Wang C, Subbarao KV., Xu X, Shang W & Hu X (2017) Vayg1 is required for microsclerotium formation and melanin production in *Verticillium dahliae*. *Fungal Genet. Biol.* **98:** 1–11.

Fang Y, Klosterman SJ, Tian C & Wang Y (2019) Insights into VdCmr1-mediated protection against high temperature stress and UV irradiation in *Verticillium dahliae*. *Environ. Microbiol.* **21:** 2977–2996.

Fellbrich G, Romanski A, Varet A, Blume B, Brunner F, Engelhardt S, Felix G, Kemmerling B, Krzymowska M & Nürnberger T (2002) NPP1, a *Phytophthora*-

associated trigger of plant defense in parsley and *Arabidopsis*. *Plant J.* **32:** 375–390.

Fichtner L, Schulze F & Braus GH (2007) Differential Flo8p-dependent regulation of *FLO1* and *FLO11* for cell-cell and cell-substrate adherence of *S. cerevisiae* S288c. *Mol. Microbiol.* **66:** 1276–1289.

Fischer R, Aguirre J, Herrera-Estrella A & Corrochano LM (2016) The complexity of fungal vision. *Microbiol. Spectr.* **4:** 441–461.

Fradin EF & Thomma BPHJ (2006) Physiology and molecular aspects of Verticillium wilt diseases caused by *V. dahliae* and *V. albo-atrum*. *Mol. Plant Pathol.* **7:** 71–86.

Fradin EF, Zhang Z, Ayala JCJ, Castroverde CDM, Nazar RN, Robb J, Liu C-M & Thomma BPHJ (2009) Genetic dissection of Verticillium wilt resistance mediated by tomato Ve1. *Plant Physiol.* **150:** 320–332.

Froehlich AC, Liu Y, Loros JJ & Dunlap JC (2002) White Collar-1, a circadian blue light photoreceptor, binding to the frequency promoter. *Science* **297:** 815–819.

Fujita A, Kikuchi Y, Kuhara S, Misumi Y, Matsumoto S & Kobayashi H (1989) Domains of the SFL1 protein of yeasts are homologous to Myc oncoproteins or yeast heat-shock transcription factor. *Gene* **85:** 321–328.

Fuller KK, Ringelberg CS, Loros JJ & Dunlap JC (2013) The fungal pathogen *Aspergillus fumigatus* regulates growth, metabolism, and stress resistance in response to light. *MBio* **4:** e00142-13.

Gao F, Zhou B-J, Li G-Y, Jia P-S, Li H, Zhao Y-L, Zhao P, Xia G-X & Guo H-S (2010) A glutamic acid-rich protein identified in *Verticillium dahliae* from an insertional mutagenesis affects microsclerotial formation and pathogenicity. *PLoS One* **5:** e15319.

Geer LY, Marchler-Bauer A, Geer RC, Han L, He J, He S, Liu C, Shi W & Bryant SH (2010) The NCBI BioSystems database. *Nucleic Acids Res.* **38:** D492-6.

Geldner N & Salt DE (2014) Focus on roots. *Plant Physiol.* **166:** 453–454.

Gijzen M & Nürnberger T (2006) Nep1-like proteins from plant pathogens: Recruitment and diversification of the NPP1 domain across taxa. *Phytochemistry* **67:** 1800–1807.

Görl M, Merrow M, Huttner B, Johnson J, Roenneberg T & Brunner M (2001) A PEST-like element in FREQUENCY determines the length of the circadian period in *Neurospora crassa*. *EMBO J.* **20:** 7074–7084.

Gui YJ, Chen JY, Zhang DD, Li NY, Li TG, Zhang WQ, Wang XY, Short DPG, Li L, Guo W, Kong ZQ, Bao YM, Subbarao KV. & Dai XF (2017) *Verticillium dahliae* manipulates plant immunity by glycoside hydrolase 12 proteins in conjunction with carbohydrate-binding module 1. *Environ. Microbiol.* **19:** 1914–1932.

Guo J, Cheng P & Liu Y (2010) Functional significance of FRH in regulating the phosphorylation and stability of *Neurospora* circadian clock protein FRQ. *J. Biol. Chem.* **285:** 11508–11515.

Hall R & Ly H (1972) Development and quantitative measurement of microsclerotia of *Verticillium dahliae*. *Can. J. Bot.* **50:** 2097–2102.

Hamel L-P, Nicole M-C, Duplessis S & Ellis BE (2012) Mitogen-activated protein kinase signaling in plant-interacting fungi: distinct messages from conserved messengers. *Plant Cell* **24:** 1327–1351.

Han LB, Li YB, Wang FX, Wang WY, Liu J, Wu JH, Zhong NQ, Wu SJ, Jiao GL, Wang HY & Xia GX (2019) The cotton apoplastic protein CRR1 stabilizes chitinase 28 to facilitate defense against the fungal pathogen *Verticillium dahliae*. *Plant Cell* **31:** 520–536.

He Q, Cha J, He Q, Lee H-C, Yang Y & Liu Y (2006) CKI and CKII mediate the FREQUENCY-dependent phosphorylation of the WHITE COLLAR complex to close the *Neurospora* circadian negative feedback loop. *Genes Dev.* **20:** 2552–2565.

He Q, Cheng P, Yang Y, He Q, Yu H & Liu Y (2003) FWD1-mediated degradation of FREQUENCY in *Neurospora* establishes a conserved mechanism for circadian clock regulation. *EMBO J.* **22:** 4421–4430.

Heale JB & Isaac I (1965) Environmental factors in the production of dark resting structures in *Verticillium alboatrum*, *V. dahliae* and *V. tricorpus*. *Trans. Br. Mycol. Soc.* **48:** 39-50.

Henson JM, Butler MJ & Day AW (1999) The dark side of the mycelium: melanins of phytopathogenic fungi. *Annu. Rev. Phytopathol.* **37:** 447–471.

Hevia MA, Canessa P & Larrondo LF (2016) Circadian clocks and the regulation of virulence in fungi: getting up to speed. *Semin. Cell Dev. Biol.* **57:** 147–155.

Hevia MA, Canessa P, Müller-Esparza H & Larrondo LF (2015) A circadian oscillator in the fungus *Botrytis cinerea* regulates virulence when infecting *Arabidopsis thaliana*. *Proc. Natl. Acad. Sci. U. S. A.* **112:** 8744–8749.

Hoffmann B, Valerius O, Andermann M & Braus GH (2001) Transcriptional autoregulation and inhibition of mRNA translation of amino acid regulator gene *cpcA* of filamentous fungus *Aspergillus nidulans*. *Mol. Biol. Cell* **12:** 2846–2857.

Hollensteiner J, Wemheuer F, Harting R, Kolarzyk AM, Diaz Valerio SM, Poehlein A, Brzuszkiewicz EB, Nesemann K, Braus-Stromeyer SA, Braus GH, Daniel R & Liesegang H (2017) *Bacillus thuringiensis* and *Bacillus weihenstephanensis* inhibit the growth of phytopathogenic *Verticillium* species. *Front. Microbiol.* **7:** 2171.

Hung CY, Seshan KR, Yu JJ, Schaller R, Xue J, Basrur V, Gardner MJ & Cole GT (2005) A metalloproteinase of *Coccidioides posadasii* contributes to evasion of host detection. *Infect. Immun.* **73:** 6689–6703.

Hwang CS, Flaishman MA & Kolattukudy PE (1995) Cloning of a gene expressed during appressorium formation by *Colletotrichum gloeosporioides* and a marked decrease in virulence by disruption of this gene. *Plant Cell* **7:** 183–193.

Igbalajobi O, Yu Z & Fischer R (2019) Red-and blue-light sensing in the plant pathogen *Alternaria alternata* depends on phytochrome and the white-collar protein LreA. *MBio* **10:** e00371-19.

Inderbitzin P, Bostock RM, Davis RM, Usami T, Platt HW & Subbarao KV (2011a)

Phylogenetics and taxonomy of the fungal vascular wilt pathogen *Verticillium*, with the descriptions of five new species. *PLoS One* **6:** e28341.

Inderbitzin P, Davis RM, Bostock RM & Subbarao KV. (2011b) The ascomycete *Verticillium longisporum* is a hybrid and a plant pathogen with an expanded host range. *PLoS One* **6:** e18260.

Inderbitzin P & Subbarao KV. (2014) *Verticillium* systematics and evolution: how confusion impedes Verticillium wilt management and how to resolve it. *Phytopathology* **104:** 564–574.

Inoue H, Nojima H & Okayama H (1990) High efficiency transformation of *Escherichia coli* with plasmids. *Gene* **96:** 23–28.

Isaac I (1967) Speciation in *Verticillium*. *Annu. Rev. Phytopathol.* **5:** 201–222.

Jashni MK, Dols IHM, Iida Y, Boeren S, Beenen HG, Mehrabi R, Collemare J & de Wit PJGM (2015) Synergistic action of a metalloprotease and a serine protease from *Fusarium oxysporum* f. sp. *lycopersici* cleaves chitin-binding tomato chitinases, reduces their antifungal activity, and enhances fungal virulence. *Mol. Plant-Microbe Interact.* **28:** 996–1008.

Jiang C, Zhang X, Liu H & Xu JR (2018) Mitogen-activated protein kinase signaling in plant pathogenic fungi. *PLoS Pathog.* **14:** e1006875.

Jiménez-Ruiz J, Leyva-Pérez M de la O, Cabanás CGL, Barroso JB, Luque F & Mercado-Blanco J (2019) The transcriptome of *Verticillium dahliae* responds differentially depending on the disease susceptibility level of the olive (*Olea europaea* L.) cultivar. *Genes (Basel).* **10:** 251.

Jones JDG & Dangl JL (2006) The plant immune system. *Nature* **444:** 323–329.

Jones P, Binns D, Chang HY, Fraser M, Li W, McAnulla C, McWilliam H, Maslen J, Mitchell A, Nuka G, Pesseat S, Quinn AF, Sangrador-Vegas A, Scheremetjew M, Yong SY, Lopez R & Hunter S (2014) InterProScan 5: Genome-scale protein function classification. *Bioinformatics* **30:** 1236–1240.

de Jonge R, Bolton MD, Kombrink A, Van Den Berg GCM, Yadeta KA & Thomma BPHJ (2013) Extensive chromosomal reshuffling drives evolution of virulence in an asexual pathogen. *Genome Res.* **23:** 1271–1282.

de Jonge R, Bolton MD & Thomma BP (2011) How filamentous pathogens co-opt plants: the ins and outs of fungal effectors. *Curr. Opin. Plant Biol.* **14:** 400–406.

de Jonge R, van Esse HP, Kombrink A, Shinya T, Desaki Y, Bours R, van der Krol S, Shibuya N, Joosten MHAJ & Thomma BPHJ (2010) Conserved fungal LysM effector Ecp6 prevents chitin-triggered immunity in plants. *Science* **329:** 953–955.

de Jonge R, Peter van Esse H, Maruthachalam K, Bolton MD, Santhanam P, Saber MK, Zhang Z, Usami T, Lievens B, Subbarao KV. & Thomma BPHJ (2012) Tomato immune receptor Ve1 recognizes effector of multiple fungal pathogens uncovered by genome and RNA sequencing. *Proc. Natl. Acad. Sci.* **109:** 5110–5115.

Jyothishwaran G, Kotresha D, Selvaraj T, Srideshikan SH, Rajvanshi PK & Jayabaskaran C (2007) A modified freeze–thaw method for efficient

transformation of *Agrobacterium tumefaciens*. *Curr. Sci.* **93:** 770–772.

Kaever A, Landesfeind M, Possienke M, Feussner K, Feussner I & Meinicke P (2012) MarVis-filter: Ranking, filtering, adduct and isotope correction of mass spectrometry data. *J. Biomed. Biotechnol.* **2012:** 263910.

Kersey PJ, Allen JE, Allot A, Barba M, Boddu S, Bolt BJ, Carvalho-Silva D, Christensen M, Davis P, Grabmueller C, Kumar N, Liu Z, Maurel T, Moore B, McDowall MD, Maheswari U, Naamati G, Newman V, Ong CK, Paulini M, et al (2018) Ensembl Genomes 2018: An integrated omics infrastructure for non-vertebrate species. *Nucleic Acids Res.* **46:** D802–D808.

Kinoshita E, Kinoshita-Kikuta E & Koike T (2009) Separation and detection of large phosphoproteins using phos-tag sds-page. *Nat. Protoc.* **4:** 1513–1521.

Klebahn H (1913) Beiträge zur Kenntnis der Fungi imperfecti. I. Eine Verticillium-Krankheit auf Dahlien. *Mycol. Cent.* **3:** 49–66.

Klimes A, Amyotte SG, Grant S, Kang S & Dobinson KF (2008) Microsclerotia development in *Verticillium dahliae*: regulation and differential expression of the hydrophobin gene *VDH1*. *Fungal Genet. Biol.* **45:** 1525–1532.

Klimes A & Dobinson KF (2006) A hydrophobin gene, *VDH1*, is involved in microsclerotial development and spore viability in the plant pathogen *Verticillium dahliae*. *Fungal Genet. Biol.* **43:** 283–294.

Klimes A, Dobinson KF, Thomma BPHJ & Klosterman SJ (2015) Genomics spurs rapid advances in our understanding of the biology of vascular wilt pathogens in the genus *Verticillium*. *Annu. Rev. Phytopathol.* **53:** 181–198.

Klosterman SJ, Atallah ZK, Vallad GE & Subbarao KV. (2009) Diversity, pathogenicity, and management of *Verticillium* species. *Annu. Rev. Phytopathol.* **47:** 39–62.

Klosterman SJ, Subbarao KV., Kang S, Veronese P, Gold SE, Thomma BPHJ, Chen Z, Henrissat B, Lee Y-H, Park J, Garcia-Pedrajas MD, Barbara DJ, Anchieta A, de Jonge R, Santhanam P, Maruthachalam K, Atallah Z, Amyotte SG, Paz Z, Inderbitzin P, *et al* (2011) Comparative genomics yields insights into niche adaptation of plant vascular wilt pathogens. *PLoS Pathog.* **7:** e1002137.

Kolar M, Punt PJ, van den Hondel CAMJJ & Schwab H (1988) Transformation of *Penicillium chrysogenum* using dominant selection markers and expression of an *Escherichia coli lacZ* fusion gene. *Gene* **62:** 127–134.

Kosugi S, Hasebe M, Tomita M & Yanagawa H (2009) Systematic identification of cell cycle-dependent yeast nucleocytoplasmic shuttling proteins by prediction of composite motifs. *Proc. Natl. Acad. Sci.* **106:** 10171–10176.

Laemmli UK (1970) Cleavage of structural proteins during the assembly of the head of bacteriophage T4. *Nature* **227:** 680–685.

Langfelder K, Streibel M, Jahn B, Haase G & Brakhage AA (2003) Biosynthesis of fungal melanins and their importance for human pathogenic fungi. *Fungal Genet. Biol.* **38:** 143–158.

Lazo GR, Stein PA & Ludwig RA (1991) A DNA transformation-competent *Arabidopsis* genomic library in *Agrobacterium*. *Biotechnology* **9:** 963–7.

Levasseur A, Drula E, Lombard V, Coutinho PM & Henrissat B (2013) Expansion of the enzymatic repertoire of the CAZy database to integrate auxiliary redox enzymes. *Biotechnol. Biofuels* **6:** 1.

Li G, Zhou X, Kong L, Wang Y, Zhang H, Zhu H, Mitchell TK, Dean RA & Xu JR (2011) MoSfl1 is important for virulence and heat tolerance in *Magnaporthe oryzae*. *PLoS One* **6:** e19951.

Li J & Zhang KQ (2014) Independent expansion of zincin metalloproteinases in onygenales fungi may be associated with their pathogenicity. *PLoS One* **9:** e90225.

Li Y, Su C, Mao X, Cao F & Chen J (2007) Roles of *Candida albicans* Sfl1 in hyphal development. *Eukaryot. Cell* **6:** 2112–2121.

Li Y, Zhang X, Hu S, Liu H & Xu JR (2017) PKA activity is essential for relieving the suppression of hyphal growth and appressorium formation by MoSfl1 in *Magnaporthe oryzae*. *PLoS Genet.* **13:** e1006954.

Li Z-F, Liu Y-J, Feng Z-L, Feng H-J, Klosterman SJ, Zhou F-F, Zhao L-H, Shi Y-Q & Zhu H-Q (2015) *VdCYC8*, encoding CYC8 glucose repression mediator protein, is required for microsclerotia formation and full virulence in *Verticillium dahliae*. *PLoS One* **10:** e0144020.

Liu T, Chen G, Min H & Lin F (2009) *MoFLP1*, encoding a novel fungal fasciclin-like protein, is involved in conidiation and pathogenicity in *Magnaporthe oryzae*. *J. Zhejiang Univ. Sci. B* **10:** 434–444.

Liu X, Li H, Liu Q, Niu Y, Hu Q, Deng H, Cha J, Wang Y, Liu Y & He Q (2015) Role for protein kinase A in the *Neurospora* circadian clock by regulating White Collar-independent frequency transcription through phosphorylation of RCM-1. *Mol. Cell. Biol.* **35:** 2088–2102.

Liversage J, Coetzee MPA, Bluhm BH, Berger DK & Crampton BG (2018) LOVe across kingdoms: blue light perception vital for growth and development in plant–fungal interactions. *Fungal Biol. Rev.* **32:** 86–103.

Lombardi LM & Brody S (2005) Circadian rhythms in *Neurospora crassa*: clock gene homologues in fungi. *Fungal Genet. Biol.* **42:** 887–892.

Luo C, Loros JJ & Dunlap JC (1998) Nuclear localization is required for function of the essential clock protein FRQ. *EMBO J.* **17:** 1228–1235.

Luo X, Xie C, Dong J, Yang X & Sui A (2014) Interactions between *Verticillium dahliae* and its host: vegetative growth, pathogenicity, plant immunity. *Appl. Microbiol. Biotechnol.* **98:** 6921–6932.

Madeira F, Park Y, Lee J, Buso N, Gur T, Madhusoodanan N, Basutkar P, Tivey A, Potter S, Finn R & Lopez R (2019) The EMBL-EBI search and sequence analysis tools APIs in 2019. *Nucleic Acids Res.* **47:** W636-W641.

McCotter SW, Horianopoulos LC & Kronstad JW (2016) Regulation of the fungal secretome. *Curr. Genet.* **62:** 533–545.

Möller M & Stukenbrock EH (2017) Evolution and genome architecture in fungal plant pathogens. *Nat. Rev. Microbiol.* **15:** 756–771.

Montenegro-Montero A, Canessa P & Larrondo LF (2015) Around the fungal clock: recent advances in the molecular study of circadian clocks in *Neurospora* and

other fungi. *Adv. Genet.* **92:** 107–184.

Mösch HU, Scheier B, Lahti R, Mäntsälä P & Braus GH (1991) Transcriptional activation of yeast nucleotide biosynthetic gene *ADE4* by GCN4. *J. Biol. Chem.* **266:** 20453–20456.

Mullins ED, Chen X, Romaine P, Raina R, Geiser DM & Kang S (2001) *Agrobacterium*-mediated transformation of *Fusarium oxysporum*: An efficient tool for insertional mutagenesis and gene transfer. *Phytopathology* **91:** 173–180.

Murashige T & Skoog F (1962) A Revised Medium for Rapid Growth and Bio Assays with Tobacco Tissue Cultures. *Physiol. Plant.* **15:** 473–497.

Naumann TA & Price NPJ (2012) Truncation of class IV chitinases from *Arabidopsis* by secreted fungal proteases. *Mol. Plant Pathol.* **13:** 1135–1139.

Naumann TA, Wicklow DT & Price NPJ (2011) Identification of a chitinase-modifying protein from *Fusarium verticillioides*: truncation of a host resistance protein by a fungalysin metalloprotease. *J. Biol. Chem.* **286:** 35358–35366.

Nees von Esenbeck CG (1817) Das System der Pilze und Schwämme. Würzburg: In der Stahelschen Buchhandlung.

Neumann MJ & Dobinson KF (2003) Sequence tag analysis of gene expression during pathogenic growth and microsclerotia development in the vascular wilt pathogen *Verticillium dahliae*. *Fungal Genet. Biol.* **38:** 54–62.

Novakazi F, Inderbitzin P, Sandoya G, Hayes RJ, von Tiedemann A & Subbarao KV. (2015) The three lineages of the diploid hybrid *Verticillium longisporum* differ in virulence and pathogenicity. *Phytopathology* **105:** 662–673.

de O. Barsottini MR, de Oliveira JF, Adamoski D, Teixeira PJPL, do Prado PF V., Tiezzi HO, Sforça ML, Cassago A, Portugal R V., de Oliveira PSL, de M. Zeri AC, Dias SMG, Pereira GAG & Ambrosio ALB (2013) Functional diversification of cerato-platanins in *Moniliophthora perniciosa* as seen by differential expression and protein function specialization. *Mol. Plant-Microbe Interact.* **26:** 1281–1293.

Odenbach D, Breth B, Thines E, Weber RWS, Anke H & Foster AJ (2007) The transcription factor Con7p is a central regulator of infection-related morphogenesis in the rice blast fungus *Magnaporthe grisea*. *Mol. Microbiol.* **64:** 293–307.

Olmedo M, Ruger-Herreros C, Luque EM & Corrochano LM (2010) A complex photoreceptor system mediates the regulation by light of the conidiation genes *con-10* and *con-6* in *Neurospora crassa*. *Fungal Genet. Biol.* **47:** 352–363.

Pan X & Heitman J (2002) Protein kinase A operates a molecular switch that governs yeast pseudohyphal differentiation. *Mol. Cell. Biol.* **22:** 3981–93.

Pegg GF & Brady BL (2002) Verticillium wilts. Pegg GF & Brady BL (eds) Wallingford, UK: CABI Pub.

Pöggeler S, Nowrousian M, Teichert I, Beier A & Kück U (2018) 16 Fruiting-body development in ascomycetes. In *Anke T, Schüffler (eds) The Mycota XV, physiology and genetics, 2nd edn.* Berlin-Heidelberg: Springer.

Prabakaran S, Lippens G, Steen H & Gunawardena J (2012) Post-translational

modification: nature's escape from genetic imprisonment and the basis for dynamic information encoding. *Wiley Interdiscip. Rev. Syst. Biol. Med.* **4:** 565–83.

Lo Presti L, Lanver D, Schweizer G, Tanaka S, Liang L, Tollot M, Zuccaro A, Reissmann S & Kahmann R (2015) Fungal effectors and plant susceptibility. *Annu. Rev. Plant Biol.* **66:** 513–545.

Prieto P, Navarro-Raya C, Valverde-Corredor A, Amyotte SG, Dobinson KF & Mercado-Blanco J (2009) Colonization process of olive tissues by *Verticillium dahliae* and its *in planta* interaction with the biocontrol root endophyte *Pseudomonas fluorescens* PICF7. *Microb. Biotechnol.* **2:** 499–511.

Pruß S, Fetzner R, Seither K, Herr A, Pfeiffer E, Metzler M, Lawrence CB & Fischer R (2014) Role of the *Alternaria alternata* blue-light receptor LreA (White-Collar 1) in spore formation and secondary metabolism. *Appl. Environ. Microbiol.* **80:** 2582–2591.

Punt PJ, Oliver RP, Dingemanse MA, Pouwels PH & van den Hondel CAMJJ (1987) Transformation of *Aspergillus* based on the hygromycin B resistance marker from *Escherichia coli*. *Gene* **56:** 117–124.

Querfurth C, Diernfellner ACR, Gin E, Malzahn E, Höfer T & Brunner M (2011) Circadian conformational change of the *Neurospora* clock protein FREQUENCY triggered by clustered hyperphosphorylation of a basic domain. *Mol. Cell* **43:** 713–722.

Rauyaree P, Ospina-Giraldo MD, Kang S, Bhat RG, Subbarao KV., Grant SJ & Dobinson KF (2005) Mutations in VMK1, a mitogen-activated protein kinase gene, affect microsclerotia formation and pathogenicity in *Verticillium dahliae*. *Curr. Genet.* **48:** 109–116.

Ravid T & Hochstrasser M (2008) Diversity of degradation signals in the ubiquitin-proteasome system. *Nat. Rev. Mol. Cell Biol.* **9:** 679–689.

Reusche M, Truskina J, Thole K, Nagel L, Rindfleisch S, Tran VT, Braus-Stromeyer SA, Braus GH, Teichmann T & Lipka V (2014) Infections with the vascular pathogens *Verticillium longisporum* and *Verticillium dahliae* induce distinct disease symptoms and differentially affect drought stress tolerance of *Arabidopsis thaliana*. *Environ. Exp. Bot.* **108:** 23–37.

Robertson LS & Fink GR (1998) The three yeast A kinases have specific signaling functions in pseudohyphal growth. *Proc. Natl. Acad. Sci. U. S. A.* **95:** 13783–13787.

Roden LC & Ingle RA (2009) Lights, rhythms, infection: the role of light and the circadian clock in determining the outcome of plant-pathogen interactions. *Plant Cell* **21:** 2546–2552.

Rodriguez-Romero J, Hedtke M, Kastner C, Müller S & Fischer R (2010) Fungi, hidden in soil or up in the air: light makes a difference. *Annu. Rev. Microbiol.* **64:** 585–610.

Romero-Calvo I, Ocón B, Martínez-Moya P, Suárez MD, Zarzuelo A, Martínez-Augustin O & de Medina FS (2010) Reversible Ponceau staining as a loading control alternative to actin in Western blots. *Anal. Biochem.* **401:** 318–320.

van Rosmalen M, Krom M & Merkx M (2017) Tuning the flexibility of glycine-serine linkers to allow rational design of multidomain proteins. *Biochemistry* **56:** 6565–6574.

Rovenich H, Boshoven JC & Thomma BPHJ (2014) Filamentous pathogen effector functions: of pathogens, hosts and microbiomes. *Curr. Opin. Plant Biol.* **20:** 96–103.

Rupp S, Summers E, Lo H, Madhani H & Fink G (1999) MAP kinase and cAMP filamentation signaling pathways converge on the unusually large promoter of the yeast FLO11 gene. *EMBO J.* **18:** 1257–1269.

Saiki RK, Gelfand DH, Stoffel S, Scharf SJ, Higuchi R, Horn GT, Mullis KB & Erlich HA (1988) Primer-directed enzymatic amplification of DNA with a thermostable DNA polymerase. *Science* **239:** 487–491.

Salichos L & Rokas A (2010) The diversity and evolution of circadian clock proteins in fungi. *Mycologia* **102:** 269–278.

Santhanam P, van Esse HP, Albert I, Faino L, Nürnberger T & Thomma BPHJ (2013) Evidence for functional diversification within a fungal NEP1-like protein family. *Mol. Plant-Microbe Interact.* **26:** 278–286.

Sarikaya Bayram Ö, Bayram Ö, Valerius O, Park HS, Irniger S, Gerke J, Ni M, Han K-H, Yu J-H & Braus GH (2010) LaeA control of velvet family regulatory proteins for light-dependent development and fungal cell-type specificity. *PLoS Genet.* **6:** e1001226.

Sarmiento-Villamil JL, García-Pedrajas NE, Baeza-Montañez L & García-Pedrajas MD (2018a) The APSES transcription factor Vst1 is a key regulator of development in microsclerotium- and resting mycelium-producing *Verticillium* species. *Mol. Plant Pathol.* **19:** 59–76.

Sarmiento-Villamil JL, Prieto P, Klosterman SJ & García-Pedrajas MD (2018b) Characterization of two homeodomain transcription factors with critical but distinct roles in virulence in the vascular pathogen *Verticillium dahliae*. *Mol. Plant Pathol.* **19:** 986–1004.

Schafmeier T, Káldi K, Diernfellner A, Mohr C & Brunner M (2006) Phosphorylation-dependent maturation of *Neurospora* circadian clock protein from a nuclear repressor toward a cytoplasmic activator. *Genes Dev.* **20:** 297–306.

Schindelin J, Arganda-Carreras I, Frise E, Kaynig V, Longair M, Pietzsch T, Preibisch S, Rueden C, Saalfeld S, Schmid B, Tinevez J-Y, White DJ, Hartenstein V, Eliceiri K, Tomancak P & Cardona A (2012) Fiji: an open-source platform for biological-image analysis. *Nat. Methods* **9:** 676–682.

Schnathorst WC (1963) Theoretical relationships between inoculum potential and disease severity based on a study of the variation in virulence among isolates of *V. albo-atrum*. *Phytopathology* **53:** 906.

Schnathorst WC (1981) Life cycle and epidemiology of *Verticillium*. In *Fungal Wilt Diseases of Plants* pp 81-111. Mace M (ed), San Diego, USA: Elsevier Academic Press.

Schumacher J (2017) How light affects the life of *Botrytis*. *Fungal Genet. Biol.* **106:**

26–41.

Sewell GWF & Wilson JF (1964) Occurrence and dispersal of *Verticillium* conidia in xylem sap of the hop (*Humulus lupulus* L.). *Nature* **204:** 901.

Shevchenko A, Wilm M, Vorm O & Mann M (1996) Mass spectrometric sequencing of proteins from silver-stained polyacrylamide gels. *Anal. Chem.* **68:** 850–858.

Shi Z, Christian D & Leung H (1998) Interactions between spore morphogenetic mutations affect cell types, sporulation, and pathogenesis in *Magnaporthe grisea*. *Mol. Plant-Microbe Interact.* **11:** 199–207.

Short DPG, Gurung S, Hu X, Inderbitzin P & Subbarao KV (2014) Maintenance of sex-related genes and the co-occurrence of both mating types in *Verticillium dahliae*. *PLoS One* **9:** e112145.

Singh S, Braus-Stromeyer SA, Timpner C, Tran VT, Lohaus G, Reusche M, Knüfer J, Teichmann T, von Tiedemann A & Braus GH (2010) Silencing of *Vlaro2* for chorismate synthase revealed that the phytopathogen *Verticillium longisporum* induces the cross-pathway control in the xylem. *Appl. Microbiol. Biotechnol.* **85:** 1961–1976.

Singh S, Braus-Stromeyer SA, Timpner C, Valerius O, von Tiedemann A, Karlovsky P, Druebert C, Polle A & Braus GH (2012) The plant host *Brassica napus* induces in the pathogen *Verticillium longisporum* the expression of functional catalase peroxidase which is required for the late phase of disease. *Mol. Plant-Microbe Interact.* **25:** 569–581.

Sorrell TC & Chen SCA (2009) Fungal-derived immune modulating molecules. In *Pathogen-derived immunomodulatory molecules. Advances in Experimental Medicine and Biology*, Fallon PG (ed) pp 108–120. New York, NY: Springer.

Southern EM (1975) Detection of specific sequences among DNA fragments separated by gel electrophoresis. *J. Mol. Biol.* **98:** 503–17.

Soyer JL, El Ghalid M, Glaser N, Ollivier B, Linglin J, Grandaubert J, Balesdent MH, Connolly LR, Freitag M, Rouxel T & Fudal I (2014) Epigenetic control of effector gene expression in the plant pathogenic fungus *Leptosphaeria maculans*. *PLoS Genet.* **10:** e1004227.

Starke J (2019) Interplay of Verticillium signaling genes favoring beneficial or detrimental outcomes in interactions with plant hosts. *Dissertation at the Georg-August-Universität Göttingen*.

Sun L, Qin J, Rong W, Ni H, Guo HS & Zhang J (2019) Cellophane surface-induced gene, *VdCSIN1*, regulates hyphopodium formation and pathogenesis via cAMP-mediated signalling in *Verticillium dahliae*. *Mol. Plant Pathol.* **20:** 323–333.

Sun Q, Yoda K & Suzuki H (2005) Internal axial light conduction in the stems and roots of herbaceous plants. *J. Exp. Bot.* **56:** 191–203.

Szewczyk E, Nayak T, Oakley CE, Edgerton H, Xiong Y, Taheri-Talesh N, Osmani SA & Oakley BR (2006) Fusion PCR and gene targeting in *Aspergillus nidulans*. *Nat. Protoc.* **1:** 3111–3120.

Tan KC & Oliver RP (2017) Regulation of proteinaceous effector expression in phytopathogenic fungi. *PLoS Pathog.* **13:** e1006241.

Thompson S, Croft NJ, Sotiriou A, Piggins HD & Crosthwaite SK (2008) *Neurospora crassa* heat shock factor 1 is an essential gene; a second heat shock factor-like gene, *hsf2*, is required for asexual spore formation. *Eukaryot. Cell* **7:** 1573–1581.

Tian L, Wang Y, Yu J, Xiong D, Zhao H & Tian C (2016) The mitogen-activated protein kinase kinase VdPbs2 of *Verticillium dahliae* regulates microsclerotia formation, stress response, and plant infection. *Front. Microbiol.* **7:** 1532.

Tian L, Xu J, Zhou L & Guo W (2014) VdMsb regulates virulence and microsclerotia production in the fungal plant pathogen *Verticillium dahliae*. *Gene* **550:** 238–244.

Timpner C, Braus-Stromeyer SA, Tran VT & Braus GH (2013) The Cpc1 regulator of the cross-pathway control of amino acid biosynthesis Is required for pathogenicity of the vascular pathogen *Verticillium longisporum*. *Mol. Plant-Microbe Interact.* **26:** 1312–1324.

Traeger S & Nowrousian M (2015) Analysis of circadian rhythms in the basal filamentous ascomycete *Pyronema confluens*. *G3 GENES, GENOMES, Genet.* **5:** 2061–2071.

Tran V-T (2011) Adhesion of the rapeseed pathogen *Verticillium longisporum* to its host *Brassica napus*. *Dissertation at the Georg-August-Universität Göttingen*.

Tran VT, Braus-Stromeyer SA, Kusch H, Reusche M, Kaever A, Kühn A, Valerius O, Landesfeind M, Aßhauer K, Tech M, Hoff K, Pena-Centeno T, Stanke M, Lipka V & Braus GH (2014) *Verticillium* transcription activator of adhesion Vta2 suppresses microsclerotia formation and is required for systemic infection of plant roots. *New Phytol.* **202:** 565–581.

Tzima AK, Paplomatas EJ, Rauyaree P & Kang S (2010a) Roles of the catalytic subunit of cAMP-dependent protein kinase A in virulence and development of the soilborne plant pathogen *Verticillium dahliae*. *Fungal Genet. Biol.* **47:** 406–415.

Tzima AK, Paplomatas EJ, Rauyaree P, Ospina-Giraldo MD & Kang S (2010b) VdSNF1, the sucrose nonfermenting protein kinase gene of *Verticillium dahliae*, is required for virulence and expression of genes involved in cell-wall degradation. *Mol. Plant-Microbe Interact.* **24:** 129–142.

Tzima AK, Paplomatas EJ, Tsitsigiannis DI & Kang S (2012) The G protein β subunit controls virulence and multiple growth- and development-related traits in *Verticillium dahliae*. *Fungal Genet. Biol.* **49:** 271–283.

Uitenbroek DG (1997) SISA Binomial. Available at: https://www.quantitativeskills.com/sisa/distributions/binomial.htm.

Vallad GE & Subbarao KV. (2008) Colonization of resistant and susceptible lettuce cultivars by a green fluorescent protein-tagged isolate of *Verticillium dahliae*. *Phytopathology* **98:** 871–885.

Vu K, Tham R, Uhrig JP, Thompson GR, Pombejra SN, Jamklang M, Bautos JM & Gelli A (2014) Invasion of the central nervous system by *Cryptococcus neoformans* requires a secreted fungal metalloprotease. *MBio* **5:** e01101-14.

Wang B, Kettenbach AN, Zhou X, Loros JJ & Dunlap JC (2019) The phospho-code

determining circadian feedback loop closure and output in *Neurospora*. *Mol. Cell* **74:** 771-784.

Wang B, Zhou XY, Loros JJ & Dunlap JC (2016a) Alternative use of DNA binding domains by the *Neurospora* White Collar complex dictates circadian regulation and light responses. *Mol. Cell. Biol.* **36:** 781–793.

Wang C & St Leger RJ (2007) The MAD1 adhesin of *Metarhizium anisopliae* links adhesion with blastospore production and virulence to insects, and the MAD2 adhesin enables attachment to plants. *Eukaryot. Cell* **6:** 808–816.

Wang JY, Cai Y, Gou JY, Mao YB, Xu YH, Jiang WH & Chen XY (2004) *VdNEP*, an elicitor from *Verticillium dahliae*, induces cotton plant wilting. *Appl. Environ. Microbiol.* **70:** 4989–4995.

Wang W, Barnaby JY, Tada Y, Li H, Tör M, Caldelari D, Lee D, Fu X-D & Dong X (2011) Timing of plant immune responses by a central circadian regulator. *Nature* **470:** 110–114.

Wang Y, Hu X, Fang Y, Anchieta A, Goldman PH, Hernandez G & Klosterman SJ (2018a) Transcription factor VdCmr1 is required for pigment production, protection from UV irradiation, and regulates expression of melanin biosynthetic genes in *Verticillium dahliae*. *Microbiology* **164:** 685–696.

Wang Y, Tian L, Xiong D, Klosterman SJ, Xiao S & Tian C (2016b) The mitogen-activated protein kinase gene, VdHog1, regulates osmotic stress response, microsclerotia formation and virulence in *Verticillium dahliae*. *Fungal Genet. Biol. FG B* **88:** 13–23.

Wang Z, Wang J, Li N, Li J, Trail F, Dunlap JC & Townsend JP (2018b) Light sensing by opsins and fungal ecology: NOP-1 modulates entry into sexual reproduction in response to environmental cues. *Mol. Ecol.* **27:** 216–232.

Wilhelm S (1955) Longevity of the Verticillium wilt fungus in the laboratory and field. *Phytopathology* **45:** 180–181.

Woodcock DM, Crowther PJ, Doherty J, Jefferson S, DeCruz E, Noyer-Weidner M, Smith SS, Michael MZ & Graham MW (1989) Quantitative evaluation of Escherichia coli host strains for tolerance to cytosine methylation in plasmid and phage recombinants. *Nucleic Acids Res.* **17:** 3469–3478.

Xiong D, Wang Y, Tang C, Fang Y, Zou J & Tian C (2015) VdCrz1 is involved in microsclerotia formation and required for full virulence in *Verticillium dahliae*. *Fungal Genet. Biol.* **82:** 201–212.

Xiong D, Wang Y, Tian L & Tian C (2016) MADS-Box transcription factor VdMcm1 regulates conidiation, microsclerotia formation, pathogenicity, and secondary metabolism of *Verticillium dahliae*. *Front. Microbiol.* **7:** 1192.

Yang Y, Zhang Y, Li B, Yang X, Dong Y & Qiu D (2018) A *Verticillium dahliae* pectate lyase induces plant immune responses and contributes to virulence. *Front. Plant Sci.* **9:** 1271.

Yellareddygari SKR & Gudmestad NC (2018) Effect of soil temperature, injection depth, and rate of metam sodium efficacy in fine-textured soils with high organic matter on the management of Verticillium wilt of potato. *Am. J. Potato Res.* **95:** 413–422.

Yu J, Li T, Tian L, Tang C, Klosterman SJ, Tian C & Wang Y (2019) Two *Verticillium dahliae* MAPKKKs, VdSsk2 and VdSte11, have distinct roles in pathogenicity, microsclerotial formation, and stress adaptation. *mSphere* **4:** e00426-19.

Yu Z, Armant O & Fischer R (2016) Fungi use the SakA (HogA) pathway for phytochrome-dependent light signalling. *Nat. Microbiol.* **1:** 16019.

Yu Z & Fischer R (2019) Light sensing and responses in fungi. *Nat. Rev. Microbiol.* **17:** 25–36.

Zeise K & von Tiedemann A (2002) Host specialization among vegetative compatibility groups of *Verticillium dahliae* in relation to *Verticillium longisporum*. *J. Phytopathol.* **150:** 112–119.

Zhang H, Yohe T, Huang L, Entwistle S, Wu P, Yang Z, Busk PK, Xu Y & Yin Y (2018) dbCAN2: A meta server for automated carbohydrate-active enzyme annotation. *Nucleic Acids Res.* **46:** W95–W101.

Zhang T, Zhang B, Hua C, Meng P, Wang S, Chen Z, Du Y, Gao F & Huang J (2017a) VdPKS1 is required for melanin formation and virulence in a cotton wilt pathogen *Verticillium dahliae*. *Sci. China Life Sci.* **60:** 868–879.

Zhang Y, Gao Y, Liang Y, Dong Y, Yang X, Yuan J & Qiu D (2017b) The *Verticillium dahliae* SnodProt1-like protein VdCP1 contributes to virulence and triggers the plant immune system. *Front. Plant Sci.* **8:** 1880.

Zhao YL, Zhou TT & Guo HS (2016) Hyphopodium-specific VdNoxB/VdPls1-dependent ROS-Ca2+ signaling is required for plant infection by *Verticillium dahliae*. *PLoS Pathog.* **12:** 1–23.

Zhou BJ, Jia PS, Gao F & Guo HS (2012) Molecular characterization and functional analysis of a necrosis-and ethylene-inducing, protein-encoding gene family from *Verticillium dahliae*. *Mol. Plant-Microbe Interact.* **25:** 964–975.

Zhou G, Ying SH, Hu Y, Fang X, Feng MG & Wang J (2018) Roles of three HSF domain-containing proteins in mediating heat-shock protein genes and sustaining asexual cycle, stress tolerance, and virulence in *Beauveria bassiana*. *Front. Microbiol.* **9:** 1677.

Zhou L, Hu Q, Johansson A & Dixelius C (2006) *Verticillium longisporum* and *V. dahliae*: infection and disease in *Brassica napus*. *Plant Pathol.* **55:** 137–144.

Zhou TT, Zhao YL & Guo HS (2017) Secretory proteins are delivered to the septin-organized penetration interface during root infection by *Verticillium dahliae*. *PLoS Pathog.* **13:** e1006275.

Appendix

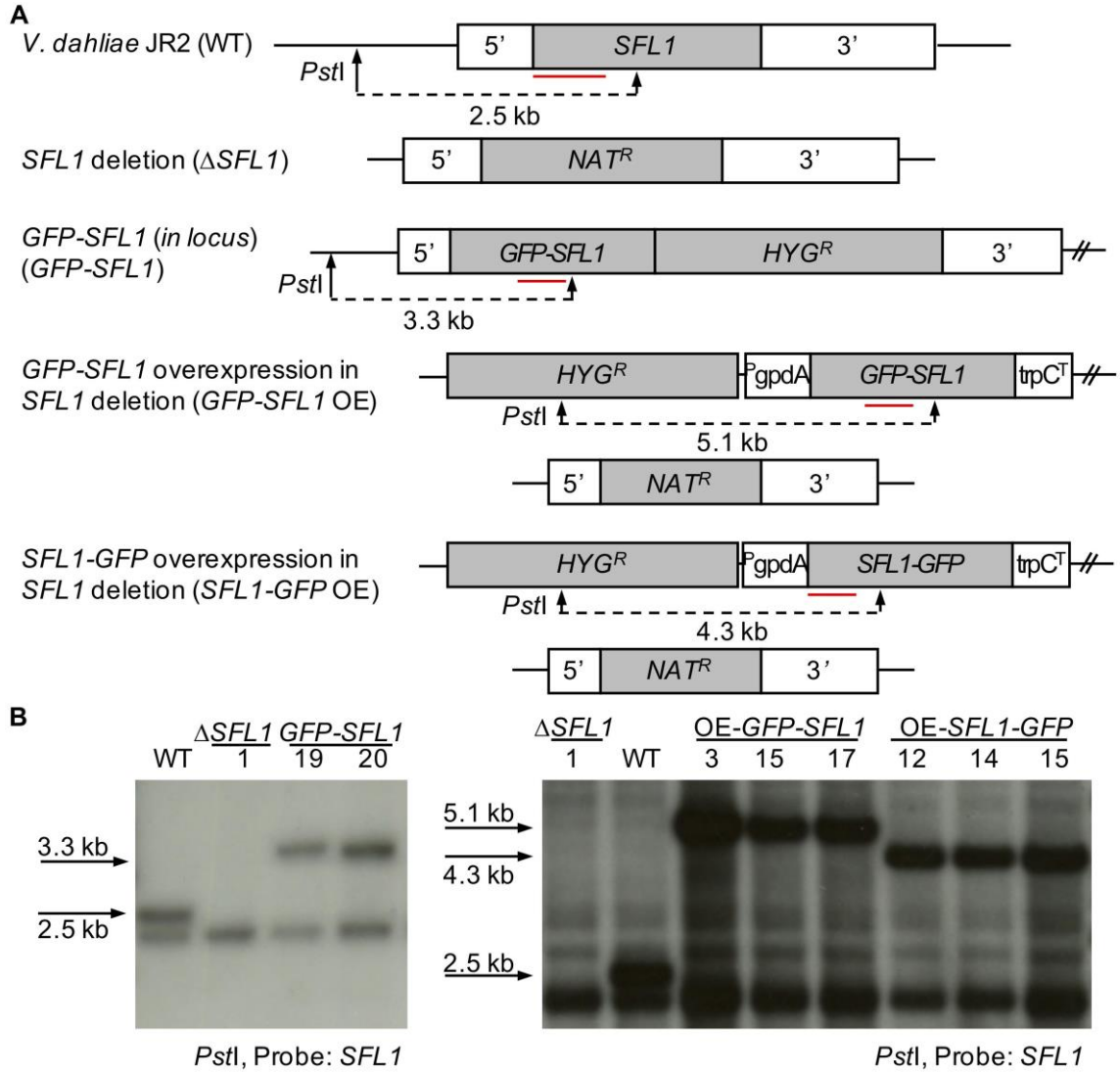

Figure S1. Verification of *V. dahliae SFL1* deletion strain carrying *GFP-SFL1 in locus* or overexpression constructs for *GFP-SFL1* or *SFL1-GFP*.

The strain harboring *GFP-SFL1 in locus* was generated via homologous recombination between the *GFP-SFL1* construct (driven by the native promoter and terminator) and the *SFL1* deletion strain VGB324 (Δ*SFL1*). Δ*SFL1* overexpressing *GFP-SFL1* and *SFL1-GFP* strains were obtained by ectopical integration (indicated by //) of the constructs (controlled by *gpdA* promoter and a *trpC* terminator) into the deletion strain. The constructs contain resistance cassettes (*HYG*^{R}: hygromycin resistance; *NAT*^{R}: nourseothricin resistance) with *gpdA* promoter and *trpC* terminator. The schemes in **A** show restriction sites (arrows) and probes (red lines) used for Southern hybridizations. Restriction enzyme *Pst*I with part of *SFL1* as probe were used for verification of the *in locus* integration of *GFP-SFL1,* the ectopic integration of *GFP-SFL1* and *SFL1-GFP* into Δ*SFL1* strain. **(B)** Blots of Southern hybridizations confirm the constructed strains: *V. dahliae* expressing endogenous *GFP-SFL1*: #19 = VGB433, #20 = VGB434; *SFL1* deletion overexpressing *GFP-SFL1*: #3 = VGB266, #15 = VGB348, #17 = VGB349; *SFL1* deletion overexpressing *SFL1-GFP: #12* = VGB350, #14 = VGB351, #15 = VGB352). Genomic WT DNA served as control. Restriction enzymes, probes and sizes of expected fragments are indicated.

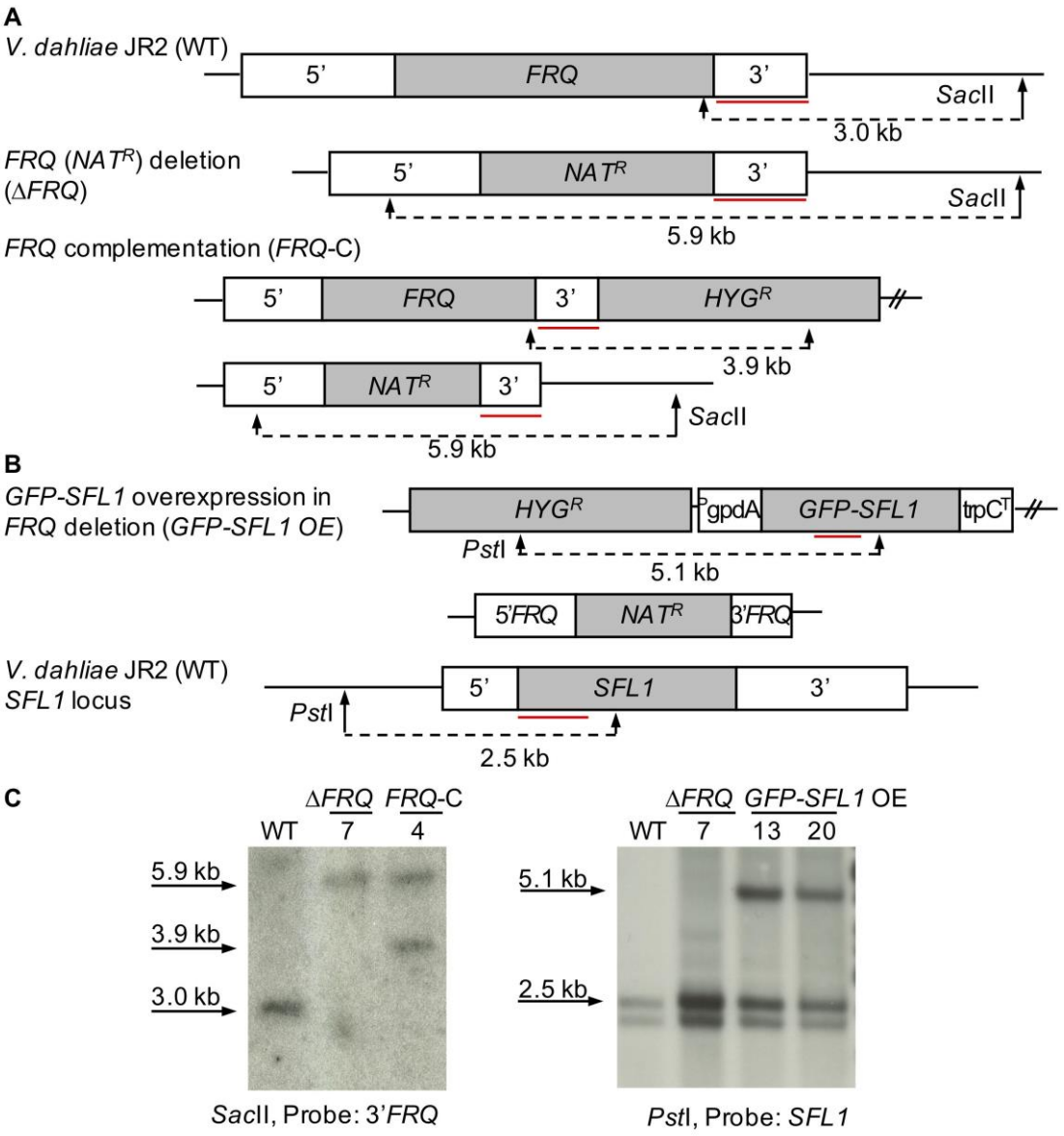

Figure S2. Verification of *V. dahliae FRQ* deletion and complementation strain and *FRQ* deletion strain ectopically overexpressing *GFP-SFL1*.

Deletion strains were constructed via homologous recombination between the deletion construct and *V. dahliae* JR2 wildtype (WT). The complementation construct (*FRQ*-C) was ectopically (indicated by //) integrated into the deletion strain (Δ*FRQ*). Δ*FRQ* overexpressing *GFP-SFL1* strain (*GFP-SFL1* OE) was obtained by ectopical integration of the constructs (with *gpdA* promoter and *trpC* terminator) into Δ*FRQ* strain. The constructs contain resistance cassettes (*HYG*^{R}: hygromycin resistance; *NAT*^{R}: nourseothricin resistance) under control of the *gpdA* promoter and a *trpC* terminator. The schemes display restriction sites (arrows) and probes (red lines) used for Southern hybridizations **(A, B)**. **(A)** *FRQ* deletion and complementation strains were confirmed using the enzyme *Sac*II with 3' flanking region as probe. **(B)** Restriction enzyme *Pst*I with part of *SFL1* as probe was used for verification of the ectopic integration of *GFP-SFL1* into *FRQ* deletion strain. **(C)** Blots of Southern hybridizations show the confirmation of the constructed strains: *FRQ* deletion #7 = VGB296; *FR*Q complementation #4 = VGB411; *FRQ* deletion overexpressing *GFP-SFL1*: #13 = VGB435; #20 = VGB436. Genomic WT DNA served as control. Restriction enzymes, probes and sizes of expected fragments are indicated.

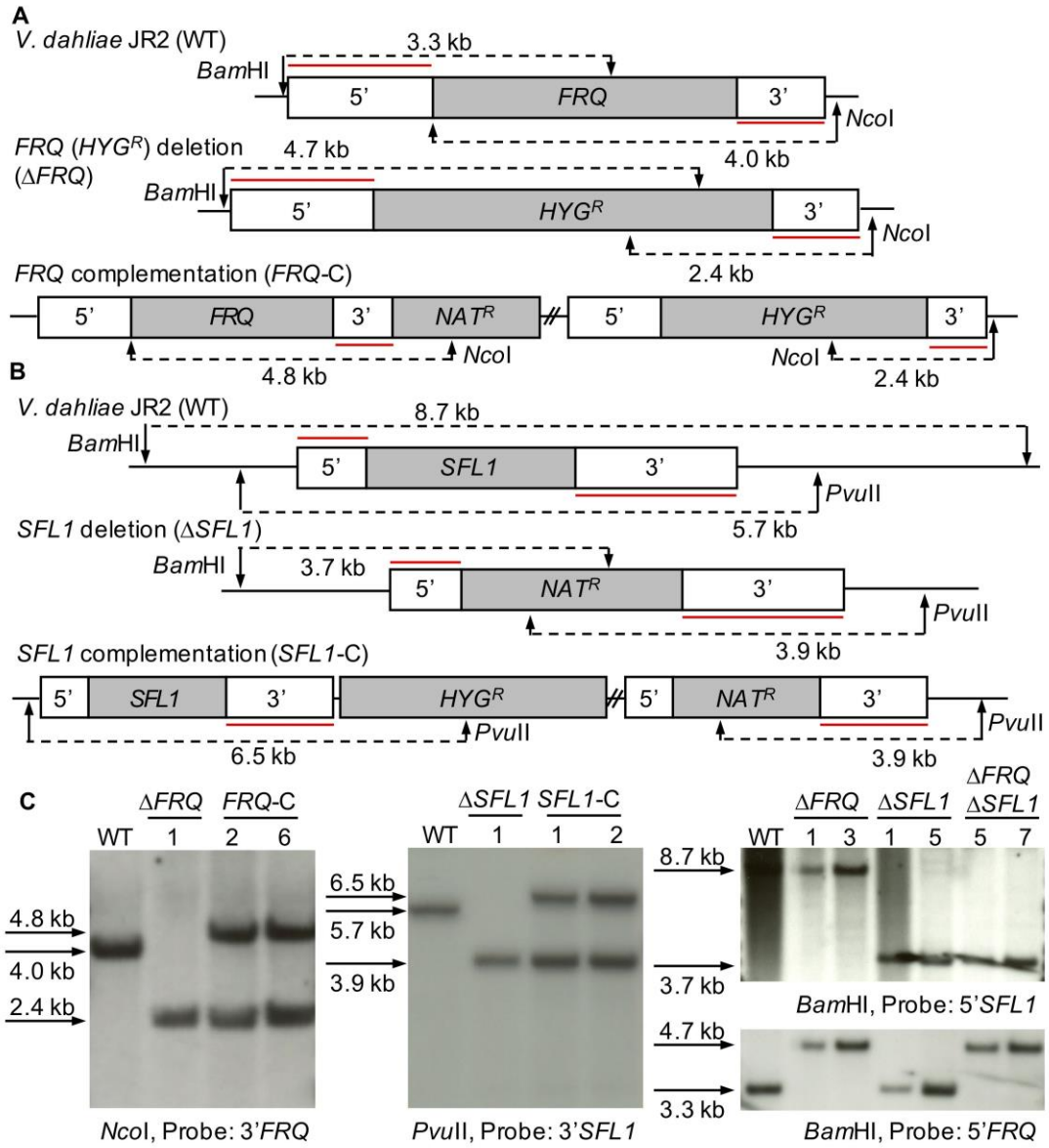

Figure S3. Verification of *V. dahliae FRQ* and *SFL1* deletion and complementation strains.

Deletion strains were obtained via homologous recombination between the deletion construct and *V. dahliae* JR2 wildtype (WT). The complementation constructs were ectopically (indicated by //) integrated into the deletion strain. The constructs contain resistance cassettes (*HYG*^{R}: hygromycin resistance; *NAT*^{R}: nourseothricin resistance) with *gpdA* promoter and *trpC* terminator. The schemes show restriction sites (arrows) and probes (red lines) used for Southern hybridizations **(A, B)**. **(A)** *FRQ* deletion (Δ*FRQ)* and complementation strains (*FRQ*-C) were confirmed using the enzyme *Nco*I with 3' flanking region as probe or *Bam*HI with 5' flanking for the double deletion. **(B)** Restriction enzyme *Pvu*II with 3' flanking or *Bam*HI with 5' flanking region were used for verification of *SFL1* deletion (Δ*SFL1*) and complementation strains (*SFL1*-C). **(C)** Blots of Southern hybridizations verify the deletion (Δ*FRQ* (*HYG*^{R}) #1 = VGB402, #3 = VGB403; Δ*SFL1* #1 = VGB324, #5 = VGB325; Δ*FRQ*Δ*SFL1* #5 = VGB403, #7 = VGB404) and complementation strains (*FRQ*-C #2 = VGB441, #6 = VGB442; *SFL1*-C #1 = VGB342, #2 = VGB343). Genomic WT DNA served as control. Restriction enzymes, probes and sizes of expected fragments are indicated.

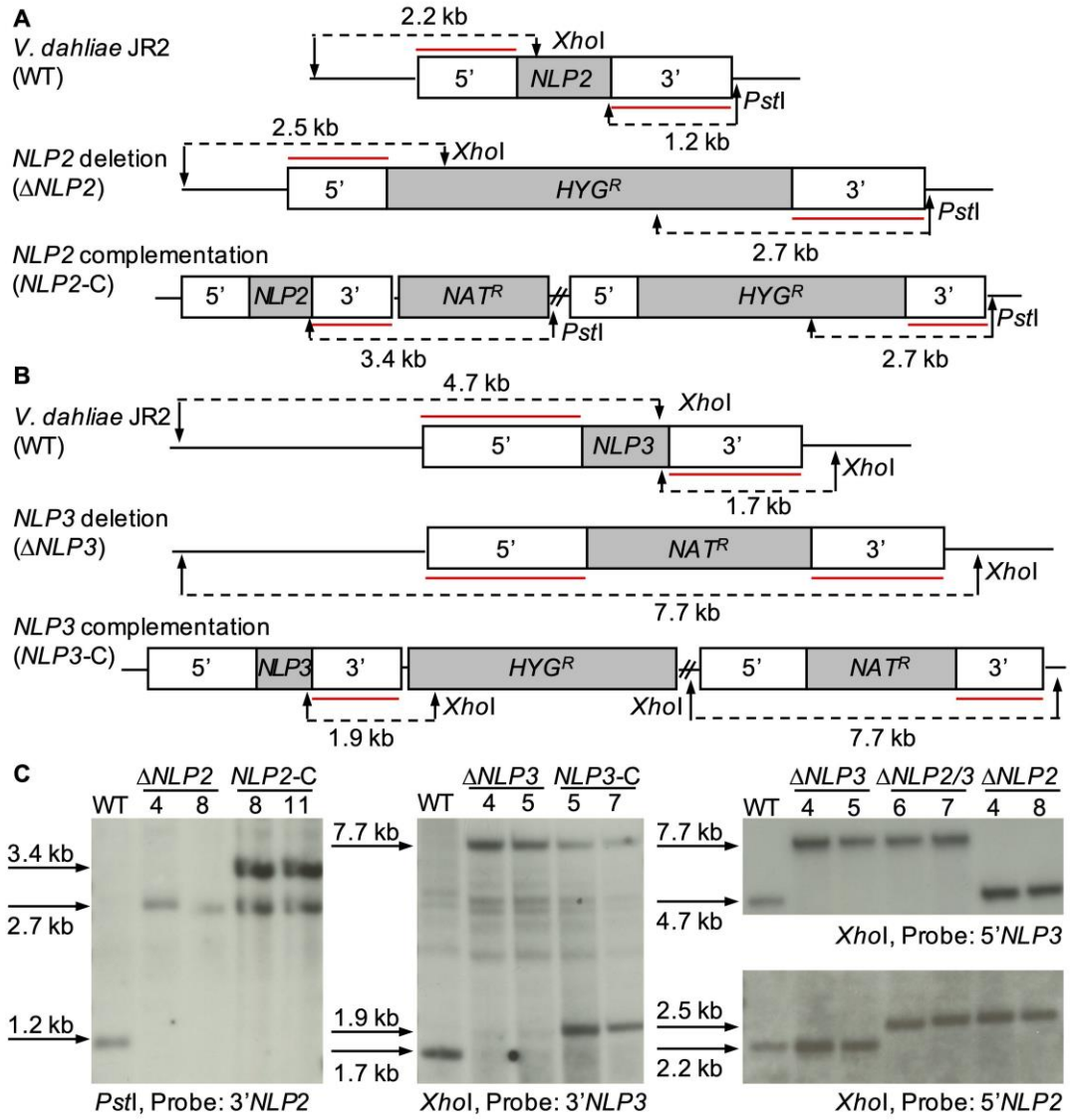

Figure S4. Verification of *V. dahliae NLP2* and *NLP3* deletion and complementation strains.

V. dahliae JR2 wildtype (WT) was transformed with respective deletion cassettes and via homologous recombination *NLP2* deletion (Δ*NLP2*) and *NLP3* deletion (Δ*NLP3*) strains were generated. The *NLP2/3* double deletion strain (Δ*NLP2/3*) was obtained by transforming Δ*NLP3* strain with the Δ*NLP2* construct. The complementation constructs (*NLP2*-C, *NLP3*-C) were ectopically integrated into the corresponding deletion strains as indicated by //. The constructs contain resistance cassettes (HYG^R: hygromycin resistance; NAT^R: nourseothricin resistance) with a *gpdA* promoter and a *trpC* terminator. The schemes show restriction sites (arrows) and probes (red lines) used for Southern hybridization **(A, B)**. **(A)** *Pst*I with 3' flanking region or *Xho*I with 5' flanking region as probe were used for verification of *NLP2* deletion and complementation strains. **(B)** Δ*NLP3* and complementation strains were confirmed using *Xho*I with 5' or 3' flanking region as probe. **(C)** Confirmation of deletion and complementation strains by Southern hybridization is shown for Δ*NLP2* #4 = VGB390, #8 = VGB391; *NLP2*-C #8 = VGB427, #11 = VGB428; Δ*NLP3* #4 = VGB384, #5 = VGB385; *NLP3*-C #5 = VGB435, #7 = VGB426 and Δ*NLP2/3* #6 = VGB400, #7 = VGB401. Genomic WT DNA served as control. Restriction enzymes, probes and sizes of expected fragments are indicated.

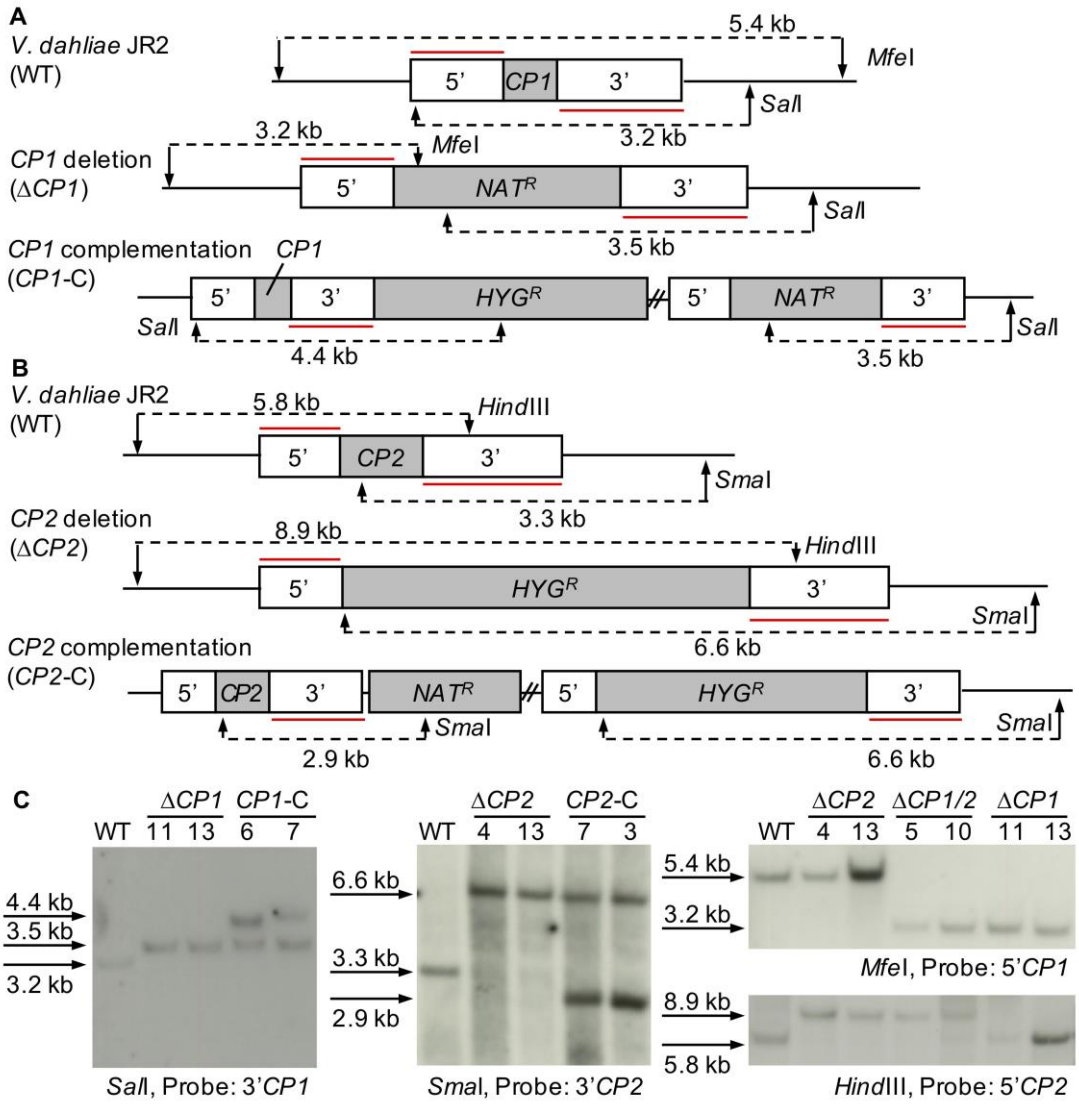

Figure S5. Verification of *V. dahliae CP1* and *CP2* deletion and complementation strains.

Deletion strains (Δ*CP1 and* Δ*CP2*) were obtained via homologous recombination between the deletion constructs and *V. dahliae* JR2 wildtype (WT). The *CP2* deletion (Δ*CP2*) strain was transformed with the *CP1* deletion construct to generate the double deletion strain Δ*CP1/2*. To generate ectopic complementation strains the constructs were integrated into the deletion strain as indicated by //. The constructs contain resistance cassettes (*HYG*^{R}: hygromycin resistance; *NAT*^{R}: nourseothricin resistance) controlled by the *gpdA* promoter and the *trpC* terminator. Schemes with used restriction enzymes, corresponding cutting sites (arrows) and probes (red lines) used for Southern hybridization are presented in **A** and **B**. **(A)** Confirmation of *CP1* deletion and complementation strain was achieved by enzyme restriction with *Sal*I and 3' flanking region as probe or *Mfe*I and 5' flanking region as probe. **(B)** *Sma*I with 3' flanking region or *Hind*III with 5' flanking region as probe was used for *CP2* deletion and complementation strains. **(C)** Deletion and complementation strains were verified by Southern hybridization: Δ*CP1* #11 = VGB316, #13 = VGB317; *CP1*-C #6 = VGB489, #7 = VGB490; Δ*CP2* #4 = VGB406, #14 = VGB422; *CP2*-C #3 = VGB429, #7 = VGB430; Δ*CP1*Δ*CP2* #5 = VGB423, #10 = VGB424. Genomic WT DNA was used as control. Restriction enzymes, probes and sizes of expected fragments are depicted.

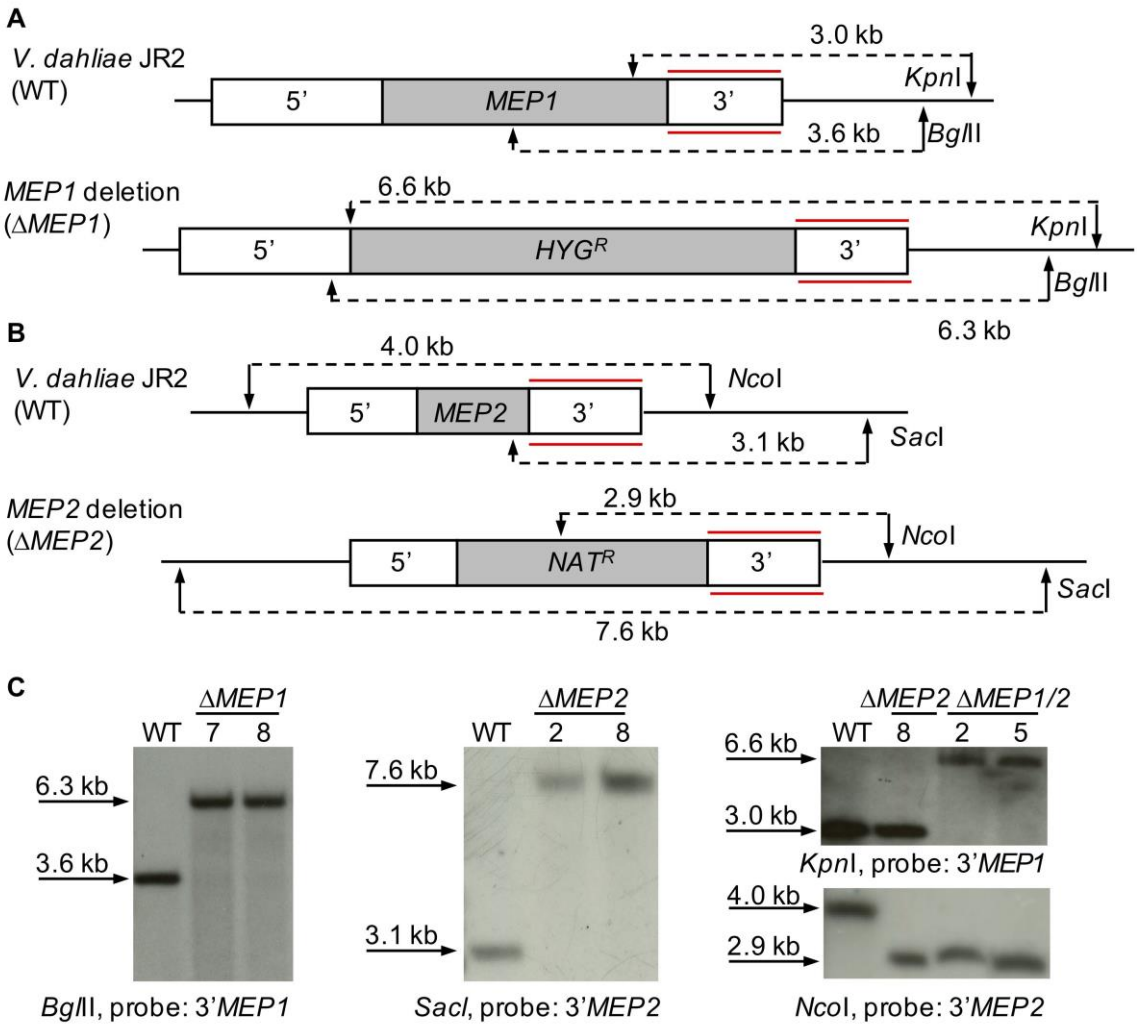

Figure S6. Verification of *V. dahliae MEP1* and *MEP2* deletion strains.
Deletion strains were constructed via homologous recombination between the deletion construct and *V. dahliae* JR2 wildtype (WT) and confirmed by Southern hybridization. In **A** and **B** used restriction enzymes and their restriction sites (arrows) and probes (red lines) used for Southern hybridization are depicted. **(A)** Deletion of *MEP1* was confirmed after enzyme restriction with *Kpn*I or *Bgl*II and 3' flanking region as probe. *MEP1* deletion construct contains hygromycin resistance (*HYG*^{R}) cassette controlled by the *gpdA* promoter and the *trpC* terminator. **(B)** Verification of *MEP2* deletion strain containing the nourseothricin resistance (*NAT*^{R}) cassette under control of the *gpdA* promoter and the *trpC* terminator was achieved with *Sac*I or *Nco*I restriction and 3' flanking region as probe. **(C)** Deletion strains were confirmed by Southern hybridization: Δ*MEP1* #7 = VGB226, #8 = VGB227; Δ*MEP2* #2 = VGB133, #8 = VGB126; Δ*MEP1/2* #2 = VGB204, #5 = VGB203. Genomic WT DNA served as control. Restriction enzymes, probes and sizes of expected fragments are indicated.

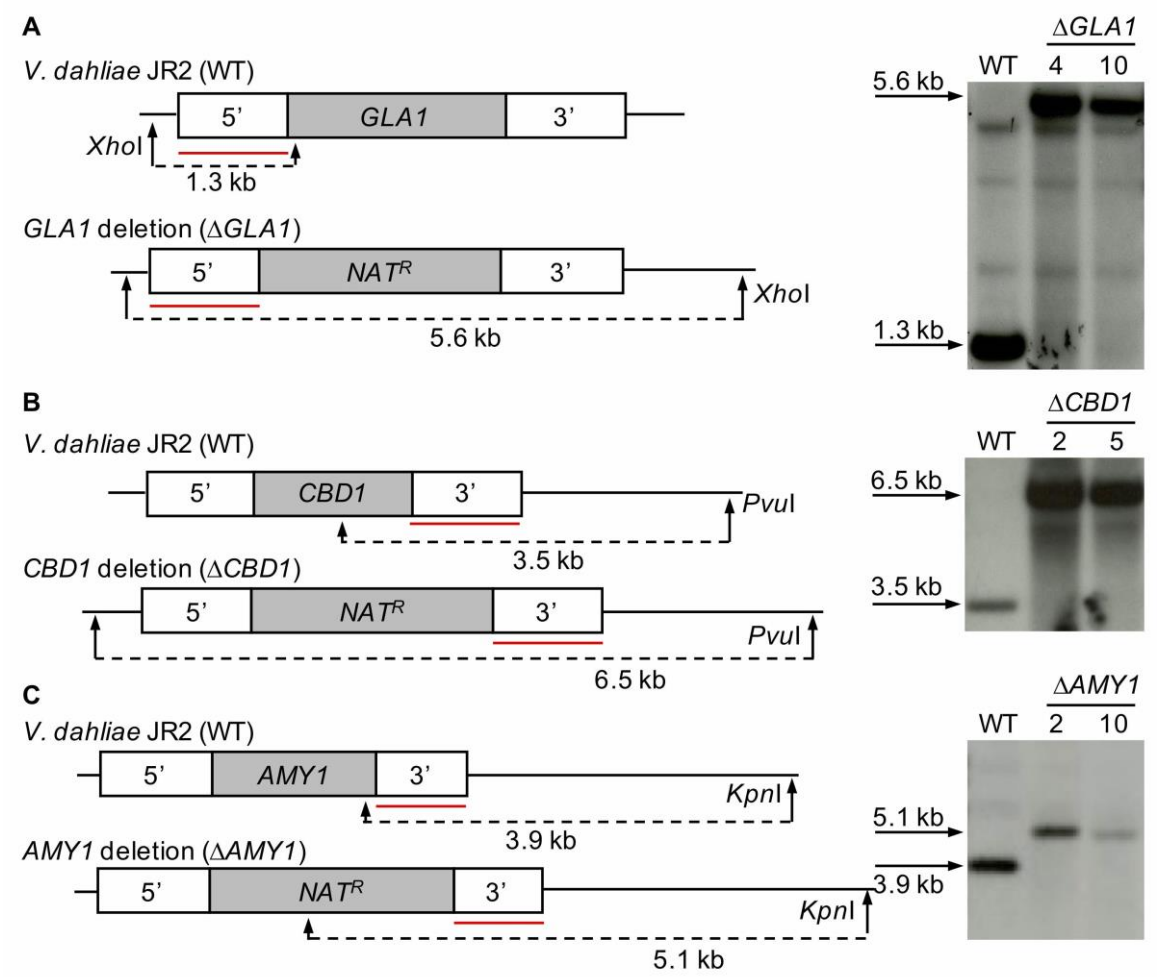

Figure S7. Verification of *V. dahliae CBD1*, *GLA1* and *AMY1* deletion strains.
Deletion strains were obtained via homologous recombination between the deletion construct and *V. dahliae* JR2 wildtype (WT) and confirmed by Southern hybridization. The deletion constructs contain a nourseothricin resistance (*NAT*^{R}) cassette controlled by the *gpdA* promoter and the *trpC* terminator. The used probes (red lines) and restriction enzymes with their cutting sites (arrows) are illustrated in the schemes (left). The expected fragments were confirmed by Southern hybridization for each deletion strain with WT as control (right). **(A)** With *Xho*I and 5' flanking region as probe *GLA1* deletion strains #4 = VGB129 and #10 = VGB131 were verified. **(B)** Verification of *CBD1* deletion strains (#2 = VGB127, #5 = VGB132) was achieved with *Pvu*I enzyme restriction and 3' flanking region as probe and *AMY1* deletion strains (#2 = VGB130, #10 = VGB128) were verified with *Kpn*I and 3' flanking region as probe **(C)**.

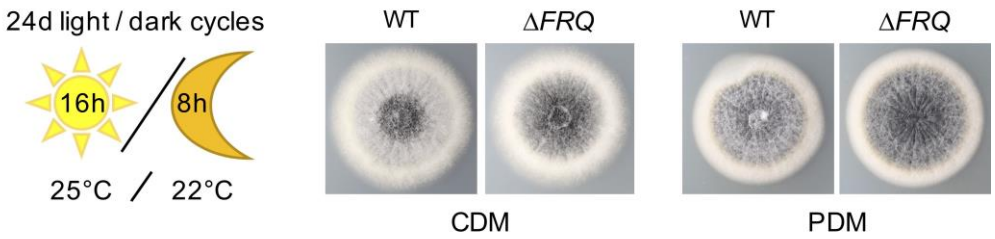

Figure S8. *V. dahliae* vegetative growth was tested in light:dark cycles.
50 000 spores of *V. dahliae* JR2 (WT) and *FRQ* deletion (*NAT*^{R}) strain VGB296 were point inoculated on minimal medium (CDM) and complete medium (PDM) and incubated for 14 days with cycles of 16 h of light at 25°C and 8 h of darkness at 22°C. Top views of the colonies, display the different phenotypes.

List of Figures

List of Supplementary Figures

List of Tables

Abbreviations

%	percent
5´	upstream flanking region
3´	downstream flanking region
α	antibody
°C	degree Celsius
Δ	deletion
λ	wavelength
µg	microgram
µl	microliter
µm	micrometer
µmol	micromol
aa	amino acid(s)
APS	ammonium persulfate
ATMT	*Agrobacterium tumefaciens* mediated transformation
ATP	adenosine triphosphate
BLAST	basic local alignment search tool
bp	base pair(s)
cAMP	cyclic adenosine monophosphate
CAZy(s)	carbohydrate-active enzymes
Cbd	carbohydrate-binding domain
CBM20	family 20 carbohydrate-binding module
CDM	Czapek-Dox medium
cDNA	complementary DNA
cm	centimeter
CP1-C/*CP2*-C	cerato-platanin 1/2 complementation strains
Cpc	cross-pathway control
C-terminus	carboxy terminus
CWDE(s)	cell wall degrading enzyme(s)
d	days
Da	Dalton
DAPI	4′,6-diamidino-2-phenylindole
dH_2O	deionized water
DHN	1,8-dihydroxynaphthalene
DNA	deoxyribonucleic acid
dpi	days post inoculation
DTT	dithiothreitol
ECL	enhanced chemiluminescence
EDTA	2,2´,2´´,2´´´-(Ethane-1,2-diyldinitrilo) tetra-acetic acid
et al	*et alii* (and others)
EtOH	ethanol
FAD	flavin adenine dinucleotide
FCD	FRQ-CK1-interacting domains
FFC	FRQ-FRH-complex
FFD	FRQ-FRH-interacting domain
FRH	FRQ-interacting RNA helicase

FRQ-C	frequency complementation strain
FTP	fungalysin/thermolysin propeptide
g	gram
GFP	green fluorescent protein
GH13	glycosyl hydrolase family 13
GmbH	Gesellschaft mit beschränkter Haftung
^{p}*gpdA*	*A. nidulans* glyceraldehyde-3-phosphate dehydrogenase promoter
H_2O_2	hydrogen peroxide
h	hour(s)
HOG	high osmolarity glycerol
HSF	heat shock factor
IRTG	international research training group
KAN^{R}	kanamycin resistance marker cassette
kb	kilobase(s)
kDA	kilo Dalton
KGaA	Kommanditgesellschaft auf Aktien
l	liter
LB	lysogeny broth
LC-MS/MS	Liquid chromatography-tandem mass spectrometry
M	molar
MAMP(s)	microbe-associated molecular pattern(s)
mer	meros (part)
MES	2-(N-Morpholino)-ethane sulphonic acid monohydrate
mg	milli gram(s)
min	minute(s)
ml	milliliter(s)
mm	millimeter(s)
mM	millimolar
mRNA	messenger RNA
n	number of elements
NAT^{R}	nourseothricin resistance marker cassette
Nc	*Neurospora crassa*
NLP2-C/*NLP3*-C	necrosis and ethylene inducing-like protein 2/3 complementation strain
NLS	nuclear localization signal
nm	nanometer
NPP1	necrosis-inducing *Phytophtora* protein 1
ns	non-significant difference
N-terminus	amino terminus
OE	overexpression
ORF	open reading frame
PAGE	polyacrylamide gel electrophoresis
PAMP(s)	pathogen-associated molecular pattern(s)
PCA	principle component analysis
PCR(s)	polymerase chain reaction(s)
PDM	potato dextrose medium

PRoTECT	plant responses to eliminate critical threats
PTI	pathogen-associated molecular pattern-triggered immunity
p-value(s)	probability value(s)
ROS	reactive oxygen species
rpm	revolutions per minute
RNA	ribonucleic acid
RR	response receiver
SCF	Skp1-Cul1-F-box-protein
SDS	sodium dodecyl sulfate
SFL1-C	suppressor of flocculation 1 complementation strain
SISA	*Simple Interactive Statistical Analysis*
s/l	signal-to-level
SOC	super optimal broth supplemented with glucose
spp.	species
SXM	simulated xylem medium
TEMED	*N,N,N′,N′*-tetramethylethane-1,2-diamine
THN	tetrahydroxynaphthalene
Tris	2-Amino-2-hydroxymethyl-propane-1,3-diol
trpC^{t}	*A. nidulans* tryptophane biosynthesis gene terminator
UV	ultra-violet
V	volt
V8	vegetable juice
Vd	*V. dahliae*
VGB	*Verticillium* strain collection Gerhard H. Braus
v/v	volume per volume
WT	wild type
w/v	weight per volume
XyS	xylem sap
YNB	yeast nitrogen base

Acknowledgments

First of all, I would like to thank Prof. Gerhard H. Braus for his guidance throughout my PhD. I deeply appreciate his supervision, the insightful discussions and the time he invested to support my PhD project.

Secondly, I want to thank my Thesis Committee Members for helpful advice and suggestions during meetings. I am grateful to apl. Prof. Kai Heimel for his motivation and sharing his knowledge. I thank the members of the Heimel group for generously sharing their experiences and protocols. I sincerely thank Prof. James W. Kronstad and his lab for the friendly welcome during my stay in Vancouver. I deeply appreciate his guidance and the time he took for additional meetings and discussions.

Thank you to Prof. Volker Lipka, Dr. Marcel Wiermer and Dr. Till Ischebeck for participation on my Examination board as well as for taking part in discussions during “Plant Responses To Eliminate Critical Threats” (PRoTECT) meetings.

I am grateful for the opportunity to join the International Research Training Group (IRTG) 2172, PRoTECT, a doctoral program of the Göttingen Graduate School for Neuroscience, Biophysics and Molecular Biosciences (GGNB). I am thankful to all PRoTECT members including principle investigators, secretary, coordinators and students who together made this program very special. Within the frame of seminars, we invited and met experts of the field plant-microbe interactions. We were involved in the organization of methodology as well as soft skill courses. I had the opportunity to plan an industry excursion to companies. As a highlight, through collaborative work we organized the International Plant Immunity Symposium (IPIS) 2018. Through organizing and participating at such seminars, courses and excursions, I was able to develop important competences beneficial for my future career. Furthermore, my fellow students and I had the chance to spend part of our PhDs in cooperating research groups of the University of British Columbia in Vancouver. This provided us international experiences and let us build up an international network. I am thankful to the Canadian PRoTECT fellow students who hosted us not only in the labs but were also very helpful in everyday life.

I would like to acknowledge the GGNB program and coordination office as the GGNB offered a broad selection of courses that we were additionally able to

participate in. I also had the opportunity to visit the 12th International Verticillium Symposium in Slovenia by financial support of the GGNB.

My gratitude further goes to the whole Verticillium group, including Rebekka, Nicole, Jessica, Annalena, Thuc, Alexandra and Isabel, for the nice working environment. A deeply sincere thank you to Rebekka for the supervision throughout my whole PhD. I am grateful for the discussions, patience, experimental support and for always being available for any kind of matter and especially for all efforts on the PhD thesis during the last phase. I would like to thank Thuc for sharing protocols and experience. Warm thanks to my bench partner Annalena who helped me in finding solutions. I could not have asked for a better bench partner. I would like to express my sincere gratitude to Nicole for most competent technical assistance as well as for being so cheerful all the time. A special thank you to Alex and Isabel for all their efforts in frame of their research assistant jobs as well as beyond. I could always count on them and their reliable and diligent work. I express my special indebtedness to Jessica for constant encouragement throughout my PhD. I am grateful to have spent my masters and PhD together with a friend who helped me through challenges and shared the joy in good moments.

Furthermore, I want to thank Alisa Keyl and Anja Pelizaeus who supported my project in frame of lab rotations. I also express my gratitude for experimental support of Rica Bremenkamp and Jan Teer as research assistants.

Anika Kühn and Alexander Kaever are gratefully acknowledged for their initial work on the secretome studies.

I would like to thank all members of the department of “Molecular Microbiology and Genetics” for the great working atmosphere. A special thanks to former lab members and finished PhD students for their constant willingness to help in trouble shooting and sharing protocols as well as other experiences. Thank you to current and new lab members for the friendly working environment and fruitful discussions during seminars. I am sincerely grateful to Heidi Northemann, Andrea Wäge, Katharina Ziese-Kubon, Gabriele Heinrich and Verena Große for supporting administrative issues as well as for maintenance of the everyday lab works.

Last but not least, I would like to thank my family and friends for their continuous encouragement. Even if they can’t imagine the challenges of a PhD, they were always there to support me in every possible way. Thank you!